Clickable lipid-based nanoparticles for targeted theranostics

A thesis submitted for the degree of
DOCTOR OF PHILOSOPHY
from the
Monash Institute of Pharmaceutical Sciences
Monash University
by
Nicolas Alejandro Alcaraz
B. Pharm Sci (Hons)
July 2018

Drug Delivery, Disposition and Dynamics

Monash Institute of Pharmaceutical Sciences

Monash University

381 Royal Parade,

Parkville, Victoria, 3052

Declaration of Authorship

In accordance with Monash University Doctorate Regulation 17/Doctor of Philosophy and Master of Philosophy (MPhil) regulations the following declarations are made:

I hereby declare that this thesis contains no material which has been accepted for the award of any other degree or diploma at any university or equivalent institution and that, to the best of my knowledge and belief, this thesis contains no material previously published or written by another person, except where due reference is made in the text of the thesis.

This thesis includes texts and figures from 2 original papers published in peer reviewed journals and at least 3 unpublished publications. The inclusion of co-authors in the published papers reflects the fact that this work came from active collaborations. Work from published papers may have been modified and altered to improve consistency and readability of the thesis.

The core theme of the thesis is clickable nanoparticles for drug delivery. The ideas, development and authorship of all the papers in the thesis were the principal responsibility of myself, the candidate, working within the Monash Institute of Pharmaceutical Sciences under the supervision of Ben J. Boyd.
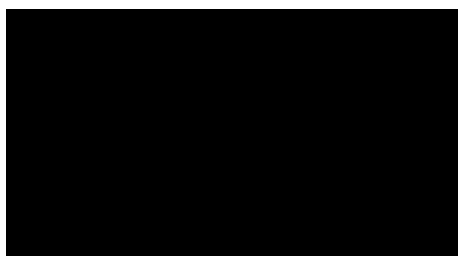
Nicolas Alejandro Alcaraz   Ben Boyd
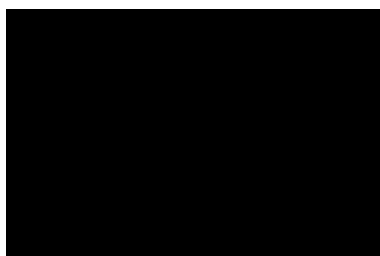
Publications

I hereby declare that this thesis contains no material which has been accepted for the award of any other degree or diploma at any university or equivalent institution and that, to the best of my knowledge and belief, this thesis contains no material previously published or written by another person, except where due reference is made in the text of the thesis.

This thesis includes *2* original papers published in peer reviewed journals. The core theme of the thesis is Lipid-based clickable nanoparticles. The ideas, development and writing up of all the papers in the thesis were the principal responsibility of myself, the student, working within the Doctor of Philosophy under the supervision of Ben Boyd.

The inclusion of co-authors reflects the fact that the work came from active collaboration between researchers and acknowledges input into team-based research. In the case of the published papers, my contribution to the work involved the following:

Thesis Chapter	Publication Title	Status	Nature and % of student contribution	Co-author name(s) Nature and % of Co-author's contribution*	Co-author(s), Monash student Y/N*
3	Clickable Cubosomes for Antibody-Free Drug Targeting and Imaging Applications	*Published*	*80% Concept, experimental work, data analysis and writing of manuscript*	1) *Ben Boyd, Concept and input into manuscript 8%* 2) *Angus Johnston, input into manuscript 4%* 3) *Jason Liu, input into manuscript and concept 4%* 4) *Eric Hanssen, CryoTEM imaging 4%*	*No*
5	Lipidated polymers for the stabilization of cubosomes: nanostructured drug delivery vehicles.	Published	39% Concept, experimental work, data anaylsis and considerable input itno the manuscript	1) James Grace Concept, experimental work, data anaylsis and considerable input itno the manuscript 39% 2) Nghia P. Truong *Concept and input into manuscript 5%* 3) Thomas P. Davis Concept 2% 4) Ben J. Boyd *Concept 5%* 5) John F. Quinn *Concept and input into manuscript 5 %* 6) Michael R. Whittaker *Concept and input into manuscript 5%*	Yes
Appendix	Cubosomes as carriers for MRI contrast agents.	Published	90% Concept and writing of manuscript	Ben Boyd, input into manuscript 10%	No

I have renumbered sections of submitted or published papers in order to generate a consistent presentation within the thesis.
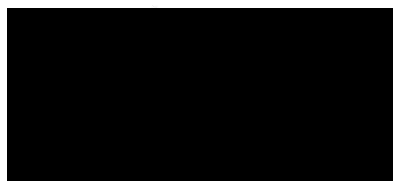
Student signature: ███████████ Date: 8/11/18

The undersigned hereby certify that the above declaration correctly reflects the nature and extent of the student's and co-authors' contributions to this work. In instances where I am not the responsible author I have consulted with the responsible author to agree on the respective contributions of the authors.

Main Supervisor signature: ███████ **Date:** 8/11/18

Manuscripts in preparation

First Author

1. Nicolas Alcaraz, James L. Grace, Nghia P. Truong, Thomas P. Davis, John F. Quinn, Michael R. Whittaker and Ben J. Boyd. Effect of Lipidated polymer structure on cubosome size, shape and structure. Intended for submission to Langmuir.

2. Nicolas Alcaraz, James L. Grace, Nghia P. Truong, Thomas P. Davis, John F. Quinn, Michael R. Whittaker and Ben J. Boyd. Azide-lipidated polymers for clickable cubosomes. Intended for submission to Bioconjugate chem.

Communications

Alcaraz N., Boyd BJ., Johnston A., Graham B., Hanley T.; (2015) Targeting Drug Carriers Using "Copper-Free" Click Chemistry and Metabolic Labelling; poster abstract (809) at the Annual Meeting of the Controlled Release Society in Edinburgh , Scotland.

Alcaraz N., Boyd BJ., Johnston A., Graham B., Hanley T.; (2015) Targeting Drug Carriers Using "Copper-Free" Click Chemistry and Metabolic Labelling; poster abstract at the annual Australasian Colloid and Interface Society in Hobart, Australia.

Alcaraz N., Liu J., Johnston A., Boyd BJ.; (2016) Targeting Lipid Based Liquid Crystalline Nanoparticles to Cell Surfaces Through Metabolic Labelling and Copper-Free Click Chemistry; poster abstract at the Drug Carriers in Medicine and Biology hosted by Gordon Research Conference/Seminar group in New Hampshire, U.S.A.

Acknowledgements

I'd like to begin my acknowledgements by thanking my supervisors Ben J. Boyd. The opportunity to undertake this challenging yet rewarding project was a privilege. All the support throughout this time was invaluable in completing this body of work, especially during all the difficult times.

I'd also like to extend a thanks to all those that collaborated and contributed to parts of this research such as Dr. Nigel Kirby, Dr. Adrian Hawley and Dr. Steven Mudie (SAXS/WAXS beamline, Australian Synchrotron) with their help during X-ray scattering experiments and Dr Eric Hansenn (Bio21, Melbourne University) and Lynn Waddington (CSIRO) for their help in conducting Cryo-TEM. Additionally, a thank you to all of those in the CBNS and at MIPS that have aided me over the course of my PhD that got me out of difficult situations. Thanks for those in the Boyd group that have come and gone over the years that have made the daily grind easier.

An extra special mention for three people who acted as great mentors and friends since the first day. Dr. Michael R. Whittaker for his constant advice and help over coffees, Igor C. for being a great friend and form of support and also to Dr. Joe Nicolazzo for being a true friend, mentor and maker of fine coffee and cured meats.

Finally, the biggest thanks is reserved to my friends who have understood and supported me over the last four years. My Mum and Dad who made this feat possible through their continual support, encouragement and love. Finally to Rebekah Culhane who has had to deal with me during my candidacy but never failed to always be a loving, understanding, supportive and positive even when I was being difficult and unreasonable.

Table of Contents

Abstract

Sophisticated drugs often require nanoparticles as carriers. These nanoparticles can have more than one function, such as targeted delivery or controlled release. One such nanoparticle system that has desirable properties for controllable drug release are dispersed lipid-based liquid crystalline matrices, including particles known as cubosomes. These systems are made from amphiphilic lipids which have hydrophilic and hydrophobic regions allowing for incorporation of drug molecules with varying properties.

Bioorthogonal chemistry involves chemical reactions that can occur in vivo, rapidly and specifically without interacting with the natural processes of the cell. Briefly, it involves a two-step process where chemical reporters (such as azide-alkyne click chemistry groups) are generated on a cell surface through the hijacking of the cells' natural metabolic pathways and then targeting the reporters with probes of interest such as a fluorescent dye possessing the complimentary functional group. There have been limited reports of this technique being utilised for delivery of nanoparticles for a therapeutic or diagnostic purpose.

Consequently, this thesis aims to understand the potential to utilise biorthogonal chemistry as a means of in vivo targeting of cubosomes in the effort to develop a novel theranostic system. Utilising a series of key techniques, nanoparticles that could partake in biorthogonal chemistry were created and characterised using dynamic light scattering, cryo-TEM and small angle X-ray scattering whilst their binding ability was assessed with size exclusion chromatography, fluorescence and total internal reflection fluorescence microscopy. Cubosomes were initially functionalized through doping of phospholipids functionalized with click groups. These systems displayed similar properties to traditional Pluronic F108 stabilised phytantriol cubosomes.

Additionally, they displayed excellent click binding in solution to a click-fluorophore. The binding to A549 cell surfaces was then assessed and an inherent limitation was discovered. The nature of the cubosomes appears to cause a high level of non-specific binding caused by hydrophobic interactions with the cell's lipid membrane. As a result, the subsequent experiments were dedicated to understanding some of the key variables that are critical in nanoparticle development to effectively use biorthogonal chemistry for drug delivery. The effect of size and azide concentration on surface binding was investigated using micelles, liposomes and quantum dots. It was clear that sizes under 30 nm were important in minimising non-specific binding and that a higher azide concentration on the nanoparticle lead to higher specific cell surface clicking. Finally, in an attempt to improve cubosome performance a series of lipidated polymers were synthesised to be used as stabilisers that could replace Pluronic F108. An azide modified polymer was developed, confirmed to stabilise cubosomes and their click capabilities assessed. In solution, like the phospholipid doped cubosomes, the binding efficiency with a click dye was nearly 100% but once again when applied to cells there was a high degree of non-specific binding observed.

These findings show that cubosomes can be effectively modified by two different pathways and undergo a specific click reaction in solution. These studies also showed that for future studies with nanoparticles, ensuring that the size is below about 50 nm and that the click group concentration on the nanoparticle surface is high is key. It is apparent that further optimisation and understanding is required to achieve the most out of biorthogonal chemistry for drug delivery purposes.

List of Abbreviations

PEG	Polyethylene glycol
EPR	Enhanced permeation and retention
RES	Reticuloendothelial system
MPS	Mononuclear phagocyte system
NP	Nanoparticle
ML	Metabolic labelling
CuACC	Copper catalysed click chemistry
CFCC	Copper free click chemistry
DBCO	Dibenzocyclooctyne
BCN	Bicyclononyne
Cyp	Cyclopropenes
TCO	Trans-cyclooctenes
sTCO	Strained Trans-cycloctenes
CNP	Glycol chitosan nanoparticle
cryoTEM	Cryo-transmission electron microscopy
SAXS	Small angle X-ray scattering
a	Lattice parameter
DLS	Dynamic light scattering
TIRF	Total internal reflective fluorescence
ATR-FTIR	Attenuated total reflective Fourier transform infrared
NIR	Near infrared
SEC	Size exclusion chromatography
PBS	Phosphate buffered saline

CHCl₃	Chloroform
GMO	Glycerol monooleate
PHYT	Phytantriol
LC	Liquid-crystalline
Im3m	Inverse bicontinuous cubic phase Im3m with space group
Pn3m	Inverse bicontinuous cubic phase Pn3m with space group
L₂	Inverse micellar phase
Lα	Lamellar phase
H₂	Inverse hexagonal phase
Ia3d	Inverse bicontinuous cubic phase with Ia3d space group
PL	Phospholipid
DSPE	1,2-Distearoylphosphatidylethanolamine
DOPC	Dipalmitoylphosphatidylcholine
Rhodamine B	1,2-dipalmitoyl-sn-glycero-3-phosphoethanolamine-N-(lissamine rhodamine B sulfonyl) (ammonium salt)
FBS	Fetal bovine serum
DMEM	Dulbecco's Modified Eagle's Medium
GRAS	Generally recognized as safe
LABOR	Liposome assisted biooorthogonal reporter

List of Figures

List of Tables

Chapter 1 - Introduction

1.1 A statement of the problem

The primary goal of the pharmaceutical science field has been to improve drug efficacy and patient compliance, while reducing the cost, amount of active required and side effects. As a result, there have been a range of technologies studied and developed that have come to market and provided huge benefits to patients around the globe. One key example from more recent times is the use of liposomes to encapsulate anti-tumour drugs to improve their efficacy. Liposomes are now on the market and being used clinically with success [1]. This has spawned further liposomal based drug formulations in clinical trials [2]. Many other nanoparticles are constantly being reported in the literature indicating a huge effort to realise novel methods to achieve the goals mentioned above [3-7]. The most commonly reported nanoparticle systems are solid drug, metallic, polymeric and lipid based nanoparticles with their array of positive and negative attributes for use as specific and controlled drug formulations detailed below.

Harnessing the benefits of nanoparticles is crucial in diseases such as cancer as the current treatment can be extremely cytotoxic which causes non-specific toxicity to organs and an array of severe side effects [8]. By improving specificity of delivery and controlling doses to be localised to the tumor, the side effects and unwanted damage can be minimised.

Currently, a popular approach to obtain specificity in nanoparticle targeting is to conjugate antibodies to the surface of the drug carrier and to target diseased cell surface receptors. Although promising, antibodies are not without their drawbacks such as low stability, difficult synthesis, high costs and limited binding restricted by cell-surface receptor density and the heterogeneity seen across and within tumors [9-12].

To this end, this project investigates the potential to specifically deliver drugs to tumor cells without the need for antibodies by utilising bioorthogonal chemistry comprising metabolic labelling and copper-free click chemistry. Building an improved understanding if how biorthogonal chemistry can be used with lipid nanoparticles to develop a theranostic agent that can lead to targeted controlled delivery of drugs.

1.2 General introduction to nanomedicine and nanoparticles in drug delivery

Modern treatment of disease and illness is strongly focussed on developing better compounds with higher efficacies and reduced side effects. However, research and clinical trials for new drugs are a long and costly endeavour that often fail at the later stages of development [13]. An alternative approach which has become more popular in the past four decades is using nanotechnology or other smart formulation designs to improve the efficacy of current drugs.

There are a range of means by which this can be achieved and they are listed briefly below:

- Encapsulation: Drugs molecules can be encapsulated into nanoparticles of different materials to protect the drug in vivo until it can access the site of action [14, 15].
- Sustained release: To ensure prolonged effective dose administration it is common to find hydrogel or polymer matrix based formulations that ensure continuous and steady release of drug via passive diffusion from their intricate structure or by the slow degradation of the structure [16].
- Triggered release: This approach allows for passive or active stimuli triggered formulations that ensure drug release is localised to the site of action to minimise unwanted cell-drug interactions [17].

- Targeted: The nanoparticle can actively or passively target cells of interest increasing localised drug release for greater efficacy and lesser side effects. Common approaches include coating the nanoparticle in PEG so the body does not recognise it, i.e. giving it a 'stealth' behaviour thereby increasing its residence in blood, or modifying the surface with ligands such as folate or antibodies so it will bind to specific receptors overexpressed by the cells in the target tissue [18, 19].

Nanoparticles are defined as sub-micron particles that can be utilised as colloidal vehicles for an active drug molecule or imaging agents [20]. Some benefits and limitations can be found in Table 1.1. Albanese *et al.* [21] has described the nanoparticle field to have entered its third generation of advances.

The first generation addressed toxicity and biocompatibility by manipulating composition and preparation methods. The second generation of nanoparticle development involved optimising the nanoparticle by improving stability, stealth behaviour and targeting capabilities by altering the surface chemistry.

The third and current generation involves the development of "smart" systems that are more dynamic improving localised delivery, reducing side effects and gaining diagnostic capabilities.

Table 1.1. Benefits and limitations of nanoparticle based drug formulations.

Benefits	Limitations
Small	Can be expensive
Inert	Difficulties synthesising, characterising and purifying
Easily chemically modified	
Can carry hydrophilic or hydrophobic compounds	Potential toxicity
	Limit to drug loading
Flexible (lipids and polymers)	Potential plasma stability issues
Rigid (metals and polymers)	
Biocompatible	
Can be biodegradable	
Normally solution based allowing for I.V administration	
Improved bioavailability	
Improves drug stability in vivo	

Two key factors have emerged of high importance when developing nanoparticle drug formulations; how the particle interacts with proteins in the blood stream through formation of the 'protein corona' (as this affects stability and targeting) and the effective size, shape and surface chemistry of the nanoparticle in the body as this affects its biodistribution and ultimate site of accumulation [21]. Below in Table 1.2 the role of size is explored.

Table 1.2. Role of particle size in intravenous applications. Adapted from [22].

Particle size (assuming a rigid sphere)	Fate	Advantages	Disadvantages	Ref
<10 nm	Rapidly cleared through extravasation or renally	Toxic agents are quickly and efficiently cleared	Poor for drugs that require long circulation and retention times to be effective	[23]
10-200 nm	Escapes most physiological barriers and has a high circulation time	Ideal for targeted drug delivery	Some potential for liver and spleen accumulation	[23, 24]
200 nm – 1 μm	High chance of clearance via the spleen	Cleared rapidly if dangerous	Chance of pulmonary embolism, difficult to manufacture and sterilise	[25]
>1 μM	High chance of opsonisation and accumulation in liver and spleen. Quickly cleared.		Not suitable for IV due to high risk of pulmonary embolism and stroke	[23, 24]

1.1.1 Theranostic capabilities

The bulk of these "smart" drug formulations utilise polymeric, metal or lipid based nanoparticles to impart their improved delivery capabilities which in turn improves efficacy and reduces side effects and costs. These more popular nanoparticle types can be visualised in Figure 1.1. A secondary benefit is found when the nanoparticles have diagnostic abilities to allow for both therapy and diagnosis, these have been given the term a theranostic formulation [26-28]. This greatly aids the clinicians in further tailoring the treatment for the patient's needs.
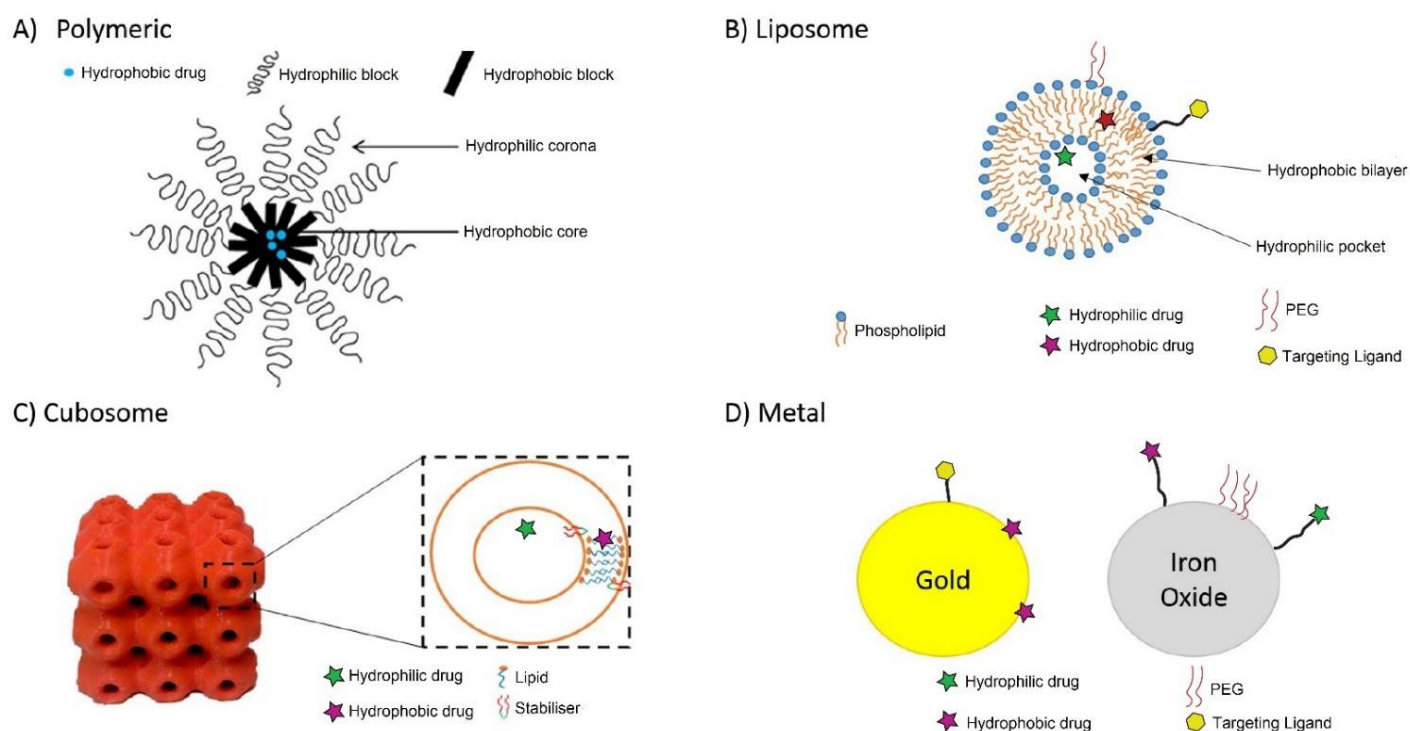
Figure 1.1. Simplified diagrams of common types of nanoparticles recreated and adapted from [34].

Further understanding of cellular interactions such as internalization mechanisms and metabolic pathways is also crucial to the development of nanoparticles for *in vivo* use. It should also be noted the use of nanoparticles is not exclusive to pharmaceuticals as other fields such as cosmetics [29], personal care [29], food [30-32] and environmental protection [33] all have an interest in improving active delivery through the use of nanoparticles.

1.1.2 Challenges for nanoparticle formulations

There are a range of challenges that all nanoparticle formulations will face during development. They can be classed as challenges before administration and those after entering the body.

1.1.2.1 Pre-administration

In forming a nanoparticle formulation for drug delivery one must be wary of and prepared for some challenges listed below [35]:

- Drug loading: Formulators must ensure efficient and high loading of the drug or imaging agent into their nanoparticle carrier. A common issue is poor loading efficiencies or poor control over loading which can result in low concentrations of drug in the formulation and a large high dose required when used for treatment.

- Drug stability: The drug compound is the key asset of the formulation and its stability is crucial to its function upon administration. A possible challenge is ensuring the stability of the drug is maintained in the nanosystem.

- Uniformity, size and sterility: When injecting a formulation there are some biological limitations and requirements that must be adhered to during preparation. Size and polydispersity play a large role with in vivo distribution, biological fate, toxicity and passive targeting of the nanoparticle. A secondary factor to consider is that the system must be sterile to prevent direct injection of harmful entities to the patient.

- Surface chemistry: The properties on the surface of the nanoparticle control its interactions *in vivo* with molecules such as proteins and also cell surfaces upon arrival to the site of action. A key property is hydrophobicity which is an important factor in protein binding and removal from the bloodstream via the MPS.

- Colloidal stability: Nanoparticle formulations generally involve a carrier being dispersed in a solvent to form a suspension. This is extremely important for injectable formulations as poor colloidal stability can result in very severe consequences for the patient, one example being a potentially fatal embolism [36]. The size also plays a crucial role in its in vivo fate and aggregation due to instability can lead to a loss of designed function.

1.1.2.2 Post-administration

As nanoparticles enter the blood stream or the gut they must overcome biological challenges to reach their target site and exhibit a beneficial response. This introduction will only focus on I.V administration as it is the most relevant to the study.

The body has a number of ways to remove foreign and unknown substances or particles to avoid harm. Understanding potential modes of clearance is essential in developing a nanoparticle formulation.

Smaller nanoparticles (below 10 nm in size) are likely to be renally cleared as they pass through and are excreted during the kidney's natural glomerular filtering process [37]. Additionally, once a foreign object enters the bloodstream another main challenge involves opsonin proteins that attach to it, making it more visible to phagocytes which then respond by clearing it from the bloodstream within minutes to hours [35, 38].

1.1.3 Passive vs Active targeting

The term 'theranostic', intends to combine therapeutics with diagnostics to help clinicians bett

er diagnose, track and treat patients. In order to develop these systems, targeting is critical to improve specificity which in turn should lead to better treatment but also reduced side effects from drug uptake in healthy cells.

Targeting has been considered either passive or active depending on the techniques and modifications used to get the nanosystem or drug molecule to the site of desired action.

Passive targeting involves nanoparticles that are small, inert, biocompatible and stable in plasma by having a hydrophilic surface [39]. At the same time they require that the tissue or cell of interest has leakier vasculature than healthy tissue as a means to escape the general circulation. A limitation of this approach is that the nanoparticle is not directed as such to the cell, and uptake can occur in undesired locations. This has predominately been seen in mice tumor models with polymeric micelles and liposomes but has had mixed clinical effectiveness. The PEG chains attached to the particle surface allow the nanoparticle to be invisible to the body's natural protection mechanisms due to the hydrophilic nature they give to the nanoparticle surface. In doing so the circulation time of the nanoparticles is greatly increased as they do not get removed or destroyed by biological systems.

This led to the discovery that nanoparticles with a long circulation time can exhibit higher accumulation in disease states, such as cancer. This was explained by the change in vasculature seen in tumors which leads to gaps in the cell walls that the nanoparticles can enter into if they are not removed in the bloodstream.

This is a phenomenon known as the enhanced permeation and retention (EPR) effect [40-42]. The EPR effect is a key method used for passive targeting of nanoparticles *in vivo*. It has had wide success in preclinical models but limited translation into humans. Focus on nanoparticles for drug delivery grew with the reporting of a stealth-like nanoparticle that could avoid clearance and termination by the mononuclear phagocytes system [43, 44]. Compared to PEGylated particles, bare nanoparticles do not circulate in vivo for long periods of time, as they are rapidly cleared from the blood by the reticuloendothelial system (RES) or accumulate in the liver before excretion by evading the mononuclear phagocytic system [43].

What is called active targeting involves having probes that specifically and covalently bind to the cell surface through the use of receptors such as folate [45], antibody-antigen [46], enzymes [43] and aptamers [47]. Each of these work via a different mechanism but have the same goal by allowing the nanosystem or drug to circulate until it binds to a corresponding target [48]. Antibody and folate receptor targeting nanoparticles are the most popular and successful approaches for specifically binding to the target cell surface.

Both modes of targeting require prolonged circulation time and therefore one of the biggest challenges they face is rapid clearance from the blood, as mentioned above, however this had been somewhat overcome with the success of "stealth" nanoparticles.

Further problems can occur once at the cell due to the cells own defence mechanisms such as efflux proteins, metabolising enzymes and sequestration into lysozymes.

Recently, there has been a shift in the drug delivery field that is described well by Josh Reineke's perspective in the Journal of Controlled Release [49]. This shift describes the need for more accurate terminology and how misnomers can hinder the progress of the field by being misleading. Reineke proposes that active targeting should be labelled as ligand retention and passive targeting more appropriately titled as evading the MPS. The key to both methods succeeding is the ability to avoid clearance and be able to accumulate and distribute into the target area (which is similar in both cases), with the systems utilising ligand binding having a higher chance of interacting with the target area. Therefore, Reineke also suggests the term targeting be replaced with more accurate language such as biodistribution and/or accumulation. It is still too soon to see the effects of this change in thinking occurring within the field. For the purpose of clarity this Thesis will continue to use currently established terminology.

1.1.4 Common nanoparticle types

There are three commonly investigated classes of nanoparticles that are described below in further detail.

1.1.4.1 Polymeric nanoparticles

Polymers have been of great interest in the field of nanomedicine for their versatility in structure and composition. Amphiphilic polymers can assemble into nanoparticles and are utilised for drug delivery and imaging [50-52].

Polymer-based nanoparticle formulations give a great amount of control to scientists over crucial formulation properties by altering the monomer type, its molecular weight, charge and solubility [53]. The polymers used can be of either a natural [54] or synthetic [55] origin, with each having advantages and disadvantages.

Natural polymers tend to be biocompatible but restricted in customisation and limited by extraction methods whereas synthetic polymers can exhibit some cytotoxicity or immune response but are usually tailor-made from the bottom up, allowing for a high degree of customisation, unique physicochemical properties and generally lower costs [56].

There is a large range of options with polymeric nanoparticles as they are often tailored for a specific use or outcome such as being thermo-responsive [57, 58], pH-responsive [59-62] or enzyme-cleavable [63, 64] which are examples of modifying a polymer to gain controlled release. Additionally, as mentioned previously, the development of PEGylated passive delivery created interest and a whole range of novel "stealth" polymeric nanoparticles utilising polyethylene glycol [65-68].

Polymers show great promise as tailored systems for targeted drug and imaging release but there has been no translation of this science into a clinical setting, unlike liposomes, indicating that there are still limitations that must be overcome through further research. It should be noted that some polymeric nanoparticles are in phase I/II trials [69, 70].

1.1.4.2 Solid metal nanoparticles

Metal nanoparticles, typically prepared from gold (for a photothermal capability) or iron oxide (for imaging purposes) are comprised of a solid metal core and specialised surface chemistry [71-73]. There are multiple means of adding or incorporating a payload, such as a drug molecule, that can include adsorbing it to the surface or tethering it with a covalent bond [71-73].

This ease and degree of control of surface modification is desirable as the surface area to volume of the metal nanoparticles is high allowing for a high degree of functionality to be imparted but also for a large amount of drug to be carried. This also allows for a high degree of complexity where the surface can have more than one drug attached, ligands can also be added to provide a stealth effect or for targeting for improved delivery [74].

Recently, metal nanoparticles have been investigated for their ability to also act as treatment, for example gold or superparamagnetic iron oxide metal nanoparticles can be heated externally through near infrared lasers and magnetic fields respectively which can lead to controlled localised cell death by utilising hyperthermia [75, 76].

1.1.4.3 Lipid-based nanoparticles

These systems are normally a collection of lipids, phospholipids and other lipidic materials that combine together to assemble into a nanoparticle that can be utilised for drug delivery. The most well-known lipid nanoparticle is the liposome, due to its utility across a range of products already in clinical use.

The benefit of these systems when compared to the two mentioned above is that they generally have better toxicity profiles (especially compared to synthesised polymers), have an accepted regulatory status (especially compared to new polymer constructs) are cheaper and simpler to prepare. However, due to their self-assembled nature they also give less control over characteristics such as size, shape and structure in comparison to polymer systems [77, 78].

1.1.4.3.1 Liposomal systems

Liposomes are generally composed of phospholipids, other lipids and cholesterol and self-assemble into spherical lipid bilayers that contain a lipid membrane and an internal aqueous pocket [79, 80]. This allows liposomes to be loaded with hydrophobic and hydrophilic drugs respectively. The use of cholesterol in the preparation of liposomes is extremely important as it helps to improve membrane rigidity and limits permeability while increasing stability. The cholesterol arranges itself among the phospholipid and lipid molecules with the hydroxyl group facing towards the water phase and the ring inserting itself between the carbons of the hydrocarbon region [80].

Liposomes are often PEGylated using PEG-conjugated phospholipids to impart stealth behaviour, as PEG is hydrophilic and provides steric hindrance for plasma proteins that would otherwise adsorb onto the liposome surface leading to rapid recognition.

If the liposomes are not PEGylated they can be rapidly cleared due to protein binding and resulting recognition and clearance by macrophages [81].

The surface can be further modified with ligands that can improve the targeting capabilities of the nanoparticle [82]. By combining both passive and active targeting strategies the efficacy can be improved.

Figure 1.2 lists a number of the current clinically used liposomes. According to the EPR theory, their small size and long circulation times enables them to accumulate in high enough concentrations at the active site where the contents are released upon lipid membrane breakdown or slow diffusion-controlled release.
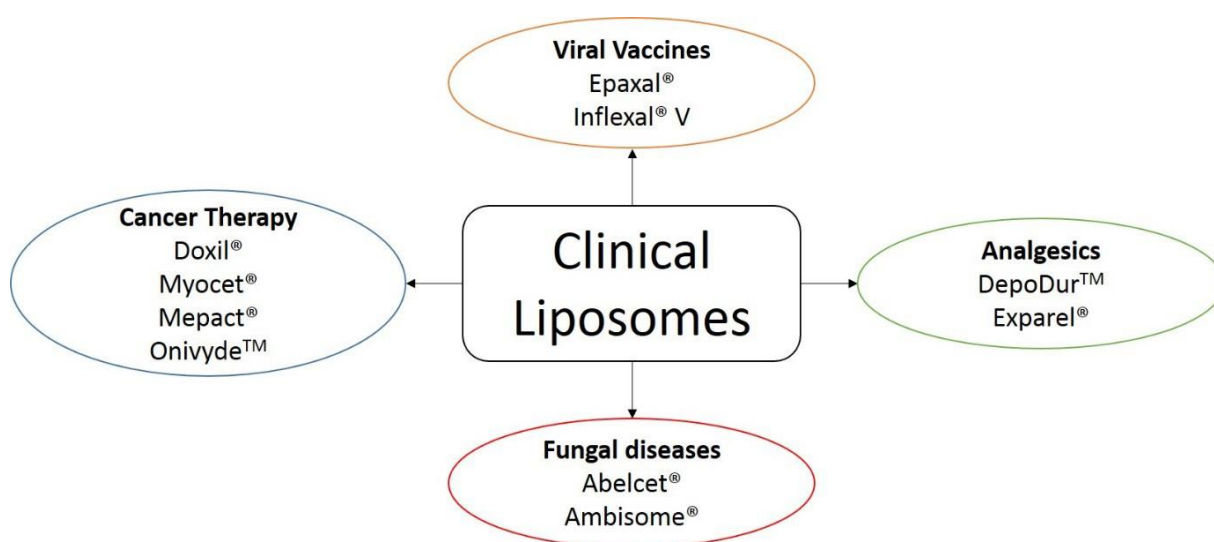
Figure 1.2. Liposomal formulations used clinically. Adapted from [2].

1.1.4.3.2 Lipid based liquid-crystalline systems

Amphiphilic lipids, such as glyceryl monooleate (GMO) and phytantriol (PHYT), can self-assemble to form a range of different structures in excess water. Their internal structure, known as the mesophase, is dictated by the properties of the lipid being used and its geometric packing according to the critical packing parameter (CPP).

The CPP is one framework used to consider what structure will be formed by a given lipid system and it is based on the theory by Israelachvili *et al.* [83] and defined by the equation:

$$CPP = V_s/a_0l$$

Where V_s is the effective volume of the hydrophobic chain, a_0 is the area of the head group and l is the hydrophobic chain length. The value indicates which phase is likely to form and can be affected by factors such as lipid structure, lipid concentration, temperature [84], water content [85], ionic strength [86] and pH [85].

For values less than 1 a normal phase will form where the hydrophobic chains face inwards towards the core of the structure and for values greater than 1 the inverse phase will form where the opposite occurs. A positive curvature means that the structure will curve towards the hydrocarbon and are attributed to the normal phase whereas inverse phases exhibit negative curvatures. The range of structures at different CPP values include micellar, hexagonal, cubic and lamellar in both the normal and inverse phases.

Those that are of most current interest to drug delivery and clinical use are the lamellar (Lα), inverse hexagonal (H$_2$), inverse bicontinuous cubic (V$_2$) and inverse micellar (L$_2$) phases. These can be visualised in Figure 1.3. Within the cubic phase there are three phases that have been observed, they include the double-diamond (Pn3m/Q$_{IID}$), primitive (Im3m/Q$_{IIP}$) and gyroid (Ia3d/Q$_{IIG}$) phases.
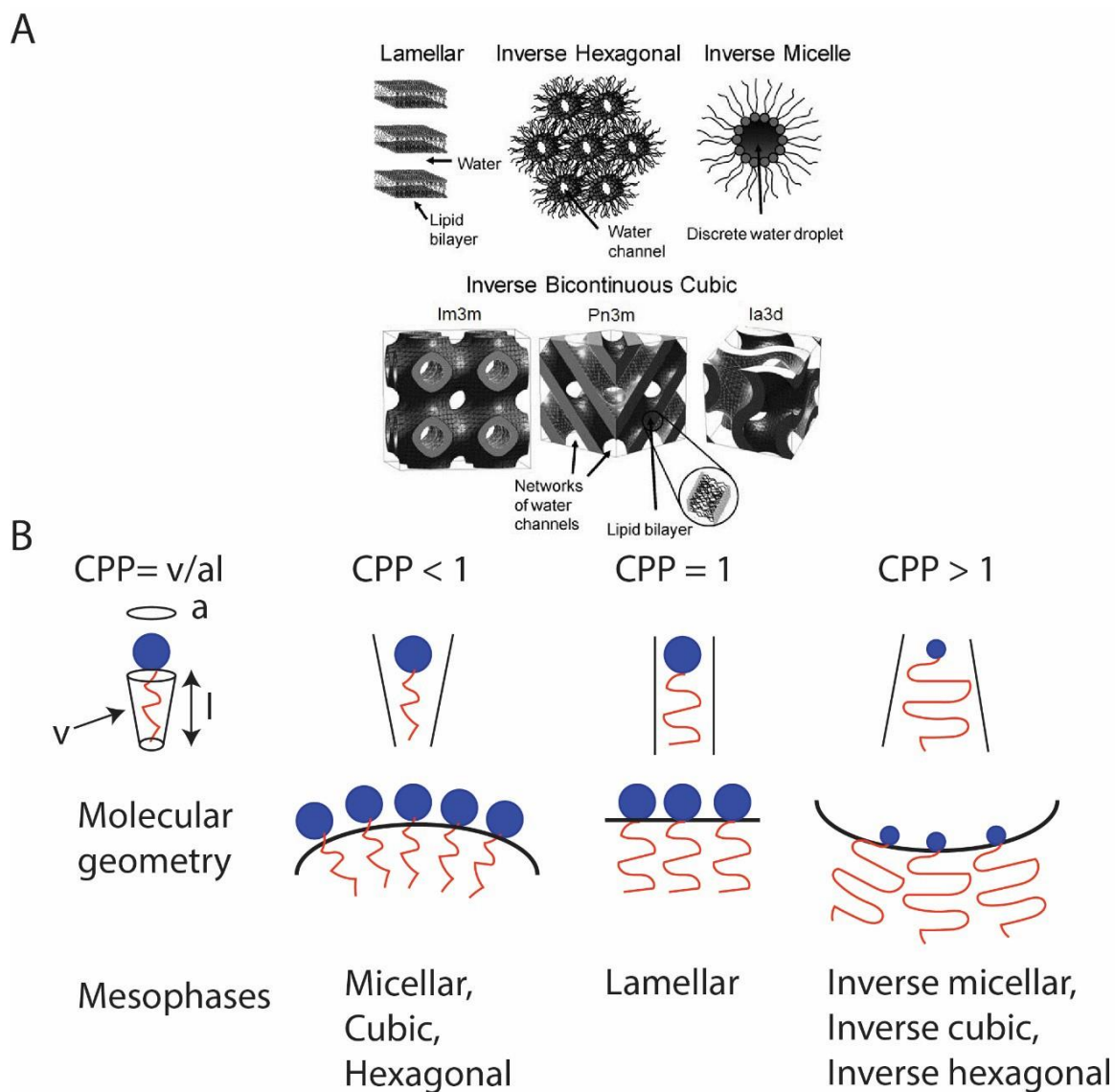
Figure 1.3. A) Depiction of mesophases of interest to this project and drug delivery. Adapted with permission from [87] via Rightslink. B) Illustration of lipid packing based on CPP for the most common mesophases. Recreated with permission from [88].

Drug release from these systems is under diffusion control and differs between the different structures (Figure 1.4). An added benefit of these systems is that they can be designed to reversibly change between the different phases under a range of stimuli allowing for controllable drug release behaviour [89-92].

These phase changes have been shown to be controllable through the use of external stimuli such as temperature [84], after the addition of additives such as vitamin E acetate [93] or using triggers such as near-infrared laser [94]. Ideally for drug delivery, a system will begin in the H_2 or $L\alpha$ phase which exhibit slow to no release due to the closed nature of the structure, and would then be triggered to form the V_2 phase which has a much faster release rate before returning to a more closed structure to prevent further release, enabling a multiple pulsatile release behaviour. A further benefit of these systems, much like liposomes, is their biocompatibility due to the nature of the lipids and phospholipids used [89, 90, 92].
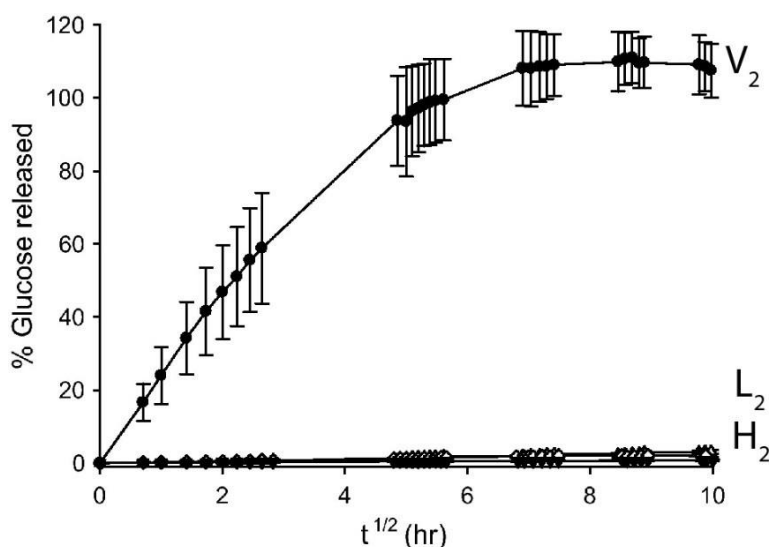
Figure 1.4. Different release rates from the mesophases of interest. Adapted with permission from [95].

Bulk liquid crystalline mesophases, like those described above, can often be dispersed in excess water, and with the aid of a stabiliser, generate nanoparticles that retain the internal structure and properties of the bulk mesophases.

To prevent aggregation of particles, a colloidal stabiliser such as Pluronic F108 or F127 is required. The dispersed cubic phase is known as cubosomes, dispersed hexagonal phase particles are known as hexosomes. These appear to be strong candidates for drug delivery systems but there is limited *in vivo* work and some reported stability issues in plasma that could be a key limitation [96].

1.1.5 Bioorthogonal Chemistry

Bioorthogonal chemistry refers to a chemical reaction that can occur inside living systems without interfering with its natural processes [97-99]. For a reaction or chemical group to be considered bioorthogonal it must be biologically inert, the reaction must proceed quickly and it must be non-toxic.

The objective of developing these technologies has primarily been for imaging and tracking biological processes to help visualise and deduce what occurs, specifically with respect to glycans [100-103]. Subsequent reaction of the new functional group at the cell surface with a 'probe' is intended to yield stable covalent linkages with no or innocuous by-products. The allure of using bioorthogonal chemistry as opposed to some more traditional and established methods for biologists is that it does not interfere with the natural processes of the cell and ensures a more accurate depiction of what is occurring, when compared to current methods.

Additionally, it is an exciting alternative to antibody-based targeting which is currently being regularly reported. Some limitations of antibodies that could be avoided by using biorthogonal chemistry include the cost and difficulty of antibody synthesis, low stability, heterogeneity of disease states and receptor surface density or availability which can limit the active targeting [10-12].

1.1.5.1 Metabolic labelling

Metabolic labelling is a technique where the natural processes of cells are harnessed to provide a 'label' for further reaction. In metabolic labelling an unnatural compound is introduced that appears to the cell to be sufficiently chemically similar to a natural compound that it does not interfere or disrupt the metabolic process [100, 104-107]. Sugars possessing unnatural reactive groups are the most common metabolic labelling systems utilised to date [107-112]. This has more recently expanded with successful labelling of proteins [106], DNA [113, 114] and even RNA [115]. Additionally, reports show that this technique is not exclusive to mammalian cells with biorthogonal chemistry also being used in bacterial systems [116-120].

In the case of using sugars as the labelling agent, monosaccharides are introduced to cells and taken up into the cytosol. Once in the cytosol, the sugars are further metabolised, typically into nucleoside sugars. There are numerous ways that the exogenous monosaccharides can be metabolised into the nucleoside sugars. These building blocks are transported to the secretory compartments of the cell where they are assembled by glycosyltransferases into oligosaccharides that are bound to a protein or lipid scaffold [121].

This process is illustrated in Figure 1.5. N-linked glycoproteins assemble a core oligosaccharide in the cytosol which is then transported into the endoplasmic reticulum where they are processed by glycosidases and are further modified by glycosyltransferases. These oligosaccharides are then expressed on the cell surface which can be used as a target for probes.
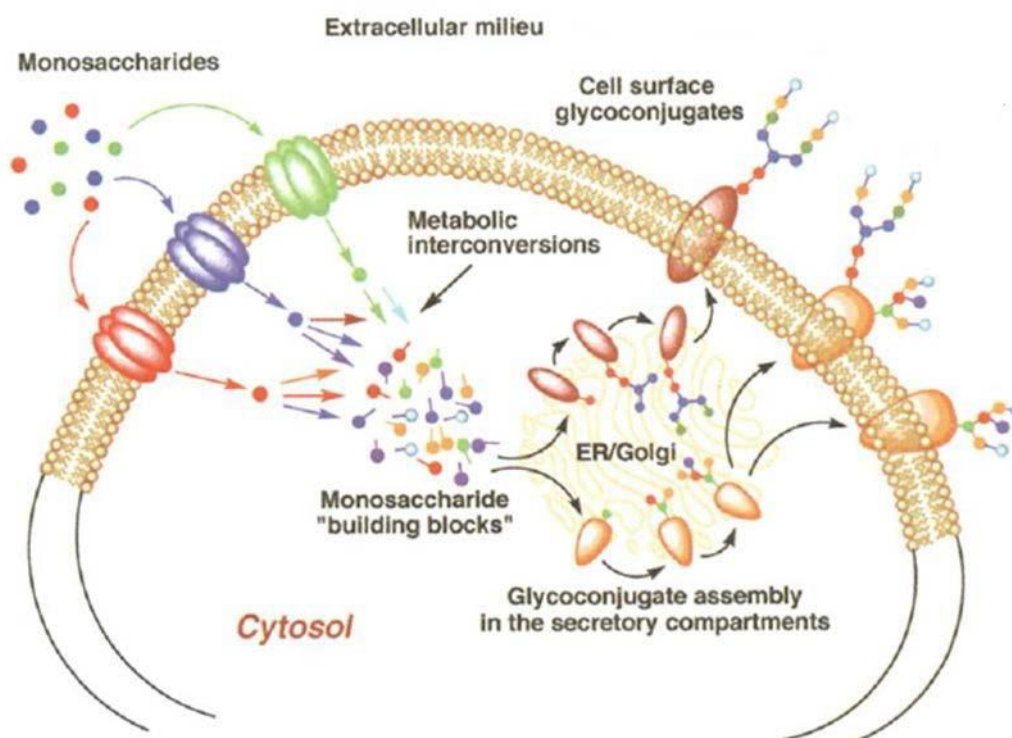
Figure 1.5. Simplified diagram of sugar metabolism in cells. Monosachharides are taken into the cytosol and broken down through a range of metabolic pathways. They then get processed through the endoplasmic reticulum and golgi complex where glycoconjugates for cellular use are assembled. Some of these become cell-surface glycoconjugates used for roles such as signalling. In metabolic labelling the modified monosaccharide retains its unnatural functional group as it is utilised in the creation of cell-surface glycoconjugates [121].

The term 'unnatural sugar' is given to sugars that have been engineered to be different to those that occur in nature. In metabolic labelling, sugars have previously been modified with azide functional groups, by replacing one of the six hydroxyl groups, for labelling [100, 121].

Sialic acid is of interest as a high level of sialic acid expression is usually found in tumor cells and has been shown to correlate with metastatic potential in several cancer types, therefore, making it of interest as a potential avenue for cancer treatment and detection [122, 123].

1.1.5.2 Click Chemistry (Copper catalysed and copper free)

The second step in biorthogonal chemistry is the binding of a probe to the reporter that the unnatural sugar has generated on the cell surface. This is often through the formation of a covalent bond using a click reaction with high thermodynamic drive resulting in high yield and specificity [124].

Click reactions also often have minimal by-products and can occur as a single synthetic step under ambient conditions [124]. These can be copper catalysed or copper-free with new functional groups and reactions being developed to achieve greater binding specificity and higher reaction speeds. Below are some of the more common reactions utilised.

1.1.5.2.1 Copper catalysed alkyne-azide (CuACC)

Copper catalysed click reactions are the traditional and simplest click reaction. They involve the use of copper ions to act as a catalyst between two chemical groups to help the reaction occur at a faster rate. Most commonly the two groups being reacted are an alkyne and azide which results in the formation of a triazole [125]. This method has been explored greatly already and has been shown to be a specific and rapid reaction making it ideal for *in vivo* labelling. However, an issue with this method is that copper can be toxic to the living systems [65, 126, 127] and requires co-delivery with a copper chelating agent to be effectively utilised [128].
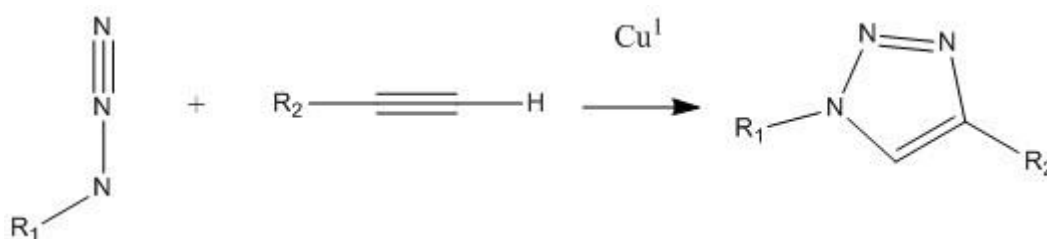
Figure 1.6. Reaction pathway for CuACC reaction.

1.1.5.2.2 Staudinger ligations

Staudinger reactions occur between an azide and a phosphine or phosphite and produce an iminophosphorane intermediate [129]. This intermediate is produced through nucleophilic addition of the phosphine at the terminal nitrogen atom of the azide and expulsion of the nitrogen. The Staudinger ligation is a modification of the traditional Staudinger reaction [130]. The end result of the ligation is a covalent bond after hydration. It has been used previously in biology to aid with cell imaging as the reaction can lead to site specific binding. However, this reaction has limitations on the speed, making it not ideal for scenarios that require fast reaction times such as during in vivo imaging [131].
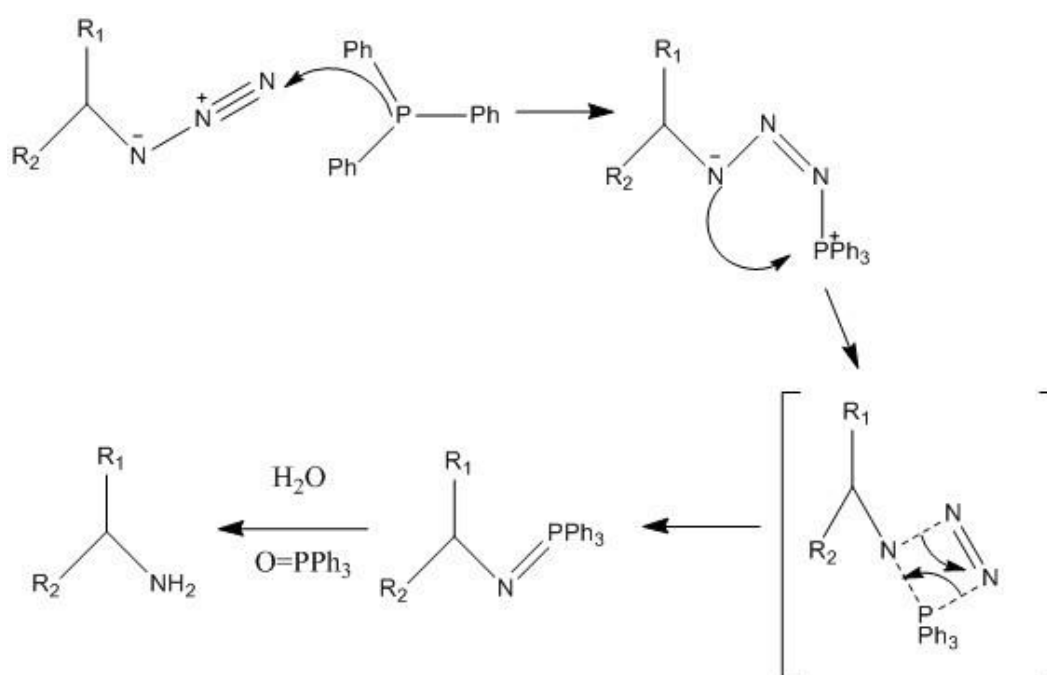
Figure 1.7. Reaction pathway for a Staudinger ligation.

1.1.5.2.3 Strain promoted copper-free click chemistry

This method was developed by Carolyn Bertozzi as a modified version of an azide-alkyne Huisgen cycloaddition [109]. This is an alternative to CuACC that doesn't require a copper ion to catalyse the reaction, therefore eliminating the possibility of copper induced toxicity. A strained cyclooctyne with an alkyne is covalently attached to an azide group. This reaction occurs faster than the Staudinger ligation making it better suited for imaging [132]. There are different types of cyclooctynes that have been developed for this method with the most popular being dibenzocyclooctyne [133, 134].
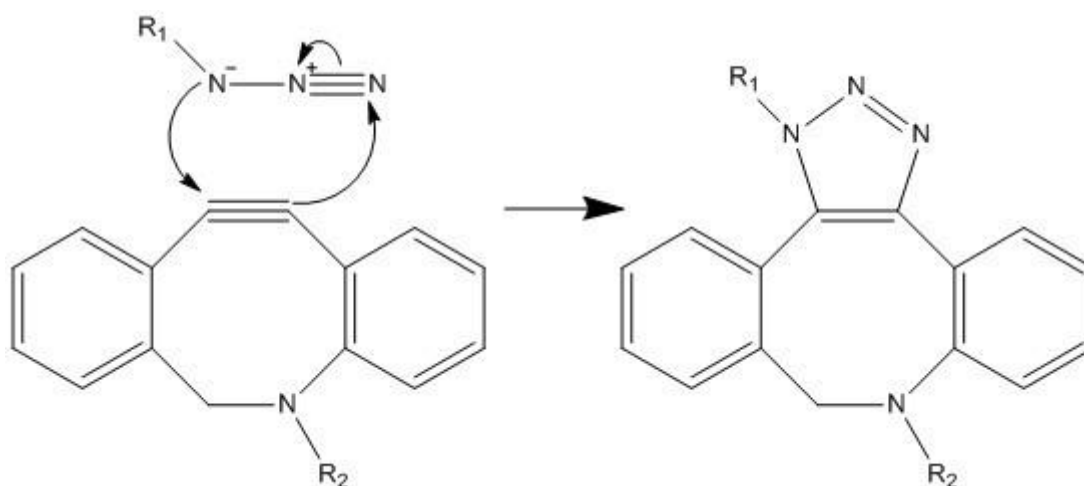
Figure 1.8. Reaction pathway for a SPAAC reaction between DBCO and an azide.

1.1.5.2.4 Inverse-electron demand Diels Alder reaction

This reaction has been increasing in popularity due to the range of reactants that can be used and its fast reaction times. The reaction differs to a traditional Diels-Alder reaction as this reaction is a cycloaddition between an electron rich dienophile and an electron poor diene [135].

These reactions can occur without the need of a catalyst between a tetrazine and strained alkenes or alkynes such as norbornenes [96], cyclopropenes (Cyp), bicyclononynes (BCN), trans-cyclooctenes (TCO) and strained trans-cyclooctynes (sTCO) [136].

The reaction yields dihydropyridazines or pyridazines with nitrogen gas as the only by-product. These reactions occur extremely quickly [137]. A favourable quality of this reaction type is that red fluorophores can be conjugated to the tetrazine involved, where there is only fluorescence present when the cycloaddition has occurred as it was quenched previously. The BCN and TCO involving reactions are currently the most popular [138, 139].
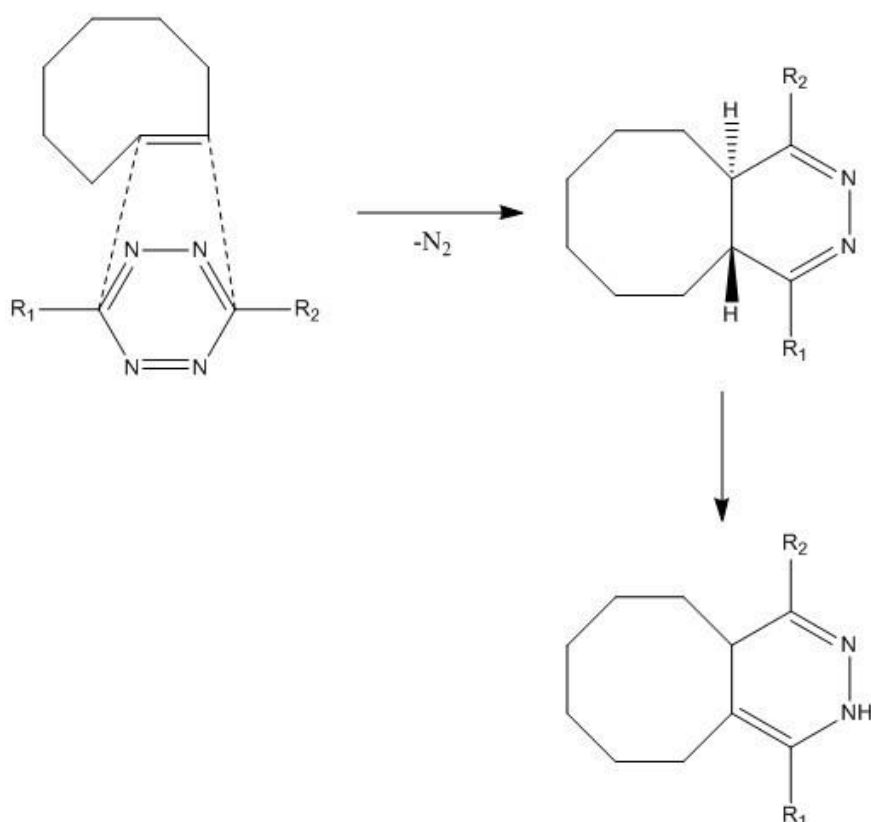
Figure 1.9. Reaction pathway for an Inverse electron-Diels Alder reaction between a trans-cyclooctene and a tetrazine.

1.1.5.3 Common uses of biorthogonal chemistry

Currently, the bulk of bioorthogonal chemistry in the literature has involved utilising the non-invasive nature of the technique to visualise natural processes *in vivo*.

Generally, a probe such as a fluorophore is attached to a cell of interest or a region within a cell and the probe is then imaged using fluorescence-based microscopy techniques over time to help biologists deduce the inner workings of a cell and the metabolic pathways of the type of unnatural chemical introduced to the system.

This technique has been used to study and visualise fucosylation during zebrafish development [103]. It was noted that the unnatural azido fucose sugars did not interfere with the natural metabolism of the cell or the growth of the embryo. Recently, metabolic labelling was used to image rat hearts during cardiac hypertrophy which showed an upregulation of sialylation [140] and also to image tumor associated glycans in live animals through the use of liposomal active targeting and metabolic labelling [141, 142]. These earlier works using biorthogonal chemistry have catalysed the pursuit of biorthogonal chemistry to aid in drug delivery, which has occurred primarily in parallel with the work in this thesis.

1.1.5.4 Active targeting of nanoparticles using biorthogonal chemistry

There have been few publications regarding the use of metabolic labelling and SPAAC reactions to selectively target a cell of interest with a nanoparticle.

The first known example was a study published by Koo *et al.* [143] who expanded on Bertozzi's work in the field by functionalising the surface of a liposome with DBCO chemical groups at the end of a PEG chain by incorporating DBCO-PEG-DSPE into the formulation.

The liposomes were then administered to the blood stream of a mouse that had previously received an intratumoral injection with azide-mannose to metabolically label the cells. Clear specific binding of the DBCO-liposomes was evident in the treated tumor compared to a control tumor with no labelling. The amount of binding was shown to be concentration dependent and that the nanoparticles were being taken into the cell to deliver their contents. The importance of sugar concentration for the success of these techniques was further supported by findings from the Chen group [144, 145].

To avoid the need for direct intratumoral injection, in a subsequent report Lee *et al*. loaded a glycol chitosan nanoparticle (CNP) with sugar that would passively target tumor tissue utilising the EPR effect and release the sugar locally, reporting a tumor concentration of 25 μg/mL within 30 minutes of administration [146]. A second CNP with BCN chemical groups present on the surface was injected intravenously and their ability to specifically bind to tumor tissues was determined. This revealed that the critical step in these techniques is the azide generation on the cell surface as if the nanoparticles circulate for a sufficiently long period of time without being cleared or altered they will eventually bind to the azide groups present in the body. They also showed that by passively targeting the sugar through an initial CNP the azide groups generated had a longer lifetime over Ac$_4$ManNAz on its own. These results show promise for the expansion of the field as it minimises non-specific binding, avoids using natural biological targets and only uses IV injections.

In past studies the sugar has almost exclusively been labelled with an azide, and the 'probe' with the alkyne containing functional group. However, the first example of metabolic labelling involving a DBCO modified sugar was presented by Wang *et al.* [147] in 2016 during the course of this PhD.

This finding showed that the hijacking of the natural metabolism of the cells was fairly robust and that the DBCO group could be transferred to the cell surface unchanged throughout the process and be a reporter that could be targeted by nanoparticles.

This finding is important for several key reasons, the first is that the DBCO group is more hydrophobic and will interact with the cell better than an azide group from a permeability perspective when labelling cells. It should be noted that non-azide bearing nanoparticles had similar uptake to those bearing azides in the DBCO-sugar treated cells [147] indicating that further studies are needed to fully understand whether the DBCO-mannose can be utilised for effective metabolic labelling. The ability to modify a cell surface with DBCO groups is of huge benefit when involving nanoparticles with this technique as the functional group is larger than azides perhaps making it an easier target *in vivo* but also that the azide can be incorporated onto the nanoparticle in much higher densities due to its smaller size whilst still being hydrophilic, which as mentioned is preferred. Not to pre-empt the contents of this thesis, but there are also clear likely advantages from a colloidal stability perspective in having the charged azide on the particles, and the relatively hydrophobic cyclooctyne on the cell surface.

One drawback of the previous study was that the sugar was directly injected into established tumors in mice for three days, like the first Koo *et al.* [143] paper, which does not translate to a clinical setting. This creates an artificially optimal situation where in reality the unnatural sugar is likely to be introduced intravenously which would result in the sugar being metabolised in all cells throughout the body if no further targeting is utilised.

It can be argued that due to a higher metabolic rate that tumors will uptake and therefore express more of the desired chemical probe but current nanoparticles using other targeting techniques are likely to be more favourable.

This issue was addressed by the Cheng group [148] who created azide mannose derivatives with chemical groups that prevented cellular uptake and metabolism until said chemical groups were removed from the sugar. They showed that an ethyl ether bond at the C1 position failed to be metabolically labelled. Once the inability to metabolise was determined, the sugar was further modified so the bond was UV cleavable (Figure 1.10).
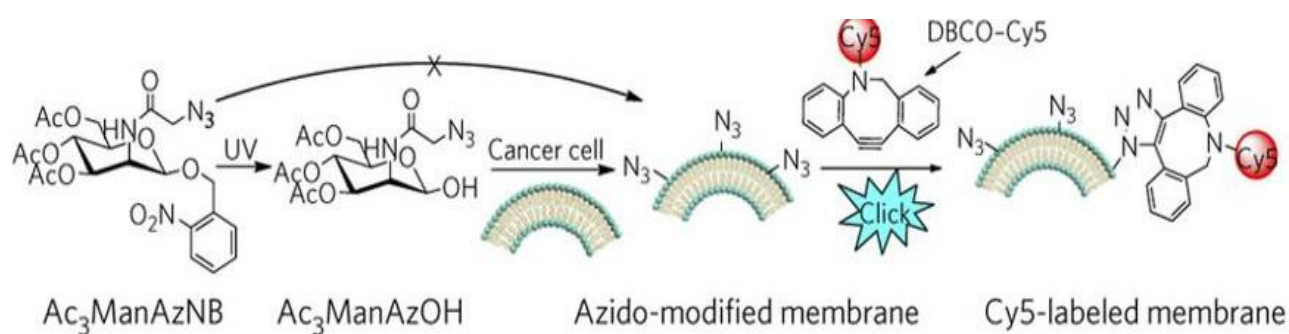
Figure 1.10. Schematic illustration of the UV activated Ac3ManAzNB and the subsequent metabolic labelling and cell-surface probe clicking. Reused with permission from [148].

The on-demand uptake after the cleaving of the ether bond was determined *in vitro* and also assessed *in vivo*. The *in vitro* experiments were expanded with a new more practical cleavable group that used natural enzymes overexpressed by cancer cells to enable uptake.

The results showed a clear specific binding and uptake of fluorescent dye probes on the cancer cell lines as opposed to the normal cell lines as the sugar was only in a form it could be metabolised in the presence of the enzymes overexpressed by the cancer cells. Additionally, no cytotoxicity was induced by these altered sugars or any degradation products.

The findings indicate that it takes around 24 hours for the sugar to be expressed on the cell surface but the amount of azide expressed on the cell surface from 200 µM of sugar was 2-4 orders of magnitude greater than the number of endogenous protein receptors on the cell surface further illustrating the untapped potential for targeted drug delivery.

Currently, the most common forms of targeted drug delivery use specific recognition of endogenous protein receptors such as the antibody-antigen technique. As mentioned, these methods have some limitations such as the receptor and targeting ligand being large, a limited number of endogenous groups to target, immunogenicity, poor stability, expensive and difficult manufacturing [9-12]. The term coined by the Cheng group for the method mentioned above is ATTACK, which circumvents a lot of the limitations of antibodies. This technique can be expanded on by improving the library of sugars and respective triggers such as oxidants, reductases and capthesin subsets.

This technique is not limited to cancer cells and has expanded to other cell types such as stem cells. There is a need to be able to track transplanted stem cells *in vivo* with non-invasive methods. This is because many modern treatments are beginning to use stem cells in regenerative medicine and to ensure the treatment is working as intended the exact information of the stem cell *in vivo* is critical.

The Kim group [149] was able to generate reporters on stem cells used for regenerative purposes and showed nanoparticle binding and uptake did not appear to interfere with the natural processes of the stem cells and allowed for non-invasive imaging for up to 15 days post-transplant. This is promising for the stem cell transplant field as further development could greatly aid in a clinical setting.

In an attempt to improve the sugar specificity the Chen group looked at assisted delivery methods much like the works mentioned above that utilised a nanoparticle and the so called EPR effect, ligand targeted or localised cleaving to unlock the sugar allowing it to be taken up by the tumor and metabolised [150]. The term coined LABOR (liposome assisted bioorthogonal reporter) and the mechanisms by which it works were studied as there was a lack of understanding of the more fundamental processes at play. They showed that LABOR uses receptor-mediated endocytosis and the salvage pathways of monosaccharides to label cells selectively.

The technique is able to specifically target the cell of interest using surface bound ligands on the liposome that specifically bind to receptors. In traditional uses, such as drug delivery, the liposome is then taken into the cell via the lysosomes and is degraded where the drug often degrades during this process [151]. When used for azido-sugar delivery the monosaccharide is salvaged and transported to the cytosol by lysosomal sugar transporters where it is utilised by the cell and surface sialoglycans. They recommend the LABOR technique to be used for sugars that have lysosomal transporters which do not include the commonly studied ManNAz. In these cases it might be more practical to utilise liposomes that fuse with the cell membrane and have cargo that is directly introduced into the cytosol for use.

This brief summary of the key studies indicate a growing interest in expanding the range of applications of biorthogonal chemistry that Bertozzi *et al.* began investigating two decades ago for biological imaging purposes. This project involves furthering the information and understanding of the mechanisms at play but also how to improve the targeting and delivery of nanoparticles to the cell of interest for theranostic purposes.

1.2 Hypothesis

1. That "copper-free" click chemistry can be used to attach a click capable cubosome to a corresponding click group in solution.

2. That "copper-free" click chemistry can be used to attach a click capable cubosome to a corresponding click group on a cell surface.

3. That smaller click nanoparticles will exhibit better cell surface binding capabilities to larger ones.

4. That a higher concentration of surface based click groups will result in higher cell-surface nanoparticle attachment.

5. That polymer-based cubosome surface functionalisation will exhibit better binding capabilities than phospholipid based cubosome surface functionalisation.

1.3 Aims

The aim of this project is to develop the understanding of whether nanoparticles can carry drugs to a site of action by covalently binding to a cell surface using bioorthogonal chemistry, specifically the combination of metabolic labelling of cells with unnatural sugars and copper free click chemistry.

The aims to be achieved in order to address the hypotheses stated above can be found below:

1. Design and characterise a novel click capable cubosome.

2. Assess the efficacy of the novel cubosomes for covalently binding to the corresponding chemical group in solution, on solid surfaces and on cell surfaces.

3. To determine the ability of chemical reporters to be generated on cell surfaces through metabolic labelling and the effect of size on surface binding of nanoparticles.

4. To develop polymer stabilisers that can functionalize the surface of cubosomes and assess their ability to undergo click reactions

1.4 References

1.   Barenholz, Y., *Doxil® — The first FDA-approved nano-drug: Lessons learned.* Journal of Controlled Release, 2012. **160**(2): p. 117-134.

2.   Bulbake, U., et al., *Liposomal Formulations in Clinical Use: An Updated Review.* Pharmaceutics, 2017. **9**(2): p. 12.

3.   Dobson, J., *Magnetic nanoparticles for drug delivery.* Drug Development Research, 2006. **67**(1): p. 55-60.

4.   Slowing, I.I., et al., *Mesoporous Silica Nanoparticles for Drug Delivery and Biosensing Applications.* Advanced Functional Materials, 2007. **17**(8): p. 1225-1236.

5.   Müller, R.H., et al., *Solid lipid nanoparticles (SLN) for controlled drug delivery – a review of the state of the art.* European Journal of Pharmaceutics and Biopharmaceutics, 2000. **50**(1): p. 161-177.

6.   Agnihotri, S.A., et al., *Recent advances on chitosan-based micro- and nanoparticles in drug delivery.* Journal of Controlled Release, 2004. **100**(1): p. 5-28.

7.   Cho, K., et al., *Therapeutic Nanoparticles for Drug Delivery in Cancer.* Clinical Cancer Research, 2008. **14**(5): p. 1310-1316.

8.   Pearce, A., et al., *Incidence and severity of self-reported chemotherapy side effects in routine care: A prospective cohort study.* PLOS ONE, 2017. **12**(10): p. e0184360.

9.   Wu, A.M., et al., *Arming antibodies: prospects and challenges for immunoconjugates.* Nature Biotechnology, 2005. **23**: p. 1137.

10.   Beck, A., et al., *Strategies and challenges for the next generation of therapeutic antibodies.* Nature Reviews Immunology, 2010. **10**: p. 345.

11.   Leavy, O., *Therapeutic antibodies: past, present and future.* Nat Rev Immunol, 2010. **10**(5): p. 297-297.

12.   Chames, P., et al., *Therapeutic antibodies: successes, limitations and hopes for the future.* British Journal of Pharmacology, 2009. **157**(2): p. 220-233.

13.   Grove, A., *Rethinking Clinical Trials.* Science, 2011. **333**(6050): p. 1679-1679.

14.   Zahr, A.S., et al., *Encapsulation of Drug Nanoparticles in Self-Assembled Macromolecular Nanoshells.* Langmuir, 2005. **21**(1): p. 403-410.

15.   Pinto Reis, C., et al., *Nanoencapsulation I. Methods for preparation of drug-loaded polymeric nanoparticles.* Nanomedicine: Nanotechnology, Biology and Medicine, 2006. **2**(1): p. 8-21.

16.   Leroux, J.-C., et al., *Biodegradable nanoparticles — From sustained release formulations to improved site specific drug delivery.* Journal of Controlled Release, 1996. **39**(2): p. 339-350.

17.   Reimhult, E., *Nanoparticle-triggered release from lipid membrane vesicles.* New Biotechnology, 2015. **32**(6): p. 665-672.

18.   Loomis, K., et al., *Nanoparticles with targeting, triggered release, and imaging functionality for cancer applications.* Soft Matter, 2011. **7**(3): p. 839-856.

19.   Singh, R. and Lilalrd, J.W., *Nanoparticle-based targeted drug delivery.* Experimental and molecular pathology, 2009. **86**(3): p. 215-223.

20.   Mudshinge, S.R., et al., *Nanoparticles: Emerging carriers for drug delivery.* Saudi Pharmaceutical Journal, 2011. **19**(3): p. 129-141.

21.   Albanese, A., et al., *The Effect of Nanoparticle Size, Shape, and Surface Chemistry on Biological Systems.* Annual Review of Biomedical Engineering, 2012. **14**(1): p. 1-16.

22.   Banik, B.L., et al ., *Polymeric nanoparticles: the future of nanomedicine.* Wiley Interdisciplinary Reviews: Nanomedicine and Nanobiotechnology, 2016. **8**(2): p. 271-299.

23.   Elsabahy, M. and Wooley, K.L., *Design of polymeric nanoparticles for biomedical delivery applications.* Chemical Society reviews, 2012. **41**(7): p. 2545-2561.

24.   Petros, R.A. and Desimone, J.M., *Strategies in the design of nanoparticles for therapeutic applications.* Nature Reviews Drug Discovery, 2010. **9**: p. 615.

25.   Swami, A., et al., *Nanoparticles for Targeted and Temporally Controlled Drug Delivery*, in *Multifunctional Nanoparticles for Drug Delivery Applications: Imaging, Targeting, and Delivery*, S. Svenson and R.K. Prud'homme, Editors. 2012, Springer US: Boston, MA. p. 9-29.

26.   Xie, J., et al., *Nanoparticle-based theranostic agents.* Advanced drug delivery reviews, 2010. **62**(11): p. 1064-1079.

27. Jeelani, S., et al., *Theranostics: A treasured tailor for tomorrow.* Journal of Pharmacy & Bioallied Sciences, 2014. **6**(Suppl 1): p. S6-S8.

28. Chen, F., et al., *Theranostic Nanoparticles.* Journal of nuclear medicine : official publication, Society of Nuclear Medicine, 2014. **55**(12): p. 1919-1922.

29. Kulkarni, V.S., *13 - Liposomes in Personal Care Products A2 - Rosen, Meyer R*, in *Delivery System Handbook for Personal Care and Cosmetic Products.* 2005, William Andrew Publishing: Norwich, NY. p. 285-302.

30. Yuli, I., et al., *Solubilization of food bioactives within lyotropic liquid crystalline mesophases.* Vol. 14. 2009. 21-32.

31. Leser, M., et al., *Self-assembly of polar food lipids.* Vol. 123-126. 2006. 125-36.

32. Mezzenga, R., et al., *Understanding foods as soft materials.* Nature Materials, 2005. **4**: p. 729.

33. Garti, N., et al., *Solubilization of active molecules in microemulsions for improved environmental protection.* Colloids and Surfaces A: Physicochemical and Engineering Aspects, 2003. **230**(1): p. 183-190.

34. Jhaveri, A.M. and Torchilin, V.P., *Multifunctional polymeric micelles for delivery of drugs and siRNA.* Frontiers in Pharmacology, 2014. **5**(77).

35. Desai, N., *Challenges in Development of Nanoparticle-Based Therapeutics.* The AAPS Journal, 2012. **14**(2): p. 282-295.

36.   Bukofzer, S., et al., *Industry Perspective on the Medical Risk of Visible Particles in Injectable Drug Products.* PDA Journal of Pharmaceutical Science and Technology, 2015. **69**(1): p. 123-139.

37.   Choi, H.S., et al., *Renal Clearance of Nanoparticles.* Nature biotechnology, 2007. **25**(10): p. 1165-1170.

38.   Karmali, P.P. and Simberg, D., *Interactions of nanoparticles with plasma proteins: implication on clearance and toxicity of drug delivery systems.* Expert Opinion on Drug Delivery, 2011. **8**(3): p. 343-357.

39.   Bazak, R., et al., *Passive targeting of nanoparticles to cancer: A comprehensive review of the literature.* Molecular and Clinical Oncology, 2014. **2**(6): p. 904-908.

40.   Maeda, H., et al., *Tumor vascular permeability and the EPR effect in macromolecular therapeutics: a review.* Journal of Controlled Release, 2000. **65**(1): p. 271-284.

41.   Fang, J., et al., *The EPR effect: Unique features of tumor blood vessels for drug delivery, factors involved, and limitations and augmentation of the effect.* Advanced Drug Delivery Reviews, 2011. **63**(3): p. 136-151.

42.   Maeda, H., et al., *Polymeric drugs for efficient tumor-targeted drug delivery based on EPR-effect.* European Journal of Pharmaceutics and Biopharmaceutics, 2009. **71**(3): p. 409-419.

43. Callmann, C.E., et al., *Therapeutic Enzyme-Responsive Nanoparticles for Targeted Delivery and Accumulation in Tumors.* Advanced materials (Deerfield Beach, Fla.), 2015. **27**(31): p. 4611-4615.

44. Owens, D.E. and Peppas, N.A., *Opsonization, biodistribution, and pharmacokinetics of polymeric nanoparticles.* International Journal of Pharmaceutics, 2006. **307**(1): p. 93-102.

45. Werner, M.E., et al., *Folate-targeted nanoparticle delivery of chemo- and radiotherapeutics for the treatment of ovarian cancer peritoneal metastasis.* Biomaterials, 2011. **32**(33): p. 8548-8554.

46. Fay, F. and Scott, C.J., *Antibody-targeted nanoparticles for cancer therapy.* Immunotherapy, 2011. **3**(3): p. 381-394.

47. Zhang, Y., et al., *Tumor-Targeted Drug Delivery with Aptamers.* Current Medicinal Chemistry, 2011. **18**(27): p. 4185-4194.

48. Bazak, R., et al., *Cancer active targeting by nanoparticles: a comprehensive review of literature.* Journal of Cancer Research and Clinical Oncology, 2015. **141**(5): p. 769-784.

49. Reineke, J., *Terminology matters: There is no targeting, but retention.* Journal of Controlled Release, 2018. **273**: p. 180-183.

50. Zhang, Y., et al., *Polymeric Micelles: Nanocarriers for Cancer-Targeted Drug Delivery.* AAPS PharmSciTech, 2014. **15**(4): p. 862-871.

51. Davis, M.E., et al., *Nanoparticle therapeutics: an emerging treatment modality for cancer.* Nature Reviews Drug Discovery, 2008. **7**: p. 771.

52. Letchford, K. and Burt, H., *A review of the formation and classification of amphiphilic block copolymer nanoparticulate structures: micelles, nanospheres, nanocapsules and polymersomes.* European Journal of Pharmaceutics and Biopharmaceutics, 2007. **65**(3): p. 259-269.

53. Brian, E.G., et al., *Polymeric Nanoparticles for a Drug Delivery System.* Current Drug Metabolism, 2013. **14**(8): p. 840-846.

54. Hamid Akash, et al., *Natural and Synthetic Polymers as Drug Carriers for Delivery of Therapeutic Proteins.* Polymer Reviews, 2015. **55**(3): p. 371-406.

55. Neuse, E.W., *Synthetic Polymers as Drug-Delivery Vehicles in Medicine.* Metal-Based Drugs, 2008. **2008**: p. 469531.

56. Bhatia, S., *Natural Polymers vs Synthetic Polymer*, in *Natural Polymer Drug Delivery Systems: Nanoparticles, Plants, and Algae.* 2016, Springer International Publishing: Cham. p. 95-118.

57. Schmaljohann, D., *Thermo- and pH-responsive polymers in drug delivery.* Advanced Drug Delivery Reviews, 2006. **58**(15): p. 1655-1670.

58. Ward, M.A. and Georgiou T.K., *Thermoresponsive Polymers for Biomedical Applications.* Polymers, 2011. **3**(3): p. 1215.

59. Li, Y., et al., *pH-Sensitive Polymeric Nanoparticles as Carriers for Cancer Therapy and Imaging*, in *Bioinspired and Biomimetic Polymer Systems for Drug and Gene Delivery*, Z.Gu (Ed.)

60.   Martín-Saldaña, S., et al., *pH-sensitive polymeric nanoparticles with antioxidant and anti-inflammatory properties against cisplatin-induced hearing loss.* Journal of Controlled Release, 2018. **270**: p. 53-64.

61.   Eun-Kyung, L., et al., *Recent Advances in pH-Sensitive Polymeric Nanoparticles for Smart Drug Delivery in Cancer Therapy.* Current Drug Targets, 2018. **19**(4): p. 300-317.

62.   Cheng, R., et al., *Dual and multi-stimuli responsive polymeric nanoparticles for programmed site-specific drug delivery.* Biomaterials, 2013. **34**(14): p. 3647-3657.

63.   Hu, J., et al., *Enzyme-responsive polymeric assemblies, nanoparticles and hydrogels.* Chemical Society Reviews, 2012. **41**(18): p. 5933-5949.

64.   De la Rica, R., et al., *Enzyme-responsive nanoparticles for drug release and diagnostics.* Advanced Drug Delivery Reviews, 2012. **64**(11): p. 967-978.

65.   Kennedy, D.C., et al., *Cellular Consequences of Copper Complexes Used To Catalyze Bioorthogonal Click Reactions.* Journal of the American Chemical Society, 2011. **133**(44): p. 17993-18001.

66.   Cheng, J., et al., *Formulation of functionalized PLGA–PEG nanoparticles for in vivo targeted drug delivery.* Biomaterials, 2007. **28**(5): p. 869-876.

67.   Gref, R., et al., *'Stealth' corona-core nanoparticles surface modified by polyethylene glycol (PEG): influences of the corona (PEG chain length and surface density) and of the core composition on phagocytic uptake and plasma*

protein adsorption. Colloids and Surfaces B: Biointerfaces, 2000. **18**(3): p. 301-313.

68.   Bazile, D., et al., *Stealth Me.PEG-PLA nanoparticles avoid uptake by the mononuclear phagocytes system.* Journal of Pharmaceutical Sciences, 1995. **84**(4): p. 493-498.

69.   Prabhu, R.H., et al., *Polymeric nanoparticles for targeted treatment in oncology: current insights.* International Journal of Nanomedicine, 2015. **10**: p. 1001-1018.

70.   Ulbrich, K., et al., *Targeted Drug Delivery with Polymers and Magnetic Nanoparticles: Covalent and Noncovalent Approaches, Release Control, and Clinical Studies.* Chemical Reviews, 2016. **116**(9): p. 5338-5431.

71.   Ghosh, P., et al., *Gold nanoparticles in delivery applications.* Advanced Drug Delivery Reviews, 2008. **60**(11): p. 1307-1315.

72.   Paciotti, G.F., et al., *Colloidal gold nanoparticles: a novel nanoparticle platform for developing multifunctional tumor-targeted drug delivery vectors.* Drug Development Research, 2006. **67**(1): p. 47-54.

73.   Liong, M., et al., *Multifunctional Inorganic Nanoparticles for Imaging, Targeting, and Drug Delivery.* ACS Nano, 2008. **2**(5): p. 889-896.

74.   Han, G., et al., *Functionalized gold nanoparticles for drug delivery.* Nanomedicine, 2007. **2**(1): p. 113-123.

75.   Gupta, A.K. and Gupta, M., *Synthesis and surface engineering of iron oxide nanoparticles for biomedical applications.* Biomaterials, 2005. **26**(18): p. 3995-4021.

76.   Cherukuri, P., et al., *Targeted hyperthermia using metal nanoparticles.* Advanced Drug Delivery Reviews, 2010. **62**(3): p. 339-345.

77.   Allen, T.M. and Cullis, P.R., *Liposomal drug delivery systems: From concept to clinical applications.* Advanced Drug Delivery Reviews, 2013. **65**(1): p. 36-48.

78.   Fielding, R.M., *Liposomal Drug Delivery.* Clinical Pharmacokinetics, 1991. **21**(3): p. 155-164.

79.   Torchilin, V.P., *Liposomes as targetable drug carriers.* Critical reviews in therapeutic drug carrier systems, 1985. **2**(1): p. 65-115.

80.   Couvreur, P. and Vautheir, C., *Nanotechnology: Intelligent Design to Treat Complex Disease.* Pharmaceutical Research, 2006. **23**(7): p. 1417-1450.

81.   Immordino, M.L., et al., *Stealth liposomes: review of the basic science, rationale, and clinical applications, existing and potential.* International Journal of Nanomedicine, 2006. **1**(3): p. 297-315.

82.   Forssen, E. and Willis, M., *Ligand-targeted liposomes.* Advanced Drug Delivery Reviews, 1998. **29**(3): p. 249-271.

83.   Israelachvili, J.N., et al., *Theory of self-assembly of lipid bilayers and vesicles.* Biochimica et Biophysica Acta (BBA) - Biomembranes, 1977. **470**(2): p. 185-201.

84.   Fong, W.-K., et al., *Stimuli responsive liquid crystals provide 'on-demand' drug delivery in vitro and in vivo.* Journal of Controlled Release, 2009. **135**(3): p. 218-226.

85.   Negrini, R., et al., *pH-responsive lyotropic liquid crystals and their potential therapeutic role in cancer treatment.* Chemical Communications, 2015. **51**(30): p. 6671-6674.

86.   Muir, B.W., et al., *Salt Induced Lamellar to Bicontinuous Cubic Phase Transitions in Cationic Nanoparticles.* The Journal of Physical Chemistry B, 2012. **116**(11): p. 3551-3556.

87.   Squires, A.M., et al., *Quantitative model for the kinetics of lyotropic phase transitions involving changes in monolayer curvature.* Soft Matter, 2009. **5**(23): p. 4773-4779.

88.   Gupta, A., *Highly Ordered Supramolecular Nanoassemblies of Paramagnetic Amphiphilic Chelates as Potential MRI Contrast Agents.* Australian Journal of Chemistry, 2018. **71**(3): p. 195-196.

89.   Xin, P., et al., *Nanostructed Cubosomes as Advanced Drug Delivery System.* Current Pharmaceutical Design, 2013. **19**(35): p. 6290-6297.

90.   Spicer, P.T., *Progress in liquid crystalline dispersions: Cubosomes.* Current Opinion in Colloid & Interface Science, 2005. **10**(5): p. 274-279.

91.   Naga, M.L., et al., *Cubosomes as Targeted Drug Delivery Systems - A Biopharmaceutical Approach.* Current Drug Discovery Technologies, 2014. **11**(3): p. 181-188.

92.   Garg, G., et al., *Cubosomes: An Overview.* Biological and Pharmaceutical Bulletin, 2007. **30**(2): p. 350-353.

93.   Dong, Y.-D., et al., *Bulk and Dispersed Aqueous Phase Behavior of Phytantriol: Effect of Vitamin E Acetate and F127 Polymer on Liquid Crystal Nanostructure.* Langmuir, 2006. **22**(23): p. 9512-9518.

94.   Fong, W.-K., et al., *Controlling the Nanostructure of Gold Nanorod–Lyotropic Liquid-Crystalline Hybrid Materials Using Near-Infrared Laser Irradiation.* Langmuir, 2012. **28**(40): p. 14450-14460.

95.   Phan, S., et al., *Evaluating the link between self-assembled mesophase structure and drug release.* International Journal of Pharmaceutics, 2011. **421**(1): p. 176-182.

96.   Leesajakul, W., et al., *Interaction of cubosomes with plasma components resulting in the destabilization of cubosomes in plasma.* Colloids and Surfaces B: Biointerfaces, 2004. **34**(4): p. 253-258.

97.   Saxon, E. and Bertozzi, C.R., *Chemical and Biological Strategies for Engineering Cell Surface Glycosylation.* Annual Review of Cell and Developmental Biology, 2001. **17**(1): p. 1-23.

98.   Bertozzi, C.R. and Kiessling L.L., *Chemical Glycobiology.* Science, 2001. **291**: p. 2357.

99.   Sletten, E.M. and Bertozzi, C.R., *From Mechanism to Mouse: A Tale of Two Bioorthogonal Reactions.* Accounts of Chemical Research, 2011. **44**(9): p. 666-676.

100. Laughlin, S.T., et al., *Metabolic Labeling of Glycans with Azido Sugars for Visualization and Glycoproteomics*, in *Methods in Enzymology*, F. Minoru, Editor. 2006, Academic Press. p. 230-250.

101. Prescher, J.A. and Bertozzi C.R., *Chemical Technologies for Probing Glycans.* Cell, 2006. **126**(5): p. 851-854.

102. Laughlin, S.T., et al., *In Vivo Imaging of Membrane-Associated Glycans in Developing Zebrafish.* Science, 2008. **320**(5876): p. 664-667.

103. Dehnert, K.W., et al., *Metabolic labeling of fucosylated glycans in developing zebrafish.* ACS Chem Biol, 2011. **6**(6): p. 547-52.

104. Krijgsveld, J., et al., *Metabolic labeling of C. elegans and D. melanogaster for quantitative proteomics.* Nat Biotech, 2003. **21**(8): p. 927-931.

105. Vocadlo, D.J., et al., *A chemical approach for identifying O-GlcNAc-modified proteins in cells.* Proceedings of the National Academy of Sciences, 2003. **100**(16): p. 9116-9121.

106. Beynon, R.J. and Pratt, J.M., *Metabolic labeling of proteins for proteomics.* Molecular & Cellular Proteomics, 2005. **4**(7): p. 857-872.

107. Baskin, J.M., et al., *Copper-free click chemistry for dynamic in vivo imaging.* Proceedings of the National Academy of Sciences, 2007. **104**(43): p. 16793-16797.

108. Agard, N.J., et al., *A Comparative Study of Bioorthogonal Reactions with Azides.* ACS Chemical Biology, 2006. **1**(10): p. 644-648.

109. Agard, N.J., et al., *A Strain-Promoted [3 + 2] Azide−Alkyne Cycloaddition for Covalent Modification of Biomolecules in Living Systems.* Journal of the American Chemical Society, 2004. **126**(46): p. 15046-15047.

110. Baskin, J.M. and Bertozzi, C.R., *Bioorthogonal Click Chemistry: Covalent Labeling in Living Systems.* QSAR & Combinatorial Science, 2007. **26**(11-12): p. 1211-1219.

111. Beahm, B. and Bertozzi, C.R., *Imaging Cell-Surface Glycans in Animals with Bioorthogonal Chemistry*, in *Glycoscience: Biology and Medicine*, T. Endo, et al., Editors. 2014, Springer Japan. p. 1-11.

112. Breidenbach, M.A., et al., *Targeted metabolic labeling of yeast N-glycans with unnatural sugars.* Proc Natl Acad Sci U S A, 2010. **107**(9): p. 3988-93.

113. Neef, A.B. and Luedtke, N.W., *Dynamic metabolic labeling of DNA in vivo with arabinosyl nucleosides.* Proceedings of the National Academy of Sciences, 2011. **108**(51): p. 20404-20409.

114. Neef, A.B. and Luedtke, N.W., *An Azide-Modified Nucleoside for Metabolic Labeling of DNA.* ChemBioChem, 2014. **15**(6): p. 789-793.

115. Rabani, M., et al., *Metabolic labeling of RNA uncovers principles of RNA production and degradation dynamics in mammalian cells.* Nature biotechnology, 2011. **29**(5): p. 436.

116. Tra, V.N. and Dube, D.H., *Glycans in pathogenic bacteria - potential for targeted covalent therapeutics and imaging agents.* Chemical Communications, 2014. **50**(36): p. 4659-4673.

117.   Geva-Zatorsky, N., et al., *In vivo imaging and tracking of host-microbiota interactions via metabolic labeling of gut anaerobic bacteria.* Nat Med, 2015. **21**(9): p. 1091-1100.

118.   MacKenzie, D.A., et al., *Bioorthogonal labelling of living bacteria using unnatural amino acids containing nitrones and a nitrone derivative of vancomycin.* Chemical Communications, 2015. **51**(62): p. 12501-12504.

119.   Pidgeon, S.E., et al., *Metabolic Profiling of Bacteria by Unnatural C-terminated D-Amino Acids.* Angewandte Chemie International Edition, 2015: p. n/a-n/a.

120.   Clark, E.L., et al., *Development of Rare Bacterial Monosaccharide Analogs for Metabolic Glycan Labeling in Pathogenic Bacteria.* ACS Chemical Biology, 2016.

121.   Bertozzi, C.R., et al., *Chemical Glycobiology.* Science, 2001. **291**(5512): p. 2357-2364.

122.   Pearce, O.M.T. and Läubli, H., *Sialic acids in cancer biology and immunity.* Glycobiology, 2016. **26**(2): p. 111-128.

123.   Dube, D.H. and Bertozzi, C.R., *Glycans in cancer and inflammation — potential for therapeutics and diagnostics.* Nature Reviews Drug Discovery, 2005. **4**: p. 477.

124.   Kolb, H.C., et al., *Click Chemistry: Diverse Chemical Function from a Few Good Reactions.* Angewandte Chemie International Edition, 2001. **40**(11): p. 2004-2021.

125. Liang, L. and Astruc, D., *The copper(I)-catalyzed alkyne-azide cycloaddition (CuAAC) "click" reaction and its applications. An overview.* Coordination Chemistry Reviews, 2011. **255**(23–24): p. 2933-2945.

126. Kate, A.N., et al., *Monitoring Cellular Uptake and Cytotoxicity of Copper(II) Complex Using a Fluorescent Anthracene Thiosemicarbazone Ligand.* Bioconjugate Chemistry, 2014. **25**(1): p. 102-114.

127. Agarwal, K., et al., *Effects of copper on mammalian cell components.* Chemico-Biological Interactions, 1989. **69**(1): p. 1-16.

128. Hong, V., et al., *Labeling Live Cells by Copper-Catalyzed Alkyne−Azide Click Chemistry.* Bioconjugate Chemistry, 2010. **21**(10): p. 1912-1916.

129. Saxon, E. and Bertozzi, C.R., *Cell Surface Engineering by a Modified Staudinger Reaction.* Science, 2000. **287**(5460): p. 2007-2010.

130. Staudinger, H. and Meyer, J. *Über neue organische Phosphorverbindungen III. Phosphinmethylenderivate und Phosphinimine.* Helvetica Chimica Acta, 1919. **2**(1): p. 635-646.

131. Lin, F.L., et al., *Mechanistic Investigation of the Staudinger Ligation.* Journal of the American Chemical Society, 2005. **127**(8): p. 2686-2695.

132. Jewett, J.C. and Bertozzi, C.R., *Cu-free click cycloaddition reactions in chemical biology.* Chemical Society Reviews, 2010. **39**(4): p. 1272-1279.

133. Dommerholt, J., et al., *Highly accelerated inverse electron-demand cycloaddition of electron-deficient azides with aliphatic cyclooctynes.* Nature Communications, 2014. **5**: p. 5378.

134.   Dommerholt, J., et al., *Strain-Promoted 1,3-Dipolar Cycloaddition of Cycloalkynes and Organic Azides.* Topics in Current Chemistry, 2016. **374**(2): p. 16.

135.   Kang, K., J. Park, and E. Kim, *Tetrazine ligation for chemical proteomics.* Proteome Science, 2017. **15**(1): p. 15.

136.   Oliveira, B.L., et al., *Inverse electron demand Diels-Alder reactions in chemical biology.* Chemical Society Reviews, 2017. **46**(16): p. 4895-4950.

137.   Karver, M.R., et al., *Bioorthogonal Reaction Pairs Enable Simultaneous, Selective, Multi-Target Imaging.* Angewandte Chemie (International ed. in English), 2012. **51**(4): p. 920-922.

138.   Še kut, J. and Devaraj, N.K., *Expanding Room for Tetrazine Ligations in the in vivo Chemistry Toolbox.* Current opinion in chemical biology, 2013. **17**(5): p. 761-767.

139.   Dommerholt, J., et al., *Readily Accessible Bicyclononynes for Bioorthogonal Labeling and Three-Dimensional Imaging of Living Cells.* Angewandte Chemie International Edition, 2010. **49**(49): p. 9422-9425.

140.   Rong, J., et al., *Glycan Imaging in Intact Rat Hearts and Glycoproteomic Analysis Reveal the Upregulation of Sialylation during Cardiac Hypertrophy.* Journal of the American Chemical Society, 2014. **136**(50): p. 17468-17476.

141.   Xie, R., et al., *In vivo metabolic labeling of sialoglycans in the mouse brain by using a liposome-assisted bioorthogonal reporter strategy.* Proceedings of the National Academy of Sciences, 2016. **113**(19): p. 5173-5178.

142. Xie, R., et al., *Cell-Selective Metabolic Glycan Labeling Based on Ligand-Targeted Liposomes.* Journal of the American Chemical Society, 2012. **134**(24): p. 9914-9917.

143. Koo, H., et al., *Bioorthogonal Copper-Free Click Chemistry In Vivo for Tumor-Targeted Delivery of Nanoparticles.* Angewandte Chemie International Edition, 2012. **51**(47): p. 11836-11840.

144. Feng, L., et al., *Bifunctional unnatural sialic acids for dual metabolic labeling of cell-surface sialylated glycans.* J Am Chem Soc, 2013. **135**(25): p. 9244-7.

145. Xie, R., et al., *Cell-selective metabolic labeling of biomolecules with bioorthogonal functionalities.* Curr Opin Chem Biol, 2013. **17**(5): p. 747-52.

146. Lee, S., et al., *Chemical Tumor-Targeting of Nanoparticles Based on Metabolic Glycoengineering and Click Chemistry.* ACS Nano, 2014. **8**(3): p. 2048-2063.

147. Wang, H., et al., *In Vivo Targeting of Metabolically Labeled Cancers with Ultra-Small Silica Nanoconjugates.* Theranostics, 2016. **6**(9): p. 1467-1476.

148. Wang, H., et al., *Selective in vivo metabolic cell-labeling-mediated cancer targeting.* Nat Chem Biol, 2017. **13**(4): p. 415-424.

149. Lee, S., et al., *In vivo stem cell tracking with imageable nanoparticles that bind bioorthogonal chemical receptors on the stem cell surface.* Biomaterials, 2017. **139**: p. 12-29.

150. Sun, Y., et al., *Mechanistic Investigation and Multiplexing of Liposome-Assisted Metabolic Glycan Labeling.* Journal of the American Chemical Society, 2018. **140**(10): p. 3592-3602.

151.   Braun, T., et al., *A bioanalytical assay to distinguish cellular uptake routes for liposomes.* Cytometry Part A, 2016. **89**(3): p. 301-308.

Chapter 2: Materials and Methods

General and repeated materials and methods will be outlined in this chapter. Those that are specific to a particular chapter will be included in the corresponding chapter.

Materials

2.1.1 Lipid based components

Phytantriol (3,7,11,15-tetramethylhexadecane-1,2,3-triol) (PHYT) was a gift from DSM Nutritional Products (Kaiseraugst, Switzerland) (≥95%). 1,2-distearoyl-*sn*-glycero-3- phosphocholine (DSPC) (≥99%), 1,2-dipalmitoyl-sn-glycero-3-phosphoethanolamine- N-(lissamine rhodamine B sulfonyl) (ammonium salt) (16:0 Liss RhoD PE) (≥99%), 1,2-distearoyl-sn-glycero-3-phosphoethanolamine-N-[dibenzocyclooctyl(polyethylene glycol)-2000] (ammonium salt) (DSPE-PEG$_{2000}$-DBCO) (≥99%), 1,2-distearoyl-sn- glycero-3-phosphoethanolamine-N-[azido(polyethylene glycol)-$_{2000}$] (ammonium salt) (DSPE-PEG$_{2000}$-Azide) (≥99%), 1,2-distearoyl-sn-glycero-3-phosphoethanolamine-N- [methoxy(polyethylene glycol)-$_{2000}$] (ammonium salt) (DSPE-PEG$_{2000}$) (≥99%), 1,2- dipalmitoyl-sn-glycero-3-phosphoethanolamine-N-dibenzocyclooctyl (DPPE-DBCO) (≥99%) and 1,2-dipalmitoyl-sn-glycero-3-phosphoethanolamine-N-(6- azidohexanoyl)(ammonium salt) (DPPE-Azide) (≥99%) were purchased from Avanti Polar Lipids (Alabaster, USA).

PHYT with a minimum purity of 95 % was used to ensure the phase transition occurs around 60 °C [2]. Upon sonication and the addition of a polymer stabiliser the lipid matrix can be dispersed with the internal structure generally being retained. Phytantriol was chosen over glyceryl monooleate (GMO), another popular lipid for forming cubosomes, as it exhibits greater stability due to a lack of an ester bond, meaning it cannot be degraded through hydrolysis.

The functionalized phospholipids were chosen due to their availability with click functional groups already installed which are necessary for the SPAAC reaction.

Ideally, the phospholipids would incorporate into the lipid portion of the cubosomes and have the ability to impart functionality to the cubosome surface whilst not interfering with size, stability and structure. The PEG$_{2000}$ variants were selected as a means to assess the impact of the hydrophilic PEG chain on reactivity of the click group by comparison with the no-PEG equivalent phospholipids.

2.1.2 Other components

Pluronic F108 was purchased from Sigma-Aldrich (St Louis, MO). Phosphate Buffered Saline (PBS) 1x pH 7.4 was prepared by dissolving 137 mM sodium chloride (purity ≥99.7%), 2.7 mM potassium chloride (purity ≥99%), 2 mM potassium dihydrogen phosphate (purity ≥99%) and 8 mM disodium hydrogen phosphate (purity ≥99%). The salts were purchased from Chemsupply (Port Adelaide, SA, Australia). Sulfo-Cy5-dibenzocyclooctyne (DBCO) (purity ≥95%) and Sulfo-Cy5-Azide (purity ≥95%) was purchased from Click Chemistry Tools (Scottsdale, USA). Water used in these studies was obtained from a Millipore Milli-Q purification system (Billerica, USA).

Pluronic F108 is a triblock co-polymer that acts as a steric stabiliser for cubosomes. The polymer is effective as it interacts with the interface between lipid and the external aqueous media where the polymer chains help prevent aggregation and colloidal instability. Pluronic F108 has been reported to provide the best stability for phytantriol-based cubosomes while having the least impact on internal structure compared to other Pluronic stabilisers [3, 4].

Sulfo-Cy5 variants were chosen as the click-dye for binding experiments, both in solution and in vitro, as they are water soluble and do not overlap with the RhodamineB fluorescence spectrum or other commonly used dyes in biological studies [5]. They were also one of the only commercially available click-dyes at the time the project was started.

A549 human lung carcinoma cells were purchased from ATCC (Manassas, Virginia), Dulbecco's Modified Eagle's Medium (DMEM), PBS, Fetal Bovine Serum (FBS), Trypsin-EDTA 0.25% and Penicillin-Streptomycin was purchased from Sigma Aldrich (St Louis MO).

Mannosamine hydrochloride (purity ≥ 98%), triethylamine (purity ≥ 98%), azidoacetic acid (purity ≥ 93%), 1-hydroxybenzotriazole hydrate (1-HOBt) (purity ≥ 98%), N-(3-Dimethylaminopropyl)-N′-ethylcarbodiimide hydrochloride (EDC) (purity ≥ 98%), pyridine (purity ≥ 99%) and acetic anhydride (purity ≥ 99%) all were purchased from Sigma-Aldrich (St Louis, MO). DBCO-NHS (purity ≥ 97%) was purchased from Lumiprobe Corporation (Maryland). Chloroform and methanol were purchased from Merck (Kilsyth, Australia).

2.2 Methods

2.2.1 Phosphate buffered saline (PBS) preparation

PBS was prepared as required following the procedure below. A 1 litre volumetric flask was filled with 800 ml of milli-Q water and 8 g of NaCl, 0.2 g of KCl, 1.44 g of Na_2HPO_4 and 0.24 g of KH_2PO_4 were added. The pH was adjusted to 7.4 using NaOH or HCl as needed. The volume was made up to a litre and the PBS was sterilized by vacuum filtration into a Schott bottle.

2.2.2 Cubosome preparation

Cubosomes were prepared through probe sonication of mixtures of PHYT and other lipid additives in excess PBS. Unless specifically stated otherwise, the samples consisted of 10% lipid (w/w) and 1.5% (w/v) Pluronic F108 with the remainder being PBS 1X pH 7.4. Once mixed together the system was given 12 hours on rollers in a 37°C oven to equilibrate. The hydrated lipid was sonicated with a Misonix S-4000 (Farmingdale, NY, USA) with the parameters, 25 amplitude for 5 minutes with 2 seconds pulse on with 1 second pulse off or until well dispersed and an appearance similar to milk was obtained.

For cubosomes with extra additives, the lipid components were weighed out and chloroform was added for mixingfor each sample individually. The chloroform was removed with a combination of evaporation for the majority of the solvent under a stream of nitrogen gas and then a vacuum oven overnight at 35°C. Once any residual chloroform had been removed from the system the PBS containing the Pluronic F108 was introduced and the sample was placed on rollers in the oven at 37°C to equilibrate for 12 hrs. Finally, the sample was sonicated as mentioned above.

2.2.3 Liposome preparation

Liposomes were prepared through probe sonication using the same process as for cubosomes. The lipid and phospholipid based components were mixed together in a small volume of chloroform. The majority of this was removed using nitrogen gas and any residual chloroform was dried from the system using a vacuum oven overnight at 35°C. Once a thin lipid layer had formed on the inside of the vial the PBS was added and the system was sonicated with the Misonix probe using the same parameters as described above.

2.2.4 Dynamic Light Scattering (DLS)

DLS was used to determine particle size and dispersion uniformity which is an essential first technique to characterise the nanoparticles. This technique utilises a laser which passes through a polarizer into the sample. The molecules and particles interacting with the laser and causes photons to be scattered. An autocorrelator then compares the light intensity over time and tracks any changes. These changes are a result of Brownian motion and when combined with the principles of Rayleigh's scattering the diffusion and size of molecules and particles can be calculated [6].

DLS was conducted using a Malvern Zetasizer Nano ZS. Samples were diluted prior to measurement and placed in quartz cells. The cells were placed inside the instrument and size was measured at 25°C at a backscatter angle of 173°. The refractive index was 1.333 for the solvent (water) and 1.456 for the lipid and phospholipid based nanoparticles with an absorbance value of 0.001. All records and analysis were carried out using the software provided by the instrument manufacturer, Malvern Instruments LTD.

The accuracy of the instrument was ensured through calibration with polymer standards, Nanospheres, from the Duke Scientific Corp, Palo Alto, CA.

2.2.5 Small Angle X-ray Scattering (SAXS)

X-ray scattering is a common technique utilised in soft matter studies and was essential to studying the liquid crystalline structures present in this body of work. The X-ray beam is collimated and passed through the sample. Differences in electron density in the material causes the X-rays to be scattered at characteristic angles depending on the symmetry and spatial attributes of the electron density in the material [7, 8].

All SAXS experiments were conducted at the Australian Synchrotron where a much higher flux is available allowing for high resolution scattering profiles and much faster acquisition times when compared to lab based synchrotron instruments [9] (typically 1 sec acquisition per sample to obtain the same information as 1 hour on a lab instrument). This allows for much greater throughput. The higher throughput specifically allows for up to 100 samples to be loaded into capillaries or into a gel plate where a temperature ramp can then be run at small temperature intervals to provide over 1000 diffractograms in several hours to give rapid determination of phase diagrams.

The internal structure of the cubosomes was assessed using SAXS to characterise the novel surface modified cubosomes and compare them to cubosomes without functionalisation. The X-ray beam from the synchrotron was tuned to a wavelength of 1.127 Å (11.0 keV) at a camera to detector distance of 1034.97 mm which gave the q-range of $0.0176 < q < 1.016$ Å^{-1}, where q is the length of the scattering vector defined by $q = (4\pi/\lambda)\sin(\theta/2)$. The q range was calibrated by a silver behenate standard.

The 2D SAXS patterns were acquired within 1 s using a Pilatus 1M detector with an active area of 169 x 179 mm^2 and with a pixel size of 172 μm. The dispersions were transferred to 1.5 mm diameter glass capillaries and loaded into the capillary holder and the SAXS profiles were acquired between 25-75°C. The 2D scattering patterns were integrated into the 1D scattering function I(q) using the in-house developed software package Scatterbrain. Intensity of scattering was plotted as a function of magnitude of the scattering vector. Phase structures are identified by indexing the Bragg peaks using Miller indices (hkl) to known relative spacing ratios that describes the unique geometry of the reflecting plane within a three-dimensional lattice [10], this can be seen in Figure 2.1 below.
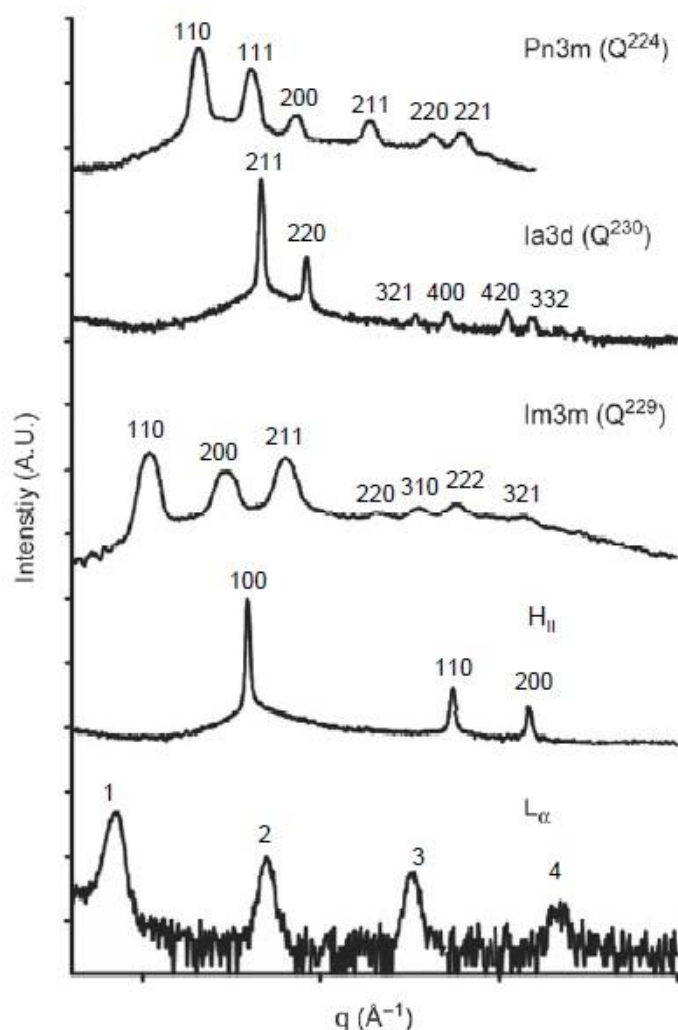
Figure 2.1. Examples of the scattering patterns of the various liquid crystal phase structures seen commonly in this Thesis with their Miller indices [11].

The scattering vector can be utilised to calculate the interplanar spacing, d, between two reflecting planes which is determined with d = 2π/q. This can then be used to calculate the mean lattice parameters, a, are determined from the SAXS data by indexing the Miller indices and using the appropriate equation based on the known internal structure of the system. For cubic phases equation 1 is used and for hexagonal phases equation 2 is used:

$$(1)\ a = \ d(h^2 + k^2\ l^2)^{1/2} \qquad\qquad (2)\ a = \frac{4d}{3}(h^2 + k^2)^{1/2}$$

Where a is the mean lattice parameter, d is the corresponding interplanar spacing (from SAXS) and h, k and l are the miller indices for the known phase. As there is only a broad peak indicating L_2 phase, d is used as the characteristic distance [10].

2.2.6 Cryo-Transmission Electron Microscopy (Cryo-TEM)

Cryogenic transmission electron microscopy is heavily utilised in lipid based studies as it is one of the only means of high resolution images that can give insight into size, shape, structure and polydispersity. In this style of microscopy the sample is cooled to cryogenic temperatures, meaning below -150°C. The cryogenic method was chosen over normal TEM as it avoids introducing artefacts that can form during sample preparation such as the staining, fixation and adsorption process.

A laboratory-built humidity-controlled vitrification system was used to prepare the samples for cryo-TEM. Ambient humidity was approximately 40% for all experiments and ambient temperature was 22°C. Copper grids (200-mesh) coated with perforated carbon film (Lacey carbon film: ProSciTech, Qld, Australia) were glow discharged in nitrogen to render them hydrophilic. Aliquots (4 μL) of the sample (which was diluted if necessary) were pipetted onto each grid prior to plunging.

After 30 seconds adsorption time the grid was blotted manually using Whatman 541 filter paper, for approximately 2 seconds. Blotting time was optimised for each sample. The grid was then plunged into liquid ethane cooled by liquid nitrogen. Frozen grids were stored in liquid nitrogen until required. The samples were examined using a Gatan 626 cryoholder (Gatan, Pleasanton, CA, USA) and Tecnai 12 Transmission Electron Microscope (FEI, Eindhoven, The Netherlands) at an operating voltage of 120 KV.

At all times low dose procedures were followed, using an electron dose of 8-10 electrons/$Å^2$ for all imaging. Images were recorded using a FEI Eagle 4k x 4k CCD camera at magnifications ranging from 15 000x to 50 000x. All images were produced by either Lynne Waddington (CSIRO) or Dr. Eric Hansen Gilles (Bio21).

2.2.7 Fluorescence detection

Fluorescence is the emission of light by a substance that has absorbed light. The emitted light generally has a longer wavelength, meaning lower energy, to the light that was adsorbed. Upon absorption the orbital electrons from a molecule become excited and change plane. Once the light is removed, the relaxation of the excited electron back to its ground state results in the emission of photons seen, this is known as the Stokes shift. This can be detected and used to quantify in the case of this project, either the presence of fluorescent dye in a sample, or fluorescent phospholipid used to track particle concentrations during microscopy or size exclusion separations.

Standards were prepared through a series of serial volumetric dilutions of stock (1 mg/mL) dye solution and sample concentrations determined by comparison to this standard curve.

The Enspire Multimode Plate Reader (Perkin Elmer) was used for all fluorescence measurements.

2.2.8 Size Exclusion Chromatography (SEC)

SEC is one mode of chromatography also known as molecular sieve chromatography which involves separating molecules and/or particles in solution by their size or molecular weight. The basic concept is that a column is loaded with porous beads of a particular pore size and chemical composition and that small molecules take longer to traverse the pores and gaps of the beads than larger molecules or colloidal particles. A key factor that must be considered is that the analyte and the beads do not interact chemically as this will alter the separation process and it will not be solely decided by analyte size.

A 10 cm column was filled with superfine G50 silica beads (GE healthcare, Uppsala, Sweden) that had been degassed in PBS 1X pH 7.4 overnight. PBS was also used as the eluent during the experiments. To begin, 100 µL of analyte solution was loaded onto the column and washed past the physical filter on top of the gel bed by the addition of 100 µL of PBS three more times. Following this 5 mL of PBS was added and the collection of elutes was commenced. Each elute was approximately 500 µL and the column was continually loaded with 5 mL of PBS until the analytes had passed through the system. This was commonly used in conjunction with fluorescence measurements from the plate reader mentioned in segment 2.2.7.

2.2.9 Click-Sugar synthesis

All the click-sugars used throughout the cell studies were synthesised and characterised by Dr Jason Liu (MIPS) which can be found in the appendix.

2.2.10 Cell culture

A549 human lung carcinoma cells were cultured in DMEM + 10% FBS + 1% penicillin medium. Cells were grown and maintained at 37°C with 5% CO_2. Upon 80% confluency, cells were split (using trypsin-EDTA 0.25%) and reseeded as necessary. For TIRF microscopy experiments the cells were seeded into singular glass bottom well plates where they were incubated for 24 hrs to allow for growth and adherence to the glass before being introduced to medium containing click sugars at 100 µM. After exposure to the sugar, the cells were incubated for three days before being fixed (4% formaldehyde solution) and nanoparticles or dye were introduced to the system in order to study the click reactivity after a change in media.

After a further 24 hours of incubation the samples were washed with PBS five times to remove any excess unbound nanoparticles before the samples remained hydrated with PBS and were imaged.

2.2.11 Total internal reflection (TIRF) microscopy

TIRF is a specialised fluorescence microscopy technique used to achieve high resolution images of membrane associated processes by visualising the interface of the glass and specimen.

It differs to traditional fluorescence microscopy as the fluorophores are excited by an evanescent wave rather than direct illumination. This is made possible by utilising mirrors that reflect the laser across the surface as opposed to through it.
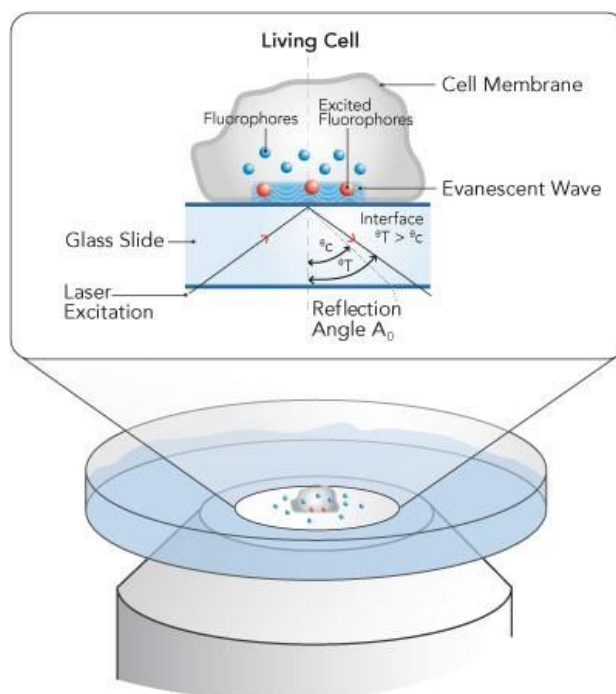
Figure 2.2. Diagram of TIRF microscopy from https://www.semrock.com/tirf.aspx (7/5/18)

TIRF was selected as the main form of imaging for the cell studies as the key interest of the experiments was to determine the cell surface binding of the novel nanoparticles.

Cells were imaged using a Leica TIRF microscope. Settings were controlled through the propriety Leica LAS software and images processed with ImageJ.

For cubosome imaging a depth of 250 nm was used based on DLS measurements and the average size of a lipid membrane [12]. The camera was aligned prior to imaging and settings such as angle, height and plate holder chosen based per the individual samples needs.

Additionally, the ability to quantify the amount of nanoparticles was achieved through an in-house script developed by Cameron Nowell (MIPS). Analysis of TIRF image data was carried out using a custom macro written in the Fiji distribution of ImageJ [13]. Nearest neighbour calculations were performed using the NND plugin developed by Yuxiong Mao. Details of the analysis are as follows. Background was subtracted from the images (rolling ball 50 pixels) to allow even extraction of particles. Local contrast enhancement was applied to improve detection (block size 64, slope 3). Particles were then segmented with watershed segmentation. The resulting particle masks were used to measure nearest neighbour distances and intensity of the original particles. Intensity measurements were performed by using the extracted particle masks to measure the original unprocessed image. With the nanoparticles investigated being relatively large and hydrophobic, there were complications utilising other common quantitative and qualitative techniques popular in cell studies such as flow cytometry and standard fluorescence which will be addressed in the appropriate chapters.

2.2.12 Lipidated polymer synthesis

All the lipidated polymers used throughout this Thesis were synthesised and characterised by James Grace (MIPS) and can be found in the Appendix.

2.3 References

1.   Barauskas, J. and Landh, T., *Phase Behavior of the Phytantriol/Water System.* Langmuir, 2003. **19**(23): p. 9562-9565.

2.   Dong, Y.-D., et al., *Impurities in commercial phytantriol significantly alter its lyotropic liquid-crystalline phase behavior.* Langmuir, 2008. **24**(13): p. 6998-7003.

3.   Chong, J.Y.T., et al., *Steric stabilisation of self-assembled cubic lyotropic liquid crystalline nanoparticles: high throughput evaluation of triblock polyethylene oxide-polypropylene oxide-polyethylene oxide copolymers.* Soft Matter, 2011. **7**(10): p. 4768-4777.

4.   Chong, J.Y.T., et al., *High-Throughput Discovery of Novel Steric Stabilizers for Cubic Lyotropic Liquid Crystal Nanoparticle Dispersions.* Langmuir, 2012. **28**(25): p. 9223-9232.

5.   Sabnis, R.W., *Handbook of biological dyes and stains: synthesis and industrial applications.* 2010: John Wiley & Sons.

6.   Goldburg, W., *Dynamic light scattering.* American Journal of Physics, 1999. **67**(12): p. 1152-1160.

7.   Ehrenberg, W. and Franks, A., *Small-Angle X-Ray Scattering.* Nature, 1952. **170**: p. 1076.

8.   Glatter, O. and Kratky, O., *Small Angle X-ray Scattering.* 1982: Academic Press.

9.   Kirby, N.M., et al., *A low-background-intensity focusing small-angle X-ray scattering undulator beamline.* Journal of Applied Crystallography, 2013. **46**(6): p. 1670-1680.

10.   Hyde, S., *The Language of Shape: The Role of Curvature in Condensed Matter- -physics, Chemistry, and Biology.* 1997: Elsevier.

11.   Dong, Y.D., *Investigation of nanostructured liquid crystal particles as novel agrochemical delivery agents*, in *Drug Discovery, Dynamics and Disposotion.* 2009, Monash.

12.   Meyer, R.A., *Light scattering from biological cells: dependence of backscatter radiation on membrane thickness and refractive index.* Applied optics, 1979. **18**(5): p. 585-588.

13.   Schindelin, J., et al., *Fiji: an open-source platform for biological-image analysis.* Nature Methods, 2012. **9**: p. 676.

Chapter 3 – Creating, characterising and assessing click capable lipid based nanoparticles

3.1 Declaration for Chapter 3

Some of the research presented in this chapter has been published as detailed below, hence some of the introductory statements are repetitive of Chapter One.

- Clickable Cubosomes for Antibody-Free Drug Targeting and Imaging Applications. Nicolas Alcaraz, Qingtao Liu, Eric Hanssen, Angus Johnston, Ben J. Boyd, *Bioconjugate Chem.*, **2018**, *29* (1), pp 149-157 **DOI**: 10.1021/acs.bioconjchem.7b00659

3.2 Introduction

A current trend in nanomedicine and drug delivery is to improve specificity of the treatment to in turn improve efficacy and avoid side effects. Nanoparticles have played a large role in this trend as they can accumulate in target tissues either passively (via the so-called Enhanced Permeation and Retention effect [1]) and actively using surface conjugated targeting ligands [2].

Self-assembled lipid based liquid crystalline nanoparticles (LCNP) possessing an internal cubic phase structure, known as cubosomes, have been gathering attention as a drug delivery system as they can be loaded with both lipophilic and hydrophilic drugs and the have potential for on-demand reversible release which offers advantages over more commonly used liposomes [3-6]. Amphiphilic lipids such as phytantriol (PHYT) and glycerol monoleate (GMO) can self-assemble in excess water to form thermodynamically stable liquid crystalline phases such as the bicontinuous cubic phase [7, 8]. Phytantriol is a generally recognized as safe (GRAS) excipient used commonly in personal care products and gaining popularity in pre-clinical research for a range of uses. It is known to form different liquid crystalline phases in excess water depending on the temperature.

At ambient temperature a bicontinuous cubic phase (V_2) is formed and transforms to the inverse hexagonal (H_2) and inverse micellar (L_2) phases at higher temperatures [1]. Cubosomes can then be formed by the dispersion of the 'bulk' cubic liquid crystalline phase, usually with the aid of a polymer stabiliser, such as Pluronic F127 or F108 (Figure 3.1)

The internal structure of the particles, and approaches to modification for drug delivery or imaging capabilities by incorporation of other agents such as lipids, phospholipids or metallic nanoparticles have been well studied [9-11], as has the influence of the stabiliser [8]. The cubosomes often have the same mesostructure as the bulk liquid crystalline phases but have a larger surface area and are much less viscous, enabling their potential deployment as injectable drug delivery or imaging systems [5, 12, 13]. The internal structure of the cubic phase particles makes them particularly interesting as MRI contrast agents, as the bound water behaves very differently to bulk water, providing a boost in relaxivity [14, 15]. The use of cubosomes as contrast agent enhancers was recently reviewed [16].
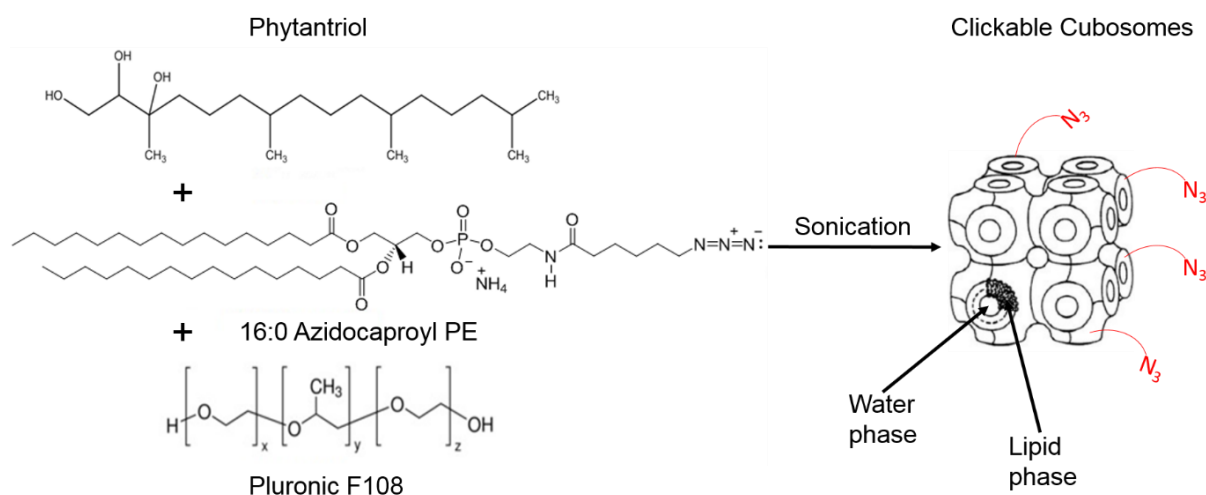
Figure 3.1. Schematic for the formation of copper-free 'clickable' cubosomes. The lipid and phospholipid are mixed together and then hydrated with Pluronic F108 solution. The system is sonicated and the cubic phase is dispersed to form cubosomes. The click phospholipid is potentially present in the interface within the internal aqueous channels, as well as at the external surface of the particles. Cubosome figure on right modified from [17] thanks to http://creativecommons.org/licenses/by/2.0.

Active targeting of drug carriers is a challenge, with the most common approach involving the use of antibodies or ligands for a specific cell surface receptor. In cancer therapy an antibody or folic acid group targeting a receptor overexpressed by the diseased cells is often conjugated to the surface of the carrier particle. Potential drawbacks of these approaches include being expensive, having poor stability, lack of specificity if the target receptor is common or can mutate in the target cells, competition with other ligands and poor pharmacokinetic consequences for the particle after injection [18-20]

Metabolic labelling is gaining popularity as an approach to enable covalent attachments of 'probes' to cell surfaces. Metabolic labelling normally involves chemically modifying a monosaccharide to contain a functional group of interest, normally an azide, without affecting its metabolic pathway *in vivo* [21-24]. Some commonly used sugars can be seen in Figure 3.2. It has expanded past azido-based chemical modifications with studies showing DBCO-based sugars being metabolically labelled onto cell-surface glycoproteins successfully [25], which is studied in this Chapter.
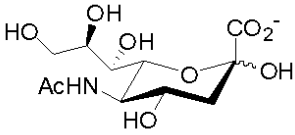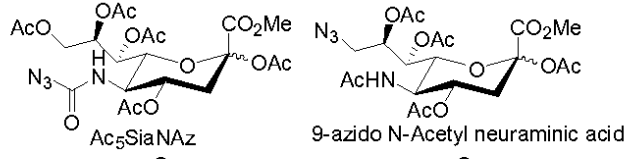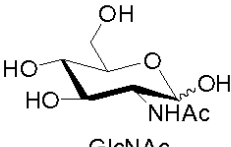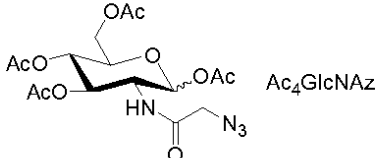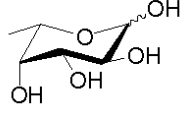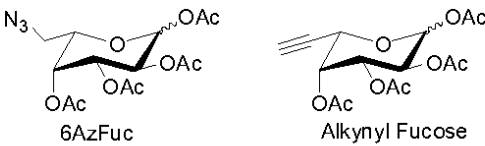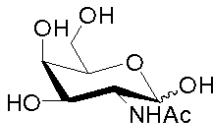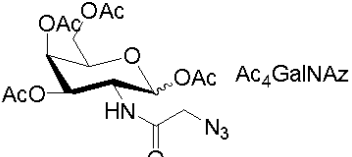
Figure 3.2. Chemical structures of some natural sugars and their unnatural variants commonly used for metabolic labelling. Reused with permission from [26].

Following this surface expression, the functional group on the non-natural sugar can then be targeted by a probe molecule that contains the complimentary functional group using biorthogonal chemical approaches [27-37]. It was initially improved and expanded on by Bertozzi *et al.* in the early 2000's as a means of being able to better understand glycans in living systems [28, 29, 31, 34, 35, 38, 39]. Since then it has risen in popularity and expanded in its use, some examples include; protein labelling [40-42], DNA labelling [43-45], cell surface labelling [46, 47], nanoparticle preparation [48, 49], and drug [50-54] or imaging delivery [55-60].

Additionally, the chemistry and reaction types that can partake in biorthogonal chemistry have been optimised and expanded greatly from the adapted Staudinger ligation described by Bertozzi and Saxon [29, 38]. This was detailed in Chapter One.

The benefits of bioorthogonal chemistry as an active targeting technique over other approaches are better stability, the materials are expectedly cheaper to synthesise than antibodies and the process is not reliant on overexpression of natural receptors to target non-functionalized cell populations [30, 33, 36, 61].

Using this approach, imaging biological processes associated with sugars in cells and in live animals, such as zebrafish, has been achieved [56, 57, 59, 60, 62-65]. Recently, nanoparticles have begun to be used as probes as opposed to simple dyes and imaging agents. Chitosan nanoparticles and liposomes have been covalently reacted to tumours that had metabolised azide bearing sugars [52, 53]. A simplified illustration of the biorthogonal chemistry approach to cubosome targeting can be seen in Figure 3.3.
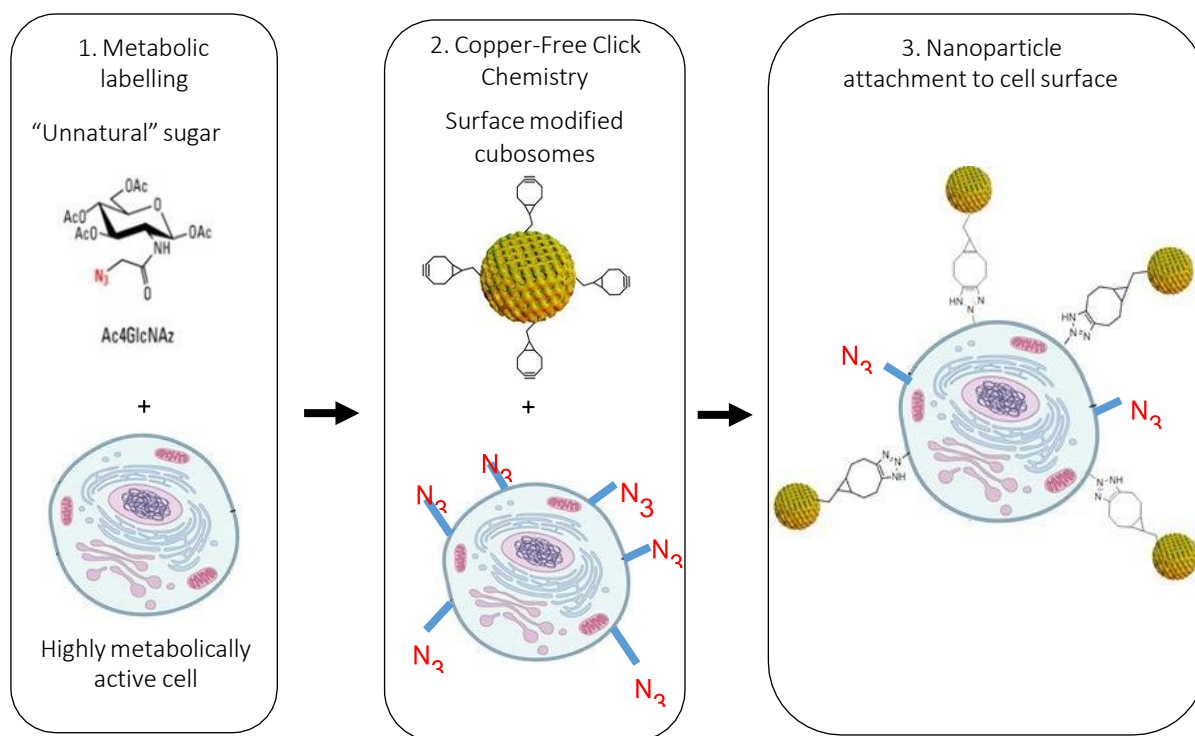
Figure 3.3. Simplified depiction of biorthogonal chemistry's two main components of metabolic labelling and copper-free click chemistry in relation to covalent cubosome attachment to cell surfaces. Cell adapted and reused with permission from Nature Education 2010 © and cubosome adapted and reused from [66].

There is no record of cubosomes designed to participate in copper-free click chemistry for use as cell-surface targeting systems through metabolic labelling. Given their aforementioned potential benefits in drug delivery and imaging this chapter begins by exploring the ability to incorporate click-phospholipids into the structure of cubosomes to impart the ability to partake in copper-free click chemistry and comparing them to liposomes as a well-known, previously studied comparator system. These novel lipid nanoparticles were then characterised to ensure that these additions did not greatly alter their function and properties.

The internal liquid crystalline nanostructure was confirmed before and after the reaction using synchrotron small angle X-ray scattering (SAXS) whilst the morphology was assessed by cryogenic-transmission electron microscopy (cryo-TEM). Size measurements were carried out with dynamic light scattering (DLS). Binding efficiency of the cubosomes via copper-free click chemistry in solution was assessed through size exclusion chromatography and fluorescence measurements. The "clickability" of the "clickosomes" was assessed in solution with a click-Cy5 molecule and finally in A549 cells following metabolic labelling. To this end we utilise total internal reflection fluorescence microscopy (TIRF) to specifically image cell surfaces at a high resolution.

3.3 Hypothesis and Aims

With the above mentioned potential for cubosomes to function as clickable delivery particles, the following hypotheses were posed to probe this:

1. That the addition of click group-modified additives will not significantly alter the structure and properties of cubosomes and liposomes.

2. That clickable cubosomes will have greater binding capacity with the click-cy5 dye in solution than the clickable liposomes.

3. That after the reaction of the click group with the complimentary probe, the structure and properties of cubosomes will not be significantly altered.

4. That the clickable cubosomes will selectively and covalently attach to A549 cells in vitro that have been treated with unnatural sugar containing media.

In order to investigate these hypotheses, the following aims will be achieved:

1. Determine the effect on structure and properties of the click cubosome and liposomes using characterisation of size and morphology (DLS/CryoTEM) and internal structure (CryoTEM/SAXS).

2. To compare the performance of click cubosomes to click liposomes using fluorescent measurements and SEC.

3. Determine the effect on structure and properties of the click cubosomes after reaction with the complimentary dye in solution.

4. To determine the ability at which clickosomes can bind to a cell surface using TIRF microscopy.

3.4 Materials and Methods

3.4.1 Materials

Please refer to Chapter Two for the materials used within this chapter.

3.4.2 Methods

Please refer to Chapter Two for general methods used in this chapter. Below are some specific methods that were used.

3.4.2.1 Cubosome preparation

Cubosome dispersions were prepared per the method described in Chapter Two. Specifically, there was a total lipid weight of 100 mg with 900 mg of 1.5% (w/v) Pluronic F108 PBS solution. Into the lipid portion 0.0025 molar ratio of Rhodamine B phospholipid and 0.02 molar ratio of the respective phospholipid was added.

3.4.2.2 Liposome preparation

Liposome dispersions were prepared per the method described in Chapter Two. Specifically, there was a total phospholipid weight of 100 mg with 900 mg of PBS added. The phospholipids added to the DSPC were doped at 0.02 molar ratio.

3.4.2.3 Binding efficiency studies

SEC was used to separate bound and unbound dye from the nanoparticles before measuring fluorescence of the fractions eluted from the column. The details to the techniques used can be found in Chapter Two. The dispersions were mixed at a 1:1 ratio (of azide to DBCO) with Sulfo-DBCO-Cy5 or Sulfo-N_3-Cy5 in PBS for 24 h protected from light.

Following this, SEC was conducted and methanol was added to the elutions to break down the lipid structure and prevent quenching of the Cy5. The fluorescence from Rhodamine B was measured at 560/583 nm and from Cy5 at 649/662 nm.

For two samples the above method was not possible due to colloidal instability. Upon introduction to the column the PL-PEG$_{2000}$-click liposomes would be sequestered at the top and not pass through the physical barrier. As a result, an alternative was chosen in order to determine bound percentage.

Samples were mixed in the same manner and 200 µL of the mixture was loaded into an 18 mm 2000 MWCO CelluSep H1 membrane (Membrane Filtration Products Inc, Texas) that was placed in to 20 mL of PBS in a beaker. The system was stirred, while covered form light, for 24 hours before the fluorescence on both sides of the membrane was tested.

3.5 Results

3.5.1 Characterisation of size and morphology of cubosomes and liposomes

The size and polydispersity of the cubosomes doped with phospholipid differed from non-click control cubosomes (Table 3.1). The systems with PEG_{2000} phospholipid displayed two populations indicating the formation of other lipid nanostructures, possibly some coexisting liposomal structures. This was also observed in the PL-DBCO doped system. It should be noted that the PL-PEG_{2000}-azide modified cubosomes did exhibit considerably larger average size and higher polydispersity which is likely due to the presence of the charged polar head group which changes the dispersion behaviour of the system. It has previously been shown that additives can alter the size and internal structure of cubosomes [67].

Table 3.1. Volume-based particle size distribution measurements (mean ± SD, n =3) of the different cubosome dispersions. PL denotes phospholipid.

Additive into cubosome dispersion	Size (nm) Peak 1	Size (nm) Peak 2	PDI
None	160 ± 10		0.15
PL-Azide	114 ± 1		0.11
PL-DBCO	102 ± 4	244 ± 56	0.19
PL-DSPC	151 ± 1		0.22
PL-PEG_{2000}-DBCO	32 ± 8	226 ± 67	0.27
PL-PEG_{2000}-Azide	91 ± 1	519 ± 19	0.52
PL-PEG_{2000}-DSPE	17 ± 3	129 ± 12	0.23

The size measurements taken of the liposomal dispersions were similar when compared to the cubosomes making them a good comparison system (Table 3.2). One key noticeable difference is the lack of a second peak indicating that there was only one nanostructure present, even in the samples doped with the phospholipid with the PEG$_{2000}$ chain present.

Table 3.2. Volume-based particle size distribution measurements (mean ± SD, n =3) of the different liposome dispersions. PL denotes phospholipid.

Additive into liposome dispersion	Size (nm) Peak 1	PDI
None	131 ± 10	0.28
PL-Azide	116 ± 6	0.22
PL-DBCO	124 ± 5	0.2
PL-PEG$_{2000}$-DBCO	201 ± 11	0.26
PL-PEG$_{2000}$-Azide	123 ± 3	0.21
PL-PEG$_{2000}$-DSPE	139 ± 4	0.27

Dynamic light scattering provides the size distribution, assuming spherical particles, but does not provide information about the shape or structure of the cubosomes. Therefore, further techniques were required to fully characterise these systems.

The cryo-TEM data (Figure 3.3) supported the DLS measurements with the particle size populations apparent in the micrographs being in general agreement with the DLS data. The formulations containing phospholipids were mainly cubosomes but did show presence of other structures such as some lipid vesicles and liposomal like structures. Again, this finding was reflected in the DLS data with more than one peak being detected.

It is likely that the liposomes and other lipid structures in the samples containing PEG$_{2000}$ phospholipid led to the larger PDI values observed. This was more noticeable in the formulations containing a PEG phospholipid.

This might be expected as the addition of phospholipid can alter the packing parameter of the system and this dictates the final structure described throughout portions of this Thesis [68].
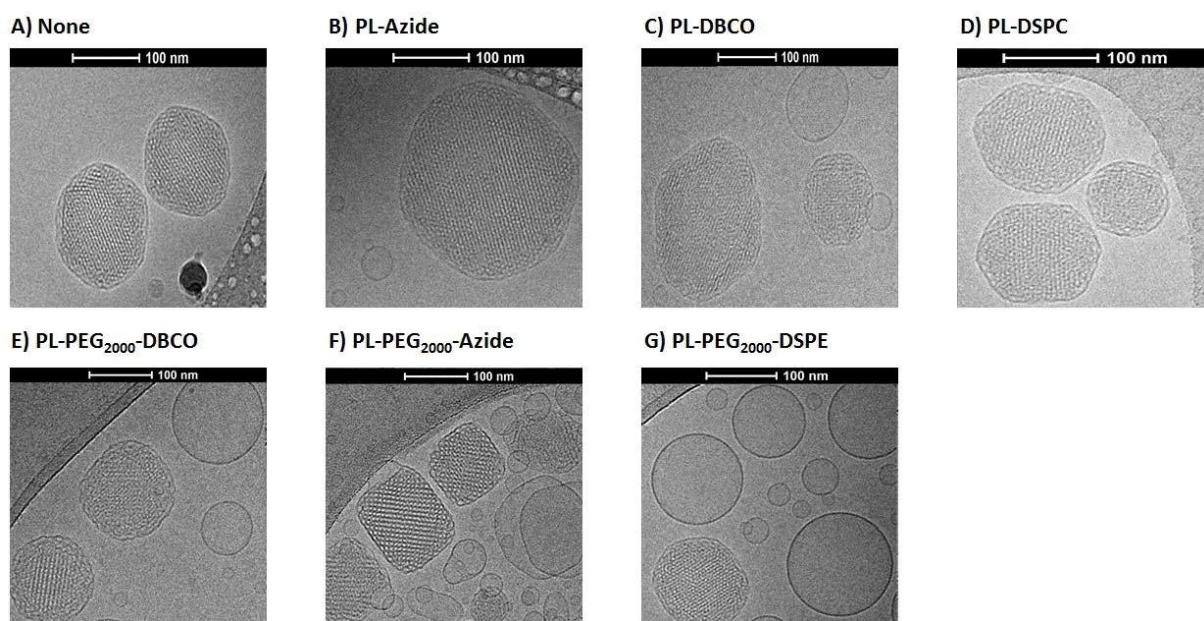
Figure 3.3. Cryo-TEM images of cubosome dispersions containing different additives as indicated on the respective panels.

As seen in figure 3.3, there appears to be a much higher non-cubosome population relative to the other samples imaged in both the PL-PEG$_{2000}$-Azide and PL-PEG$_{2000}$-DSPE systems. It is unusual that the other PEG-$_{2000}$ PL containing system did not also show this. This could potentially be explained due to the hydrophobic nature of the DBCO group making liposome formation less favourable for the system.

3.5.2 Internal structure of modified cubosomes

The internal structure of the cubosomes was determined using SAXS where the Bragg peaks were indexed and the internal structure thereby determined. The scattering profiles of the systems at 25°C can be seen in Figure 3.4.
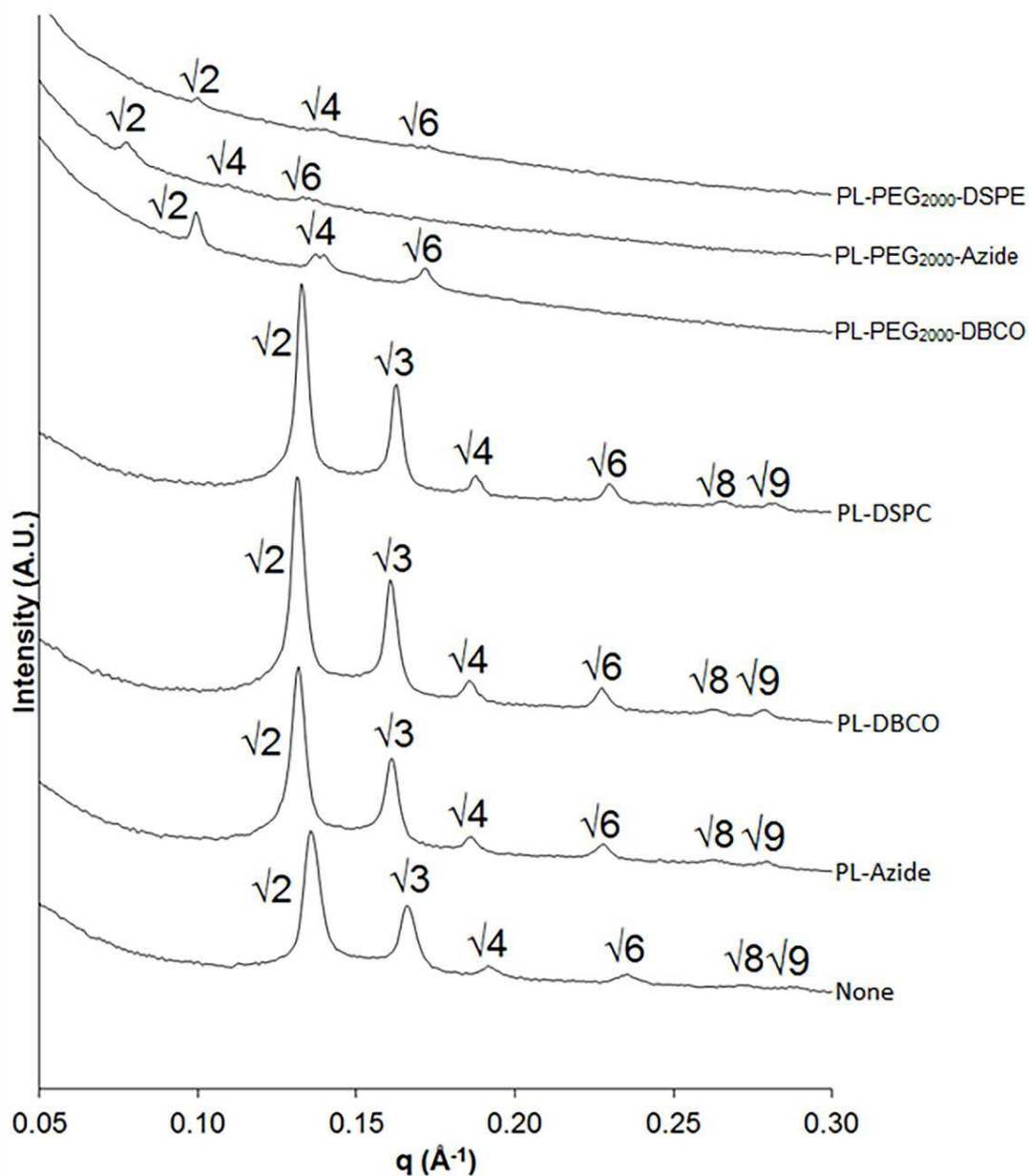
Figure 3.4. Dependence of internal structure on phospholipid-based additives in phytantriol-based cubosomes measured by small angle X-ray scattering at 25°C. The different cubosome dispersions contained different phospholipids loaded at 2 mol % relative to phytantriol.

The cubosomes without PL-PEG$_{2000}$ additives retained the Pn3m internal structure of unmodified cubosomes. In contrast, the cubosomes with PEG$_{2000}$-based additives showed that the internal structure shifted to the more swollen Im3m phase. This behaviour is consistent with the addition of hydrophilic additives to phytantriol-based cubic phases [69]. The scattering for the PL-PEG$_{2000}$ phospholipid doped systems is also much weaker than the other systems and this is potentially due to the presence of less geometrically ordered lipid structures that do not provide discrete diffraction peaks compared to the cubosomes.

The lattice parameters of the internal structures (Table 3.3) were determined from the SAXS data and showed similar spacing to previously reported systems with Pn3m and Im3m spacing. The PL-PEG$_{2000}$-Azide containing cubosomes were the exception, having a considerably larger lattice parameter than the other PL-PEG$_{2000}$ containing systems, evident from the lower q values for the peaks, and also had a much larger lattice parameter compared to typical phytantriol cubosomes (65-70 Å) [8, 67, 70, 71].

Table 3.3 Calculated lattice parameter (Å ± SE) of cubosome dispersions from SAXS data and DLS measurements from Table 3.1.

Phospholipid added	Phase	Lattice Parameter (Å ± SE)	Size (nm) Peak 1	Size (nm) Peak 2	PDI
None	Pn3m	65.54 ± 0.18	160 ± 10		0.15
PL-Azide	Pn3m	67.73 ± 0.10	114 ± 1		0.11
PL-DBCO	Pn3m	66.87 ± 0.15	102 ± 4	244 ± 56	0.19
PL-DSPC	Pn3m	67.53 ± 0.12	151 ± 1		0.22
PL-PEG$_{2000}$-DBCO	Im3m	89.68 ± 1.39	32 ± 8	226 ± 67	0.27
PL-PEG$_{2000}$-Azide	Im3m	114.75 ± 0.72	91 ± 1	519 ± 19	0.52
PL-PEG$_{2000}$-DSPE	Im3m	89.67 ± 0.17	17 ± 3	129 ± 12	0.23

This is supported by the larger internal spacing seen in Figure 3.3 and as mentioned above, the increased lattice parameter for the PL-PEG$_{2000}$ containing systems is due to the increased hydrophilicity of the head group, inducing increased swelling and the shift from the double diamond to the more hydrated primitive cubic phase space group. This effect has been reported previously upon addition of Tween 80 to phytantriol cubosomes as it favours a mean negative shift in spontaneous mean curvature at the lipid/water interface [72]. It is likely that a similar effect is occurring with the PEG$_{2000}$ containing systems as they will be even more hydrophilic and interact with the water at the interface.

Taken together, the cryoTEM, DLS, and SAXS data indicate that the size, shape, and structure of the clickable cubosomes are broadly retained on introduction of the click groups with an overall change in cubic phase spacegroup when PEG$_{2000}$ was present. It should be noted that a loss in long-range order and overall structure was observed in the SAXS data for the PEG$_{2000}$ PL containing systems. This is likely due to the lower cubosome population seen in the Cryo-TEM and DLS data. Additionally, this could be explained by the swelling of the bilayer once the click reaction has occurred which has been seen in other systems previously [73].

3.5.3 Binding ability of cubosomes and liposomes

After confirmation that the dispersion contained cubosomes upon incorporation of copper-free click functional phospholipids, and that they were similar to standard cubosomes, the ability of the cubosomes to covalently and specifically bind with a strained cyclooctyne or azide through copper-free click chemistry was assessed. A representative set of elution profiles showing the baseline separation between the cubosomes eluting at 2-5 mLs and the free dye eluting at 6-15 mLs are provided in Figure 3.5.
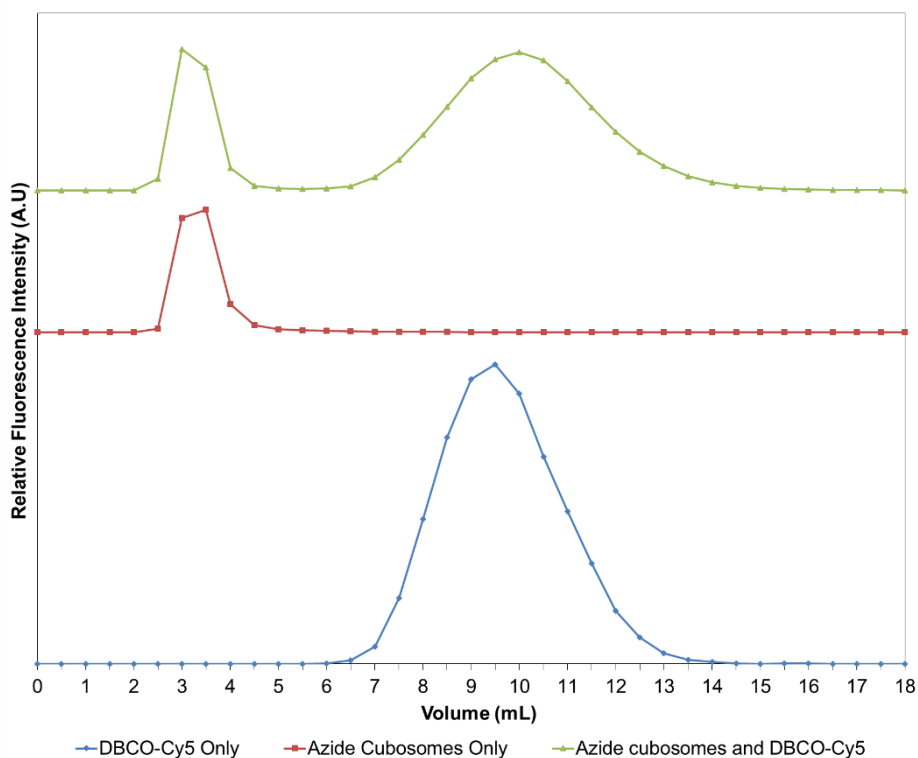
Figure 3.5. Representative elution profiles for Sulfo-DBCO-Cy5 dye only (blue), PL-Azide cubosomes only (red) and Sulfo-DBCO-Cy5 dye mixed with PL-Azide cubosomes (green) from a Sephadex G50 column with PBS as the eluent.

The PL-Azide cubosome sample was doped with Rhodamine B phospholipid to impart fluorescence to the cubosomes and this is why the total fluorescence observed is not in line with the other two elution profiles. Area under the curve for the distribution between the populations can be used to calculate a binding efficiency.

Each of the clickable cubosome systems showed over 85% binding with Sulfo-DBCO-Cy5 or Sulfo-Azide-Cy5 at 24 h after the complementary click-dye was added at a 1:1 mol ratio (Figure 3.6). The formulations with the greatest binding efficiency were the azide-containing cubosomes, specifically the PL-PEG$_{2000}$-Azide doped formulation binding to Sulfo-DBCO-Cy5 dye.
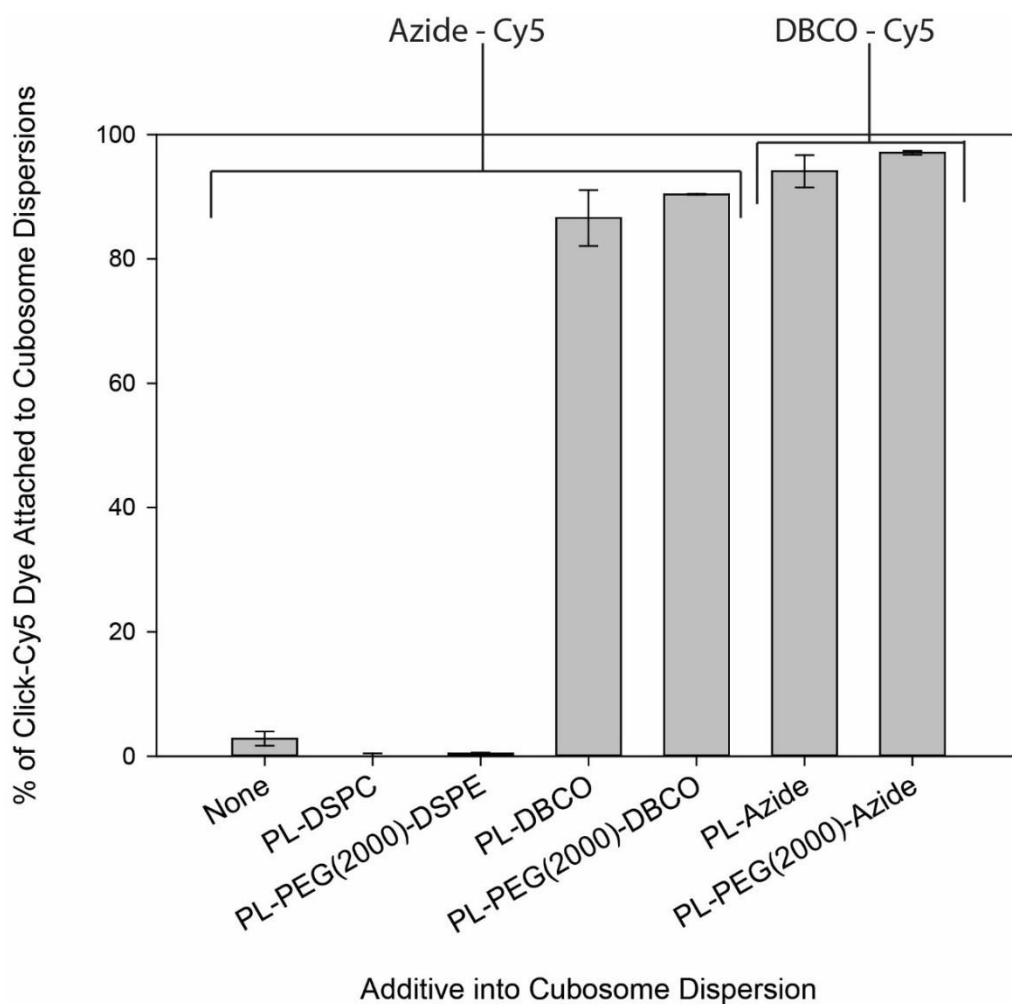
Figure 3.6. Percentage of dye bound to cubosomes (mean ± SD, n = 3) after size exclusion chromatography in a Sephadex G50 column with PBS as the eluent.

In the case of the controls, it is apparent that the dye was partially non-specifically bound to the particles but one also needs to be mindful that a fraction of the PBS that contains dye is present within the internal water channels of the cubic phase. The liposomes showed a very different binding profile to the cubosomes (Figure 3.7).
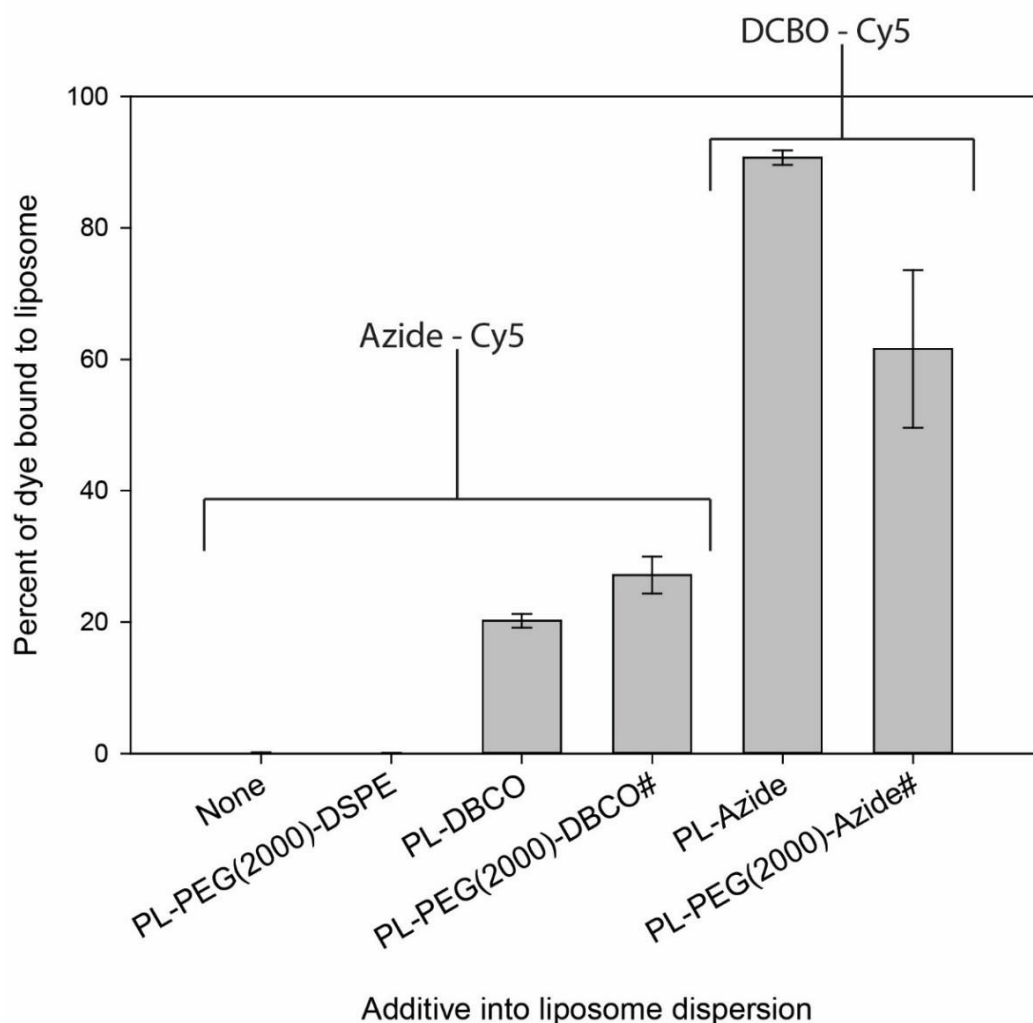
Figure 3.7. Percentage of dye bound to liposomes (mean ± SD, n = 3) after size exclusion chromatography in a Sephadex G50 column with PBS as the eluent. Samples denoted with # were not analysed via SEC as described due to colloidal stability and column bead adsorption. For this reason, membrane dialysis was utilised to assess bound and unbound Sulfo-click-Cy5.

The two control systems showed even less binding in part likely due to the fact that the liposomes are closed and contain a rigid lipid bilayer so the free dye cannot penetrate through into the internal aqueous pocket. Additionally, over all less binding was seen as perhaps some click groups are internalised and cannot be accessed, unlike the open bicontinuous cubic structure. Specifically, DBCO-bearing liposomes exhibited very poor binding which could be due to the hydrophobic and large DBCO structure which will prefer to embed itself within the lipid domain of the liposome making it unavailable for the azide-Cy5 to react with. This is a key issue if wanting to functionalize nanoparticles with DBCO entities for biorthogonal chemistry based targeting. The azide bearing liposomes had greater amounts of dye bound to them with the Azide-PL system having similar results to the cubosome variant, further supporting the idea that the hydrophilicity of the end group controls its location and availability. Finally, it is clear the PL-PEG$_{2000}$-Azide liposome performed poorly compared to all other Azide bearing nanoparticles. It has been seen before that PEG chains can fold and interact with each other [74-76] and this could have caused reduced azide availability for reacting in this particular instance or as mentioned for the DBCO systems the internalization of click groups would limit overall binding. This could also be due to the technique used to assess binding of the PL-PEG$_{2000}$-DBCO and PL-PEG$_{2000}$-Azide liposome. A membrane filter and dialysis was used to separate free dye from clicked dye on the liposomes as when they were applied to the column they would get stuck at the top layer before entering the packed beads. This change in technique may contribute to the lower binding seen in the PL-PEG$_{2000}$-Azide liposome. The cubosomes had overall more promising binding efficiency and could be a promising alternative to click-liposomes, considering the earlier highlight that liposomes reported to be effective *in vivo*.

3.5.4 Effect of click-conjugation on cubosome structure and lattice parameter

The cubosomes containing bound dye were also studied using SAXS to determine whether there was an effect of the covalent attachment of dye on the structure of the cubosome system (Figure 3.8).
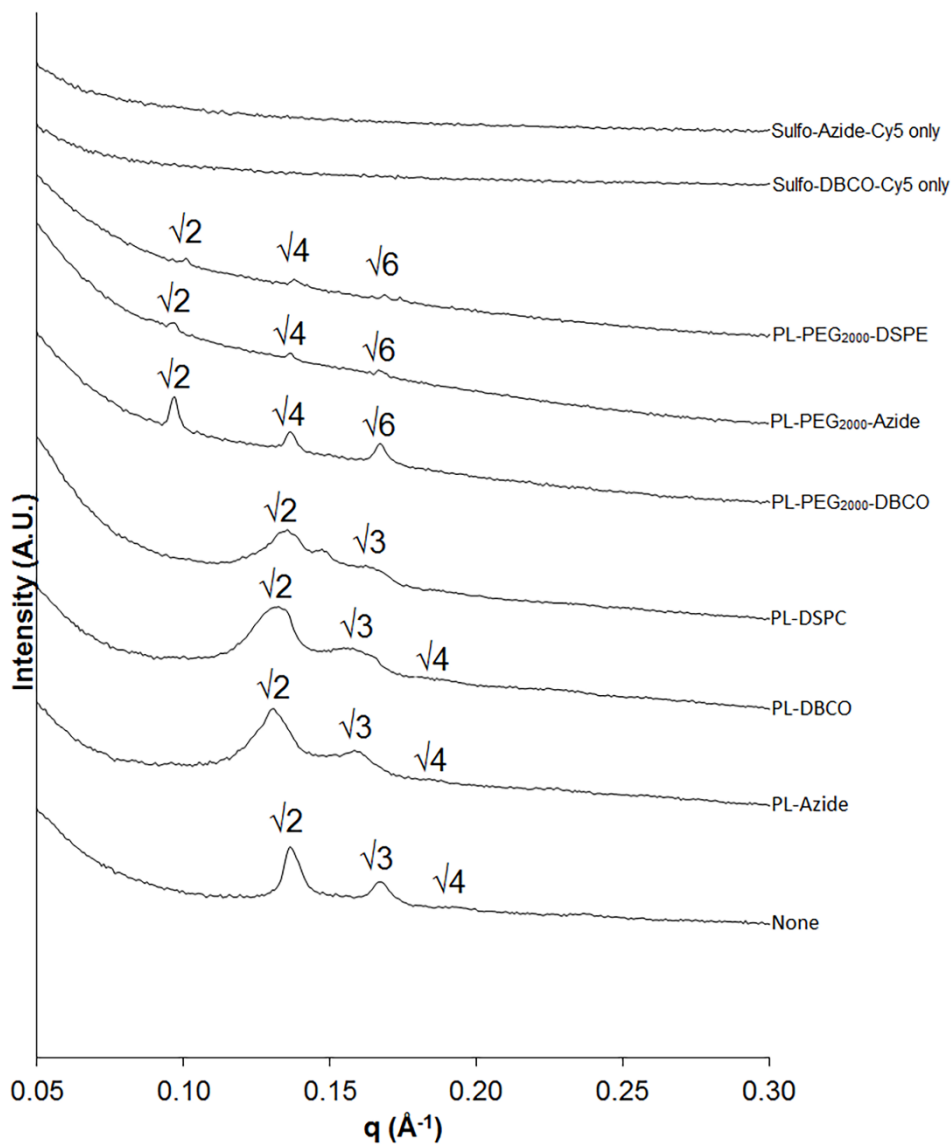
Figure 3.8. Effect of binding of the complementary dye probes on internal structures of clickable cubosomes. Scattering profiles were measured at 25°C after mixing clickable cubosomes with the complementary Cy5 dye in PBS for 24 h.

The presence of dye bound to the cubosome generally had a minor impact on the structure, as all systems retained the phases they had displayed in previous SAXS experiments. However, the scattering intensity was reduced and some peaks were less well-defined than before exposure to dye. The reduced peak intensity observed is likely due to the sample being diluted with the addition of dye solution. The peak broadening or loss of shape is related to a loss in long-range which could occur due to the binding of the dye molecule to the cubosome which may have minor effects on the packing of the system. It should be noted that the PL-DSPC containing dispersion appeared to have a third peak emerging between the first two Pn3m cubic phase peaks which is indicative of an additional phase being present but due to low peak intensity it is difficult to confirm this phase.

Additionally, lattice parameters were determined for the formulations after binding to the dye (Table 3.4) and there were no substantial differences compared to the pre-click structures in Table 3.3.

Table 3.4 Lattice parameters (Å ± SE) of cubosome dispersions after mixing with either Sulfo-Azide-Cy5 or Sulfo-DBCO-Cy5 and incubating for 24 hours.

Phospholipid added	Dye added	Phase	Lattice Parameter (Å ± SE)
None	Sulfo-Azide-Cy5	Pn3m	66.76 ± 2.50
PL-Azide	Sulfo-DBCO-Cy5	Pn3m	67.67 ± 1.20
PL-DBCO	Sulfo-Azide-Cy5	Pn3m	66.47 ± 0.80
PL-DSPC	Sulfo-Azide-Cy5	Pn3m	68.49 ± 0.27
PL-PEG$_{2000}$-DBCO	Sulfo-Azide-Cy5	Im3m	90.24 ± 1.78
PL-PEG$_{2000}$-Azide	Sulfo-DBCO-Cy5	Im3m	92.33 ± 0.13
PL-PEG$_{2000}$-DSPE	Sulfo-Azide-Cy5	Im3m	91.96 ± 0.38

Again, the exception was the PL-PEG$_{2000}$-Azide doped system, which had a high lattice parameter before clicking (~115 Å), but was similar to the other PEG systems after clicking (~92 Å) which is also similar to other systems in the literature with the same Im3m space group [77].

This difference upon click reaction is readily rationalised because before clicking on the DBCO dye, the azide phospholipid carries a net positive charge which swells the matrix even moreso than the plain PEG systems. However, when the click reaction takes place the formation of the triazole renders the system similar to the DBCO-azide dye system, hence reducing the impact of the azide's charge on packing in the cubosome structure.

3.5.5 Specifically clicking nanoparticles to A549 cell surfaces

Human lung cancer cells (A549) were cultured and treated with DBCO-mannose for three days before being exposed to the nanoparticles for 24 hours. The samples were then fixed and imaged using total internal reflection fluorescence microscopy (TIRF). These experiments were conducted three times on different days and with different passages. The cubosomes were labelled with rhodamine B-phospholipid, which provides the contrast in the images in Figure 3.9.
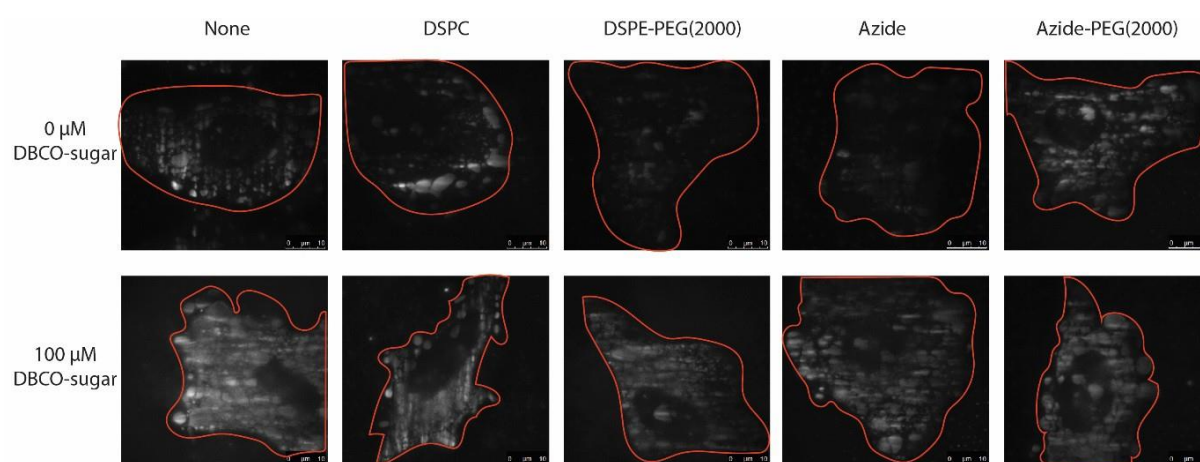
Figure 3.9. TIRF imaging of different cubosomes dispersions. The additive is detailed above the images. The white is a depiction of the cubosomes fluorescence from doped Rhodamine B phospholipid (0.25 mol %). The cells are circled in red for clarity and to depict the area analysed by Cameron Nowell's script.

The underlying concept is that unlabelled cells should show no or very little fluorescence indicating low interaction with the cells, while the cells metabolically labelled with DBCO-mannose should provide contrast due to specific permanent binding. The cubosomes appear as white circles attached onto the cell surface and can also be seen adsorbing onto the glass bottom of the well plate. Generally, the cells not exposed to DBCO-sugar appear to have less cubosomes bound to their surface than those that were, especially the DSPE-PEG$_{2000}$ and Azide modified systems. In the samples with DBCO-sugar all systems showed relatively high cell-surface binding. As samples with or without sugar show cubosome binding and also samples with or without click-capable groups show binding it suggests that the cubosomes were attaching non-specifically to the cells, even though specific attachment to azide-cubosomes was observed when DBCO-Sulfo-Cy5 was assessed in solution.

Similar findings were also seen in cells exposed to liposomal dispersions (Figure 3.10). Of particular interest was that the images indicate less overall binding when compared to the cubosomes.
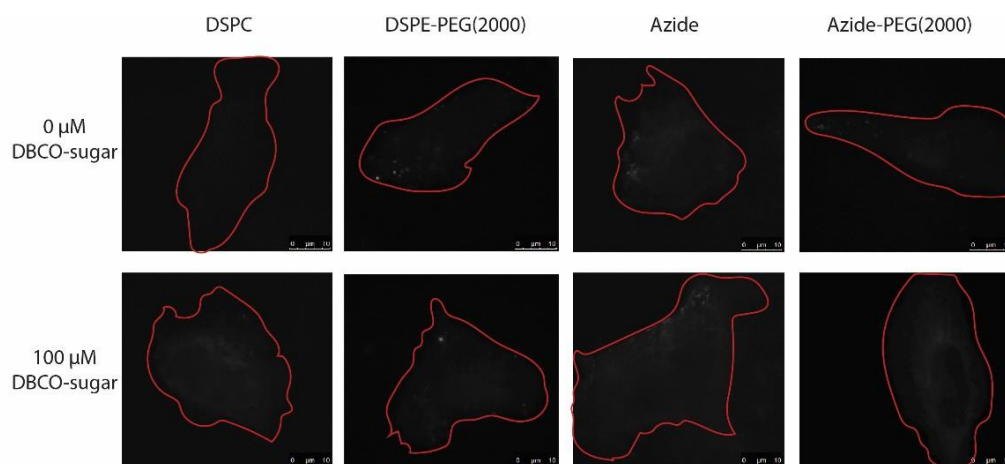
Figure 3.10. TIRF imaging of different liposomal dispersions. The additive is detailed above the images. The white is a depiction of the liposomes fluorescence from doped Rhodamine B phospholipid (0.25 mol %). The cells are circled in red for clarity and to depict the area analysed by Cameron Nowell's script.

Across all liposomes there appears to be less binding to the cell surface indicating a lower level of non-specific binding. In the systems where no sugar was introduced the non-specific binding was relatively low indicating that the liposomes do not substantially interact with the cell surface when compared to cubosomes. There is also more fluorescence observed on the cells treated with DBCO-sugar across all liposomes which could be a result of the added hydrophobicity of the DBCO groups on the cell surface. Finally, it is not apparent that specific binding is occurring as the samples without azides exhibit similar images to those with azides present. In an attempt to quantify the cell surface binding an in-house script was developed by Cameron Nowell (MIPS), described in Chapter Two. Figure 3.11 presents the mean fluorescence intensity of the cells analysed for all the samples.

A)
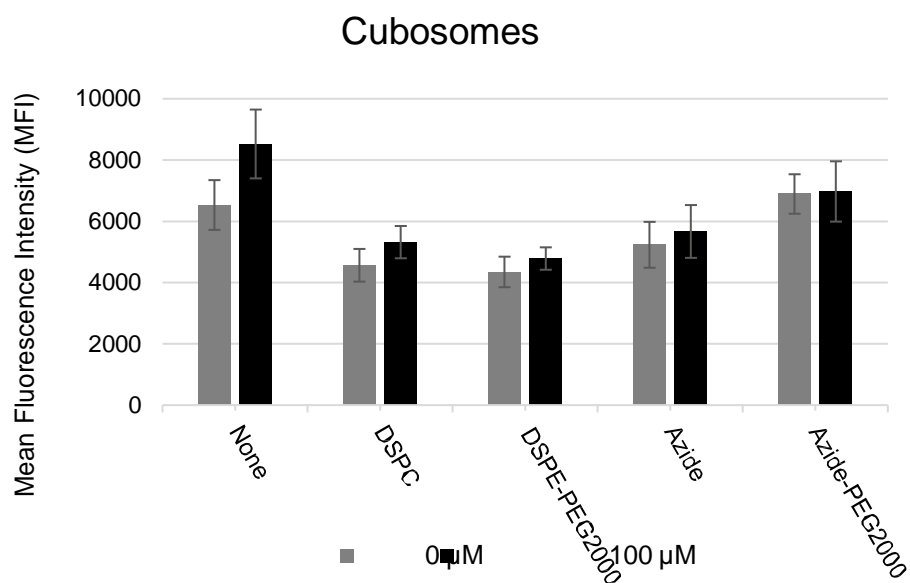
B)
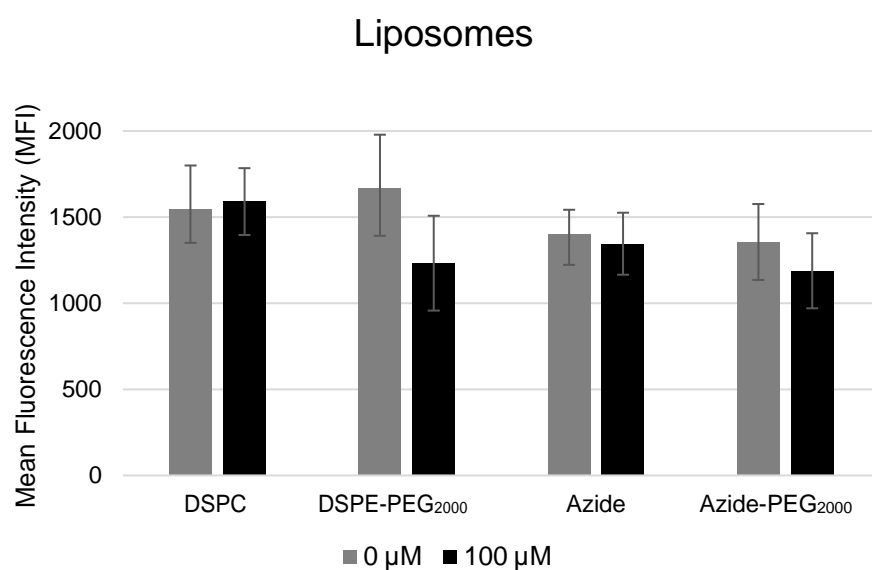
Figure 3.11. Calculated mean fluorescence intensity (MFI + SD, n >15) of the cell-surfaces from the TIRF images using the analysis script. A) Cubosome dispersions B) Liposomal dispersions. The additive is displayed on the x-axis.

All systems showed similar amount of binding regardless of the composition or whether sugar was present. This would indicate that the dominant force is hydrophobic interactions that do not allow specific binding to be detected. As seen in the images, the liposomes displayed much lower overall fluorescence on the cell surfaces. This is likely due to less non-specific binding occurring.

3.6 Discussion

This study confirms that the cubosomes can be functionalized using copper-free click reagents to enable covalent coupling to a complementary probe, and when used in a biorthogonal chemistry context they should retain their internal structure and consequently their drug delivery and imaging capabilities.

This finding is supported by other examples in the literature where cubosomes have been functionalized and used for immobilisation or targeting. To the best of our knowledge there is one previous work using antibody functionalized cubosomes for targeting [78] but none that utilise click chemistry. There have been cubosomes doped with biotin-DSPE for binding to avidin to enable immobilisation for bio-sensing [79, 80]. Similarly, cubosomes have been functionalized with biotin through a biotin-modified Pluronic F108 for active targeting of the receptors overexpressed by cancer cells [81]. Furthermore, two groups have used a folic acid-modified Pluronic F108 to stabilise and functionalize cubosomes for cancer cell targeted imaging and therapy [82, 83]. All these examples showed only minor or no changes to the cubosomes upon binding, as was the case for the clickable cubosomes in this study.

The use of the long PEG chain phospholipid bearing the azide- or DBCO- at the end is expected to increase the chance of the phospholipid being at the interface of the cubic phase due to its size and hydrophilicity. This would benefit surface interactions as there would be a greater number of click groups extended from the surface. Additionally, the hydrophilic PEG chain might help to reduce undesirable nonspecific hydrophobic interactions with a cell membrane or adsorption of opsonising proteins from the blood.

The findings presented in this chapter pave the way for the use of these cubosomes with metabolic labelling to develop an improved delivery or imaging method. While the opportunities are significant for a new approach to delivery to come to the fore, cubosomes are in their infancy as delivery and imaging agents, for example understanding the *in vitro* cellular toxicity of cubosomes is still immature [84, 85] let alone understanding the pharmacokinetic aspects of these materials. Alternatively, these techniques and nanoparticles could have other uses such as biosensing and cell capture.

One limitation to functionalisation through doping in phospholipid is the lack of control over where the reactive groups present themselves. This does not appear to limit binding of the complimentary dye in solution but could present problems for future use paired with metabolic labelling.

A potential solution is taking the approach mentioned above where the polymeric stabiliser is modified to contain the clickable functional group. Large stabiliser molecules tend to position at the external interface of the particles, presenting themselves to bulk aqueous phase rather than inside the aqueous cubic phase channels [86, 87], presenting the azides in a position where they are more readily available to react. Recently, lipid-like polymers were reported that can stabilise cubosomes [88] and an azide bearing version was synthesised to assess the two different functionalisation methods. This work is addressed in Chapter Five. An added bonus of this change would be the replacing of Pluronics as stabilisers. Although they are currently the most popular stabiliser for liquid crystalline systems they do have drawbacks. They are required in relatively high concentrations (> 1 wt. %) [89] and have been shown that there is reduced polymer-particle association resulting in more free Pluronic molecules over time [90].

In order to determine whether the cubosomes ability to take part in the click reaction was not limited to small molecules in solution a series of experiments were conducted with model surfaces before cell studies.

A range of experiments were attempted such as QCM, SAXS, GISAXS, flow cytometry with click-silica beads and fluorescence measurements with click-magnetic beads. In all these cases either the sensitivity was too low or the background and non-specific binding was high and therefore unable to be quantified in a repeatable and reproducible manner. This gave some insight into potential problems that might be present when moving *in vitro*, and for this reason TIRF was selected as the imaging technique chosen as it would indicate what is occurring at the cell-surface.

It is clear from the imaging data and the previous experiments mentioned that hydrophobic interactions play a large role in the specific surface binding of cubosomes, and to a lesser degree liposomes. This has not been a concern for many of the original studies utilising biorthogonal chemistry to selectively attach small dye molecules and track their movement to gain understanding of biological processes, but is a significant issue in considering these materials for drug delivery or imaging applications.

The images clearly show a higher amount of binding in the systems treated with DBCO-mannose and this could be due to the increased hydrophobicity of the cell surface from the DBCO groups, leading to increased non-specific hydrophobic interactions. This might also indicate why the azide bearing cubosomes showed generally less binding as their surface would be more polar and charged, leading to less non-specific interactions.

There have been reports summarising and investigating key physicochemical factors required for nanoparticles to be successful *in vitro* and *in vivo* settings [91-95], this is further addressed in Chapter Four. A common finding is that size, charge and hydrophilicity all play key roles in nanoparticle interface interactions. The liposomal systems were considerably smaller on average when compared to the cubosomes. This was seen in the DLS measurements and TIRF imaging in figures 3.6 and 3.7. This could be one of the key attributes that is limiting the selective binding of the click-capable cubosomes as their relatively large size allows for a high number of contact points where adsorption can occur. This may be further exaggerated by the lipophilic nature of both the cell surface membrane, made from lipids, and the cubosome itself, also made from lipids.

The two lipophilic surfaces are likely to have strong hydrophobic interactions leading to non-specific binding which is supported by the imaging data but also the unsuccessful experiments of QCM, SAXS, GISAXS, Flow cytometry and fluorescent measurements.

The surface of the cubosomes and liposomes are quite different in their shape and structure which may also play a role. Liposomes are spherical and when they contain PEG groups this is often found on the surface creating a hydrophilic layer around the outside of the liposome, which improves circulation and reduces non-specific interactions that lead to blood clearance *in vivo* [96-99].

Cubosomes differ in that they exhibit a sponge like appearance of bicontinuous water and oil channels and that the location of the PEG is more random, limiting the formation of this hydrophilic external layer that could be minimising hydrophobic interactions.

3.7 Conclusion

Novel functionalized cubosomes that can partake in copper-free click chemistry have been demonstrated. The incorporation of an azido or DBCO group to the cubosomes did not alter their phase and structure significantly. The liposomes that were developed as a comparison nanoparticle system did not perform as well when compared to the novel cubosomes indicating a potential role for cubosomes for which liposomes may be less suitable. Additionally, the copper-free click reaction between the "clickable" cubosomes and DBCO or Azide-Cy5 was selective and very efficient whilst retaining the structure of the unreacted cubosomes. This first study and proof of concept work is promising regarding the use of cubosomes combined with copper-free click chemistry and in the near future metabolic labelling to provide an antibody-free targeting option for these emerging drug delivery and imaging systems.

These results indicate that although click-cubosomes and liposomes are able to undergo click reactions while retaining structure and properties in solution, further application still requires more investigation due to a lack of understanding of the nature of the non-specific interactions that mask any specificity in binding. The consistent finding across all attempted experiments was that hydrophobic non-specific binding was occurring to a high degree with both types of lipid-based nanoparticles. This is likely due to the similar nature of the cubosomes, the hydrophobic surfaces assessed and also the lipid membranes of cells. An interesting development was the lower amount of non-specific binding seen in some of the click-liposome dispersions indicating that perhaps size is also important in any non-specific interactions occurring. Further insight into metabolic labelling being utilised for nanoparticle delivery, especially relatively large lipid based hydrophobic systems, is needed to truly utilise this promising targeting approach.

3.8 References

1. Iyer, A.K., et al., *Exploiting the enhanced permeability and retention effect for tumor targeting.* Drug Discovery Today, 2006. **11**(17–18): p. 812-818.

2. Torchilin, V.P., *Passive and Active Drug Targeting: Drug Delivery to Tumors as an Example*, in *Drug Delivery*, M. Schäfer-Korting, Editor. 2010, Springer Berlin Heidelberg: Berlin, Heidelberg. p. 3-53.

3. Garg, G., et al., *Cubosomes: An Overview.* Biological and Pharmaceutical Bulletin, 2007. **30**(2): p. 350-353.

4. Karami, Z. and Hamidi, M., *Cubosomes: remarkable drug delivery potential.* Drug Discovery Today.

5. Spicer, P.T., *Progress in liquid crystalline dispersions: Cubosomes.* Current Opinion in Colloid & Interface Science, 2005. **10**(5): p. 274-279.

6. Xin, P., et al., *Nanostructed Cubosomes as Advanced Drug Delivery System.* Current Pharmaceutical Design, 2013. **19**(35): p. 6290-6297.

7. Rizwan, S.B., et al., *Characterisation of bicontinuous cubic liquid crystalline systems of phytantriol and water using cryo field emission scanning electron microscopy (cryo FESEM).* Micron, 2007. **38**(5): p. 478-485.

8. Zhai, J., et al., *Lipid–PEG Conjugates Sterically Stabilize and Reduce the Toxicity of Phytantriol-Based Lyotropic Liquid Crystalline Nanoparticles.* Langmuir, 2015. **31**(39): p. 10871-10880.

9.   Azmi, I.D.M., et al., *Cubosomes and hexosomes as versatile platforms for drug delivery.* Therapeutic Delivery, 2015. **6**(12): p. 1347-1364.

10.   Chen, Y., et al., *Cubic and Hexagonal Liquid Crystals as Drug Delivery Systems.* BioMed Research International, 2014. **2014**: p. 815981.

11.   Boyd, B.J. and Fong, W.-K., *Stimuli-Responsive Lipid-Based Self-Assembled Systems*, in *Self-Assembled Supramolecular Architectures*. 2012, John Wiley & Sons, Inc. p. 257-288.

12.   Naga, M.L., et al., *Cubosomes as Targeted Drug Delivery Systems - A Biopharmaceutical Approach.* Current Drug Discovery Technologies, 2014. **11**(3): p. 181-188.

13.   Mulet, X., et al., *Advances in drug delivery and medical imaging using colloidal lyotropic liquid crystalline dispersions.* Journal of Colloid and Interface Science, 2013. **393**(Supplement C): p. 1-20.

14.   Gupta, A., et al., *Nanoassemblies of Gd-DTPA-monooleyl and glycerol monooleate amphiphiles as potential MRI contrast agents.* Journal of Materials Chemistry B, 2014. **2**(9): p. 1225-1233.

15.   Muir, B.W., et al., *Metal-free and MRI visible theranostic lyotropic liquid crystal nitroxide-based nanoparticles.* Biomaterials, 2012. **33**(9): p. 2723-2733.

16.   Alcaraz, N. and Boyd, B.J., *Cubosomes as Carriers for MRI Contrast Agents.* Current Medicinal Chemistry, 2017. **24**(5): p. 470-482.

17.   Tresset, G., *The multiple faces of self-assembled lipidic systems.* PMC Biophysics, 2009. **2**(1): p. 3.

18.   Chames, P., et al., *Therapeutic antibodies: successes, limitations and hopes for the future.* British Journal of Pharmacology, 2009. **157**(2): p. 220-233.

19.   Zwicke, G.L., et al., *Utilizing the folate receptor for active targeting of cancer nanotherapeutics.* Nano Reviews, 2012. **3**: p. 10.3402/nano.v3i0.18496.

20.   Kularatne, S.A. and Low, P.S.,*Targeting of Nanoparticles: Folate Receptor*, in *Cancer Nanotechnology: Methods and Protocols*, S.R. Grobmyer and B.M. Moudgil, Editors. 2010, Humana Press: Totowa, NJ. p. 249-265.

21.   Zaro, B.W., et al., *Incorporation of Unnatural Sugars for the Identification of Glycoproteins.* Methods in molecular biology (Clifton, N.J.), 2013. **951**: p. 57-67.

22.   Laughlin, S.T. and Bertozzi, C.R., *Metabolic labeling of glycans with azido sugars and subsequent glycan-profiling and visualization via Staudinger ligation.* Nature Protocols, 2007. **2**: p. 2930.

23.   Laughlin, S.T., et al., *Metabolic Labeling of Glycans with Azido Sugars for Visualization and Glycoproteomics*, in *Methods in Enzymology*. 2006, Academic Press. p. 230-250.

24.   Chang, P.V., et al., *Metabolic labeling of sialic acids in living animals with alkynyl sugars.* Angewandte Chemie, 2009. **121**(22): p. 4090-4093.

25.   Wang, H., et al., *In Vivo Targeting of Metabolically Labeled Cancers with Ultra-Small Silica Nanoconjugates.* Theranostics, 2016. **6**(9): p. 1467-1476.

26.   Zheng, M., et al., *Development of Bioorthogonal Reactions and Their Applications in Bioconjugation.* Molecules, 2015. **20**(2): p. 3190.

27. Agard, N.J., et al., *A Comparative Study of Bioorthogonal Reactions with Azides.* ACS Chemical Biology, 2006. **1**(10): p. 644-648.

28. Agard, N.J., et al., *A Strain-Promoted [3 + 2] Azide−Alkyne Cycloaddition for Covalent Modification of Biomolecules in Living Systems.* Journal of the American Chemical Society, 2004. **126**(46): p. 15046-15047.

29. Saxon, E. and Bertozzi, C.R., *Chemical and Biological Strategies for Engineering Cell Surface Glycosylation.* Annual Review of Cell and Developmental Biology, 2001. **17**(1): p. 1-23.

30. Bertozzi, C.R., *A Decade of Bioorthogonal Chemistry.* Accounts of Chemical Research, 2011. **44**(9): p. 651-653.

31. Bertozzi, C.R., et al., *Chemical Glycobiology.* Science, 2001. **291**(5512): p. 2357-2364.

32. Laughlin, S.T., et al., *Metabolic Labeling of Glycans with Azido Sugars for Visualization and Glycoproteomics*, in *Methods in Enzymology*, F. Minoru, Editor. 2006, Academic Press. p. 230-250.

33. Prescher, J.A. and Bertozzi, C.R., *Chemistry in living systems.* Nat Chem Biol, 2005. **1**(1): p. 13-21.

34. Prescher, J.A., et al., *Chemical remodelling of cell surfaces in living animals.* Nature, 2004. **430**(7002): p. 873-877.

35. Vocadlo, D.J., et al., *A chemical approach for identifying O-GlcNAc-modified proteins in cells.* Proceedings of the National Academy of Sciences, 2003. **100**(16): p. 9116-9121.

36.   Sletten, E.M. and Bertozzi, C.R., *Bioorthogonal Chemistry: Fishing for Selectivity in a Sea of Functionality.* Angewandte Chemie International Edition, 2009. **48**(38): p. 6974-6998.

37.   Baskin, J.M. and Bertozzi, C.R., *Bioorthogonal Click Chemistry: Covalent Labeling in Living Systems.* QSAR & Combinatorial Science, 2007. **26**(11-12): p. 1211-1219.

38.   Saxon, E. and Bertozzi, C.R., *Cell Surface Engineering by a Modified Staudinger Reaction.* Science, 2000. **287**(5460): p. 2007-2010.

39.   Dube, D.H. and Bertozzi, C.R., *Glycans in cancer and inflammation [mdash] potential for therapeutics and diagnostics.* Nat Rev Drug Discov, 2005. **4**(6): p. 477-488.

40.   Lang, K. and Chin, J.W., *Bioorthogonal Reactions for Labeling Proteins.* ACS Chemical Biology, 2014. **9**(1): p. 16-20.

41.   Lang, K. and Chin, J.W., *Cellular incorporation of unnatural amino acids and bioorthogonal labeling of proteins.* Chemical reviews, 2014. **114**(9): p. 4764-4806.

42.   Lang, K., et al., *Genetic Encoding of Bicyclononynes and trans-Cyclooctenes for Site-Specific Protein Labeling in Vitro and in Live Mammalian Cells via Rapid Fluorogenic Diels–Alder Reactions.* Journal of the American Chemical Society, 2012. **134**(25): p. 10317-10320.

43.   Song, C.-X., et al., *Selective chemical labeling reveals the genome-wide distribution of 5-hydroxymethylcytosine.* Nature biotechnology, 2010. **29**(1): p. 68.

44.   Neef, A.B and Luedtke N.W., *An Azide-Modified Nucleoside for Metabolic Labeling of DNA.* ChembioChem. 2014. **15**(6). P. 789/793

45.   Schoch, J., et al., *Site-specific one-pot dual labeling of DNA by orthogonal cycloaddition chemistry.* Bioconjugate chemistry, 2012. **23**(7): p. 1382-1386.

46.   Baskin, J.M., et al., *Copper-free click chemistry for dynamic in vivo imaging.* Proceedings of the National Academy of Sciences, 2007. **104**(43): p. 16793-16797.

47.   Devaraj, N., et al., *Readily accessible living cells Anse for bioChemical labeling and three-dimensional imaging of* 2010. **122**(49): p. 9612-9615.

48.   Wu, H. and Devaraj, N.K., *Advances in Tetrazine Bioorthogonal Chemistry Driven by the Synthesis of Novel Tetrazines and Dienophiles.* Accounts of Chemical Research, 2018. **51**(5): p. 1249-1259.

49.   Hongyan, Z., et al., *Tetrazine Bioorthogonal Reaction: A Novel Scheme for Polymer and Biomaterials.* Current Organic Chemistry, 2016. **20**(17): p. 1756-1767.

50.   Yoon, H.Y., et al., *Artificial Chemical Reporter Targeting Strategy Using Bioorthogonal Click Reaction for Improving Active-Targeting Efficiency of Tumor.* Molecular Pharmaceutics, 2017.

51.   Koo, H., et al., *Bioorthogonal Copper-Free Click Chemistry In Vivo for Tumor-Targeted Delivery of Nanoparticles.* Angewandte Chemie International Edition, 2012. **51**(47): p. 11836-11840.

52.   Lee, S., et al., *Chemical Tumor-Targeting of Nanoparticles Based on Metabolic Glycoengineering and Click Chemistry.* ACS Nano, 2014. **8**(3): p. 2048-2063.

53.   Koo, H., et al., *In Vivo Targeted Delivery of Nanoparticles for Theranosis.* Accounts of Chemical Research, 2011. **44**(10): p. 1018-1028.

54.   Lee, S., et al., *In vivo stem cell tracking with imageable nanoparticles that bind bioorthogonal chemical receptors on the stem cell surface.* Biomaterials, 2017. **139**: p. 12-29.

55.   Chang, P.V. and Bertozzi, C.R., *Imaging beyond the proteome.* Chemical Communications, 2012. **48**(71): p. 8864-8879.

56.   Beahm, B. and Bertozzim C.R., *Imaging Cell-Surface Glycans in Animals with Bioorthogonal Chemistry*, in *Glycoscience: Biology and Medicine*, T. Endo, et al., Editors. 2014, Springer Japan. p. 1-11.

57.   Laughlin, S.T., et al., *In Vivo Imaging of Membrane-Associated Glycans in Developing Zebrafish.* Science, 2008. **320**(5876): p. 664-667.

58.   Chang, P.V., et al., *A strategy for the selective imaging of glycans using caged metabolic precursors.* J Am Chem Soc, 2010. **132**(28): p. 9516-8.

59.   Agarwal, P., et al., *Systemic Fluorescence Imaging of Zebrafish Glycans with Bioorthogonal Chemistry.* Angewandte Chemie International Edition, 2015. **54**(39): p. 11504-11510.

60. Baskin, J.M., et al., *Visualizing enveloping layer glycans during zebrafish early embryogenesis.* Proc Natl Acad Sci U S A, 2010. **107**(23): p. 10360-5.

61. McKay, C.S. and Finn, M.G., *Click Chemistry in Complex Mixtures: Bioorthogonal Bioconjugation.* Chemistry & biology, 2014. **21**(9): p. 1075-1101.

62. Dehnert, K.W., et al., *Imaging the sialome during zebrafish development with copper-free click chemistry.* Chembiochem, 2012. **13**(3): p. 353-7.

63. Besanceney-Webler, C., et al., *Metabolic labeling of fucosylated glycoproteins in Bacteroidales species.* Bioorganic & Medicinal Chemistry Letters, 2011. **21**(17): p. 4989-4992.

64. Dehnert, K.W., et al., *Metabolic labeling of fucosylated glycans in developing zebrafish.* ACS Chem Biol, 2011. **6**(6): p. 547-52.

65. Jiang, H., et al., *Imaging glycans in zebrafish embryos by metabolic labeling and bioorthogonal click chemistry.* J Vis Exp, 2011(52).

66. Géral, C., et al., *From Molecular to Nanotechnology Strategies for Delivery of Neurotrophins: Emphasis on Brain-Derived Neurotrophic Factor (BDNF).* Pharmaceutics, 2013. **5**(1): p. 127.

67. Dong, Y.-D., et al., *Bulk and Dispersed Aqueous Phase Behavior of Phytantriol: Effect of Vitamin E Acetate and F127 Polymer on Liquid Crystal Nanostructure.* Langmuir, 2006. **22**(23): p. 9512-9518.

68. Israelachvili, J.N., et al., *Theory of self-assembly of hydrocarbon amphiphiles into micelles and bilayers.* Journal of the Chemical Society, Faraday Transactions 2: Molecular and Chemical Physics, 1976. **72**(0): p. 1525-1568.

69.   Bisset, N.B., et al., *Tailoring liquid crystalline lipid nanomaterials for controlled release of macromolecules.* International Journal of Pharmaceutics, 2015. **495**(1): p. 241-248.

70.   Barauskas, J. and Landh, T., *Phase Behavior of the Phytantriol/Water System.* Langmuir, 2003. **19**(23): p. 9562-9565.

71.   Hartnett, T.E., et al., *Size and Phase Control of Cubic Lyotropic Liquid Crystal Nanoparticles.* The Journal of Physical Chemistry B, 2014. **118**(26): p. 7430-7439.

72.   Azhari, H., et al., *Stabilising cubosomes with Tween 80 as a step towards targeting lipid nanocarriers to the blood–brain barrier.* European Journal of Pharmaceutics and Biopharmaceutics, 2016. **104**(Supplement C): p. 148-155.

73.   R. Bruinsma., Elasticity and excitations of minimal crystals. J. Phys. II (France), 1992. **2**(3): p. 425-451.

74.   Terashima, T., et al., *Single-Chain Folding of Polymers for Catalytic Systems in Water.* Journal of the American Chemical Society, 2011. **133**(13): p. 4742-4745.

75.   Ozcan, A. and Christopher, B.K., *Single Chain Folding of Synthetic Polymers by Covalent and Non-Covalent Interactions: Current Status and Future Perspectives.* Macromolecular Rapid Communications, 2012. **33**(11): p. 958-971.

76.   Terashima, T., et al., *Synthesis and Single-Chain Folding of Amphiphilic Random Copolymers in Water.* Macromolecules, 2014. **47**(2): p. 589-600.

77. Nilsson, C., et al., *PEGylation of Phytantriol-Based Lyotropic Liquid Crystalline Particles—The Effect of Lipid Composition, PEG Chain Length, and* Temperature on the Internal Nanostructure. Langmuir, 2014. 30(22): p. 6398-6407.

78. Zhai, J., et al., *Epidermal growth factor receptor-targeted lipid nanoparticles retain self-assembled nanostructures and provide high specificity.* Nanoscale, 2015. **7**(7): p. 2905-2913.

79. Fraser, S.J., et al., *Development of Cubosomes as a Cell-Free Biosensing Platform.* Australian Journal of Chemistry, 2011. **64**(1): p. 46-53.

80. Tajik-Ahmadabad, B., et al., *A QCM-D and SAXS Study of the Interaction of Functionalized Lyotropic Liquid Crystalline Lipid Nanoparticles with siRNA.* ChemBioChem, 2017. **18**(10): p. 921-930.

81. Aleandri, S., et al., *Biotinylated Cubosomes: A Versatile Tool for Active Targeting and Codelivery of Paclitaxel and a Fluorescein-Based Lipid Dye.* Langmuir, 2015. **31**(46): p. 12770-12776.

82. Caltagirone, C., et al., *Cancer-Cell-Targeted Theranostic Cubosomes.* Langmuir, 2014. **30**(21): p. 6228-6236.

83. Tian, Y., et al., *Folic Acid-Targeted Etoposide Cubosomes for Theranostic Application of Cancer Cell Imaging and Therapy.* Medical Science Monitor : International Medical Journal of Experimental and Clinical Research, 2017. **23**: p. 2426-2435.

84. Murgia, S., et al., *Nanoparticles from Lipid-Based Liquid Crystals: Emulsifier Influence on Morphology and Cytotoxicity.* The Journal of Physical Chemistry B, 2010. **114**(10): p. 3518-3525.

85.   Zhai, J., et al., *Amphiphilic brush polymers produced using the RAFT polymerisation method stabilise and reduce the cell cytotoxicity of lipid lyotropic liquid crystalline nanoparticles.* Faraday Discussions, 2016. **191**(0): p. 545-563.

86.   La, Y., et al., *Colloidal inverse bicontinuous cubic membranes of block copolymers with tunable surface functional groups.* Nat Chem, 2014. **6**(6): p. 534-541.

87.   Chong, J.Y.T., et al., *Novel Steric Stabilizers for Lyotropic Liquid Crystalline Nanoparticles: PEGylated-Phytanyl Copolymers.* Langmuir, 2015. **31**(9): p. 2615-2629.

88.   Grace, J.L., et al., *Lipidated polymers for the stabilization of cubosomes: nanostructured drug delivery vehicles.* Chemical Communications, 2017.

89.   Chong, J.Y.T., et al., *Steric stabilisation of self-assembled cubic lyotropic liquid crystalline nanoparticles: high throughput evaluation of triblock polyethylene oxide-polypropylene oxide-polyethylene oxide copolymers.* Soft Matter, 2011. **7**(10): p. 4768-4777.

90.   Tilley, A.J., et al., *Disposition and association of the steric stabilizer Pluronic® F127 in lyotropic liquid crystalline nanostructured particle dispersions.* Journal of colloid and interface science, 2013. **392**: p. 288-296.

91.   Khlebtsov, N. and Dykman, L., *Biodistribution and toxicity of engineered gold nanoparticles: a review of in vitro and in vivo studies.* Chemical Society Reviews, 2011. **40**(3): p. 1647-1671.

92.   Mohanraj, V. and Chen, Y., *Nanoparticles-a review.* Tropical journal of pharmaceutical research, 2006. **5**(1): p. 561-573.

93.   Cho, K., et al., *Therapeutic nanoparticles for drug delivery in cancer.* Clinical cancer research, 2008. **14**(5): p. 1310-1316.

94.   Irvine, D.J., *Drug delivery: One nanoparticle, one kill.* Nature materials, 2011. **10**(5): p. 10.1038/nmat3014.

95.   Christian, P., et al., *Nanoparticles: structure, properties, preparation and behaviour in environmental media.* Ecotoxicology, 2008. **17**(5): p. 326-343.

96.   Immordino, M.L., et al., *Stealth liposomes: review of the basic science, rationale, and clinical applications, existing and potential.* International Journal of Nanomedicine, 2006. **1**(3): p. 297-315.

97.   Paola, M., et al., *PEGylation of Proteins and Liposomes: a Powerful and Flexible Strategy to Improve the Drug Delivery.* Current Drug Metabolism, 2012. **13**(1): p. 105-119.

98.   Gabizon, A., et al., *Pharmacokinetics of pegylated liposomal doxorubicin.* Clinical pharmacokinetics, 2003. **42**(5): p. 419-436.

99.   Torchilin, V.P., *Targeted pharmaceutical nanocarriers for cancer therapy and imaging.* The AAPS journal, 2007. **9**(2): p. E128-E147.

Chapter 4 – Role of Size and Click-group Density on Cell Surface Binding of Nanoparticles through Metabolic Labelling and Copper-Free Click Chemistry

4.1 Introduction

Nanoparticles have been of increasing interest over the past 50 years as a means of improving drug efficacy, either through targeting to ensure the drug can reach the site of action [1-4] or protection and encapsulation so more drug is able to be delivered [5-7]. A key area dictating the rate of development of nanoparticle-based therapies is the importance of physicochemical properties, specifically the role that size, shape and surface properties can play *in vivo* [8-13]. The bulk of these studies have focussed on how the nanoparticle is distributed in the body when these properties have been altered in a controlled matter. There appears to be less focus on the cell surface-nanoparticle interactions, particularly non-specific interactions as seen for cubosomes in Chapter Three, which can dominate when a foreign nanoparticle enters a biological system and obscures any desired targeted interactions. Knowledge of how to avoid unwanted interactions is of great importance in improving the *in vivo* performance and viability of emerging nanosystems but is rarely discussed. The data in Chapter Three indicates that although small dyes are able to specifically bind to the metabolically labelled cells that nanoparticles, even the liposomes with relatively low non-specific binding, did not show avid specific binding. Hence, it is apparent that size, particle type, and surface chemistry including the density of reactive groups may all play a role in both non-specific binding and specific binding, but to date there has not been a systematic study of these variables to enable identification and control of the effect. Table 4.1 below summarises some findings regarding the influence of the aforementioned physico-chemical properties on nanoparticle-cell interactions. It should be mentioned that protein-nanoaprticle interactions *in vivo* are another area of interest for scientists developing nanoparticles but this is not within the scope of this Thesis and therefore will not be focussed on.

Table 4.1. A summary of the roles of physicochemical properties of a particle surface in their cellular uptake. Reproduced and adapted from [14] with permission.

Physicochemical characteristic	Role	Ref
Size	The smaller the particle the higher the surface area which results in reduced clearance and broader cellular uptake	[15, 16]
Shape	Rod shaped particles with a higher aspect ratio exhibit greater cellular uptake	[17]
Neutral charge	The greater the steric prevention, the lower the plasma protein adsorption resulting in greater circulating time and broader cellular uptake	[18, 19]
Positive charge	Facilitates the cell-membrane nanoparticle interaction due to the negatively charged cell surface	[20, 21]
Negative charge	The initial repulsive interaction of nanoparticles modulate aggregation, cluster formation and cellular uptake	[22, 23]

4.1.1 Effect of nanoparticle size and shape on cell interactions

One aspect of the system that formulators can generally control are the particle size and morphology. It has been shown that size and shape are strong determinants for cellular uptake and must be taken into consideration when creating a nanoparticle that will interact with a biological setting [23-25].

The recommended ideal size for *in vivo* delivery is between 10 and 200 nm as this allows the nanoparticle to potentially escape most physiological barriers and have a high circulation time, but studies are limited when assessing the role of size once the nanoparticle has reached the desired end point *in vivo* [26]. It has been shown with spherical PEG coated gold nanoparticles that their size heavily dictates their natural distribution in the body.

Terentyuk *et al.* tracked the biodistribution of 15 and 50 nm gold nanoparticles and 150 nm silica/gold nanoshells. They saw that the 15 nm nanoparticle remained in circulation considerably longer than the other two systems tested but also that they were removed more slowly and accumulated to a lesser degree in key organs such as the spleen, liver and kidney which would indicate less unwanted interactions occurring such as non-specific binding [27]. A similar study was conducted by Perrault *et al.* with PEG coated gold nanoparticles ranging between 25 and 119 nm with similar results observed. They were able to give further insight in the role of size by tracking the permeation and localisation of the different sizes once they had reached tumors. The larger the nanoparticle the more likely it is that the particle stays near the vasculature whereas the smaller nanoparticles will diffuse through the tumor matrix [28]. These examples show the importance in controlling nanoparticle size in order to improve control over its function.

The size recommendation for beneficial cell surface interactions is 30-60 nm as this drives membrane-wrapping and uptake as seen in Figure 4.1 [29]. Many of these studies investigating the role of size of a nanoparticle *in vivo* focus on its biodistrubution, overall fate and excretion, however there are limited studies focussing on the role of size at the cell surface.

Additionally, they often use different nanoparticles, different sizes and different models which leads to a lack of uniformity in results.
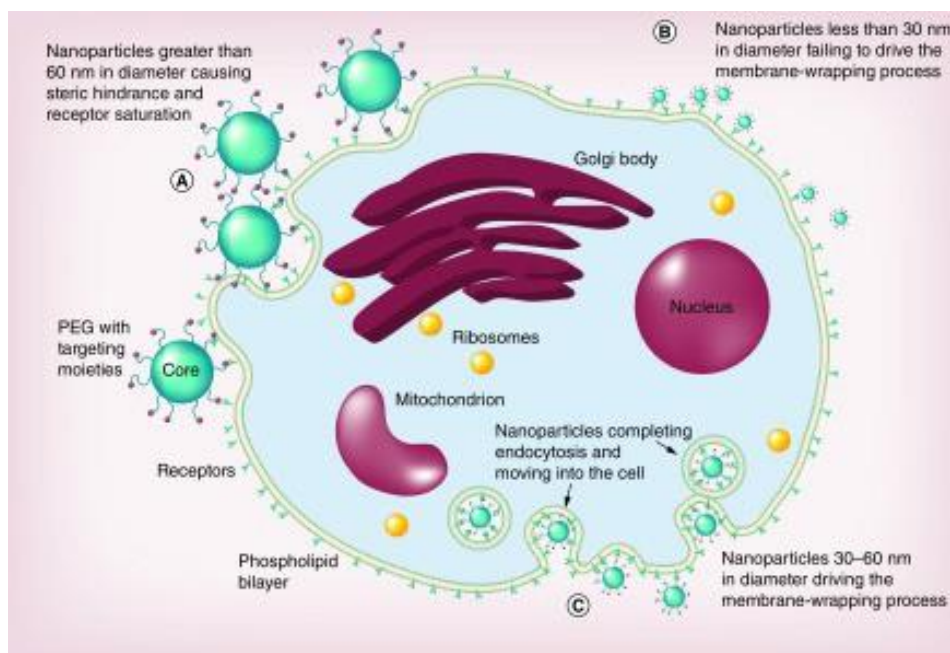
Figure 4.1. Schematic illustrating the role of size in cell membrane interaction and uptake. A) Nanoparticles over 60 nm in size can be limited by issues such as steric hindrance or receptor saturation. B) Nanoparticles under 30 nm in size cannot successfully drive the membrane-wrapping process. C) 30-60 nm is the "sweet spot" for membrane-wrapping and internalization to occur. Reproduced from [29] with permission.

Similarly, the shape of the nanoparticle can play a role in how it interacts *in vivo* with proteins but also cell surfaces. Studies have shown that an oblate sized nanoparticle is less likely to be targeted by macrophages, improving blood circulation times [30, 31]. It has also been shown that rod shaped nanoparticles exhibit more rapid uptake to spheres who are followed by cylinders and cubes. However, it should be noted that this was only the case in nanoparticles over 100 nm in size, those that were sub-100 nm behaved differently with spheres becoming taken up more quickly than rods [29, 32, 33].

The optimal size and shape for maximising uptake is dependent on the nanoparticle type being used and also the cell lines being experimented on or the area of the body being targeted [34].

A study investigating the effect of shape in silica nanoparticles found that the shape of the nanoparticle did not effect *in vivo* biocompatibility and cytotoxicity but it did effect where the nanoparticle was distributed and how it interacted *in vivo*. For this study two differently shaped mesoporous silica nanoparticles were designed that had similar particle dimensions, chemical compositions and surface charges with different aspect ratios, 1.5 and 5, short rod and long rod respectively. These nanoparticles were unable to cross the blood-brain barrier or spread into peripheral sites such as lymph nodes. Longer particles had faster clearance rates and more likely to accumulate in the spleen as opposed to the liver like the shorter particles [35]. Generally, the size, surface chemistry and nanoparticle type remain constant and the shape changes but as mentioned above, there is a lack of uniformity in the studies conducted leading to gaps in the knowledge base that still require investigation.

4.1.2 Effect of nanoparticle ligand type and density on cell interactions

Surface chemistry is also influential at the cell surface-nanoparticle interface [36-38]. Researchers will often coat the nanoparticle with PEG groups to avoid opsonisation in order to improve biodistribution [39-41] and passive targeting [42, 43], and the PEG may also functionalized with ligands for active targeting [40, 44]. This has been shown in spherical and rod shaped particles to increase circulation time as it reduces the rate of mononuclear phagocytes by creating a steric hydrophilic shield around the particle which stops plasma proteins adhering to it [45].

The type of ligand and its surface density has also been shown to affect the behaviour of the nanoparticle *in vivo* [36, 46]. The density of the coverage of the nanoparticle with a ligand and its arrangement can also negatively impact cell binding and greatly slow uptake [47-49].

This was shown with gold nanoparticles by Elias *et al*. Their study involved conjugating a range of different amounts of ligands/SPIO (0, 11.5, 23, 30.2 and 35.8). It appears that an intermediate number of ligands/SPIO was optimal with 23 exhibiting higher cell labelling compared to the other systems tested [46]. This would suggest that more is not necessarily better and in reality there will be an optimal ligand density for cell interactions. In a different study, nanoparticles were functionalized with different densities of folate and the internalisation in human epithelial mouth carcinoma cells (KB) cells was assessed using flow cytometry [50]. Higher loading on the nanographene oxide surface led to higher internalization *in vitro*, unlike the findings in the previous example. The *in vivo* results showed a similar trend with differences being explained with the extra barriers that must be overcome *in vivo*. They concluded that below a critical concentration there was no benefit and by greatly surpassing the critical concentration there were no major benefits, suggesting that *in vitro* results do not necessarily predict *in vivo* outcomes. It should be noted that internalization was always observed indicating that regardless of the ligand density there will be non-specific interactions as observed in Chapter Three.

As mentioned, the ligand arrangement is also important with clustering being shown to impact internalization and uptake. In polymer micelle nanoparticles the targeting efficiency was enhanced by increasing folate ligand clusters [51]. By having the ligands presented in clusters as opposed to a more dispersed manner an increase in epithelial cell uptake *in vitro* was seen.

It should be noted a link between ligand density and arrangement was seen where in systems with low density a dispersed arrangement had higher uptake. A similar study also showed improved uptake *in vivo* with dendrimers containing folate clusters on their surface [52].

These findings might only be applicable with folate targeting as folate receptors appear to form in discrete clusters on cell-surfaces. They also demonstrate a clear advantage that biorthogonal targeting can have as the cell-surface receptors are generated in a concentration dependent manner through unnatural sugars. It should be noted that size and shape influence the effect of surface chemistry as this effects ligand presentation for binding [53, 54].

4.1.3 Effect of nanoparticle charge on cell interactions

The charge on the ligands can also influence biological interactions [14, 22, 23, 55]. Neutral systems have been shown to undergo fewer non-specific interactions, whilst both negatively and positively charged systems having increased uptake and in some cases increased cytotoxicity. Studies have shown charged iron oxide nanoparticles get taken up better over their uncharged counterparts [56]. The cationic dextran covered magnetite system exhibited better uptake in HeLa cells. This is because the cationic nanoparticles studied appear to cause plasma-membrane disruption to a greater extent which facilitates internalization [57]. Another explanation is that the positively charged nanoparticles depolarize the negatively charged membrane. This is hypothesised to cause a Ca^{2+} influx and cell death but further studies are required to better understand what is occurring at the cell-nanoparticle interface, TEM conducted by Arvizo *et al.* did not demonstrate membrane disruption [22].

The improved uptake with positively charged nanoparticles was confirmed in eight different cell lines when the uptake and trafficking of chitosan-based nanoparticles were assessed [55]. The driving factor behind improved amount and rate of cellular uptake of cationic nanoparticles appears to be electrostatic forces. The neutral chitosan nanoparticles were deemed more suitable for delivering drugs that need longer half-lives.

Alternatively, negatively charged nanoparticles appear to diffuse quicker into tissue so might be more appropriate for drugs that need to penetrate further into tissue to exhibit their effect [58].

It should be noted that work by Chung *et al.* have shown with mesoporous silica nanoparticles that the effect of charge on cell uptake is cell type and surface charge dependent [59]. It would appear that this is another avenue to pursue to get a better idea of how charge can be utilised for improved uptake.

4.1.4 Effect of particle attributes on click chemistry in biological systems for delivery

The area of particular interest to this project are nanoparticles being specifically targeted to a cell surface for covalent attachment to a click group on the cell surface installed through metabolic labelling with an unnatural sugar. This is opposed to other more commonly used affinity based approaches such as folate targeting [60, 61] or antibody-antigen targeting [62, 63]. Before 2012, the majority of articles describing the use of biorthogonal chemistry were of small molecule probes attaching onto cell surfaces to track and visualise biological processes without interfering with the natural processing of the cell [64-69].

There are some studies that have utilised these techniques for clinical diagnostic purposes such as clicking PET [70-72] and MRI [73] agents to cells of interest. For even larger molecular agents, size does not appear to be a limitation to click-coupling to cells.

The first report of attaching a nanoparticle to cells using the metabolic labelling and click chemistry approach were Koo *et al.* who reported liposomal delivery (Figure 4.2) [74]. They doped liposomes with a DBCO functionalized phospholipid which would present the cyclooctyne on the surface of the nanoparticle.
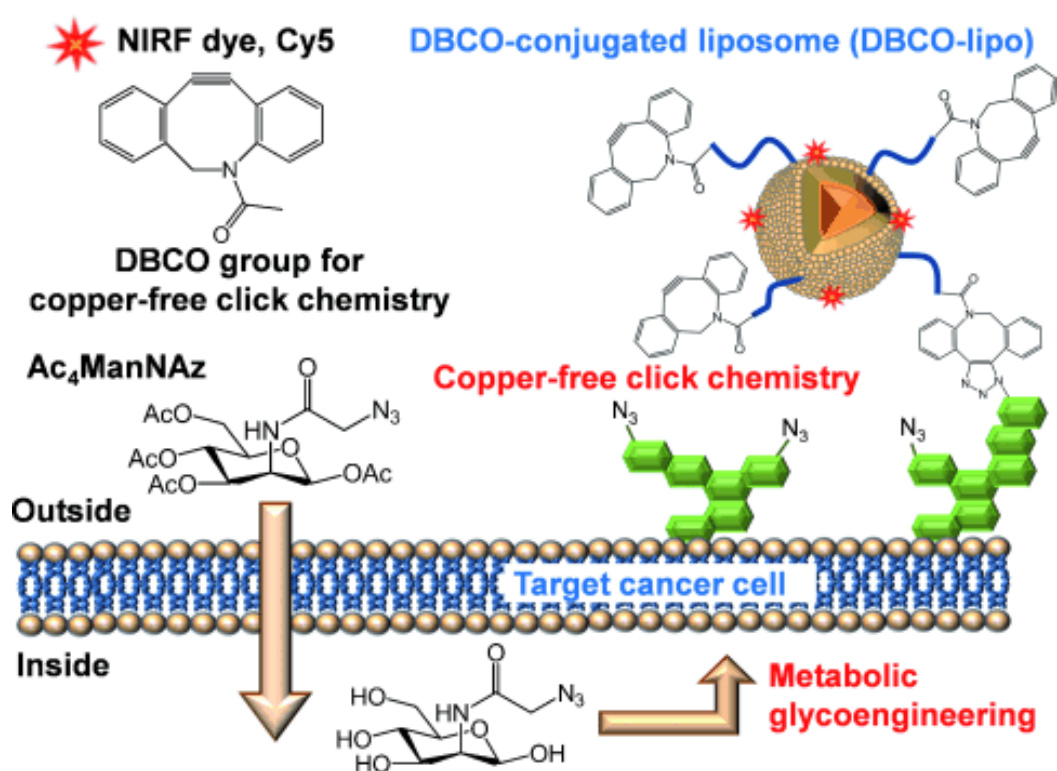
Figure 4.2. Schematic of the study by Koo *et al.* The azide sugar is metabolised by a cell and expressed on the target cancer cell surface. The azide groups are targeted with the DBCOs on the surface of the liposome. Reused with permission from [74] .

The surface cyclooctyne group could then target azido groups generated on a cell surface after metabolic labelling by intratumoral injection of the cells with Ac₄MaNAz. They were able to significantly increase liposomal accumulation at the tumor site paving the way for future similar studies. They also showed that the binding success of this technique was closely related to azide generation based on sugar concentration before nanoparticle addition. According to findings in Chapter Three, one would expect the lipophilic DBCO end groups to cause some non-specific interactions with cell surfaces.

This study was followed by a different type of nanoparticle being delivered to tumors, In this case, Lee *et al.*, created a BCN containing glycol chitosan nanoparticle that also displayed specific targeting when combined with metabolic labelling [75].

They too were able to greatly increase tumor accumulation when compared to passive accumulation. A third report by Wang *et al.* used a different nanoparticle bearing azide groups after developing a DBCO-Mannose that could be metabolically incorporated [76]. They synthesised ultra-small silica nanoconjugates bearing azido groups which could also specifically target labelled cells and increase nanoparticle accumulation.

The fourth and final report that has delivered nanoparticles using biorthogonal chemistry also chose glycol chitosan nanoparticles as their carrier and they showed that the targeting was possible in a wide range of cell types and *in vivo* [77]. Their system even outperformed an established active peptide targeting method. Unlike the cubosomes discussed in Chapter Three, no issue with non-specific binding was mentioned *in vitro* or *in vivo*. With the limited studies in the field there is a clear lack of knowledge in the interactions on the cell surface with these nanoparticle carriers.

It is of great interest to further this understanding in order to better develop nanoparticles, reactive groups and unnatural sugars to improve these techniques as these mentioned studies show great promise as an alternative to current traditional active targeting techniques.

There has not been any insight regarding the effect that the properties of the nanoparticles have over the success of this technique. As mentioned, the studies to date have all shown that sugar concentration and reporter generation play a critical role in nanoparticle binding but there is no information on the success of binding particles to cells with systematic change in variables including different shapes, sizes and types of nanoparticles.

The nanoparticles used have all been PEGylated creating a hydrophilic region around their surface and were relatively small. The liposomes and silica nanoconjugates were determined to be 90 and 50 nm respectively whereas the glycol chitosan nanoparticles were more similar to cubosomes at around 200 nm.

This would indicate that, contrary to the hypothesis arising from the data in the previous chapter, size is not a key contributor but without further studies it is difficult to come to any conclusions as a whole range of factors could be influencing the successful surface clicking. There are limited studies that have shown nanoparticle targeting and binding that use metabolic labelling and copper-free click chemistry resulting in a lack of fundamental knowledge of the key variables. One area that has not been investigated is the location of the click group along the glycoprotein following successful metabolic labelling of a cell. As described in Chapters One and Three, the unnatural sugar is broken down and repurposed by the cell. The end result is being incorporated into the structure of a surface bound glycoprotein.

There is no control over this process and the location of the sugar [78-80]. This means that the click group attached to the sugar might not be easily accessible for nanoparticles to click with as they could be surrounded by larger groups or too close to the cell-surface, which could lead it to being in difficult to access positions. This could lead to complications when trying to click on a nanoparticle if it is too large or the respective click group on its surface is not able to reach the click group on the glycoprotein. Further studies in this area would be helpful in understanding and utilising these techniques in a greater capacity.

In this chapter, the effect of nanoparticle size was investigated to give insight into why the cubosomes were unable to overcome non-specific interactions. The liposomes in Chapter Three appeared to exhibit less non-specific binding than the cubosomes. This is believed to be due to their size and also potentially their different surface properties (with PEGylation of the liposomes providing a more coherent barrier against non-specific interactions with cells compared to Pluronic on the cubosomes) and for this reason smaller liposomes were formulated to further investigate the effect of size on attachment of nanoparticles onto a cell surface. Furthermore, micelles were generated from the same phospholipids by increasing the molar concentration of PEG phospholipid in the dispersion. It has been shown that by controlling the amount of PEGylated phospholipid that makes up the lipid component of a liposomal dispersion allows control over the type of particle formed and its size [81]. Concentrations of PEGylated phospholipids over 20 mol % lead to the formation of micelles approximately 65 nm in size. If the amount is increased to 100 mol % the size can be reduced to 18 nm. The micelles were expected to exhibit similar shape and surface properties to the liposomes but be much smaller than the liposomes providing a series of particles where the primary variable was size.

To probe the impact of azide density on cellular interactions, the same micelles and liposomes were prepared with different amounts of phospholipid-PEG-azide were used.

In addition to the lipid based particles, to further probe the impact of size on particle reactivity with cells, a range of size-controlled azide-quantum dots (prepared by collaborators at Warwick University) were investigated in order to fill in the size gap between the micelles and liposomes, thereby to produce a more comprehensive idea on the effect of size.

Ideally, these experiments will lay the foundation for future work to gain better understanding of cell surface-nanoparticle interactions specifically with metabolic labelling and copper-free click chemistry to further expand the uses in this field.

4.2 Hypotheses and aims

The following hypotheses were tested in this Chapter;

1. That the smaller nanoparticles will show improved specific cell-surface clicking due to having better access to the reactive site.

2. That a higher azide concentration on a nanoparticle surface will result in higher overall specific cell-surface clicking due to having more reactive groups available.

In order to investigate these hypotheses, the following aims will be achieved:

1. To determine the ability with which differently sized nanoparticles can bind to metabolically-labelled cell surfaces using TIRF microscopy.

2. To determine the ability with which nanoparticles with different surface azide concentrations can bind to metabolically–labelled cell surfaces using TIRF microscopy.

4.3 Materials and methods

4.3.1 Materials

Please refer to Chapter Two for materials used in this chapter. Below are some specific materials that were used.

4.3.1.1 Quantum dots (QDs)

Four different sized QD samples were supplied by collaborators at University of Warwick. Sarah-Jane Richards from Professor Matthew Gibson's lab synthesised azide-polymer functionalized gold nanoparticles with the core sizes being 15, 30, 45 and 60 nm. The QDs were also surface functionalized with the fluorescent tag Hostasol (wavelengths of excitation/emission maxima are 460/530). The concentration of QD in water was determined to be ~0.3 mM. Sizes and fluorescent tagging was confirmed with DLS and fluorescence spectroscopy.

4.3.2 Methods

Please refer to Chapter Two for general methods used in this chapter. Below are some specific methods that were used.

4.3.2.1 Micelle preparation

Phospholipid based micelles were prepared using ratios determined by Kaminskas *et al.* [81] to ensure their small size. This involved mixing the appropriate amounts of PEG$_{2000}$ containing phospholipids and Rhodamine B conjugated phospholipid (560/583) at the desired concentration in chloroform.

The chloroform was then removed overnight through the use of nitrogen gas and a vacuum oven before excess 1x pH 7.4 PBS was introduced and the system was sonicated using a Misonix S-400. The ratio of lipid:water was 1:10. The samples are described below in Table 4.2.

Table 4.2. Composition and given sample name for the micelle dispersions studied.

Sample name	Composition	Mol ratios of lipid portion
1.5 mol % Azide Micelles	N_3-DSPE-PEG$_{2000}$: DSPE-PEG$_{2000}$	1.5:98.5
Azide Micelles	N_3-DSPE-PEG$_{2000}$: DSPE-PEG$_{2000}$	15:85
Micelles	DSPE-PEG$_{2000}$	100

4.3.2.2 Liposome preparation

Phospholipid-based liposomes were also prepared using ratios determined by previous work by Kaminskas *et al.* [81] to control their size. This involved mixing the required concentration of PEG containing phospholipids with DSPC and Rhodamine B-phospholipid (560/583) in chloroform. The chloroform was then removed overnight through the use of nitrogen gas and a vacuum oven before excess 1x pH 7.4 PBS was introduced and the system was sonicated using a Misonix S-400. The ratio of lipid:water was 1:10 (w/v). The samples are described below in Table 4.3.

Table 4.3. Composition and given sample name for the liposomal dispersions studied.

Sample name	Contents	Mol ratio of lipid portion
1.5 mol % Azide Liposomes	N_3-DSPE-PEG$_{2000}$:DSPC	1.5:98.5
Azide Liposomes	N_3-DSPE-PEG$_{2000}$:DSPC	15:85
1.5 mol % PEG Liposomes	DSPE-PEG$_{2000}$:DSPC	1.5:98.5
PEG Liposomes	DSPE-PEG$_{2000}$:DSPC	15:85

4.4 Results

4.4.1 Effect of size on nanoparticle clicking to a cell surface

Previous experiments displayed differences in cell-surface interactions between clickable cubosomes and liposomes therefore a range of nanoparticles with different sizes, Table 4.4, were prepared and assessed in the same manner as described in section 4.3.2. Fluorescent micelles and liposomes were created and azide bearing quantum dots (QD) were obtained from Matt Gibson's group at Warwick University (UK).

Table 4.4. Size of micelles, liposomes and QDs determined with DLS (Volume-based particle size distribution (mean $\pm$ SD, n =3)).

Nanoparticle	Size (nm)	PDI
Micelles	14 $\pm$ 3	0.476
Azide Micelles	10 $\pm$ 3	0.508
PEG Liposomes	96 $\pm$ 65	0.228
Azide Liposomes	121 $\pm$ 90	0.53
15 nm QD	14 $\pm$ 3	0.227
30 nm QD	43 $\pm$ 1	0.243
45 nm QD	49 $\pm$ 3	0.187
60 nm QD	78 $\pm$ 1	0.233

It should be noted that the QD exhibit different sizes to their gold core. For the purpose of this study they still add important information regarding the role of size by filling the gap between the sizes of the micelles and liposomes.

These differently sized nanoparticles were then incubated with cells treated with DBCO-mannose for 24 hours before being imaged using TIRF and being further analysed through the in-house script. The imaging data indicates that there is a relationship between size of nanoparticle and surface interactions with the smaller systems performing better (Figure 4.3). All liposome, micelle and QD samples exhibited less non-specific binding than the cubosomes and liposomes from Chapter Three.

It should be noted that the liposomes showed less non-specific binding than those reported in Chapter Three. This could be due to the higher loading of PEG_{2000}-phospholipid in the systems in Figure 4.3 resulting in a less hydrophobic surface (15 mol % of total phospholipid in the liposomes in Figure 4.3 compared to those in Chapter Three which had only 2 mol %).

A)
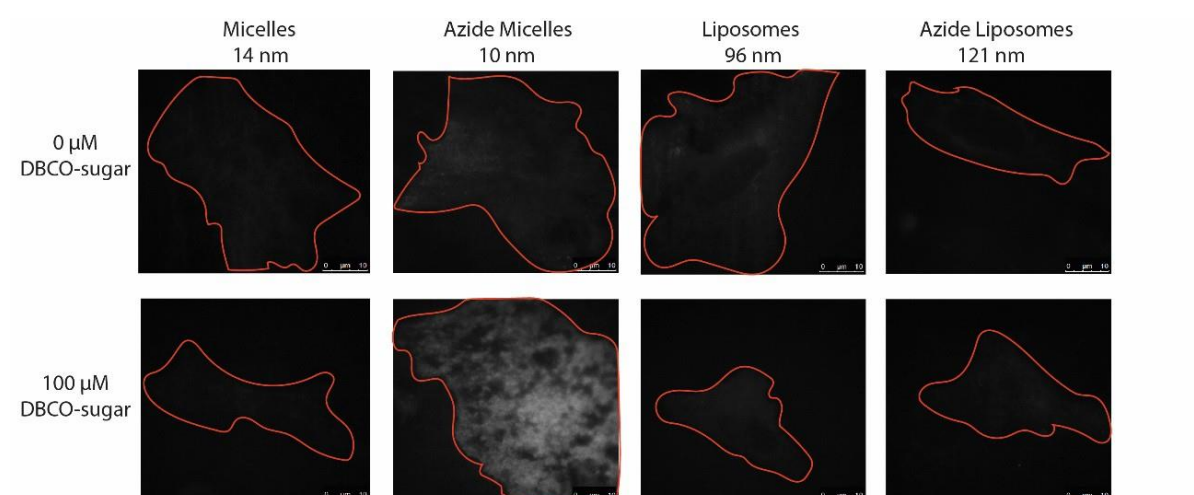
B)
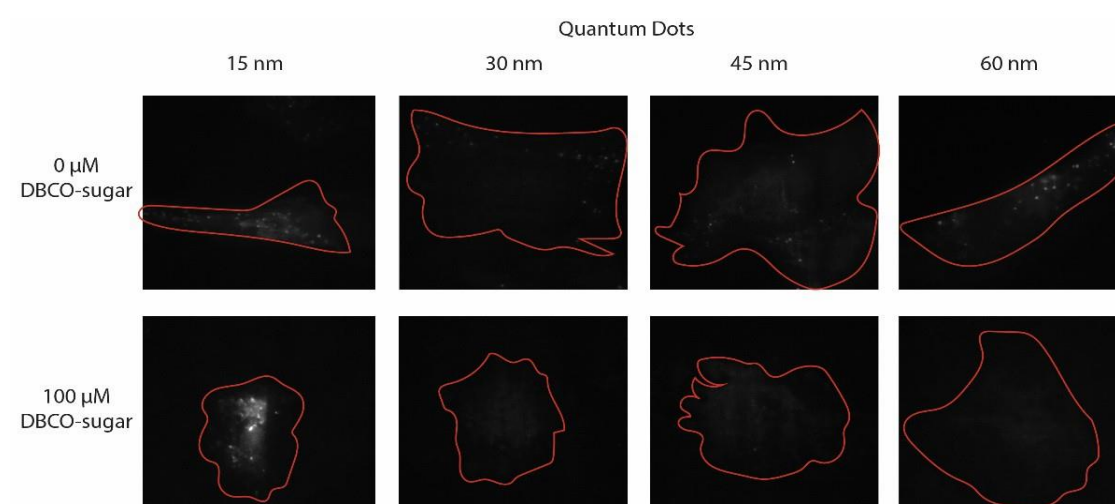
Figure 4.3. TIRF images of A549 cells grown in DMEM media containing 100 µM of DBCO-Mannose treated with differently sized nanoparticles. A) phospholipid-based nanoparticles and B) quantum dots. The cells have been circled in red for clarity and are reflective of the area considered by the quantitative analysis script.

The phospholipid micelles (Figure 4.3A), show visually similar non-specific binding to the larger liposomes which would indicate that there is always some level of hydrophobic interaction occurring regardless of nanoparticle size. Similarly to the micelles and liposomes, all QD samples showed some level of non-specific interactions (Figure 4.3B). This suggests that regardless of nanoparticle size or type there will be non-specific binding to cell surfaces. As can be seen in Figure 4.3, the two smaller azide bearing systems, Azide micelles and 15 nm QDs, show specific binding. In both cases there is greater coverage and fluorescence in the systems treated with DBCO-Mannose when compared to those without the sugar or azide group. Additionally, the larger sizes do not appear to exhibit specific binding as both the 0 µM and 100 µM DBCO-mannose images look similar. The contrast in the images was then quantified using the analysis script and the mean fluorescence of each system can be seen in Figure 4.4.

Interestingly, in Figure 4.3, the micelles and liposomes appear to have similar levels of non-specific binding but upon further analysis this appears to not be the case. Figure 4.4 indicates that the micelles have a much higher average MFI than the liposomes.

Quantitatively , the azide micelles showed high specific binding ability with a ~2 fold increase in average mean fluorescence intensity (MFI) when compared to all the other phospholipid based systems (Figure 4.4A).

A)
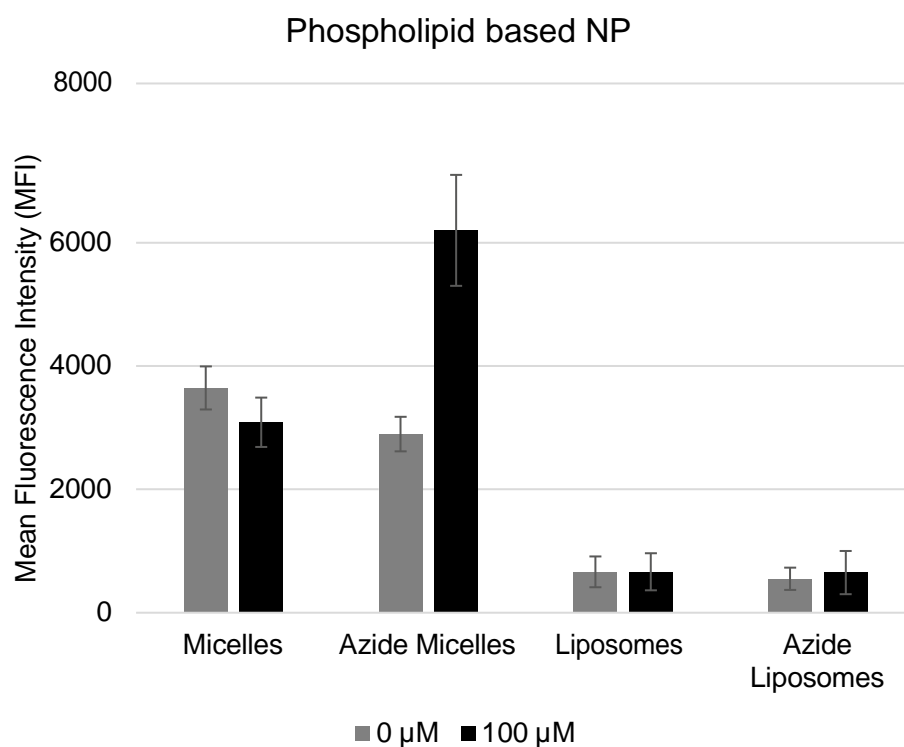
B)
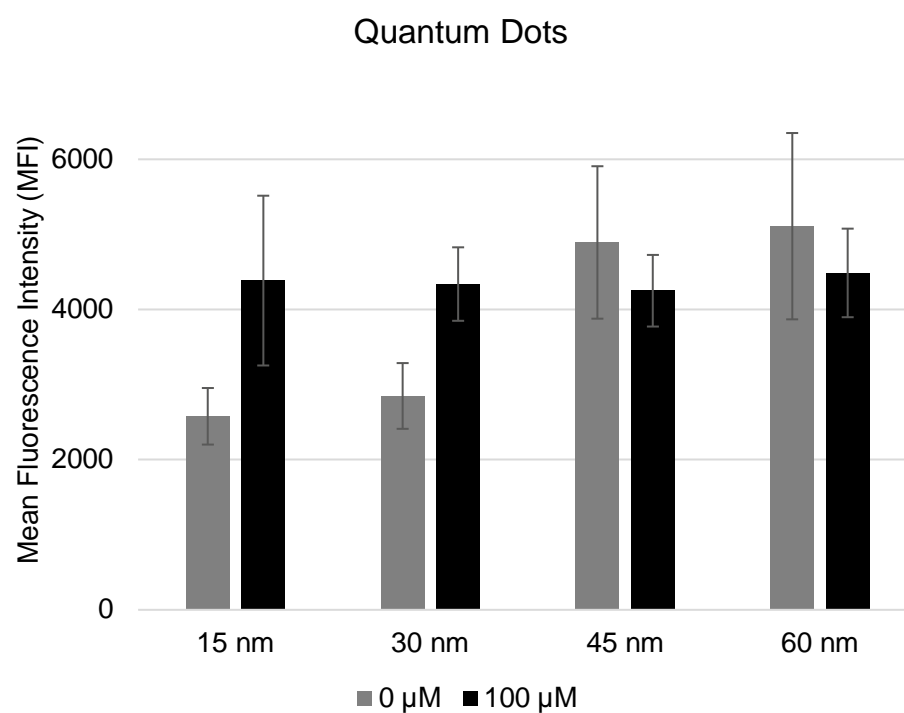
Figure 4.4. Average mean fluorescence intensity (MFI) ± SD (n > 15) of the differently sized nanoparticle dispersions. A) Phospholipid based nanoparticles and B) Quantum dots. The values were determined using Cameron Nowell's analysis script.

Surprisingly, the average mean fluorescence intensity (MFI) for the liposomal systems was considerably lower than all other systems. This would suggest that there are other factors, such as shape and surface properties, apart from size influencing what takes part at the cell surface. Another potential reason for the lower average MFI for the liposomes compared to the micelles is the role their bilayer plays. Although no SAXS data is available one would assume the liposomes are unilamellar like those imaged in Chapter 3. This potentially reduces surface area of contact when compared to cubosomes and micelles which could result in less non-specific interactions and cell membrane fusing, which has been seen before in lipids. The 15 and 30 nm QDs also showed specific binding with approximately a 1.6 and 1.5 fold increase in average MFI respectively (Figure 4.4B). The 45 and 60 nm QDs experienced a high amount of non-specific binding. This could be expected as 30-60 nm is considered the ideal size for membrane wrapping and internalization [29]. As a result, regardless of surface chemistry the size is likely playing a key role in non- specific binding and therefore affecting the ability to specifically surface bind.

4.4.2 Effect of nanoparticle azide concentration on surface clicking

Micelles and liposomes were prepared with different ratios of azide-functionalized to azide-free PEG phospholipid to determine whether the amount of azide in the formulation also affected surface binding. A low loading of azide on each nanoparticle was created with 1.5 mol % of N_3-DSPC-PEG$_{2000}$ of the total DSPE-PEG$_{2000}$ in the sample for comparison with the 15 mol % high loading of the particles described in Section 4.4.1 above. Their size distributions were determined and are shown in Table 4.5.

Table 4.5. Volume-based particle size distribution measurements of lower PEG_{2000} phospholipid loaded micelles and liposomes (mean ± SD, n =3) determined by DLS of the different dispersions.

Nanoparticle	Size (nm)	PDI
Micelles	14 ± 3	0.476
1.5 mol % Azide Micelles	13 ± 3	0.371
1.5 mol % PEG Liposomes	52 ± 27	0.533
1.5 mol % Azide Liposomes	101 ± 56	0.231

Once characterised these nanoparticles were introduced to A549 cells in the same manner as the previous cell experiments. The micelles and liposomes with ten-fold less PEG phospholipid had similar sizes to those with the higher loading. It should be noted that the liposomes with 1.5 mol % DSPC-PEG_{2000} were half the size of the previously tested liposome and this could influence the cell-surface interactions.

This is likely to influence binding and non-specific interactions. The TIRF images show that there is not a large difference seen in binding when the azide concentration was altered (Figure 4.5).
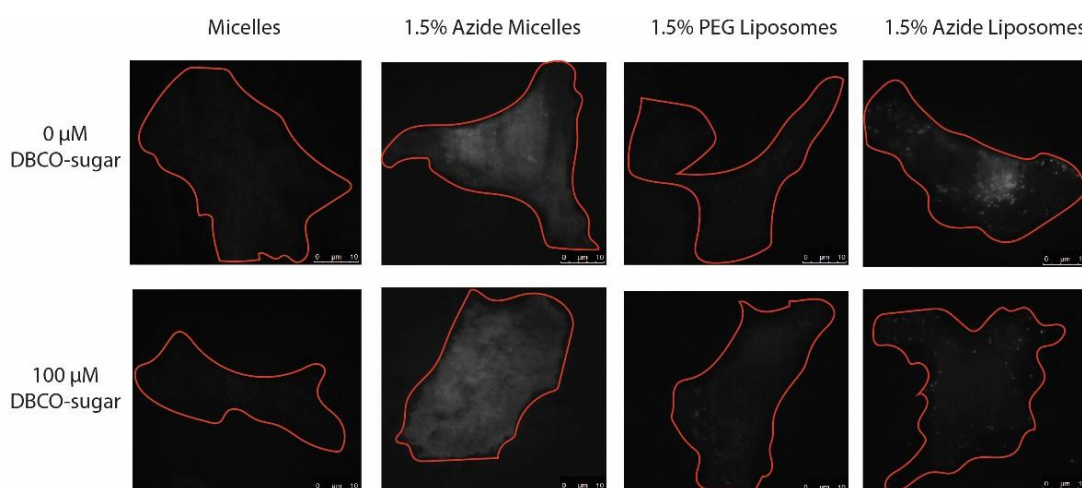
Figure 4.5. TIRF images of A549 cells grown in DMEM media containing 100 µM of DBCO-Mannose treated with micelles and liposomes with low azide loading. The cells have been circled in red for clarity and is reflective of the area analysed by the script.

Similar to the behaviour of the higher loading liposomes in Figure 4.3A, it can be seen that the lower loading liposomes behaved similarly even with a tenfold decrease in the concentration of PEG_{2000} or azide being present. Importantly, the 1.5% azide micelles in Figure 4.5 appeared to have higher non-specific binding than the 15% azide micelles (Figure 4.3A). It visually looks as if the non-specific binding has increased to match any specific binding that might be occurring resulting in an inability to differentiate them. Therefore, it would suggest that much like size, azide density on the nanoparticle's surface plays a role in the ability to specifically bind.

The average MFI calculated from the TIRF images can be seen in Figure 4.6. These reflect the imaging data above, showing a high amount of non-specific binding in the 1.5% azide micelle system and again indicating lower non-specific binding for the liposomal dispersions when compared to micelles. The lack of difference between the 1.5% azide micelles exposed to labelled and unlabelled cells is indicative of a threshold level of azide required on the particles to either provide significant levels of specific binding and/or to prevent non-specific interactions with the cells.
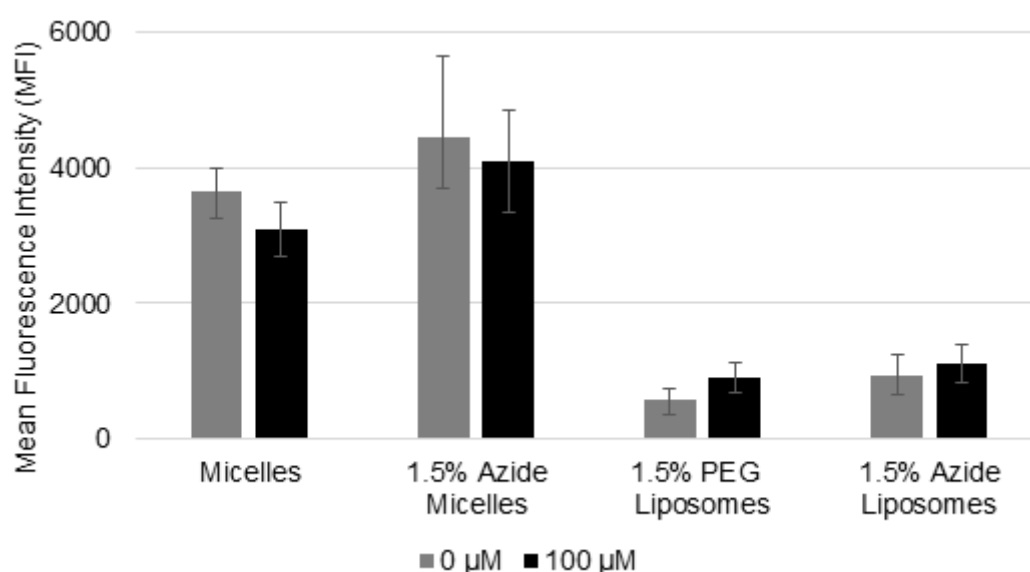
Figure 4.6. Average mean fluorescence intensity (MFI) ± SD (n > 15) of the lower PEG$_{2000}$ phospholipid loaded micelles and liposomes. The values were determined using Cameron Nowell's analysis script.

4.5 Discussion

The studies support previous findings discussed above and show a clear connection with the size and ligand density of the nanoparticle and its interactions with a cell-surface.

4.5.1 Role of size and azide loading with non-specific binding

Size does not seem to influence non-specific binding to the cell surface greatly. In regards to micelles and liposomes it would appear that size does not control the non-specific interactions as the smaller micelles have considerably higher mean cell-surface fluorescence when compared to the larger liposomes. This would indicate that there is another more dominant factor controlling the non-specific binding. The findings in Chapter Three would indicate that the size and hydrophobicity of the cubosomes led to the high non-specific binding seen. If the controlling factor is related to hydrophobic interactions one would expect that both the micelles and liposomes would show very low non-specific binding as they have PEG on their surface. In regards to the QDs tested there does appear to be a size dependent effect occurring, with the smaller the QD the less non-specific binding being determined. The differences seen are relatively small.

There are reports that link nanoparticle size with cell interactions *in vitro* and *in vivo*, these studies also stress the importance of having nanoparticles inside a "goldilocks" size range for optimal in vivo behaviour [82, 83].

The QD data is supported by the success of smaller molecule attachment using biorthogonal chemistry already heavily reported [68, 69, 84-88]. The phospholipid based nanoparticles do not follow previous observations with the larger liposomes exhibiting far less non-specific interactions with cells, indicating another factor is also influencing what occurs at the interface. It should be noted that other studies into nanoparticle systems and biorthogonal chemistry have not been reported to experience the same issues with non-specific cell binding, possibly because they describe studies straight into *in vivo* settings [74-77]. They do not describe the specific nature of the interaction with cell surfaces, nor do they discuss at all any issues of protein corona formation on the particles which could further complicate interpretation.

Of particular interest in the current study is the very low non-specific binding which is observed in all the liposomal dispersions. The low non-specific binding seen for liposomes in the current study would support the successful use of liposomes and biorthogonal chemistry *in vivo* by Koo *et al.* [74], however the lack of specific binding observed in our study for liposomes and large particles in general is not consistent with that report. The liposomes used in this chapter and Chapter Three may not be able to specifically bind due to having different surface properties compared to those used in the literature, different cell conditions, or other confounding factors at play that make the literature reports appear to selectively bind to tissues when the effect is not actually reflecting covalent binding per se. Specifically, the amount of PEGylation is likely to be different as is the location of the click groups which could lead to different cell surface-nanoparticle interactions reducing the ability of our liposomes to covalently click to the DBCO-groups. Additionally, the experiment conducted by Koo *et al.* was using azide-modified sugars and DBCO-liposomes which is the opposite of this study and this too could play a large role in the differences observed.

The systems with tenfold less azide loading showed similar results in regards to non-specific binding. Again, the small micelles had higher MFI compared to the larger liposomes further supporting that a factor other than size is affecting surface binding, requiring more research to be conducted.

4.5.2 Role of size and azide loading on specific binding

Only a few samples showed specific binding. We know from Chapter Three that the cells express DBCO, and it can be targeted with azide-Cy5, so the issue is with particle interactions, not the chemical target on the cell surface.

At higher azide loading both micelles and quantum dots under 30 nm provided specific binding. It is clear that size can play a role in enabling differences to emerge in the click attachment. For the smaller particles, increased specific binding could be a result of the ligand coating density and distribution. For the same total mass of lipid making up the dispersion, when the size of the nanoparticles are decreased the total surface area increases allowing for more space for the functional groups. As a result, they may experience less steric hindrance allowing for better availability [46, 61, 89].

Similarly, looking from the aspect of the DBCO groups on the cell surface that are being targeted, the smaller nanoparticles are likely to gain better access to the cell-surface glycoproteins that have been metabolically labelled without interacting with the cell membrane itself. This is an area of research in the metabolic labelling field that is still unexplored but important for nanoparticle delivery as the accessibility of the generated chemical reporters is one of the critical steps for successful clicking.

While azide is utilised in this context for its click capability, it also is hydrophilic and charged – which although might be favoured for colloidal stability, could also lead to interactions with charged residues on proteins in media confounding the anticipated behaviour. By lowering the amount of azide in the micelle dispersion this could have altered the surface chemistry that was favourable for specific interactions seen with 15 mol % loading. It appears that the change in surface charge and hydrophobicity may be playing a role [23, 26]. It has been shown that neutral or positively charged systems are better for cell surface interactions as cell membranes have negatively charged groups present [14, 57]. The reduced binding is supported by previous studies where ligand density plays a role in surface binding. It has been shown with antibodies and proteins that, up to a certain threshold, there is an increase in binding with an increase in ligand density on the nanoparticle [46, 89]. Alternatively, the loss of observed specific binding could be due to there being less available azide groups to click to the DBCO expressed on the cell-surfaces.

In the majority of published studies documenting the use of biorthogonal chemistry for nanoparticle targeted delivery there is little information provided on the extent of nanoparticle surface functionalisation with little indication of the amount of azide present or where the functional groups are located. This is even larger of an issue with self-assembled systems as there is uncertainty about the location of the reactive groups. They can be unavailable by being internalized in the lipid portion or if surface bound on the internal surface of the hydrophilic core of the liposome. Additionally, the PEG chains that are often used for linking can fold over themselves or cross-link making the end group unavailable for the click reaction [90-92]. That said, in the experiments detailed above there appears to be a benefit with a higher loading of azide for the micelles, indicating that this plays some role in surface binding.

One method of gaining some control over the location of the functional groups and improving their availability is through smart stabiliser design. Using a high molecular weight stabiliser to preclude it from being in the internal structures there is a greater chance that it is bound to the available for clicking [93-95]. To this end, we explore in Chapter Five the use of novel lipidated polymers to stabilise cubosomes and assess the click capabilities of an azide containing variant of these new polymers.

4.6 Conclusion

Size is a factor in nanoparticle binding to a surface when utilising metabolic labelling and copper-free click chemistry, for hard particles such as quantum dots. For self-assembled systems, the correlation was less clear – although micelles showed high non-specific binding compared to larger liposomes, they also showed clear specific binding, whereas liposomes also showed low or no specific binding.

The nanoparticles under 30 nm, both lipid or metal based, showed significantly more surface binding when compared to the same system without treatment of the DBCO-mannose. In contrast, those larger than 30 nm, like the cubosomes previously described in Chapter Three, exhibited no specific binding. The average MFI determined for these larger systems was similar for both treated and untreated cells. Additionally, it appears the role of nanoparticle azide concentration is to be considered if attempting to formulate a nanoparticle that wishes to utilise bioorthogonal chemistry for improved retention. A tenfold decrease in azide molar concentration caused micelles to no longer demonstrate specific binding indicating that a certain minimum azide concentration is required for the covalent attachment to be successful.

These studies are indicative of the need to further study the systematic changes in structural and formulation variables regarding nanosystems utilising metabolic labelling and copper-free click chemistry for targeting. Ideally, a range of nanoparticles with different sizes and shapes would be studied on a range of cell lines in order to create a clearer picture of the formulation space available to achieve specific binding.

4.7 References

1. Gu, F.X., et al., *Targeted nanoparticles for cancer therapy.* Nano Today, 2007. **2**(3): p. 14-21.

2. Friedman, A.D., et al., *The Smart Targeting of Nanoparticles.* Current pharmaceutical design, 2013. **19**(35): p. 6315-6329.

3. Anu Mary, E. and Saravanakumar, M.P., *A review on the classification, characterisation, synthesis of nanoparticles and their application.* IOP Conference Series: Materials Science and Engineering, 2017. **263**(3): p. 032019.

4. Kukowska-Latallo, J.F., et al., *Nanoparticle targeting of anticancer drug improves therapeutic response in animal model of human epithelial cancer.* Cancer research, 2005. **65**(12): p. 5317-5324.

5. Salata, O., *Applications of nanoparticles in biology and medicine.* Journal of Nanobiotechnology, 2004. **2**(1): p. 3.

6. Shaikh, J., et al., *Nanoparticle encapsulation improves oral bioavailability of curcumin by at least 9-fold when compared to curcumin administered with piperine as absorption enhancer.* European Journal of Pharmaceutical Sciences, 2009. **37**(3-4): p. 223-230.

7. Prestidge, C.A. and Simovic S., *Nanoparticle encapsulation of emulsion droplets.* International journal of pharmaceutics, 2006. **324**(1): p. 92-100.

8. Blanco, E., et al., *Principles of nanoparticle design for overcoming biological barriers to drug delivery.* Nature biotechnology, 2015. **33**(9): p. 941.

9.   Moghimi, S.M., et al., *Factors controlling nanoparticle pharmacokinetics: an integrated analysis and perspective.* Annual review of pharmacology and toxicology, 2012. **52**: p. 481-503.

10.   Tenzer, S., et al., *Nanoparticle size is a critical physicochemical determinant of the human blood plasma corona: a comprehensive quantitative proteomic analysis.* ACS nano, 2011. **5**(9): p. 7155-7167.

11.   Duan, X. and Li, Y., *Physicochemical characteristics of nanoparticles affect circulation, biodistribution, cellular internalization, and trafficking.* Small, 2013.**9**(9-10): p. 1521-1532.

12.   Li, S.-D. and Huang, L., *Pharmacokinetics and Biodistribution of Nanoparticles.* Molecular Pharmaceutics, 2008. **5**(4): p. 496-504.

13.   Chithrani, B.D., et al., *Determining the size and shape dependence of gold nanoparticle uptake into mammalian cells.* Nano letters, 2006. **6**(4): p. 662-668.

14.   Salatin, S., et al., *Effect of the surface modification, size, and shape on cellular uptake of nanoparticles.* Cell Biology International, 2015. **39**(8): p. 881-890.

15.   Karataş, Ö.F., et al., *Interaction of gold nanoparticles with mitochondria.* Colloids and Surfaces B: Biointerfaces, 2009. **71**(2): p. 315-318.

16.   Tahara, K., et al., *Improved cellular uptake of chitosan-modified PLGA nanospheres by A549 cells.* International Journal of Pharmaceutics, 2009. **382**(1): p. 198-204.

17.   Wilhelm, C., et al., *Intracellular uptake of anionic superparamagnetic nanoparticles as a function of their surface coating.* Biomaterials, 2003. **24**(6): p. 1001-1011.

18.   Oyewumi, M.O., et al., *Comparison of cell uptake, biodistribution and tumor retention of folate-coated and PEG-coated gadolinium nanoparticles in tumor-bearing mice.* Journal of Controlled Release, 2004. **95**(3): p. 613-626.

19.   Amidi, M., et al., *Chitosan-based delivery systems for protein therapeutics and antigens.* Advanced Drug Delivery Reviews, 2010. **62**(1): p. 59-82.

20.   Zhang, Y., et al., *Surface modification of superparamagnetic magnetite nanoparticles and their intracellular uptake.* Biomaterials, 2002. **23**(7): p. 1553-1561.

21.   Chiu, Y.-L., et al., *The characteristics, cellular uptake and intracellular trafficking of nanoparticles made of hydrophobically-modified chitosan.* Journal of Controlled Release, 2010. **146**(1): p. 152-159.

22.   Arvizo, R.R., et al., *Effect of nanoparticle surface charge at the plasma membrane and beyond.* Nano letters, 2010. **10**(7): p. 2543-2548.

23.   He, C., et al., *Effects of particle size and surface charge on cellular uptake and biodistribution of polymeric nanoparticles.* Biomaterials, 2010. **31**(13): p. 3657-3666.

24.   Sonavane, G., et al., *Biodistribution of colloidal gold nanoparticles after intravenous administration: effect of particle size.* Colloids and Surfaces B: Biointerfaces, 2008. **66**(2): p. 274-280.

25.   Decuzzi, P., et al., *Size and shape effects in the biodistribution of intravascularly injected particles.* Journal of Controlled Release, 2010. **141**(3): p. 320-327.

26.   Albanese, A., et al., *The Effect of Nanoparticle Size, Shape, and Surface Chemistry on Biological Systems.* Annual Review of Biomedical Engineering, 2012. **14**(1): p. 1-16.

27.   S., T.G., et al., *Circulation and distribution of gold nanoparticles and induced alterations of tissue morphology at intravenous particle delivery.* Journal of Biophotonics, 2009. **2**(5): p. 292-302.

28.   Perrault, S.D., et al., *Mediating Tumor Targeting Efficiency of Nanoparticles Through Design.* Nano Letters, 2009. **9**(5): p. 1909-1915.

29.   Hoshyar, N., et al., *The effect of nanoparticle size on in vivo pharmacokinetics and cellular interaction.* Nanomedicine, 2016. **11**(6): p. 673-692.

30.   Champion, J.A. and Mitragotri, S., *Role of target geometry in phagocytosis.* Proceedings of the National Academy of Sciences of the United States of America, 2006. **103**(13): p. 4930-4934.

31.   Chithrani, B.D., et al., *Determining the Size and Shape Dependence of Gold Nanoparticle Uptake into Mammalian Cells.* Nano Letters, 2006. **6**(4): p. 662-668.

32.   Zhao, Y., et al., *A comparison between sphere and rod nanoparticles regarding their in vivo biological behavior and pharmacokinetics.* Scientific Reports, 2017. **7**(1): p. 4131.

33.   Niikura, K., et al., *Gold Nanoparticles as a Vaccine Platform: Influence of Size and Shape on Immunological Responses in Vitro and in Vivo.* ACS Nano, 2013. **7**(5): p. 3926-3938.

34.   Toy, R., et al., *Shaping cancer nanomedicine: The effect of particle shape on the in vivo journey of nanoparticles.* Nanomedicine (London, England), 2014. **9**(1): p. 121-134.

35.   Huang, X., et al., *The Shape Effect of Mesoporous Silica Nanoparticles on Biodistribution, Clearance, and Biocompatibility in Vivo.* ACS Nano, 2011. **5**(7): p. 5390-5399.

36.   Ayush, V. and Francesco, S., *Effect of Surface Properties on Nanoparticle–Cell Interactions.* Small, 2010. **6**(1): p. 12-21.

37.   Xiao, K., et al., *The effect of surface charge on in vivo biodistribution of PEG-oligocholic acid based micellar nanoparticles.* Biomaterials, 2011. **32**(13): p. 3435-3446.

38.   Aggarwal, P., et al., *Nanoparticle interaction with plasma proteins as it relates to particle biodistribution, biocompatibility and therapeutic efficacy.* Advanced drug delivery reviews, 2009. **61**(6): p. 428-437.

39.   Li, Y.-P., et al., *PEGylated PLGA nanoparticles as protein carriers: synthesis, preparation and biodistribution in rats.* Journal of controlled release, 2001. **71**(2): p. 203-211.

40.   Otsuka, H., et al., *PEGylated nanoparticles for biological and pharmaceutical applications.* Advanced drug delivery reviews, 2012. **64**: p. 246-255.

41. Moghimi, S.M. and Szebeni, J., *Stealth liposomes and long circulating nanoparticles: critical issues in pharmacokinetics, opsonization and protein-binding properties.* Progress in lipid research, 2003. **42**(6): p. 463-478.

42. Immordino, M.L., et al., *Stealth liposomes: review of the basic science, rationale, and clinical applications, existing and potential.* International Journal of Nanomedicine, 2006. **1**(3): p. 297-315.

43. Gabizon, A.A., *Stealth liposomes and tumor targeting: one step further in the quest for the magic bullet.* 2001, AACR.

44. Brannon-Peppas, L. and Blanchette, J.O., *Nanoparticle and targeted systems for cancer therapy.* Advanced drug delivery reviews, 2012. **64**: p. 206-212.

45. Arnida, et al., *Geometry and surface characteristics of gold nanoparticles influence their biodistribution and uptake by macrophages.* European journal of pharmaceutics and biopharmaceutics : official journal of Arbeitsgemeinschaft fur Pharmazeutische Verfahrenstechnik e.V, 2011. **77**(3): p. 417-423.

46. Elias, D.R., et al., *Effect of ligand density, receptor density, and nanoparticle size on cell targeting.* Nanomedicine: Nanotechnology, Biology and Medicine, 2013. **9**(2): p. 194-201.

47. Li, L., Y. Zhang, and Wang, J., *Effects of ligand distribution on receptor-diffusion-mediated cellular uptake of nanoparticles.* Royal Society Open Science, 2017. **4**(5): p. 170063.

48.   Hongying, L., et al., *Control of Surface Ligand Density on PEGylated Gold Nanoparticles for Optimized Cancer Cell Uptake.* Particle & Particle Systems Characterization, 2015. **32**(2): p. 197-204.

49.   Chu, C., et al., *Effect of surface ligand density on cytotoxicity and pharmacokinetic profile of docetaxel loaded liposomes.* Asian Journal of Pharmaceutical Sciences, 2016. **11**(5): p. 655-661.

50.   Lee, J.H., et al., *The effect of ligand density on in vivo tumor targeting of nanographene oxide.* Journal of Controlled Release, 2015. **209**: p. 219-228.

51.   Moradi, E., et al., *Ligand density and clustering effects on endocytosis of folate modified nanoparticles.* RSC Advances, 2012. **2**(7): p. 3025-3033.

52.   Poon, Z., et al., *Ligand-Clustered "Patchy" Nanoparticles for Modulated Cellular Uptake and In Vivo Tumor Targeting.* Angewandte Chemie International Edition, 2010. **49**(40): p. 7266-7270.

53.   Muro, S., et al., *Control of Endothelial Targeting and Intracellular Delivery of Therapeutic Enzymes by Modulating the Size and Shape of ICAM-1-targeted Carriers.* Molecular Therapy, 2008. **16**(8): p. 1450-1458.

54.   Kolhar, P., et al., *Using shape effects to target antibody-coated nanoparticles to lung and brain endothelium.* Proceedings of the National Academy of Sciences, 2013. **110**(26): p. 10753-10758.

55.   Yue, Z.-G., et al., *Surface Charge Affects Cellular Uptake and Intracellular Trafficking of Chitosan-Based Nanoparticles.* Biomacromolecules, 2011. **12**(7): p. 2440-2446.

56.   Angeles, V., et al., *The influence of surface functionalization on the enhanced internalization of magnetic nanoparticles in cancer cells.* Nanotechnology, 2009. **20**(11): p. 115103.

57.   Fröhlich, E., *The role of surface charge in cellular uptake and cytotoxicity of medical nanoparticles.* International Journal of Nanomedicine, 2012. **7**: p. 5577-5591.

58.   Kim, B., et al., *Tuning Payload Delivery in Tumour Cylindroids using Gold Nanoparticles.* Nature nanotechnology, 2010. **5**(6): p. 465-472.

59.   Chung, T.-H., et al., *The effect of surface charge on the uptake and biological function of mesoporous silica nanoparticles in 3T3-L1 cells and human mesenchymal stem cells.* Biomaterials, 2007. **28**(19): p. 2959-2966.

60.   Thomas, T.P., et al., *Folate-targeted nanoparticles show efficacy in the treatment of inflammatory arthritis.* Arthritis and rheumatism, 2011. **63**(9): p. 2671-2680.

61.   Kularatne, S.A. and Low, P.S., *Targeting of Nanoparticles: Folate Receptor*, in *Cancer Nanotechnology: Methods and Protocols*, S.R. Grobmyer and B.M. Moudgil, Editors. 2010, Humana Press: Totowa, NJ. p. 249-265.

62.   Richards, D.A., et al., *Antibody fragments as nanoparticle targeting ligands: a step in the right direction.* Chemical Science, 2017. **8**(1): p. 63-77.

63.   Arruebo, M., et al., *Antibody-Conjugated Nanoparticles for Biomedical Applications.* Journal of Nanomaterials, 2009. **2009**: p. 24.

64. Bertozzi, C.R., et al., *Chemical Glycobiology.* Science, 2001. **291**(5512): p. 2357-2364.

65. Vocadlo, D.J., et al., *A chemical approach for identifying O-GlcNAc-modified proteins in cells.* Proceedings of the National Academy of Sciences, 2003. **100**(16): p. 9116-9121.

66. Prescher, J.A., et al., *Chemical remodelling of cell surfaces in living animals.* Nature, 2004. **430**(7002): p. 873-877.

67. Prescher, J.A. and Bertozzi, C.R., *Chemistry in living systems.* Nat Chem Biol, 2005. **1**(1): p. 13-21.

68. Laughlin, S.T., et al., *Metabolic Labeling of Glycans with Azido Sugars for Visualization and Glycoproteomics*, in *Methods in Enzymology*, F. Minoru, Editor. 2006, Academic Press. p. 230-250.

69. Laughlin, S.T., et al., *In Vivo Imaging of Membrane-Associated Glycans in Developing Zebrafish.* Science, 2008. **320**(5876): p. 664-667.

70. Knight, J.C. and Cornelissen, B., *Bioorthogonal chemistry: implications for pretargeted nuclear (PET/SPECT) imaging and therapy.* American Journal of Nuclear Medicine and Molecular Imaging, 2014. **4**(2): p. 96-113.

71. Rossin, R., et al., *In Vivo Chemistry for Pretargeted Tumor Imaging in Live Mice.* Angewandte Chemie International Edition, 2010. **49**(19): p. 3375-3378.

72. Zeglis, B.M., et al., *A pretargeted PET imaging strategy based on bioorthogonal Diels-Alder click chemistry.* J Nucl Med, 2013. **54**(8): p. 1389-96.

73. Neves, A.A., et al., *Imaging Glycosylation In Vivo by Metabolic Labeling and Magnetic Resonance Imaging.* Angewandte Chemie International Edition, 2016. **55**(4): p. 1286-1290.

74. Koo, H., et al., *Bioorthogonal Copper-Free Click Chemistry In Vivo for Tumor-Targeted Delivery of Nanoparticles.* Angewandte Chemie International Edition, 2012. **51**(47): p. 11836-11840.

75. Lee, S., et al., *Chemical Tumor-Targeting of Nanoparticles Based on Metabolic Glycoengineering and Click Chemistry.* ACS Nano, 2014. **8**(3): p. 2048-2063.

76. Wang, H., et al., *In Vivo Targeting of Metabolically Labeled Cancers with Ultra-Small Silica Nanoconjugates.* Theranostics, 2016. **6**(9): p. 1467.

77. Yoon, H.Y., et al., *Artificial Chemical Reporter Targeting Strategy Using Bioorthogonal Click Reaction for Improving Active-Targeting Efficiency of Tumor.* Molecular Pharmaceutics, 2017. **14**(5): p. 1558-1570.

78. Prescher, J.A.,et al., *Chemical remodelling of cell surfaces in living animals.* Nature, 2004. **430**(7002): p. 873.

79. Saxon, E., et al., *Investigating cellular metabolism of synthetic azidosugars with the Staudinger ligation.* Journal of the American Chemical Society, 2002. **124**(50): p. 14893-14902.

80. Hang, H.C., et al., *A metabolic labeling approach toward proteomic analysis of mucin-type O-linked glycosylation.* Proceedings of the National Academy of Sciences, 2003. **100**(25): p. 14846-14851.

81. Kaminskas, L.M., et al., *Differences in colloidal structure of PEGylated nanomaterials dictate the likelihood of accelerated blood clearance.* Journal of Pharmaceutical Sciences, 2011. **100**(11): p. 5069-5077.

82. Tang, L., et al., *Investigating the optimal size of anticancer nanomedicine.* Proceedings of the National Academy of Sciences, 2014.

83. Moghimi, S.M., et al., *Factors Controlling Nanoparticle Pharmacokinetics: An Integrated Analysis and Perspective.* Annual Review of Pharmacology and Toxicology, 2012. **52**(1): p. 481-503.

84. Saxon, E. and Bertozzi, C.R., *Chemical and Biological Strategies for Engineering Cell Surface Glycosylation.* Annual Review of Cell and Developmental Biology, 2001. **17**(1): p. 1-23.

85. Hsu, T.-L., et al., *Alkynyl sugar analogs for the labeling and visualization of glycoconjugates in cells.* Proceedings of the National Academy of Sciences, 2007. **104**(8): p. 2614-2619.

86. Baskin, J.M., et al., *Visualizing enveloping layer glycans during zebrafish early embryogenesis.* Proc Natl Acad Sci U S A, 2010. **107**(23): p. 10360-5.

87. Breidenbach, M.A., et al., *Targeted metabolic labeling of yeast N-glycans with unnatural sugars.* Proc Natl Acad Sci U S A, 2010. **107**(9): p. 3988-93.

88. Chang, P.V., et al., *A strategy for the selective imaging of glycans using caged metabolic precursors.* J Am Chem Soc, 2010. **132**(28): p. 9516-8.

89. Hakem, I.F., et al., *Understanding Ligand Distributions in Modified Particle and Particlelike Systems.* Journal of the American Chemical Society, 2010. **132**(46): p. 16593-16598.

90. Gref, R., et al., *'Stealth'corona-core nanoparticles surface modified by polyethylene glycol (PEG): influences of the corona (PEG chain length and surface density) and of the core composition on phagocytic uptake and plasma protein adsorption.* Colloids and Surfaces B: Biointerfaces, 2000. **18**(3-4): p. 301-313.

91. Veronese, F.M., *Peptide and protein PEGylation: a review of problems and solutions.* Biomaterials, 2001. **22**(5): p. 405-417.

92. De las Heras Alarcón, C., et al., *Stimuli responsive polymers for biomedical applications.* Chemical Society Reviews, 2005. **34**(3): p. 276-285.

93. Yaghmur, A. and Glatter, O., *Characterization and potential applications of nanostructured aqueous dispersions.* Advances in colloid and interface science, 2009. **147**: p. 333-342.

94. Yaghmur, A., et al., *Self-assembly in monoelaidin aqueous dispersions: direct vesicles to cubosomes transition.* PLoS One, 2008. **3**(11): p. e3747.

95. Chong, J.Y., et al., *Steric stabilizers for cubic phase lyotropic liquid crystal nanodispersions (cubosomes)*, in *Advances in planar lipid bilayers and liposomes.* 2015, Elsevier. p. 131-187.

Chapter 5 – Lipidated polymers for cubosome stabilisation, potential surface modification and cell-surface clicking

5.1 Declaration for Chapter 5

Some of the research presented in this chapter has been published as;

- Lipidated polymers for the stabilization of cubosomes: nanostructured drug delivery vehicles. James L. Grace, Nicolas Alcaraz, Nghia P. Truong, Thomas P. Davis, Ben J. Boyd, John F. Quinn, Michael R. Whittaker. Chem Commun., **2017**, 53, 10552-10555 **DOI:** 10.1039/C7CC005842J

5.2 Introduction

Lipid nanoparticles have attracted considerable attention in the drug delivery field for over two decades, and their ability to carry imaging agents and drug molecules has been widely documented [1-7]. In recent times, cubosomes, a particular subclass of lipid based nanoparticles, have been the subject of focused research efforts [8-15]. Cubosomes are dispersed lipid based liquid crystalline nanoparticles comprising an internal cubic phase that has self-assembled in excess water upon dispersion. Due to the unique structure of the dispersed cubic phase, which includes both hydrophobic lipid domains and hydrophilic water channels, cubosomes can carry both hydrophilic and hydrophobic molecules. An important property of these cubosomes is that the phase can be reversibly altered by the application of an external stimulus such as temperature [16]. Further, the properties of the different phases are unique, with the packing and phase structure determining the rate of encapsulated drug release via passive diffusion. As such, controlled payload release can be achieved through the external control of this phase structure [16-18]. It is these desirable properties that have generated many investigations into the potential of cubosomes as versatile nanomaterials for therapeutic delivery [8, 9, 15, 19-24].

There are three common orientations within the cubic phase: double diamond (D-surface/Pn3m), primitive (P-surface/Im3m) and gyroid (G-surface/Ia3d). Other commonly identified structures within lipid nanomaterials include inverse hexagonal (H_2), reversed micellar (L_2) and lamellar phases ($L\alpha$). The phase that is formed is dictated by the Critical Packing Parameter (CPP), which has been detailed in Chapters One and Three.

To help disperse the bulk phase and provide colloidal stability a stabiliser is generally added to the system. These stabilisers are generally amphiphilic and provide stability by sequestering at the lipid/water interface. In doing so, they are able to reduce interfacial tension and enhance the stability of the colloidal system by reducing the rate at which aggregation occurs via steric stabilisation of the nanoparticles. An excellent summary of stabilisers for lipid based colloidal dispersions was recently published by Chong *et al.* [25] which collates information on stabilisers and their performance. Currently, the most common stabilisers used are block copolymer surfactants such as Pluronic F108 or F127 [25]. Pluronics across the series, differing in their length and relative hydrophobicity have been compared for their ability to stabilise cubosomes [26], with F108 showing the best stabilising properties. Other studies have focused on utilising different compounds for stabilisation of cubosomes such as β-casein [27], other block co-polymers that aren't pluronics such as P(ODA)-*b*-P(PEGA-OMe), poly(ethylene oxide) stearate and Dansyl-conjugated copolymers [28-30] or PEG-based conjugates such as PEGylated phytanyl copolymers [31, 32]. The mechanism of stabilisation is the same across these examples as they require sufficient incorporation into the lipid domain but also have a segment that is hydrophilic to create a surrounding layer in the water domains.

The colloidal stability of the cubosome system is closely linked to the size of the stabiliser, due to the potential for inclusion or exclusion from the internal structure, and its affinity for both the lipid and aqueous regions in the dispersion. An effective stabiliser requires a sufficient degree of hydrophobicity so as to anchor into the lipid component but must also be sufficiently hydrophilic to reduce interfacial tension (Figure 5.1).
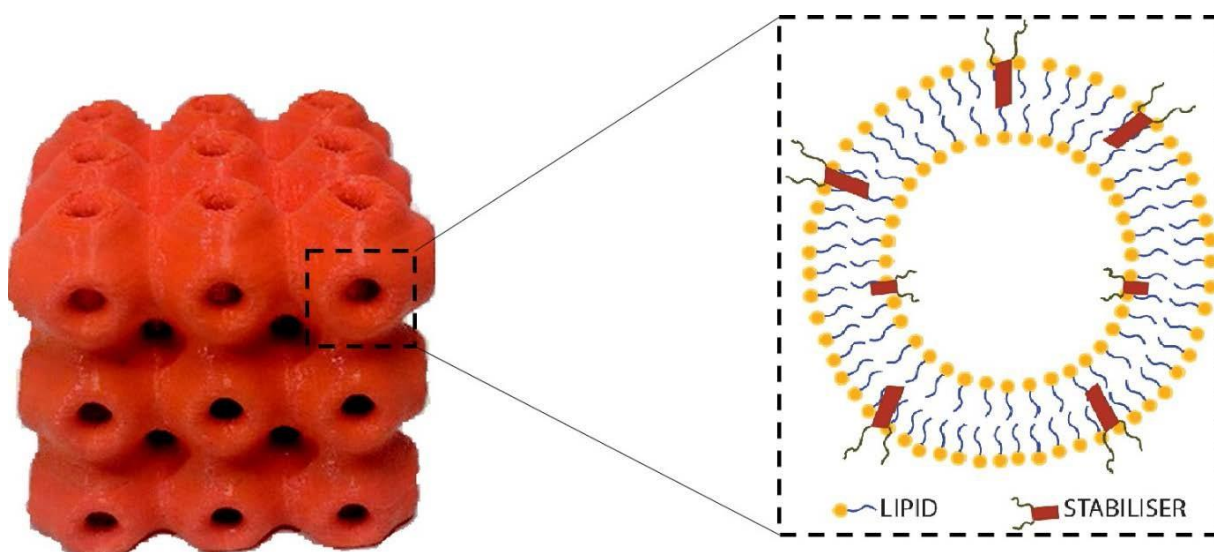
Figure 5.1. 3D printed Im3m cubic spacing model depicting the internal packing and localisation of stabilisers. The hydrophobic component of the stabiliser associates with the hydrophobic (blue) region of the lipid. The hydrophilic chain (grey) is surface bound and associates with the water and helps reduce interfacial tension. As depicted, the stabiliser can locate itself on the inside or outside of the channels but also within the lipid domain.

Pluronic stabilisers suffer from some deficiencies such as some toxicity issues [33] and high concentrations required (up to 1% wt of total mass) [34]. Their generally small size also means that they can readily enter the cubic phase structure (likely linked to the requirement for relatively high concentrations) and are liable to induce changes in phase structure [35].

The largest of the Pluronic molecules, F108, is the most efficient and also prevents a phase transition seen in monoglycerides-based cubosomes from the less swollen Pn3m phase to the most swollen Im3m seen for smaller Pluronics such as F127 [26]. This hints that even larger stabilisers may restrict access to the cubosome internal structure and provide an opportunity to retain the stabiliser on the surface rather than it distributing to the internal interface and thereby not contributing to stability, and not being available for binding. In Chapter Three, where Pluronics and relatively small click functionalized phospholipid derivatives were used, non-specific binding to cells was evident and no specific binding was detected, hypothesised to be due to poor colloidal stability leading to hydrophobic interactions with cells, and lack of availability of reactive groups at the particle surface, potentially due to incorporation into the internal interfaces of the particles.

Therefore, it is hypothesised that polymers with even larger size than Pluronics should provide even greater and more efficient colloidal stability for cubosomes, as well as opportunity for more effective surface functionalization. It is also hypothesised that polymers with a greater hydrophobic domain will have better dispersing ability due to their ability to embed into the lipid regions of the cubosomes. To this end, lipidated polymers could be a favourable alternative to Pluronics. Lipidated polymers are polymers that incorporate a lipid chain in their structure as one of their monomer building blocks.

Lipidated polymers were synthesized as the structure was of particular interest, due to the use of a dual tail lipid initiator which had not been reported for the polymerization of Cu(0)-mediated polymerization. Three polymeric variants were synthesized with this dual tail lipid initiator each containing a different charge: cationic charge from primary amine groups, anionic charge from carboxylic groups, and neutral hydrophilic charge from poly(ethylene glycol) groups. The initiator allowed for the polymerization of a range of monomers which led to the synthesis of said polymers with the three different charges. Originally, the polymers were synthesised with the intent to develop novel antibacterial but a collaboration developed when a potential alternative use was hypothesised.

In this chapter, novel defined lipidated polymers synthesised by James Grace (collaborator at Monash Institute of Pharmaceutical Sciences) were assessed for their ability to act as stabilisers for cubosome dispersions as an alternative to Pluronics. These lipidated polymers can have their molecular weight, hydrophobic-hydrophilic balances and end group functionality easily altered. Specifically, a library of neutral, cationic and anionic lipid-inspired polymer surfactants were synthesised with different elements and their ability to form and stabilise cubosome nanoparticles was assessed.

They were characterised using dynamic light scattering (DLS) for size determination and small angle X-ray scattering (SAXS) for phase and internal structure determination. The chemical structures can be seen in Figure 5.2. Following this, the polymer library was expanded to include two polymers that bear PEG-Azide end groups and assess their ability for click binding in solution and on cell surfaces following metabolic labelling.
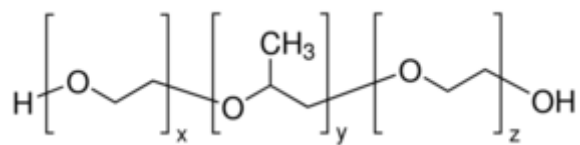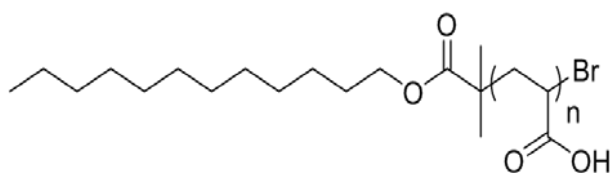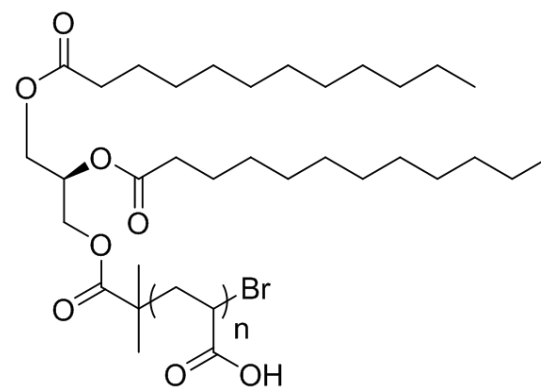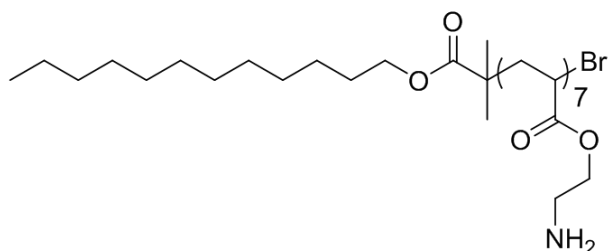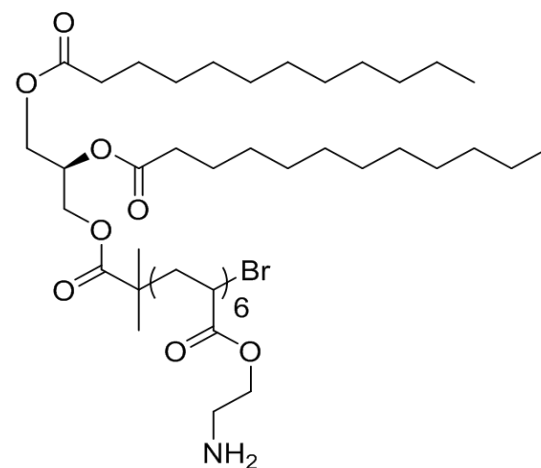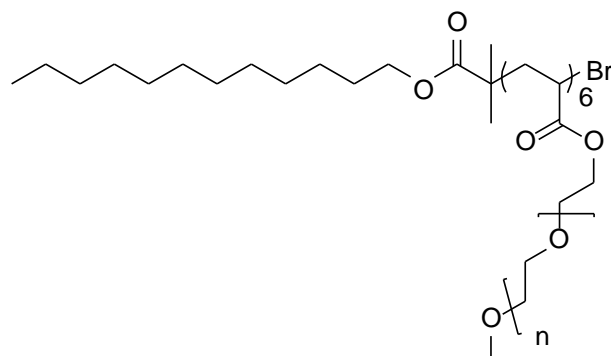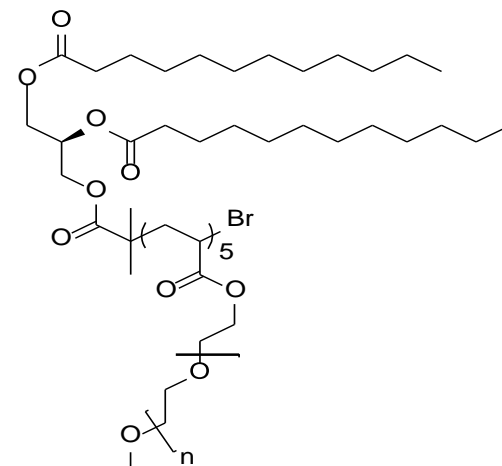
Figure 5.2. Chemical structures of Pluronic F108 (A) and the lipidated polymers synthesised. B) C_{12}-PAA, C) di-C_{12}-PAA, D) C_{12}-PAEA and E) di-C_{12}-PAEA F) C_{12}-PEGMEA G) di-C_{12}-PEGMEA

5.3 Hypothesis and aims

The following hypotheses were tested in this Chapter;

1. That two tailed polymers will have better dispersing abilities than single tailed polymers as they have a greater hydrophobic domain meaning they will be embedded more readily.

2. That neutral polymers will exhibit better dispersing ability than charged polymers as they are less likely to interact with the lipid and its packing.

3. That the azide lipidated polymer will have better binding in solution and onto cells than the phospholipid modified cubosomes due to more favourable positioning at the particle-solution interface.

In order to investigate these hypotheses, the following aims will be achieved:

1. To determine the size and structure of cubosomes stabilised by the different lipidated polymers at different concentrations using DLS, cryo-TEM and SAXS.

2. To determine the ability of the azide polymers to covalently bind to DBCO-Cy5 in solution using fluorescence measurements and size exclusion chromatography.

3. To determine the ability of the azide polymers to covalently bind to A549 cells treated with unnatural DBCO sugars using TIRF microscopy.

5.4 Materials and methods

5.4.1 Materials

Please refer to Chapter Two for the materials used within this chapter.

Phytantriol was used as the lipid component of the cubosome and PBS was the solvent used.

The lipidated polymers were synthesised and characterised by James Grace (MIPS). Information regarding these can be found in the Appendix.

5.4.2 Methods

Please refer to Chapter Two for general methods used in this chapter. Below are some specific methods that were used.

5.4.2.1 Cubosome preparation

Cubosome dispersions were prepared as described in Chapter Two with the Pluronic F108 being replaced by the novel stabilisers in the respective samples.

5.4.2.2 Binding efficiency studies

The dispersions were mixed at a 1:1 ratio (of azide to DBCO) with Sulfo-DBCO-Cy5 or Sulfo-N$_3$-Cy5 in PBS for 24 h protected from light. Following this, SEC was conducted and methanol was added to the elutions to break down the lipid structure and prevent quenching of the Cy5. The fluorescence from Rhodamine B was measured at 560/583 nm and from Cy5 at 649/662 nm.

5.5 Results

5.5.1 Cubosomes stabilised with lipidated polymers: creation and characterisation

Cubic phase was dispersed in the presence of the lipidated polymers and their colloidal stability was assessed through DLS followed by their internal structure through SAXS.

5.5.1.1 Cubosomes stabilised with lipidated polymers: colloidal stability

The polymer structure and concentration had a significant effect on the size of the dispersed nanoparticles. When examined using DLS, most of the dispersions prepared using the lipidated polyelectrolytes revealed nanoparticles with hydrodynamic sizes consistent with those produced when Pluronic F108 was used as the stabiliser (i.e., 100-500 nm) [11-13]. Table 5.1 lists the sizes measured for cubosomes prepared using the non-azide lipidated polymers. It should be noted that some polymers at some concentrations exhibited particle sizes larger than 500 nm. This size indicates poorly dispersed lipid reflecting a limited stabilising ability for those polymers. It is also important to note that DLS provides the size distribution assuming spherical particles, but does not provide information about the shape or structure of the cubosomes.

Table 5.1. Volume-based particle size distribution measurements (mean ± SD, n =3) for cubosomes stabilised by the different lipidated polymers and Pluronic F108 taken at 25°C and within 5 minutes of sonication.

Polymer stabiliser used	Concentration (w/v %)	Peak 1 (nm)	Peak 2 (nm)	PDI
Pluronic F108	1.5	160 ± 10		0.151
C$_{12}$-PEGMEA	0.5	248 ± 22		0.281
	1	325 ± 26		0.419
	1.5	632 ± 53		0.434
di-C$_{12}$-PEGMEA	0.5	259 ± 41		0.392
	1	439 ± 64		0.528
	1.5	632 ± 89		0.454
C$_{12}$-PAA	0.5	1348 ± 500	3610 ± 497	0.371
	1	363 ± 187		0.267
	1.5	95 ± 62	1736 ± 627	0.368
di-C$_{12}$-PAA	0.5	121 ± 53		0.123
	1	81 ± 62	1750 ± 437	0.357
	1.5	121 ± 111		0.241
C$_{12}$-PAEA	0.5	225 ± 101		0.243
	1	153 ± 45	515 ± 157	0.426
	1.5	200 ± 55	807 ± 341	0.404
di-C$_{12}$-PAEA	0.5	239 ± 79		0.303
	1	144 ± 71	1987 ± 306	0.437
	1.5	1168 ± 402	3728 ± 420	0.319

5.5.1.2 Cubosomes stabilised with lipidated polymers: internal structure

Next, SAXS was used at the Australian Synchrotron to investigate the internal phase structure of the dispersed lipid nanoparticles. A temperature ramp was conducted which involves assessing the internal phase structure of the dispersion every 5°C from 25°C to 75°C. The internal phase is identified by the scattering profile acquired from SAXS where the Bragg peaks that appear can be characterised and compared to known lattice spacings which are well-described in the literature.

Additionally, the lattice parameter which describes the spacing between the repeating cell units of the crystalline structure was calculated from the SAXS data.

Pore size is directly linked to the lattice parameter and can be calculated from the lattice parameter and lipid chain length as seen in Briggs *et al.* [36]. The lattice parameter, and in turn the pore size, is directly related to the diffusion rate of encapsulated therapeutics and is a critically important parameter for potential use of these nanoparticles in drug delivery [14, 17, 22, 37, 38]. The phase structures based off the SAXS scattering profiles have been summarised in Figure 5.3. The stacked plots can be found in the Appendix and individual profiles are available upon request of the author. Each polymer behaved uniquely based on whether it had one or two alkyl chains and also depending on the hydrophilic polymer moiety. This observation is supported by previous findings where the size and architecture of the polymer and also their charge had significant impacts on their stabilising ability and the final physio-chemical characteristics of the dispersed lipid nanoparticles [25, 26, 28, 29, 31, 32].
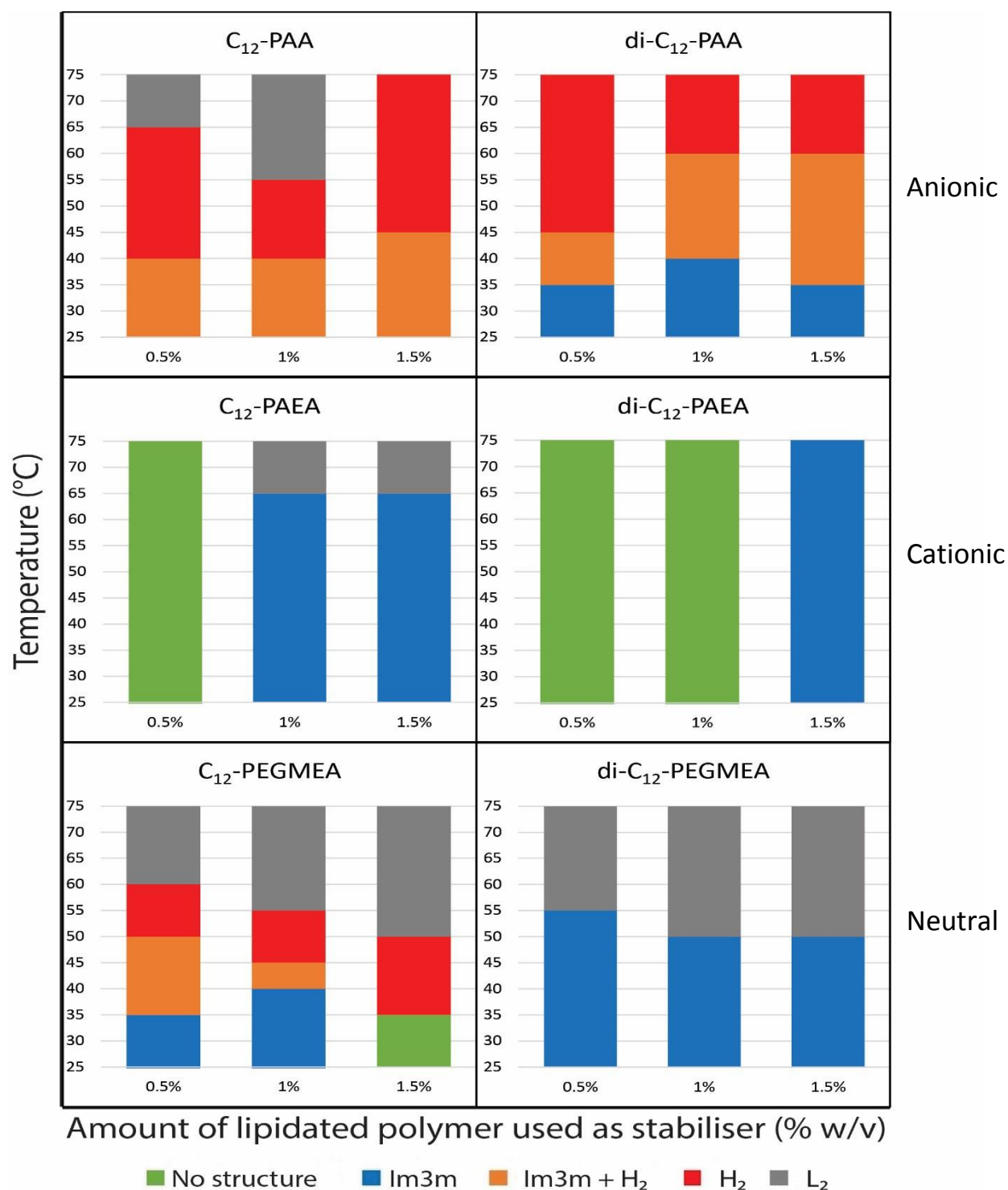
Figure 5.3. Temperature dependent phase structure of the dispersions stabilised by the novel lipidated polymers. The phase transition profile for cubosomes stabilised by 1.5% Pluronic F108 is; Pn3m (25-45°C), Pn3m + H_2 (45-50°C), H_2 (50-60°C) and L_2 (60-75°C) [26]. Stacked plots for the each system are located in the Appendix.

The scattering profiles can be understood in terms of the critical packing parameter (CCP). While phytantriol imparts a slightly negative curvature on the lipid bilayer resulting in the formation of the cubic phase, the use of the more polar charged polymers synthesised herein would be expected to draw the mean curvature back towards a lamellar phase. This would result in Im3m cubic spacing, as the apparent hydrophilic head group area (denoted A in the CPP equation) is larger. Although the lipid used is the key contributor to the CPP and therefore the phase formed, the polymer embedding its hydrophobic C_{12} tail between the lipid molecules (as would be likely as part of the stabilising mechanism) is expected to also influence CPP by affecting how the lipids can position themselves to form a mesophase. The results obtained are consistent with this mechanism and will be explained below.

As can be seen in Figure 5.3, the majority of samples had Im3m cubic spacing present at lower temperatures. This is different to cubosomes stabilised by Pluronic F108 which exhibits Pn3m spacing. We attribute this to the nature of the polymer head group, which increases the apparent hydrophilic head group packing area. It should be noted that the polymers containing different head groups and alkyl chains lead to cubosomes with very different temperature-dependent phase structures. The internal structure of cubosomes stabilised by lipidated polymers was determined as a function of temperature using SAXS. Generally, Pluronic stabilised phytantriol cubosomes will exhibit Pn3m cubic spacing until around 45°C before transitioning to H_2 phase above 45 °C and transitioning to L_2 phase above 60°C [26].

As discussed above, even though DLS measurements revealed nanoscale particles in all the tested systems some of the findings were relatively large nanoparticles and PDIs meaning the dispersability and stability was poor. The SAXS experiments give information if a liquid-crystal structure is present within the dispersion.

Only one polymer end group, PAEA, was not able to stabilise and disperse cubosomes effectively. The single chain variant was able to stabilise Im3m cubic spacing cubosomes at concentrations over 1% (w/v) and surprisingly the two chain variant was only able to stabilise effectively at 1.5% (w/v). The two chain system was also Im3m cubic spacing and remained that way even at high temperatures where normally cubic spacing is not commonly encountered. This data appears to suggest that below a certain concentration the polymer is present in too low of a quanitity to act as a stabiliser but once above this threshold there is a strong integration into the lipid and cubosomes can be formed and dispersed. This further indicates that the charge on the polymer is likely to play an important role in its ability to stabilise cubosomes [25], more so than the extent of the hydrophobic region of the stabiliser. It appears that a positively charged end group is not favourable for stabilisers.

All other systems had some liquid-crystal structure present at any concentration. In most of these cases, Im3m cubic spacing was found at room temperature. Only in the C_{12}-PAA stabilised system was a mixed phase present at 25ºC. At all three concentrations assessed, this system had no pure cubic phase present with a mixed phase of Im3m and H_2 being present until at least 40ºC in all samples. The bifunctional di-C_{12}-PAA had Im3m present before the mixed phase. It would appear that the PAA polymer systems increases interfacial curvature as H_2 was present at room temperature which is likely due to the effect of the negative charge present.

Finally, the uncharged system, PEGMEA, had very different profiles between the single and two tail polymers. The single alkyl chain bearing polymer exhibited a similar profile to that of F108 stabilised cubosomes except for the cubic phase being present determined to be Im3m instead of Pn3m. The two chained polymer exhibited Im3m spacing across all concentrations until around 50ºC. Above this temperature there was L_2 phase present. This shows the influence altering the hydrophobic block of the polymer has over cubosome stabilising ability seen when comparing to a Pluronic stabilised system and in the lack of a charged head group, like the other polymers.

Incorporating a phospholipid-mimicking end group into a polymeric stabiliser is a convenient method for stabilising cubosomes, presumably by reducing the interfacial tension of the cubic LC structures. This uncharged system helps demonstrate the benefit of the second alkyl tail in stabilising the system and giving it a temperature dependent phase profile more similar to that achieved by Pluronics, the current "gold standard". This is likely due to differences in the hydrophobicity of the polymer and in turn how it interacts and embeds itself into the lipid portion of the mesophase. This would indicate that there is some interference with internal packing suggesting some polymer is still internalised. However, it should be noted that the difference is not very significant indicating the extra tail may not be a large enough change in hydrophobicity to warrant a large change in how the polymer interacts with the phytantriol. It should also be noted that charged appeared to play a greater role in the systems with charged end groups, in comparison to the amount of hydrocarbons tails present.

Both negatively and positively charged polymers exhibited very different phase profiles over the temperatures assessed to each other but also Pluronic stabilised cubosomes. From the findings it would suggest the negatively charged polymer was able to act more similalry to Pluronic based stabilisers than the positively charged system. This is seen in both the size measurements and temperature profiles from DLS and SAXS respectively. It should be added that changes in peak intensity, visible in the stacked pltos in the Appendix, indicate a change in nanoparticle concentration whilst peak broadening, as mentioned in previous chapters, results in a loss in long-range order indicating a loss or change in structure of the mesophase which is reflected in the lattice parameter calculations. The derived lattice parameter was greatly affected by the chemistry of the stabilising polymer (Figure 5.4).
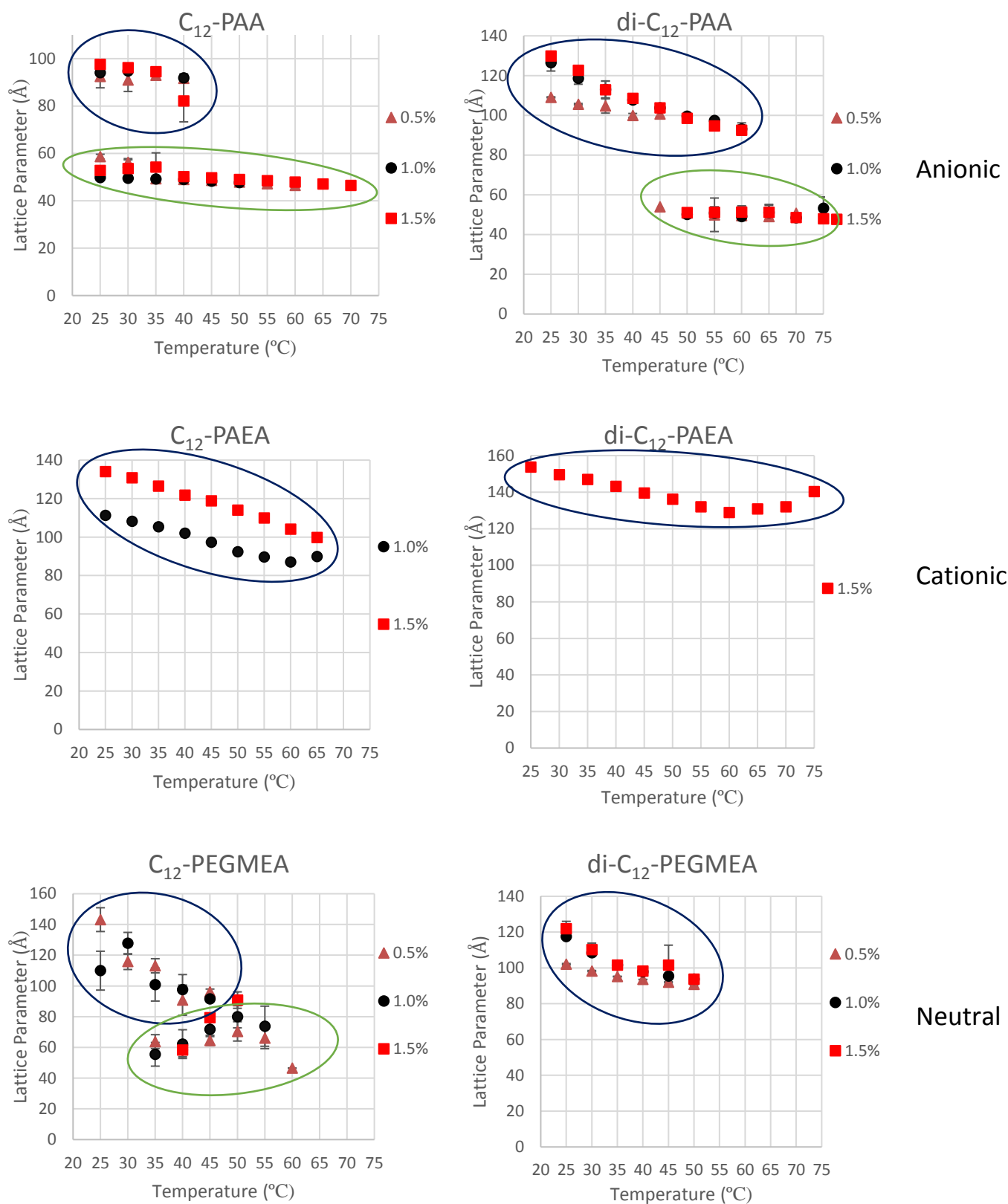
Figure 5.4. Temperature dependence of lattice parameters of lipid dispersions with different concentrations of synthesised polymers over 25°C to 75°C based on SAXS data. Data points circled in blue indicate Im3m spacing and those circled in green indicate H$_2$ spacing.

It has been shown that a charged species can alter cubic phases by causing them to swell, but only if it is present on the inside [39]. For instance, the Im3m spacing observed in dispersions stabilised with the cationic polymers, C_{12}-PAEA and di-C_{12}-PAEA, was larger than for cubosomes stabilised with Pluronic F108 that exhibit Im3m spacing. Suprinsingly, the lattice parameter increased with temperature for the 1.5% di-C_{12}-PAEA system which is uncommon. In contrast, particles stabilised with the anionic polymers, C_{12}-PAA and di- C_{12}-PAA, presented similar lattice parameters for their respective internal structures when compared to Pluronic F108 stabilised systems. This would indicate and further support previous findings that stabiliser charge plays an influential role in how the stabiliser interacts with the lipid and performs its function at the interface. There is a link between the charged end group and the internal structure of the cubosomes. For the neutral system, it appears the single tailed polymer had difficulty embedding itself with the lipid as the lattice parameters are a slightly different to Pluronic F108 stabilised systems whereas the two tailed variant, perhaps due to its higher hydrophobicity, had less difficulty embedding into the phytantriol.

As expected, with an increase in temperature the lattice parameter decreased for all systems, although not necessarily to the same extent [18, 19, 40]. Only in the di-C12-PAEA did this not occur. The lattice parameter indicates where the polymer is locating itself in the cubic structure. If the lattice parameter is swollen, the polymer is embedding itself inside the lipid domains and limiting its stabilising ability whilst if similar to Pluronic F108 stabilised cubosomes it is likely to be on the interface allowing for better stabilising properties [41]. This is reflected in those with larger lattice parameters exhibiting very different phase-temperature profiles to "traditional" cubosomes.

The negatively charged polyelectrolyte appears to prefer being embedded in the cubic structure in turn improving its stabilising ability, as described above.

Aside from expanding the library of polymers available for cubosome stabilisation and modification, these systems show promise in developing polymers that can increase the range of uses for cubosomes outside of drug delivery and imaging such as biosensing.

5.5.2 Creation and characterisation of cubosomes stabilised with azide lipidated polymer

The lipidated polymers were further modified to include an azide end group that was at the end of a PEG chain. Two variants of the di-C_{12}-PEGMEA were developed with one containing a short-PEG (SP) of 400 MW and another with a long-PEG (LP) of 2000 MW. The di-C_{12}-PEGMEA was chosen as the base polymer due to it being neutral, exhibiting some similarities in performance to Pluronic F108 and being easily modifiable. The cubosome systems were stabilised using an equimolar amount of azide lipidated polymer to that of "traditional" cubosomes stabilised by 1.5% w/v Pluronic F108.

Upon sonication the systems were analysed using DLS and the size of the nanoparticles was determined (Table 5.2). Both systems showed one peak with mean sizes around 100 nm, smaller than the majority of cubosomes reported in this Thesis. A second peak was detected in both samples, with that of the system stabilised by the LP exhibiting a size more similar to other reported cubosomes (Table 5.1) whereas the SP stabilised dispersion had a significantly larger nanoparticle population present. It should be noted that the PDI of the SP system was 0.741 which is considered high, even for self-assembled lipid nanoparticle systems. This likely indicates poorer stabilising capabilities of the SP stabiliser compared to the LP stabilised cubosomes.

Table 5.2. Volume-based particle size distribution measurements (mean ± SD, n =3) of the cubosome dispersions stabilised with PEG-azide-lipidated polymers, Pluronic F108 and their alternatives without the PEG-azide at 1.5% w/v.

Stabiliser used for cubosome dispersion	Size (nm) Peak 1	Size (nm) Peak 2	PDI
Short-PEG	113 ± 32	615 ± 199	0.741
Long-PEG	101 ± 33	287 ± 107	0.189
Pluronic F108	160 ± 10		0.151
di-C$_{12}$-PEGMEA	632 ± 89		0.454

An image of the two different cubosome dispersions can be seen in Figure 5.5. The azide lipidated polymers were both able to disperse the bulk lipid cubic phase to a high extent. Both systems gave an opaque milk-like solution with only some undispersed lipid being seen along the sides of the Eppendorf tubes. It should be noted that visually, the long-PEG version appears to be better dispersed with less large lipid chunks along the side and a more uniform and opaque white appearance.
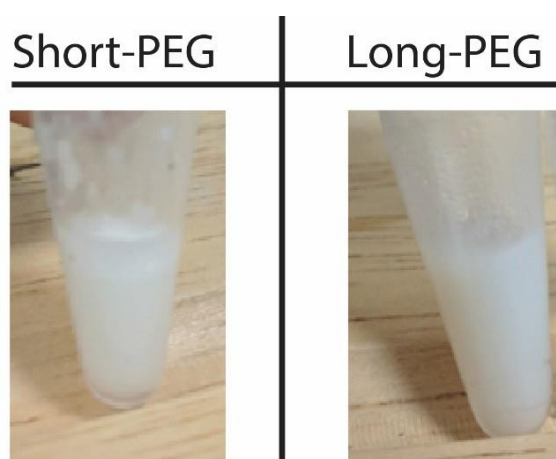
Figure 5.5. Pictures of azide lipidated polymer stabilised cubosomes after sonication.

The internal structure of the azide-polymer stabilised cubosomes was measured by SAXS (Figure 5.6). The azide-polymer stabilised cubosomes exhibited a different temperature-dependent phase profile to the other lipidated polymers mentioned earlier in this chapter and also the phospholipid doped systems in Chapter 3. The azide polymer stabilised systems were in the Pn3m cubic arrangement at room temperature and the first change in behaviour was seen at 50°C. For LP, the first transition was a mixture of Pn3m and H_2 phases until it fully shifted to H_2 phase at 55°C until there was no detectable phase at 70°C. SP behaved differently, directly transitioning to the H_2 phase before losing any identifiable structure at 55°C.
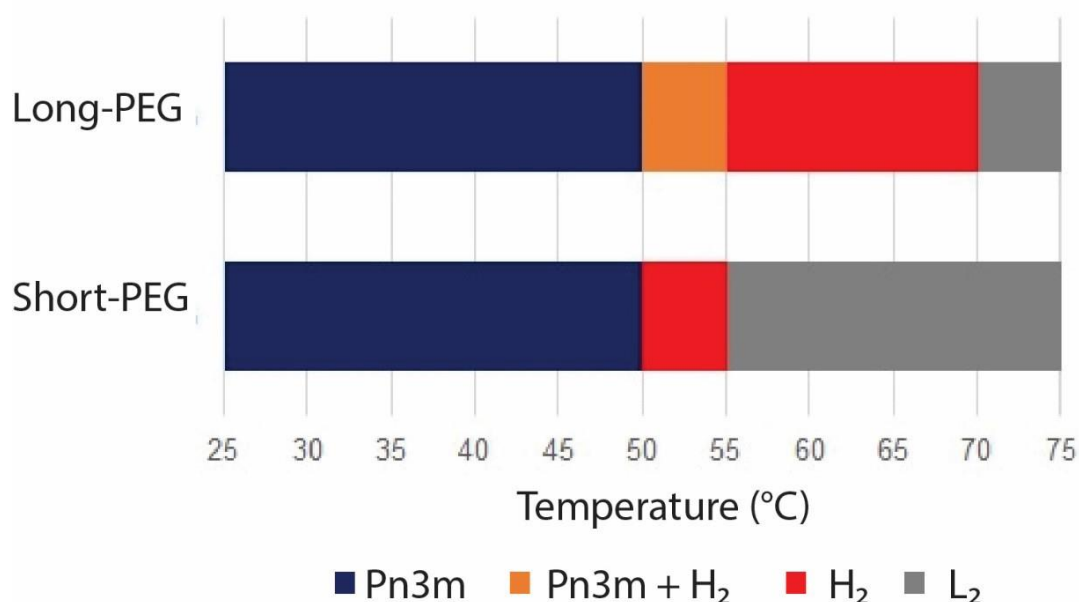
Figure 5.6. Effect of temperature on internal structure of cubosome dispersions stabilised by the short or long PEG azide lipidated polymers over 25°C to 75°C based on SAXS data.

This is considerably different to the other lipidated polymer stabilised systems that were predominately Im3m cubic phases at room temperature and had very varied temperature phase profiles. Additionally, these differed from the phospholipid doped and Pluronic F108 stabilised systems in the same way, as they too form the Im3m cubic structure at room temperature but transition similarly around 50°C to either a mixed phase or pure H_2 phase before losing any detectable internal structure though SAXS. The presence of Pn3m phase as opposed to Im3m could be due to the polymer being at the external interface much like Pluronics or also due to the charge and hydrophilicity attributed to the PEG-azide end group. The length of the PEG group did not appear to greatly alter the dispersing and stabilising ability of the polymers.

5.5.3 Click capability of azide functionalized cubosomes

After characterising the size and internal structure of the azide polymer-stabilised cubosomes, their ability to undergo a copper-free click reaction in solution with dye was assessed, using the same approach as for the cubosomes described in Chapter Three. Figure 5.7 shows that there was a high level of specific binding of the Sulfo-DBCO-Cy5 to the azide-polymer cubosomes, with both systems binding 90% or more of the dye. This is considerably more than the cubosomes stabilised with Pluronic F108 and similar to the click-phospholipid doped cubosomes reported in Chapter Three, indicating that the PEG-azide polymers could stabilise and functionalize the cubosomes.
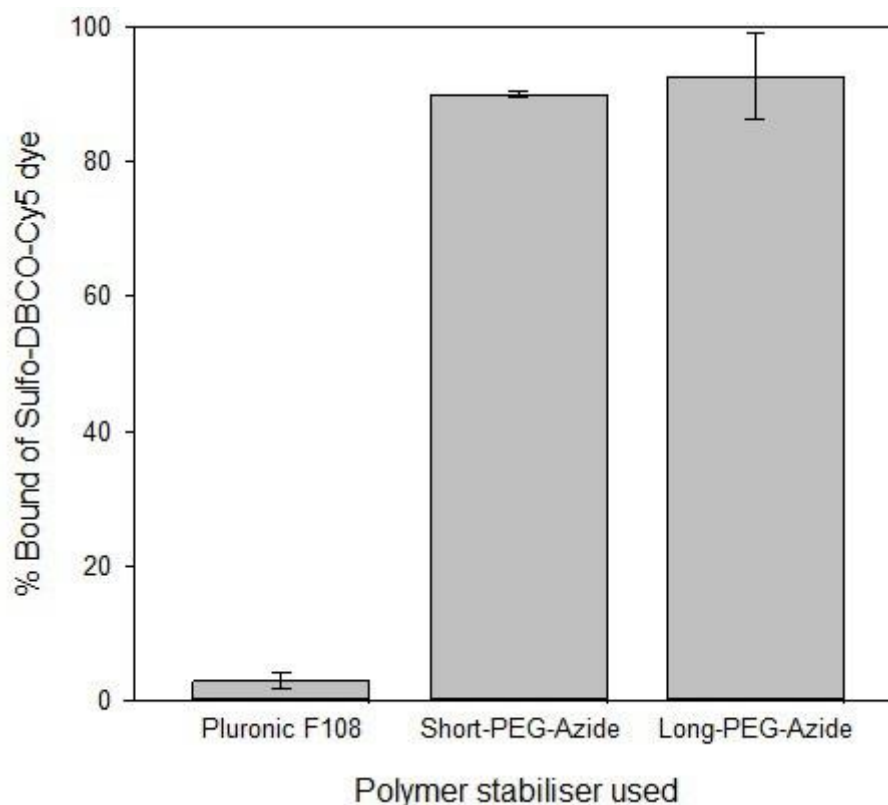
Figure 5.7. Percentage of dye bound to cubosomes (mean ± SD, n = 3) after size exclusion chromatography in Sephadex G50 column with PBS as the eluent.

After the click capability of these particles was confirmed their interaction with A549 cells was assessed using TIRF microscopy. As seen in Figure 5.8, both cubosomes stabilised with both the long and short PEG-azide polymer showed high non-specific binding regardless of whether the cells had been treated with only medium or Ac_4ManNDBCO containing medium (DBCO-labelled cells). Similar to the results observed in Figure 3.9, the cubosomes appeared to fully coat the cells outer surface likely due to hydrophobic interactions with the lipid membrane. The quantitative analysis in Figure 5.8B also shows a high amount of MFI associated with all cells, with those being treated with DBCO-sugar having similar values to those without DBCO-sugar, indicating high non-specific binding similar to the cubosomes discussed in Chapter Three.

A)

B)
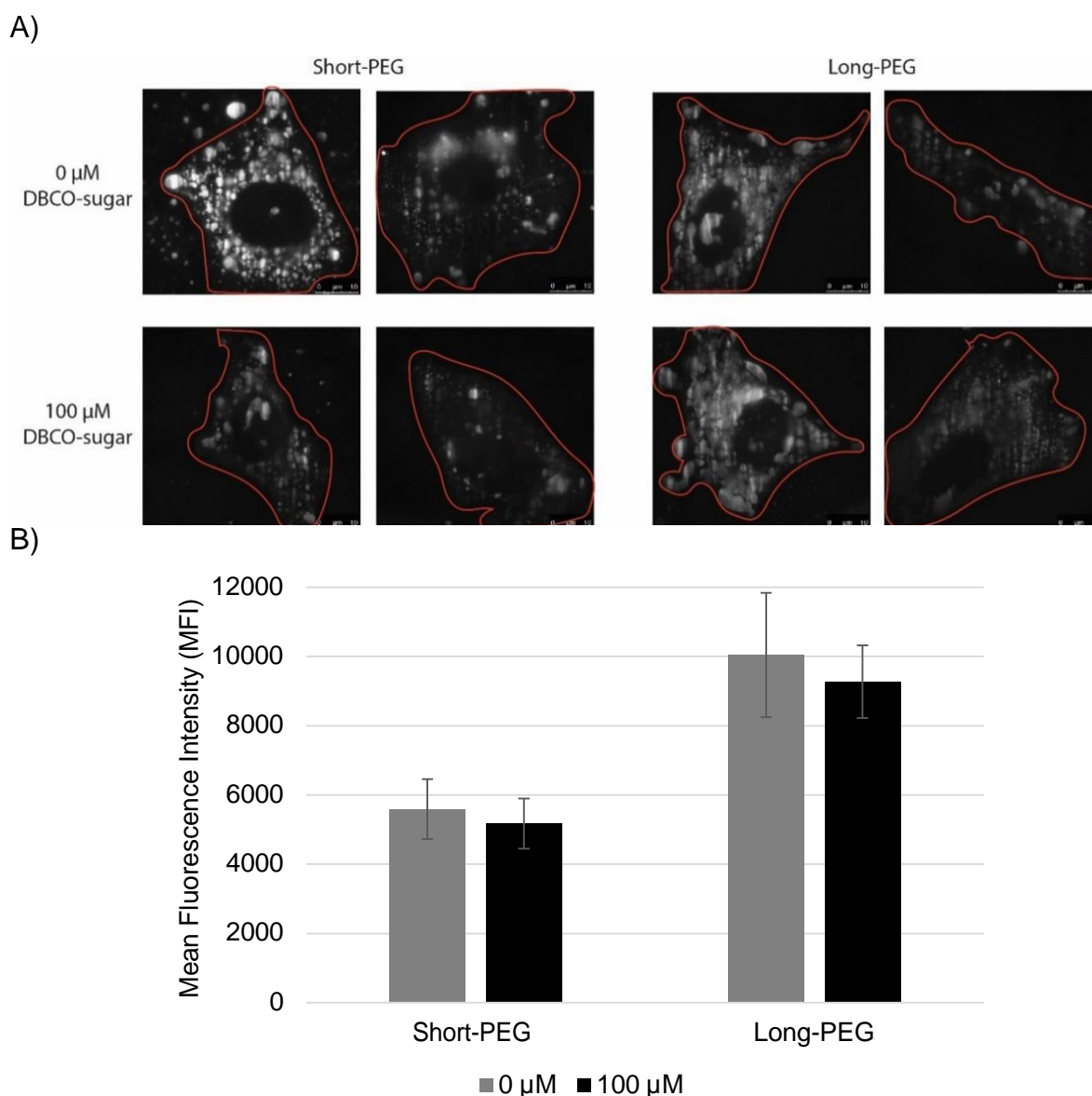
Figure 5.8. A) TIRF microscopy images of A549 cells treated with cubosomes stabilised using either Long-PEG-Azide or Short-PEG-Azide polymer stabilised cubosomes. These images are representative of the findings over three experiments conducted on different days with different passages of cells and different batches of the cubosome dispersions. The cells have been circled in red for clarity and to depict the area analysed by the script. B) The Mean fluorescence Intensity (MFI ± SD, n > 15) determined from than analysis script.

5.6 Discussion

In consideration of the results, it is clear that the charge on the hydrophilic polymer head group has a large effect on the ability of the polymer to stabilise cubosomes. The charge on the head group will influence the interaction of the polymer with the lipids, and its distribution between the particle and the water phase, altering its effectiveness in reducing interfacial tension [25]. If the goal is to identify a suitable alternative to Pluronic F108 and maintain a similar phase-temperature profile, then the negatively charged polymer with two alkyl groups at the chain terminus, di-C_{12}-PAA, provided the best stabilising ability when compared to the currently most commonly used Pluronic statbilisers (Figure 5.3).

These systems behave similarly to other previously reported polymers utilised for cubosome stabilisation. Chong *et al.* studied a large range of Pluronic based stabilisers for preparing cubosomes [26]. They found the longer the PEO segment the better the dispersing ability of the Pluronic, with Pluronic F108 (132 PEO units) performing the best, hence its use as a reference cubosome. They also showed that below 0.5 % w/v most Pluronics were ineffective as the coverage of the interface was poor and flocculation could not be mitigated through their primary stabilising method, steric repulsion. They also found that the hydrophobic portion of the stabiliser was also important as it anchors the molecule to the lipid phase through adsorption. In the case of Pluronics this is related to their PPO units, the minimum required for good stabiliser performance was determined to be 40. In general, they found that it was beneficial to have a high HLB and MW. This was further confirmed in the current study by the success of the two tail lipidated polymers and also the long-PEG-azide variant, that was developed later, as effective colloidal stabilsiers for cubosomes. This information should be considered when further optimising these polymers for better stabilising and dispersing capabilities [26].

In another of their studies, they assessed a series of custom 'brush' block copolymers and found that polymers with an increased PEG length and number of PEG groups performed as better stabilisers [29]. This is likely due to a more complete coverage of the surface by the brush-like polymers compared to linear copolymer Pluronics, resulting in better steric hindrance. Additionally, it was shown that increasing the length of the hydrophobic region also led to improved steric stabilisation likely due to the increased affinity for the particle surface rather than the free aqueous phase.

Based on these previous studies it would be anticipated that the two tail polymer system in the current work would be expected to have better stabilising capabilities than a single tailed polymer with the same or similar head group. There was no substantial improvements when comparing the stabilisation of the single and two tailed systems for the charged polymers indicating that charge appeared to be a dominating factor and that one tail was sufficient for the polymer to interact with and embed itself into the hydrophobic region of the lipid based liquid crystal mesophase. The two tailed polymers tended to be less disruptive to the structure, as the cubosomes stabilised with these polymers retained their structure until higher temperatures (Figure 5.3) and showed less peak broadening, possibly indicating a greater affinity for the particle/bulk solution interface than the internal interface in the water channels, although this has not been proven.

The SAXS measurements of the cubosomes stabilised with the azide polymers showed a profile more similar to cubosomes stabilised by Pluronic F108 (Figure 5.6) [18, 42]. This could be due to the negatively charged azido group on the end of the PEG chain. This similarity with previously reported systems would indicate the polymer sits at the interface and should have high stabilising ability.

Much like the studies in Chapter Three, the azide cubosomes were able to partake in click reactions with a dye in solution to a high extent (Figure 5.7). However, on exposure to the cells, again a high level of non-specific binding was evident that prevented any chance of seeing specific binding if it were to occur. In Chapter Four, it was proposed that this is likely to be due to the hydrophobic nature of the cubosomes and relatively ineffective surface coverage by Pluronics. However, the colloidal stability was particularly good for the long PEG-azide system (Table 5.2), yet it still showed very high non-specific binding in Figure 5.8. Keeping in mind that liposomes showed low non-specific binding (Figure 3.10 and Figure 4.3), it appears that cubosomes may be particularly difficult to stabilise against these non-specific interactions, perhaps due to the higher surface area or the bilayer type which could be more prone to fusion with a cell membrane. The cubosomes here were above the ideal size range for endocytosis, suggesting that hydrophobic interactions were still likely to be responsible, but that these interactions were specific for cell to particle interactions, and not particle to particle. Overall, the task of making cubosomes that are amenable to specific covalent binding to metabolically labelled cells may be out of reach with current small molecule azido-lipid or azido-polymer systems. Future, as yet unknown, approaches to this problem mayprovide solutions to prevent the non-specific interactions from dominating behaviour.

5.7 Conclusion

A library of lipidated polymers were synthesised and assessed as stabilisers for phytantriol cubosomes and were assessed with increasing concentration relative to the lipid present. The variables around the structure of the polymers all had an impact on cubosome structure and stability, due to possible differences in their interaction with the lipid bilayer, as well as their distribution between particle and free solution. The polymer-stabilised cubosomes were generally similar size to those stabilised using Pluronic F108 but exhibited very different phase profiles and lattice parameters. The concentration of the polymer also influenced the performance of the stabiliser, where polymers with a hydrophobic chain terminus and a charged segment distal to the chain end appeared to work best at concentrations over 1% w/v. The anionic polymer provided better cubosome stabilisation, attributed to a greater concentration at the particle-bulk solution interface. Azide-bearing lipidated polymers were then prepared to test the hypothesis that the polymer will present more azides at the surface and be less prone to non-specific interactions with the cells compared to the phospholipid based modification addressed in Chapter Three and overcome nonspecific interactions. Although their ability to specifically click to the DBCO-dye in solution was demonstrated, on exposure to cells they still showed a high degree of non-specific binding. Even with the long-PEG spacer between the polymer backbone and the azide group, and despite it provided good colloidal stability for cubosomes, the non-specific binding still dominated the cell-nanoparticle interactions. While the polymeric materials add to the potential options for preparing cubosomes with tailored interfacial properties, they do not overcome the non-specific binding evident for cubosomes prepared with other stabilisers, limiting the application in the context of antibody-free affinity coupling of particles to cells for drug delivery and imaging purposes.

5.8 References

1. Mukherjee, S., S. Ray, and Thakur, R.S., *Solid Lipid Nanoparticles: A Modern Formulation Approach in Drug Delivery System.* Indian Journal of Pharmaceutical Sciences, 2009. **71**(4): p. 349-358.

2. Puri, A., et al., *Lipid-Based Nanoparticles as Pharmaceutical Drug Carriers: From Concepts to Clinic.* Critical reviews in therapeutic drug carrier systems, 2009. **26**(6): p. 523-580.

3. Naseri, N., et al., *Solid Lipid Nanoparticles and Nanostructured Lipid Carriers: Structure, Preparation and Application.* Advanced Pharmaceutical Bulletin, 2015. **5**(3): p. 305-313.

4. Akbarzadeh, A., et al., *Liposome: classification, preparation, and applications.* Nanoscale Research Letters, 2013. **8**(1): p. 102-102.

5. Pattni, B.S., et al., *New Developments in Liposomal Drug Delivery.* Chemical Reviews, 2015. **115**(19): p. 10938-10966.

6. Sercombe, L., et al., *Advances and Challenges of Liposome Assisted Drug Delivery.* Frontiers in Pharmacology, 2015. **6**: p. 286.

7. Torchilin, V.P., *Recent advances with liposomes as pharmaceutical carriers.* Nature Reviews Drug Discovery, 2005. **4**: p. 145.

8. Azmi, I.D.M., et al., *Cubosomes and hexosomes as versatile platforms for drug delivery.* Therapeutic Delivery, 2015. **6**(12): p. 1347-1364.

9.   Caltagirone, C., et al., *Cancer-Cell-Targeted Theranostic Cubosomes.* Langmuir, 2014. **30**(21): p. 6228-6236.

10.   Garg, G., et al., *Cubosomes: An Overview.* Biological and Pharmaceutical Bulletin, 2007. **30**(2): p. 350-353.

11.   Larsson, K., *Aqueous dispersions of cubic lipid–water phases.* Current Opinion in Colloid & Interface Science, 2000. **5**(1–2): p. 64-69.

12.   Spicer, P.T., *Progress in liquid crystalline dispersions: Cubosomes.* Current Opinion in Colloid & Interface Science, 2005. **10**(5): p. 274-279.

13.   Spicer, P.T., et al., *Novel Process for Producing Cubic Liquid Crystalline Nanoparticles (Cubosomes).* Langmuir, 2001. **17**(19): p. 5748-5756.

14.   Xin, P., et al., *Nanostructed Cubosomes as Advanced Drug Delivery System.* Current Pharmaceutical Design, 2013. **19**(35): p. 6290-6297.

15.   Nazaruk, E., et al., *Lipidic Cubic-Phase Nanoparticles—Cubosomes for Efficient Drug Delivery to Cancer Cells.* ChemPlusChem, 2017. **82**(4): p. 570-575.

16.   Boyd, B.J. and Fong, W.-K., *Stimuli-Responsive Lipid-Based Self-Assembled Systems*, in *Self-Assembled Supramolecular Architectures.* 2012, John Wiley & Sons, Inc. p. 257-288.

17.   Aleandri, S., et al., *Design of Light-Triggered Lyotropic Liquid Crystal Mesophases and Their Application as Molecular Switches in "On Demand" Release.* Langmuir, 2015. **31**(25): p. 6981-6987.

18. Dong, Y.-D., et al., *Bulk and Dispersed Aqueous Phase Behavior of Phytantriol: Effect of Vitamin E Acetate and F127 Polymer on Liquid Crystal Nanostructure.* Langmuir, 2006. **22**(23): p. 9512-9518.

19. Barauskas, J., et al., *Cubic Phase Nanoparticles (Cubosome): Principles for Controlling Size, Structure, and Stability.* Langmuir, 2005. **21**(6): p. 2569-2577.

20. Deshpande, S. and Singh, N., *Influence of Cubosome Surface Architecture on Its Cellular Uptake Mechanism.* Langmuir, 2017.

21. Kluzek, M., et al., *Influence of a pH-sensitive polymer on the structure of monoolein cubosomes.* Soft Matter, 2017.

22. Mulet, X., et al., *Advances in drug delivery and medical imaging using colloidal lyotropic liquid crystalline dispersions.* Journal of Colloid and Interface Science, 2013. **393**: p. 1-20.

23. Alcaraz, N. and Boyd, B.J., *Cubosomes as Carriers for MRI Contrast Agents.* Current Medicinal Chemistry, 2017. **24**(5): p. 470-482.

24. Tian, Y., et al., *Folic Acid-Targeted Etoposide Cubosomes for Theranostic Application of Cancer Cell Imaging and Therapy.* Medical Science Monitor : International Medical Journal of Experimental and Clinical Research, 2017. **23**: p. 2426-2435.

25. Chong, J.Y.T., et al., *Chapter Five - Steric Stabilizers for Cubic Phase Lyotropic Liquid Crystal Nanodispersions (Cubosomes)*, in *Advances in Planar Lipid Bilayers and Liposomes*, A. Iglič, C.V. Kulkarni, and M. Rappolt, Editors. 2015, Academic Press. p. 131-187.

26.   Chong, J.Y.T., et al., *Steric stabilisation of self-assembled cubic lyotropic liquid crystalline nanoparticles: high throughput evaluation of triblock polyethylene oxide-polypropylene oxide-polyethylene oxide copolymers.* Soft Matter, 2011. **7**(10): p. 4768-4777.

27.   Zhai, J., et al., *Revisiting β-Casein as a Stabilizer for Lipid Liquid Crystalline Nanostructured Particles.* Langmuir, 2011. **27**(24): p. 14757-14766.

28.   Chong, J.Y.T., et al., *High-Throughput Discovery of Novel Steric Stabilizers for Cubic Lyotropic Liquid Crystal Nanoparticle Dispersions.* Langmuir, 2012. **28**(25): p. 9223-9232.

29.   Chong, J.Y.T., et al., *Novel RAFT amphiphilic brush copolymer steric stabilisers for cubosomes: poly(octadecyl acrylate)-block-poly(polyethylene glycol methyl ether acrylate).* Soft Matter, 2014. **10**(35): p. 6666-6676.

30.   Murgia, S., et al., *Cubosome formulations stabilized by a dansyl-conjugated block copolymer for possible nanomedicine applications.* Colloids and Surfaces B: Biointerfaces, 2015. **129**: p. 87-94.

31.   Zhai, J., et al., *Lipid–PEG Conjugates Sterically Stabilize and Reduce the Toxicity of Phytantriol-Based Lyotropic Liquid Crystalline Nanoparticles.* Langmuir, 2015. **31**(39): p. 10871-10880.

32.   Chong, J.Y.T., et al., *Novel Steric Stabilizers for Lyotropic Liquid Crystalline Nanoparticles: PEGylated-Phytanyl Copolymers.* Langmuir, 2015. **31**(9): p. 2615-2629.

33.   Wang, R., et al., *Generation of toxic degradation products by sonication of Pluronic(®) dispersants: implications for nanotoxicity testing.* Nanotoxicology, 2013. **7**: p. 1272-1281.

34.   Pitto-Barry, A. and Barry, N.P.E., *Pluronic[registered sign] block-copolymers in medicine: from chemical and biological versatility to rationalisation and clinical advances.* Polymer Chemistry, 2014. **5**(10): p. 3291-3297.

35.   Meikle, T.G., et al., *Incorporation of antimicrobial peptides in nanostructured lipid membrane mimetic bilayer cubosomes.* Colloids and Surfaces B: Biointerfaces, 2017. **152**: p. 143-151.

36.   Briggs, J. and Caffrey, M., *The temperature-composition phase diagram and mesophase structure characterization of monopentadecenoin in water.* Biophysical Journal, 1994. **67**(4): p. 1594-1602.

37.   Nazaruk, E., et al., *Lyotropic Cubic Phases for Drug Delivery: Diffusion and Sustained Release from the Mesophase Evaluated by Electrochemical Methods.* Langmuir, 2015. **31**(46): p. 12753-12761.

38.   Naga, M.L., et al., *Cubosomes as Targeted Drug Delivery Systems - A Biopharmaceutical Approach.* Current Drug Discovery Technologies, 2014. **11**(3): p. 181-188.

39.   Angelov, B., et al., *Identification of large channels in cationic PEGylated cubosome nanoparticles by synchrotron radiation SAXS and Cryo-TEM imaging.* Soft Matter, 2015. **11**(18): p. 3686-3692.

40. Fraser, S.J., et al., *Controlling nanostructure and lattice parameter of the inverse bicontinuous cubic phases in functionalized phytantriol dispersions.* Journal of Colloid and Interface Science, 2013. **408**: p. 117-124.

41. Tilley, A.J., et al., *Disposition and association of the steric stabilizer Pluronic® F127 in lyotropic liquid crystalline nanostructured particle dispersions.* Journal of colloid and interface science, 2013. **392**: p. 288-296.

42. Barauskas, J. and Landh, T., *Phase Behavior of the Phytantriol/Water System.* Langmuir, 2003. **19**(23): p. 9562-9565.

Chapter 6 - Summary, Lessons Learned and Future Directions

6.1 Summary of studies in this thesis

Interest in developing better and smarter drug formulations is steadily increasing as novel drug molecule design is becoming more difficult and expensive. As mentioned, this body of work attempted to create lipid nanoparticles with controlled release capabilities and combining that with the techniques known as metabolic labelling and copper-free click chemistry as a means for targeted delivery. The nanoparticles of interest to this project are known as cubosomes and have many desirable properties for drug delivery systems [1] and acting as carriers for imaging applications [2]. This thesis presents the creation, characterisation and effectiveness of novel clickable cubosomes and also the expansion of our understanding around the mechanisms that influence lipid nanoparticle-cell surface binding through metabolic labelling and copper free click chemistry, specifically the role of nanoparticle size and stabilisation on binding.

As addressed in **Chapter Three**, the cubosomes were formulated to include click-groups through the use of commercial phospholipids that possessed either an azide or a strained cyclooctyne (DBCO) group that could impart functionality to the system so they can partake in copper-free click chemistry reactions. It was found that by adding 2 mol % of phospholipid to the lipid component of the formulation it was possible to introduce a sufficiently high concentration of click groups without interfering drastically with the size, structure and stability of the cubosomes when compared to traditional Phytantriol cubosomes stabilised with 1.5% (w/v) Pluronic F108. This was confirmed through the use of DLS, cryo-TEM and SAXS. The phospholipid bearing cubosomes exhibited similar size, structure and stability to those without phospholipids indicating that it would be possible to prepare clickable cubosomes that retain the structural characteristics of the traditional Pluronic stabilised cubosomes.

The ability of these new cubosomes to undergo a copper-free click reaction was then assessed initially using the complementary small molecule sulfo-cy5 dye in solution. Specific binding was shown in all the click-capable systems with minimal non-specific binding being evident. These studies have been published in Bioconjugate Chemistry [3]. The cubosomes structure was reassessed using SAXS after being clicked to a dye molecule in solution and no significant changes to the structure of the systems was evident indicating that the clickable cubosomes had potential as targeted drug delivery systems due to retaining their structure and in turn the desirable properties.

The clickable cubosomes, together with liposomes as a control system anticipated to have low non-specific binding, were then tested for their ability to bind to surfaces. Initial experiments to bind the cubosomes to model surfaces were made, intended as a precursor to introducing them to a metabolically labelled cell surface.

These experiments are briefly discussed here, as they show development of the project, but were not successful so were not included in the main thesis, but deserve a brief mention under 'Lessons Learned'.

- Initially, a silicon wafer that had been chemically modified to contain azido groups was generated and the presence of the azide groups on the surface was confirmed with X-ray photoelectron spectroscopy (XPS) before Rhodamine B containing click-cubosomes were added and reacted with the surface for 24 hours and then imaged using fluorescent microscopy. Unfortunately, there was a high degree of non-specific binding, a lack of uniform surface modification and sensitivity resulting in inconclusive results.

- Additionally, a similar experiment was conducted at the Australian Synchrotron (AS) where the samples were mounted in a custom 3D printed holder and both transmission SAXS and grazing incidence SAXS was conducted on them. A lack of sensitivity led to no scattering detected in transmission SAXS. In order to overcome that GISAXS was attempted but also unsuccessful in detecting anything on the surface, this could be due to the novelty and lack of optimisation of the GISAXS setup at the AS.

- As a last effort at binding to a model surface, 1 µm click-functionalized magnetic beads were used as a means to mimic a cell surface. However, these were also unsuccessful due to high non-specific binding between the beads and the particles.

The primary goal of clicking the particles selectively to cells remained as the primary aim, and although the clicking to model surfaces was not successful, the soft nature of cells and 'fuzzy' glycoprotein interface meant that it was not absolutely certain that this experiment would not be successful. Consequently, clicking of the lipid particles to A549 cells was undertaken. Binding was assessed using TIRF microscopy [4, 5]. As mentioned in **Chapter Two,** TIRF was chosen as it allows for specific visualisation of the surface regions of cells and would give insight to what is occurring at the cell-nanoparticle interface but also its ability to observe single molecule fluorescence. This is possible as an evanescent wave illuminates a selected region adjacent to the glass-water interface by changing the angle of the beam to exceed the critical angle and achieve total internal reflection.

Cells were treated with click-modified mannose (or PBS) and then exposed to the different cubosome and liposomal dispersions. Binding to cells that had not been exposed to the click-sugar indicates non-specific binding. When unlabelled cells without click groups were exposed to cells, there was very high cubosome binding. The images showed every cell was covered in cubosomes indicating that a high degree of non-specific binding. In comparison, liposomes showed significantly less non-specific binding, indicating some potential for selective binding of liposomes through the click chemistry, consistent with previous reports [6-10]. Quantitative analysis of the images were then analysed using an in house script that allows the user to select a cell area and for the fluorescence to be quantified based on the known size of the nanoparticles.

The mean fluorescence intensity between no sugar and sugar treated cells was not significantly different for the cubosomes, meaning there was no ability to determine specific cell-surface binding over the high non-specific binding for the cubosomes. Somewhat surprisingly, the MFI was similar for liposomes introduced to sugar-treated cells compared to sugar-free, also indicating an absence of selective click-based binding.

These findings indicated that the specific variables of nanoparticle size, hardness and surface ligand density needed to be established to determine a direction to progress the research. Therefore, Chapter Four focused on investigating the role of nanoparticle type and size, and azide concentration on cell surface binding to aid and guide future experiments.

The studies in **Chapter Four** involved creating small (~15 nm) and large (~100 nm) liposomes with PEGylated phospholipids that also had low (1.5 mol %) or high (15 mol %) azide phospholipid loading. Cells were exposed to the different liposomes for 24 hours before rinsing off any unbound liposomes and imaged using TIRF like in the previous chapter. The studies showed that the smaller sized micelles with higher azide surface density exhibited much less non-specific binding and a greater amount of specific binding on the cell-surface.

To further define an appropriate size range and to determine whether the material from which the particles were made had an effect a series of fluorescent azide quantum dots that covered the sizes of 15, 30, 45 and 60 nm were also studied. The nanoparticles that were 30 nm or smaller should specific binding, whereas the larger nanoparticles did not. This supported the findings with the liposomes and micelles that the smaller sized nanoparticles showed higher amounts of specific binding.

This finding does not agree with some reported works where liposomes and other inorganic nanoparticles over 100 nm in size have been apparently delivered to tumors in mice successfully utilising these techniques [11-15]. However, these findings do shed some light on the results found in Chapter Three with the click cubosomes and liposomes. There was no significant specific binding of the liposomes even though there was low non-specific binding, reinforcing the finding that large particles do not offer an opportunity to click to the cells even in the case of low non-specific binding.

One hypothesis for the high non-specific binding seen for cubosomes in Chapter Three was that the stabiliser did not sufficiently cover the surface of the particle leading to hydrophobic interactions with the cells, in part due to its ready access to the internal water channels of the particle making it unavailable to prevent these interactions. To this end, an approach to improving cubosome surface chemistry was explored in **Chapter Five**.

In an attempt to better stabilise the surface of the cubosomes and provide a means of introducing the click surface functionalisation to the very outer surface of the particle, a series of novel polymers were developed in collaboration with James Grace from Monash Institute of Pharmaceutical Sciences. Initially, a series of single and two tailed lipid-like polymers with differentially charged head groups were synthesised, and their ability to be used as stabilisers for cubosome dispersions was assessed. These polymers also exhibited easily modifiable end groups meaning they could also be utilised to impart functionality to the cubosomes with a focus on the interface where the stabiliser is known to embed itself. Cubosomes were stabilised by the six different lipidated polymers at three different concentrations.

These polymers had either a neutrally, positively or negatively charge end groups and were either single or double tailed. The majority of the novel polymers at the appropriate concentration could act as stabilisers for cubosomes, adding to the pool of known stabilisers for such systems. The polymers structure impacted the size of the nanoparticle and also the internal structure behaviour of the cubosomes. It appears that the charge of the polymer end group greatly effects its ability to act as a stabiliser and not alter the mesophase.

This led to the functionalisation of two of these polymers with click azide groups which only differed in their PEG chain length. When incubated with Sulfo-DBCO-Cy5 dye in solution they performed similarly when compared to the click-phospholipid cubosomes described in Chapter Three showing over 90% selective binding with the dye. However, when incubated with A549 cells, the TIRF imaging showed a large amount of non-specific binding in the cells that were not metabolically labelled.

This would suggest that cubosomes will be very difficult to use in a metabolic labelling strategy to attach delivery particles to the cell-surface.

Many of the findings are of importance to this new field and the progression of targeting nanoparticles to cells through metabolic labelling and copper-free click chemistry. Click cubosomes were able to be formulated with intact 'clickability' towards the dye. Additionally, successful metabolic labelling with both azido and DBCO modified sugars was conducted and analysed using TIRF, which is, to our knowledge, the first time this microscopy method has been combined to biorthogonal chemistry. Finally, some insight was gained on the effect of size in relation to cell-surface binding and how to improve future lipid based nanoparticles that might take better advantage of biorthogonal chemistry.

6.2 Future directions

There is a constant need to improve pharmaceutical products and the concept of a theranostic system that is able to deliver the therapeutic agent specifically and in a controlled matter whilst also allowing for imaging and diagnostic capabilities is extremely desirable. These have the potential to improve survival rates in diseases such as cancer as the doctor can be assured that not only is the drug reaching the treatment site but that an effective dose will be delivered without causing a large amount of side effects. At the same time, they can monitor the disease and treatment progression utilising the diagnostic tools incorporated into the system. There are only a few of these systems in development and into clinical trials but preclinical reports of novel systems are being published weekly.

This body of work has attempted to add to this field and also help explain some of the more fundamental factors at play that must be understood for better design but there is still a lot unknown that should be investigated.

The ability to create click cubosomes was demonstrated and their ability to click to a dye was also proven, however the limitation arose when used with model surfaces and cell surfaces. The unsuccessful translation into specific delivery to the target surfaces and cells, even with novel effective stabiliser systems, indicates a clear need for further studies in understanding the mechanisms that dictate the non-specific binding. This can be achieved by further understanding the role of size, shape and surface properties which was started with the work from Chapter Five. One possible method to improve the success of cell-surface clicking for cubosomes and other nanoparticles in general is to limit their size, although the production of very small cubosomes <50 nm has not been reported previously.

In parallel to addressing the challenges imposed by size, the role of surface chemistry can also be investigated further. Aside from requiring the corresponding click group on the surface to react with the cell-surface it may be beneficial to reduce the hydrophobicity of the surface to reduce non-specific hydrophobic interactions with cell membranes like that observed in this Thesis. One approach can be to continue developing the library of polymers that can replace Pluronic F108 or F127 as the main means of colloidal stabilisation in an attempt to help create smaller more stable cubosomes which at the same time could have added functionalities. Studies could focus on developing DBCO and azide containing polymer stabilisers that are superior at stabilising cubosomes to those reported in Chapter Five, but provide favourable *in vivo* pharmacokinetics as observed with PEGylated liposomes in the literature.

Alternatively, another area to focus on could include the monomers used to make the lipidated polymers. The core lipid could be modified in order to influence the polymers interactions with the lipid.This could be achieved by altering the monomers used in the synthesis of the polymer, specifically including a PEG chain before the functional group to try and ensure it is away from the surface and available for reacting with the cell surface groups. The addition of a PEG chain on the surface will also change the surface properties by creating a large hydrophilic region. This would require further polymer synthesis and characterisation studies with the cubosomes. The next step would be to again assess the binding in solution and *in vitro* utilising the appropriate microscopy techniques.

Ideally, the new cubosome systems will be small, hydrophilic and stabilised by a custom polymer that adds the click functionality required for the targeted delivery. This may take some time as the fundamentals related to the cell surface interactions of nanoparticles, especially cubosomes, is not fully understood.

For this reason, it would be of interest to continue the work started in Chapter Four involving experiments that elucidate the key factors at play in order to aid others with their nanoparticle design if wanting to utilise metabolic labelling and copper-free click chemistry, especially with lipid-based nanoparticles. Further factors that need to be studied, aside from continuing at looking at the effect of size, include; the shape of the nanoparticle, the surface charge, the surface properties, the hardness of the nanoparticle, the click group concentration and overall reaction time. These are all key factors that scientists can somewhat exhibit control over and therefore is important when developing a novel nanoparticle system that will be used as a theranostic. As shown, size is a key factor when the nanoparticles get introduced to cells *in vitro* and in the literature successful nanoparticle targeting has occurred *in vivo*, indicating that the non-specific binding might be exaggerated with the protocol used when conducting cell studies.

To remove any flaws in the current method the following alternative approaches could be taken; a system where the cells are not adhered to the bottom of the well plate or using non-adherent cell lines to avoid sedimentation of nanoparticles and limit the role of gravity.

Another problem that was encountered involved the non-specific hydrophobic interactions between the cubosomes with each other and the cell membrane that didn't allow for certain separating and washing procedures which made techniques like flow cytometry or traditional fluorescent microscopy difficult as unbound cubosomes were unable to be effectively removed from the sample.

If a successful washing protocol could be developed that avoids causing aggregation or adherence of nanoparticles this would allow for better statistical analysis of cell surface binding and remove some of the noise from the analysis techniques painting a better picture of what is occurring at the cell-nanoparticle interface. What is required to fully understand the factors at play and to give a blueprint for nanoparticle development involves the creation of uniform and optimised nanoparticles that can have the key factors mentioned above altered relatively easily and analysed through more than one technique such as flow cytometry and TIRF. This would be extremely useful to the field and future researchers.

Another avenue of future research to pursue is investigating and improving the click reagents and reactions used. A very recent review [16] helps discuss the challenges and current approaches being undertaken. They emphasise the need to keep expanding the toolkits available as each option has its benefits but also limitations. Some of the more pressing limitations involve the fact that some of the click reagents will interact with each other *in vivo* meaning more than one reaction type cannot be used at the same time in the same system where another limitation is that only a select few of the reactions developed can be employed for fast conjugation *in vivo* in some of the harsher cellular environments.

One area of greater personal interest is increasing the specificity of chemical reporter generation such as that addressed with the publications utilising LABOR [17] or cleavable moieties that prevent cellular uptake and metabolism. For a successful theranostic system to utilise biorthogonal chemistry based targeting the generation of the chemical reporter on the cell of interest must be specific and significant or else specific targeting will be dramatically hindered.

Some promising avenues to pursue include using a targeted liposome to deliver the click-sugar directly to the cell of interest where a large number of chemical reporters can be generated on the surface. This could be useful in a few situations such as when disease states overexpress a particular receptor which generally has limited targeting ability. By ensuring a high concentration reaches the cell you can increase the amount of targetable groups easily and avoid any issues that may come from trying only to use those natural targets. Another option is to explore further the work by Wang *et al.* [10] where they synthesised sugars incapable of being metabolised until an extra functional group had been removed or modified.

This method can ignore trying to use natural targets by taking advantage of internal and external triggers that can ensure localised release for improved nanoparticle targeting.

Once a greater understanding of the challenges that face the nanoparticles and chemistry in the biological setting the next stage would be to further understand uptake and cell interaction mechanics such as internalization and eventual release of cargo.

In summation, there are a range of options and areas within this field to explore and different angles to tackle to help build the knowledge base and tools available for developing novel theranostics. The increase in interest can already be seen with the increasing number of publications across many relevant journals. The final goal in a more long term situation would be to move these studies into humans and create a medical product. These systems could create a new generation of treatments that can be used by clinicians to aggressively and accurately treat diseases such as cancer but also monitor the progress closely to fine tune future treatments for the highest possible efficacy and survival rates.

6.3 References

1.   Fong, W.-K., et al., *Responsive self-assembled nanostructured lipid systems for drug delivery and diagnostics.* Journal of colloid and interface science, 2016. **484**: p. 320-339.

2.   Alcaraz, N. and Boyd, B.J., *Cubosomes as Carriers for MRI Contrast Agents.* Current Medicinal Chemistry, 2017. **24**(5): p. 470-482.

3.   Alcaraz, N., et al., *Clickable Cubosomes for Antibody-Free Drug Targeting and Imaging Applications.* Bioconjugate Chemistry, 2018. **29**(1): p. 149-157.

4.   Ambrose, E.J., *A Surface Contact Microscope for the study of Cell Movements.* Nature, 1956. **178**: p. 1194.

5.   Furness, S.G.B., et al., *Ligand-Dependent Modulation of G Protein Conformation Alters Drug Efficacy.* Cell, 2016. **167**(3): p. 739-749.e11.

6.   Yoon, H.Y., et al., *Artificial Chemical Reporter Targeting Strategy Using Bioorthogonal Click Reaction for Improving Active-Targeting Efficiency of Tumor.* Molecular Pharmaceutics, 2017.

7.   Lee, S., et al., *Chemical Tumor-Targeting of Nanoparticles Based on Metabolic Glycoengineering and Click Chemistry.* ACS Nano, 2014. **8**(3): p. 2048-2063.

8.   Koo, H., et al., *In Vivo Targeted Delivery of Nanoparticles for Theranosis.* Accounts of Chemical Research, 2011. **44**(10): p. 1018-1028.

9.   Wang, H., et al., *Selective in vivo metabolic cell-labeling-mediated cancer targeting.* Nat Chem Biol, 2017. **13**(4): p. 415-424.

10. Wang, H., et al., *In Vivo Targeting of Metabolically Labeled Cancers with Ultra-Small Silica Nanoconjugates.* Theranostics, 2016. **6**(9): p. 1467-1476.

11. Perrault, S.D., et al., *Mediating tumor targeting efficiency of nanoparticles through design.* Nano letters, 2009. **9**(5): p. 1909-1915.

12. Danhier, F., et al., *To exploit the tumor microenvironment: passive and active tumor targeting of nanocarriers for anti-cancer drug delivery.* Journal of controlled release, 2010. **148**(2): p. 135-146.

13. Choi, K.Y., et al., *Self-assembled hyaluronic acid nanoparticles for active tumor targeting.* Biomaterials, 2010. **31**(1): p. 106-114.

14. Brannon-Peppas, L. and Blanchette, J.O., *Nanoparticle and targeted systems for cancer therapy.* Advanced Drug Delivery Reviews, 2012. **64**: p. 206-212.

15. Malam, Y., et al.,*Liposomes and nanoparticles: nanosized vehicles for drug delivery in cancer.* Trends in Pharmacological Sciences, 2009. **30**(11): p. 592-599.

16. Row, R.D. and Prescher, J.A., *Constructing New Bioorthogonal Reagents and Reactions.* Accounts of Chemical Research, 2018.

17. Xie, R., et al., *In vivo metabolic labeling of sialoglycans in the mouse brain by using a liposome-assisted bioorthogonal reporter strategy.* Proceedings of the National Academy of Sciences, 2016. **113**(19): p. 5173-5178.

Appendix

213

Original publications included in this section were completed during candidature that were either: (A) adapted for the thesis or (B) did not contribute to the overall coherent flow of the thesis.

Additionally, information pertaining to the synthesis and characterisation of certain molecules used can be found within this appendix.

Synthesis of Click-sugars by Dr. Jason Liu

Monash Institute of Pharmaceutical Sciences

Materials

Mannosamine hydrochloride (purity ≥ 98%), triethylamine (purity ≥ 98%), azidoacetic acid (purity ≥ 93%), 1-Hydroxybenzotriazole hydrate (1-HOBt) (purity ≥ 98%), N-(3-Dimethylaminopropyl)-N′-ethylcarbodiimide hydrochloride (EDC) (purity ≥ 98%), pyridine (purity ≥ 99%) and acetic anhydride all were purchased from Sigma-Aldrich (St Louis, MO). DBCO-NHS (purity ≥ 97%) was purchased from Lumiprobe Corporation (Maryland). Chloroform and methanol were purchased from Merck (Kilsyth, Australia).

Methods
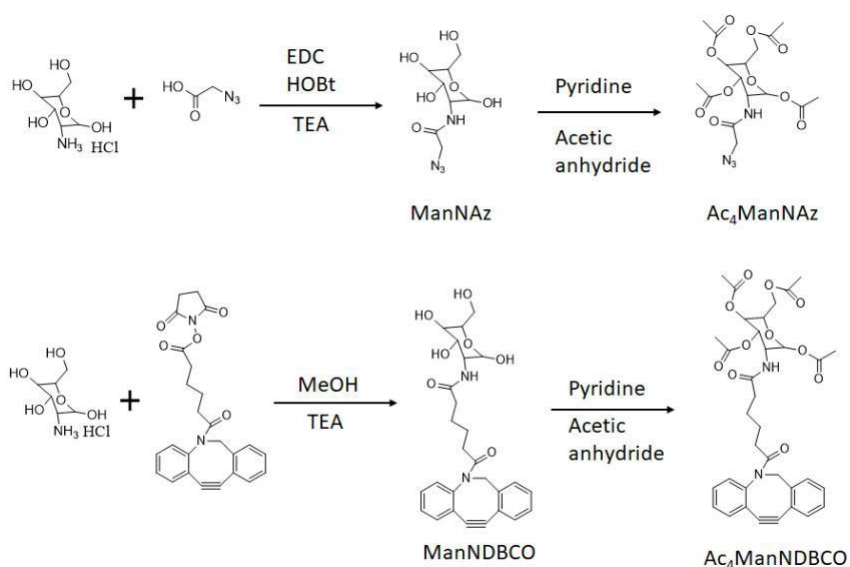
The chemical structure and synthesis route of unnatural mannosamine glycans with azido or DBCO functional group for metabolic labelling and copper free click chemistry.

The preparation of Ac4ManNAz

Mannosamine hydrochloride (5 mmol), azidoacetic acid (7.5 mmol) and triethylamine (20 mmol) were dissolved in 70 mL methanol, followed by the addition of 1-HOBt (7 mmol) and EDC (7 mmol) in methanol. The mixture was stirred at room temperature overnight. Solvent was removed under reduced pressure, the ManNAz is hardly and unnecessary completely purified, will be directly used for next step reaction.

The residue from last reaction was redissolved in 15 mL pyridine, then acetic anhydride (15 mL) was added. The reaction mixture was stirred at room temperature overnight. After removal of the solvent, the residue was resolved in milli-Q water (50 mL). The residue aqueous solution was extracted three times using chloroform (30 mL). The chloroform solutions were combined and dried by addition of anhydrous sodium sulfate. After filtration and removal of the chloroform, the crude product was pre-purified by flash chromatography, eluting with methanol/chloroform (1/50 to 1/20, v/v). Then the product was further purified by flash chromatography, eluting with methanol/chloroform (1/30, v/v). The product is light yellow oil (total 55% yield).[1] ^{1}H NMR (CDCl3, 400 MHz): δ (ppm) 1.94 (d, 3H), 2.00 (s, 3H), 2.05 (d, 3H), 2.12 (s, 3H), 3.74-3.78 (m, 0.3H), 3.96-4.10 (m, 3H), 4.15-4.21 (m, 1H), 4.27-4.30 (t, 0.2H), 4.53-4.57 (m, 0.5H), 4.66-4.69 (m, 0.3H), 4.98-5.30 (m, 2H), 5.82-5.83 (d, 0.3H), 5.98-5.99 (d, 0.3H), 6.1-6.14 (m, 0.2H), 6.5-6.6 (m, 0.8H).

The preparation of ManNAz

200 mg Ac4ManNAz was dissolved in 30 mL methanol, followed by the addition of 200 mg sodium hydroxide power. The mixture was refluxed for 4 hours. After removal of the methanol, the residue was resolved in milli-Q water (5 mL), adjusted pH to 7.0 via titration using 1 M HCl solution, and was diluted to 0.05 M. The diluted ManNAz solution was separately stored in vias, then these via was freeze dried for storage.

The preparation of ManNDBCO

Mannosamine hydrochloride (0.5 mmol) and triethylamine (1.0 mmol) were dissolved in methanol (20 mL), followed by the addition of DBCO-NHS (0.6 mmol) in methanol. The mixture was stirred at room temperature overnight. Solvent was removed under reduced pressure, crude product was purified by flash chromatography, eluting with methanol/chloroform (1/9, v/v). The product is light yellow powder (45% yield). ^{1}H NMR (CDCl3, 400 MHz): δ (ppm) 1.27-1.28 (m, 2H), 1.76-1.81 (m, 1H), 1.95-2.09 (m, 3H), 2.17-2.21 (m, 2H), 3.60-3.66 (m, 2H), 3.78-3.83 (m, 3H), 4.05-4.07 (m, 0.65H), 4.26-4.34 (m, 1.35H), 4.88-4.98 (m, 0.7H), 5.03-5.11 (m, 1.3H), 7.09-7.23 (m, 3H), 7.34-7.37 (m, 4H), 7.64-7.66 (m, 1H).

The preparation of Ac4ManNDBCO

The ManNDBCO (0.2 mmol) was redissolved in pyridine (4 mL). Then acetic anhydride (5 mL) was added. The reaction mixture was stirred at room temperature overnight. After removal of the solvent, the crude product was purified by flash chromatography, eluting with chloroform. The product is light yellow powder (95 % yield).[14] ^{1}H NMR (CDCl3, 400 MHz): δ (ppm) 1.33-1.53 (m, 4H), 1.92-2.21 (m, 16H), 3.68-3.74 (m, 1H), 3.80-3.83 (m, 0.35H), 4.06-4.18 (m, 1.65H), 4.31-4.41 (m, 1H), 4.52-4.60 (m, 0.65H), 4.72-4.73 (m, 0.35H), 5.05-5.06 (m, 0.35H), 5.14-5.35 (m, 2H), 5.57-5.62 (m, 0.2H), 5.83-5.90 (m, 0.4H), 6.02-6.10 (m, 1H), 7.02-7.46 (m, 7H), 7.71-7.77 (m, 1H).

Synthesis and characterisation of lipidated polymers by James Grace

Monash Institute of Pharmaceutical Sciences

Charged lipidated Polymer preparation

Materials

Tris(2-(dimethylamino)ethyl) amine (Me6TREN), (2-Boc-amino)ethyl acrylate (2-BocAEA), (R)-3-((2-bromo-2-methylpropanoyl)oxy)propane-1,2-diyl didodecanoate (BMPD), Dichloromethane (DCM, Sigma Aldrich), dimethyl sulphoxide (DMSO, Merck Millipore), copper (II) bromide (CuBr2, Sigma-Aldrich, 98%), triethylamine (TEA, Sigma Aldrich) dodecyl 2-bromoisobutyrate (DBiB, Sigma Aldrich), trifluoroacetic acid (TFA, Sigma Aldrich), O-(2-Aminoethyl)-O'-(2-azidoethyl)heptaethylene glycol (Azido-PEG8-amine, Sigma-Aldrich), Azide-PEG2000-amine (nanocs), 1,2-dilauroyl-*sn*-glycerol (1,2-DLG, Sapphire Biosciences) were used as received. Tert-butyl acrylate (tBA, Sigma Aldrich) and Poly(ethylene glycol) methyl ether acrylate (PEGMEA, Sigma Aldrich) was de-inhibited by percolating over a column of basic alumina. Copper wire was activated by washing in sulfuric acid for 10 min, followed by the removal of the acid with water and drying of the copper wire. The VDM was a kind gift from Prof. Fontaine's group.

Methods

Diglyceride-terminated poly(tert-butyl acrylate) (di-C12-P(tBA)

tBA (0.4467 mL, 3.05 mmol, 5 eq.), DMSO (1.0 mL), BMPD (0.3694 g, 0.610 mmol, 1 eq.), Me6TREN (0.0260 mL, 0.0976 mmol, 0.16 eq.), CuBr2 (0.0068 g, 0.0305 mmol, 0.05 eq.), were charged to a polymerization flask with a magnetic stir bar and fitted with a rubber septum and the mixture degassed via nitrogen sparging for 15 min after which pre-activated copper wire was carefully added under a nitrogen blanket. The polymerization flask was then resealed, deoxygenated for a further five minutes and polymerization was allowed to occur at room temperature for 24 hours.

Diglyceride-terminated poly((2-Boc-amino) ethyl acrylate) (di-C12-P(2-BocAEA))

2-BocAEA (0.5 g, 2.32 mmol, 5 eq.), DMSO (1.0 mL), BMPD (0.2816 g, 0.465 mmol, 1 eq.), Me6TREN (0.0198 mL, 0.0744 mmol, 0.16 eq.), CuBr2 (0.0052 g, 0.0232 mmol, 0.05 eq.), were charged to a polymerization flask with a magnetic stir bar and fitted with a rubber septum and the mixture degassed via nitrogen sparging for 15 min after which pre-activated copper wire was carefully added under a nitrogen blanket. The polymerization flask was then resealed, deoxygenated for a further five minutes and polymerization was allowed to occur at room temperature for 24 hours.

Dodecyl-terminated poly(tert-butyl acrylate) (C12-P(tBA))

tBA (0.5 mL, 3.41 mmol, 5 eq.), DMSO (1.0 mL), DBiB (0.2164 mL, 0.683 mmol, 1 eq.), Me6TREN (0.0291 mL, 0.109 mmol, 0.16 eq.), CuBr2 (0.0076 g, 0.0341 mmol, 0.05 eq.), were charged to a polymerization flask with a magnetic stir bar and fitted with a rubber septum and the mixture degassed via nitrogen sparging for 15 min after which pre-activated copper wire was carefully added under a nitrogen blanket. The polymerization flask was then resealed, deoxygenated for a further five minutes and polymerization was allowed to occur at room temperature for 24 hours.

Dodecyl-terminated poly((2-Boc-amino) ethyl acrylate) (C12-P(2-BocAEA))

2-BocAEA (0.5 g, 2.32 mmol, 5 eq.), DMSO (1.0 mL), DBiB (0.1473 mL, 0.465 mmol, 1 eq.), Me6TREN (0.0198 mL, 0.0744 mmol, 0.16 eq.), CuBr2 (0.0052 g, 0.0232 mmol, 0.05 eq.), were charged to a polymerization flask with a magnetic stir bar and fitted with a rubber septum and the mixture degassed via nitrogen sparging for 15 min after which pre-activated copper wire was carefully added under a nitrogen blanket. The polymerization flask was then resealed, deoxygenated for a further five minutes and polymerization was allowed to occur at room temperature for 24 hours.

After polymerization a sample of the reaction mixture was removed for ^{1}H NMR and GPC analysis. The sample for ^{1}H NMR was diluted with CDCl3, while the sample for GPC was first diluted with DMAc then passed over a neutral aluminium oxide column to remove metal salts. The polymers synthesized were purified by diluting with THF and passing over a neutral aluminium oxide column to remove metal salts and remaining monomer, followed by removal of the solvent by evaporation under a stream of air.
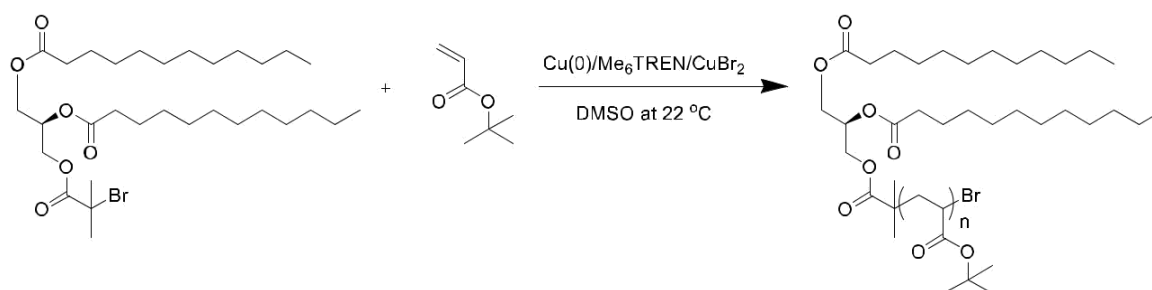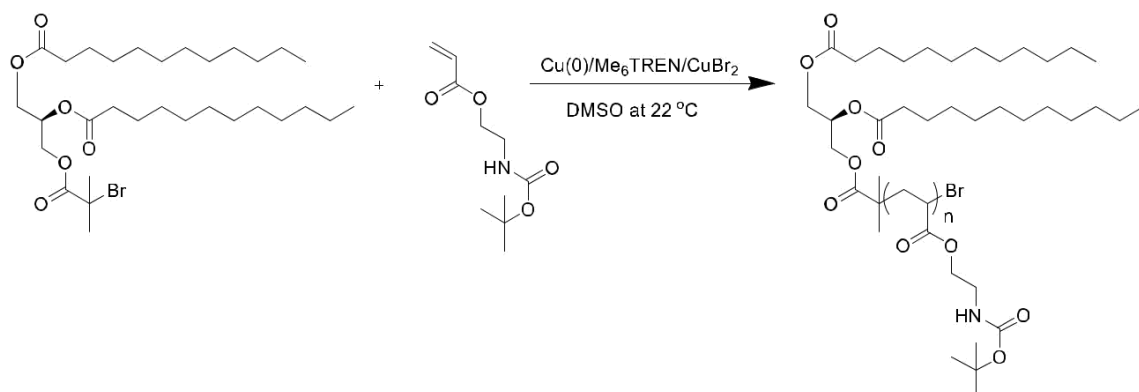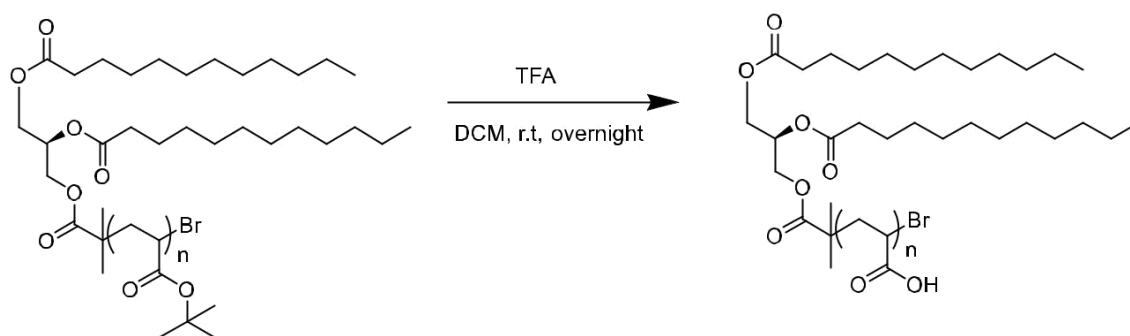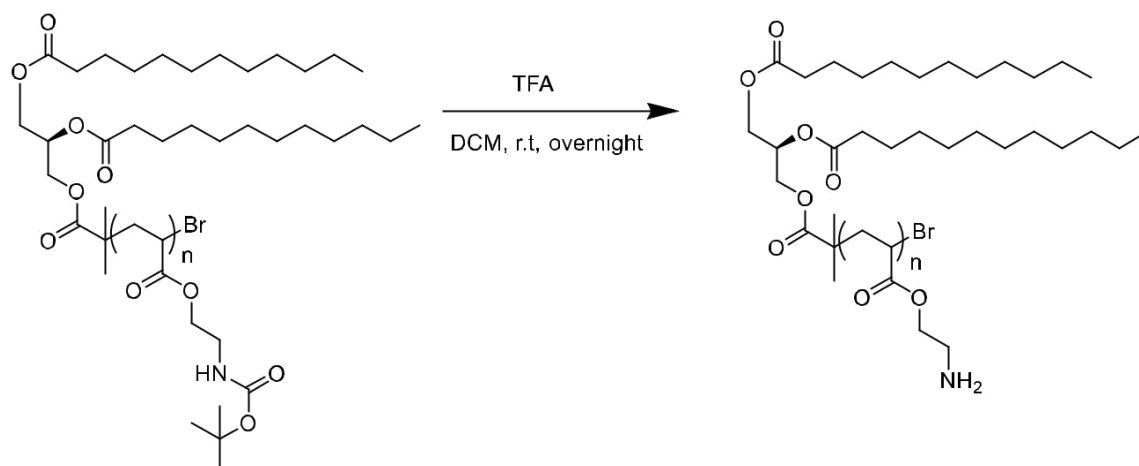
Charged lipidated polymer deprotection

Di-C12-Poly(2-BocAEA) (200 mg) was dissolved in DCM (2.0 mL) in a 20 mL glass vial, in which TFA (2.0 mL) was added and allowed to react overnight. The resulting deprotected polymer solution was then evaporated to dryness under a stream of air, after which 5.0 mL of acetone was added and evaporated to dryness under a stream of air, and this process was repeated three times. Finally, the polymer was dried in the vacuum oven at 25°C for a week to remove residual solvent. Complete deprotection was confirmed by ^{1}H NMR using MeOD. This process was repeated for the single chain initiator (DBiB), and the polymers containing tBA.

Charged lipidated polymer characterisation

Nuclear Magnetic Resonance (NMR) Spectroscopy. All NMR spectra were recorded on a Bruker Advance III 400 MHz spectrometer using an external lock and referenced to the residual nondeuterated solvent. Chemical shifts ($δH$) are reported in parts per million (ppm). NMR solvents (CD3OD and CDCl3) were purchased from Sigma-Aldrich and used as received.

Gel Permeation Chromatography (GPC). GPC analyses of polymer samples were performed using a Shimadzu modular system comprising a DGU-20A3R degasser unit, an SIL-20A HT autosampler, a 10.0 μm bead-size guard column (50 x 7.8 mm) followed by three KF-805L columns (300 x 8 mm, bead size: 10 μm, pore size maximum: 5000 Å), a SPD-20A UV/Vis detector, and an RID-10A differential refractive-index detector. The temperature of columns was maintained at 40 °C using a CTO- 20A oven.

The eluent was *N,N*-dimethylacetamide (CHROMASOLV Plus for HPLC) and the flow rate was kept at 1.0 mL min^{-1} using an LC-20AD pump. A molecular weight calibration curve was produced using commercial narrow molecular weight distribution polystyrene standards with molecular weights ranging from 500 to 2 x 10^6 g mol^{-1}. Polymer solutions at approx. 2 mg mL^{-1} were prepared and filtered through 0.45 µm PTFE filters before injection.

Reaction pathways for the lipidated polymers. The reaction pathway is the same for the single chained polymers.

Polymer Characterization using ^{1}H NMR and GPC

| Initiator	Monomer	DP[a]	Mn[a]	Mn[b]	PDI[b]
DBiB	2-BocAEA	7	1800	3200	1.07
	tBA	3	700	-	-
BMPD	2-BocAEA	6	1900	2900	1.07
	tBA	4	1100	-	-

[a]DP (degree of polymerization) values and Mn were determined by ^{1}H NMR peak integration analysis. [b]Mn and PDI were determined by GPC analysis in DMAc against polystyrene standards.
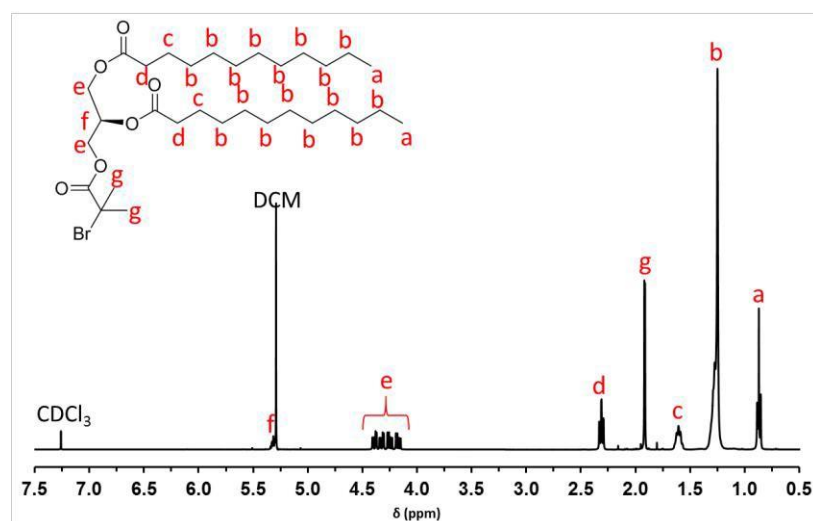
^{1}H NMR spectra of BMPD. ^{1}H NMR was recorded in CDCl3
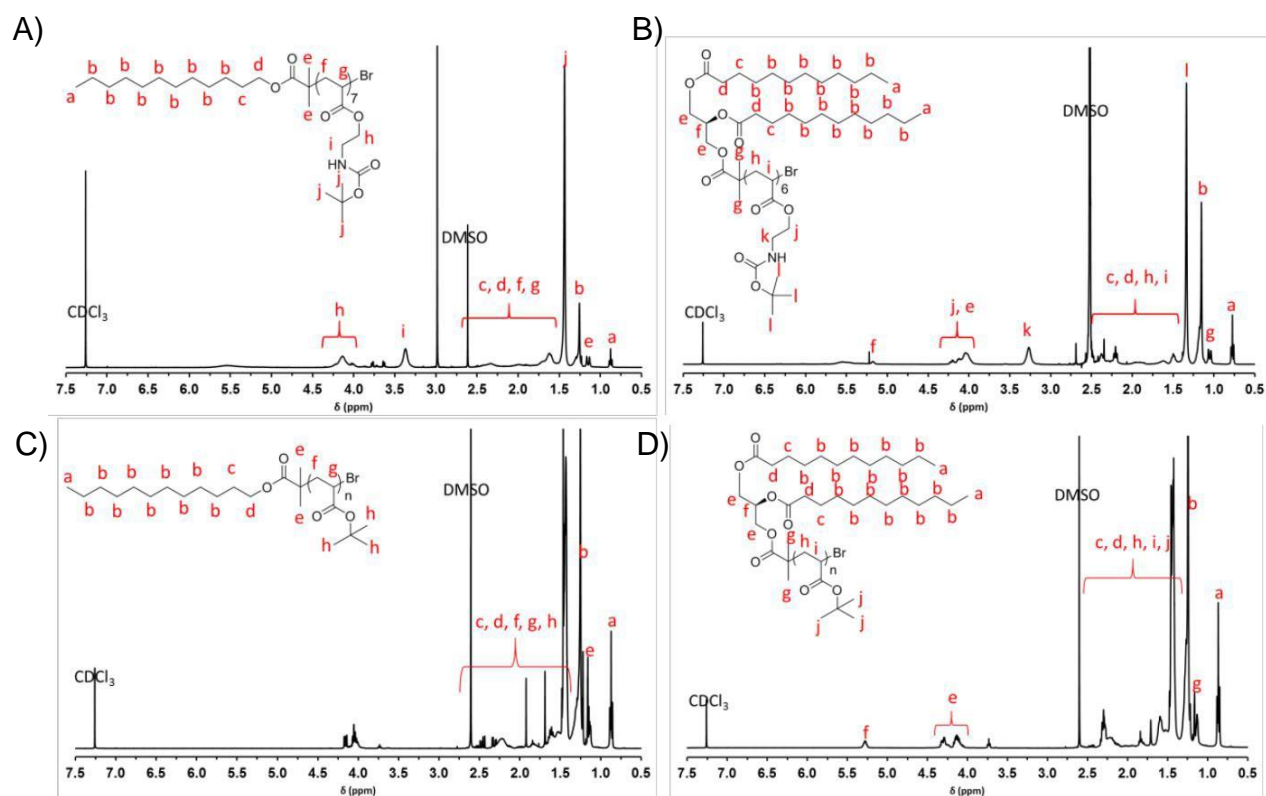
¹H NMR spectra of A) C12-terminated PBocAEA; B) di-C12-terminated PBocAEA; C) C12-terminated PtBA; D) di-C12-terminated PtBA. ¹H NMR conducted in CDCl3.
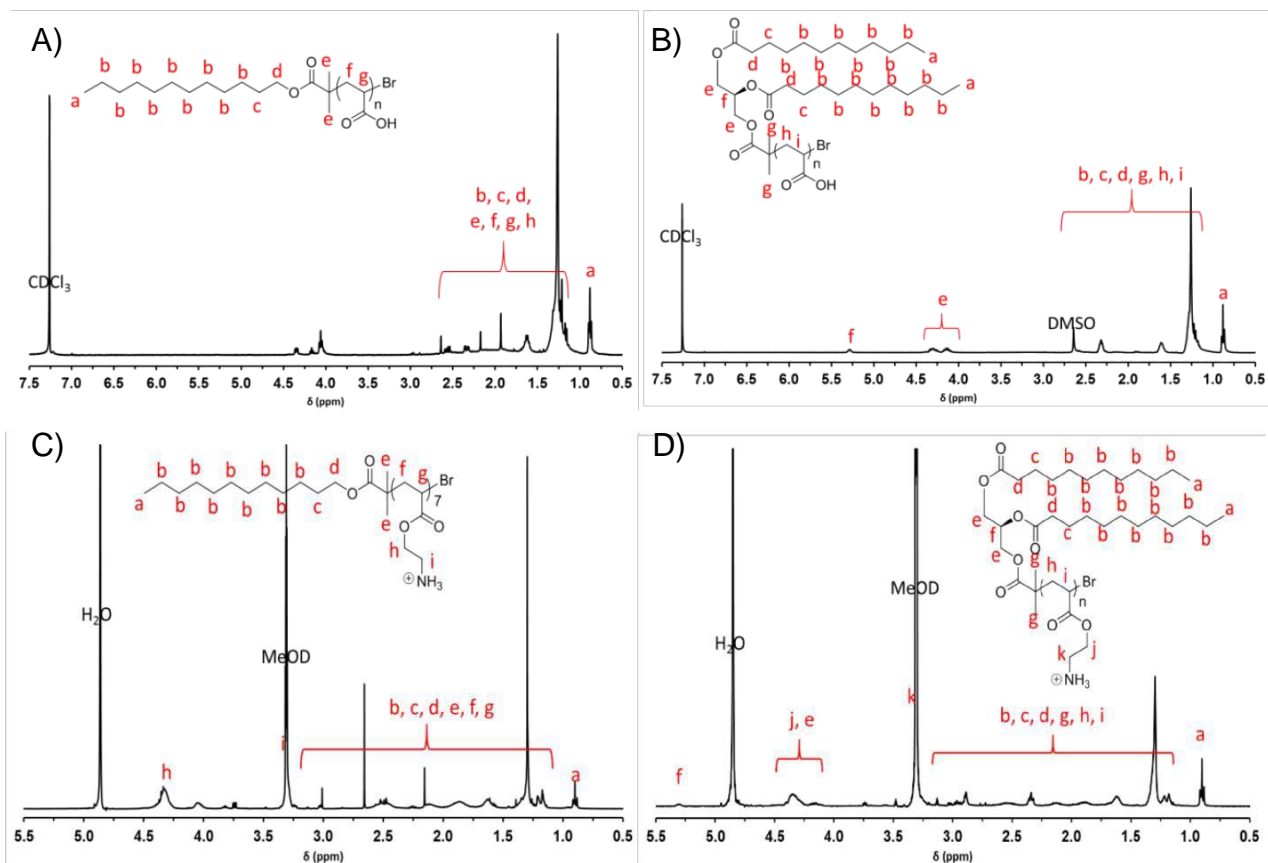
^{1}H NMR spectra of deprotected polymers; A) C12-terminated PAA; B) di-C12-terminated PAA; C) C12-terminated PAEA; D) di-C12-terminated PAEA. ^{1}H NMR conducted in CDCl3 for A) and B). ^{1}H NMR conducted in MeOD for C) and D).

Azide-PEG lipidated polymers

Methods

Polymerization

PEGMEA (0.5 mL, 1.14 mmol, 5 eq.), DMSO (1.0 mL), BMPD (0.1375 g, 0.227 mmol, 1 eq.), Me6TREN (0.0097 mL, 0.0363 mmol, 0.16 eq.), CuBr2 (0.0025 g, 0.0114 mmol, 0.05 eq.), were charged to a polymerization flask with a magnetic stir bar and fitted with a rubber septum and the mixture degassed via nitrogen sparging for 15 min after which pre-activated copper wire was carefully added under a nitrogen blanket. The polymerization flask was then resealed, deoxygenated for a further five minutes and polymerization was allowed to occur at room temperature for 5 hours.

A sample of the reaction mixture was removed for ^{1}H NMR and GPC analysis. The sample for ^{1}H NMR was diluted with CDCl3, while the sample for GPC was first diluted with DMAc then passed over a neutral aluminium oxide column to remove metal salts. The 2C12-poly(PEGMEA) was chained extended by the addition of deoxygenated vinyl azlactone (152 μL, 1.14 mmol, 5 eq.) using a deoxygenated gas-tight syringe. To allow for fast conversion, and moderate control over the reaction Me6TREN (25.4 μL, 0.0954 mmol, 0.5 eq.) was also added at the same time. The polymerization was allowed to react for 3 hours, and was then stopped by exposure to air.

A sample of the reaction mixture was removed for ^{1}H NMR and GPC analysis. The sample for ^{1}H NMR was diluted with CDCl3, while the sample for GPC was first diluted with DMAc then passed over a neutral aluminium oxide column to remove metal salts. The crude polymer solution was immediately employed for the ring-opening utilizing the amine to yield the desired functionalized polymer.

Modification of poly(PEGMEA-b-VDM)

0.353 mL of the crude 2C12-poly(PEGMEA-*b*-VDM) solution (containing 0.224 mmol of azlactone functionality) was added to a polymerization vial and diluted with 0.393 mL of DMSO and 0.0625 mL TEA . NH-PEG-N3 2K (493.30 mg, 0.247 mmol) was added to the polymer solution in 0.785 mL of DMSO and allowed to react for 3 days. The solution was dialysed in water for 5 days with MWCO 12-14k g/mol.

0.333 mL of the crude 2C12-poly(PEGMEA-*b*-VDM) solution (containing 0.211 mmol of azlactone functionality) was added to a polymerization vial and diluted with 0.370 mL of DMSO and 0.0589 mL TEA . *O*-(2-Aminoethyl)-*O'*-(2-azidoethyl)heptaethylene glycol (101.81 mg, 0.232 mmol) was added to the polymer solution in 0.739 mL of DMSO and allowed to react for 3 days. The solution was dialysed in water for 5 days with MWCO 1000 g/mol.

After purification a sample was taken for ^{1}H NMR and GPC analysis. The sample for ^{1}H NMR was diluted with CDCl3, while the sample for GPC was first diluted with DMAc then passed over a neutral aluminium oxide column to remove metal salts.

Infra-red analysis of the obtained polymer showed complete disappearance of the signals corresponding to the azlactone ring, along with the appearance of a strong signal corresponding to the azide peak. GPC analysis revealed a clear mass increase upon ring opening, and a well-defined final polymer observed.

Polymer Characterization

Nuclear Magnetic Resonance (NMR). All NMR spectra were recorded on a Bruker Advance III 400 MHz spectrometer using an external lock and referenced to the residual nondeuterated solvent. Chemical shifts (δH) are reported in parts per million (ppm). NMR solvents (CDCl3) were purchased from Sigma-Aldrich and used as received.

Gel Permeation Chromatography (GPC). GPC analyses of polymer samples were performed using a Shimadzu modular system comprising a DGU-20A3R degasser unit, an SIL-20A HT autosampler, a 10.0 µm bead-size guard column (50 x 7.8 mm) followed by three KF-805L columns (300 x 8 mm, bead size: 10 µm, pore size maximum: 5000 Å), a SPD-20A UV/Vis detector, and an RID-10A differential refractive-index detector. The temperature of columns was maintained at 40 °C using a CTO- 20A oven. The eluent was *N,N*-dimethylacetamide (CHROMASOLV Plus for HPLC) and the flow rate was kept at 1.0 mL min^{-1} using an LC-20AD pump. A molecular weight calibration curve was produced using commercial narrow molecular weight distribution polystyrene standards with molecular weights ranging from 500 to 2 x 10^6 g mol^{-1}. Polymer solutions at approx. 2 mg mL^{-1} were prepared and filtered through 0.45 µm PTFE filters before injection.

Characterization of the polymers with ^{1}H NMR and GPC

| Polymer	DP[a]		Mn[a]	Mn[b]	PDI[b]
	PEGMEA	Vinyl azlactone			
2C$_{12}$-PEGMEA	6	-	3500	3900	1.09
2C$_{12}$-PEGMEA-b-VDM	6	7	4500	6700	1.20
2C$_{12}$-PEGMEA-b-VDM-RO-2k NH-PEG-N$_3$	-	-	-	30452	1.18
2C$_{12}$-PEGMEA	6		3500	4464	1.08
2C$_{12}$-PEGMEA-b-VDM	6	9	4738	7050	1.23
2C$_{12}$-PEGMEA-b-VDM-RO-0.4k NH-PEG-N$_3$	-	-	-	12073	1.39
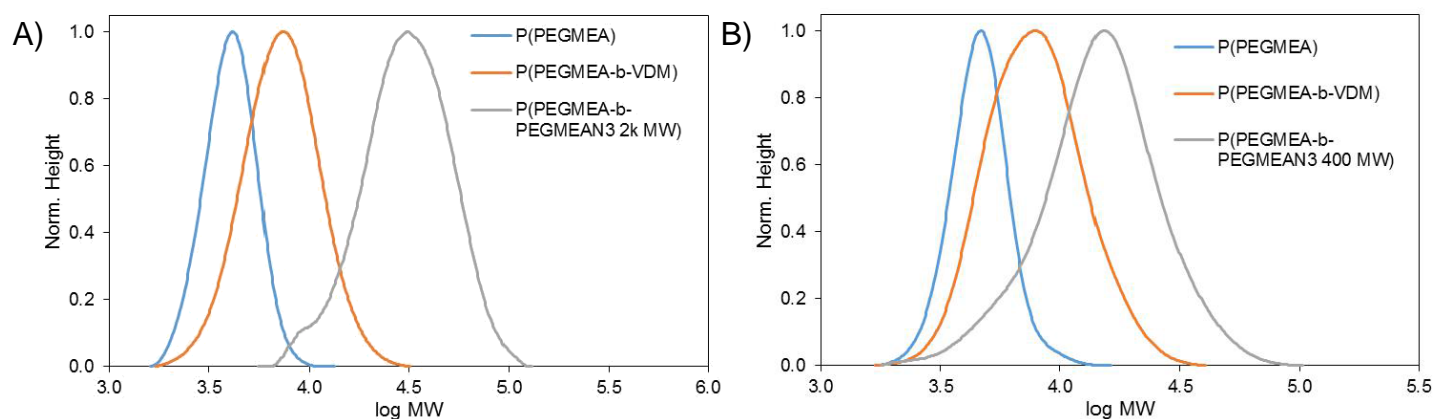
Evolution of the molecular weight of P(PEGMEA) through chain extension using VDM then ring opening with A) NH-PEG-N3 MW 2k and B) H-PEG-N3 MW 0.4k
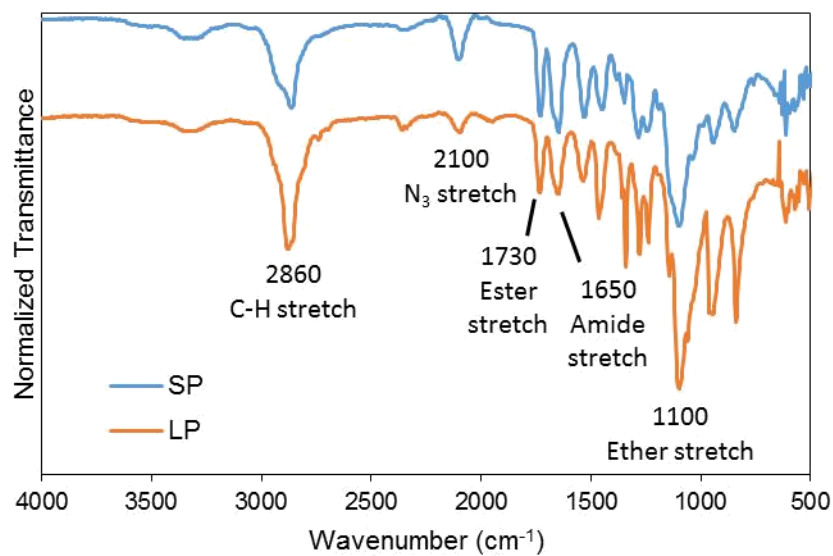
ATR-FTIR spectra of the ring opened polymers
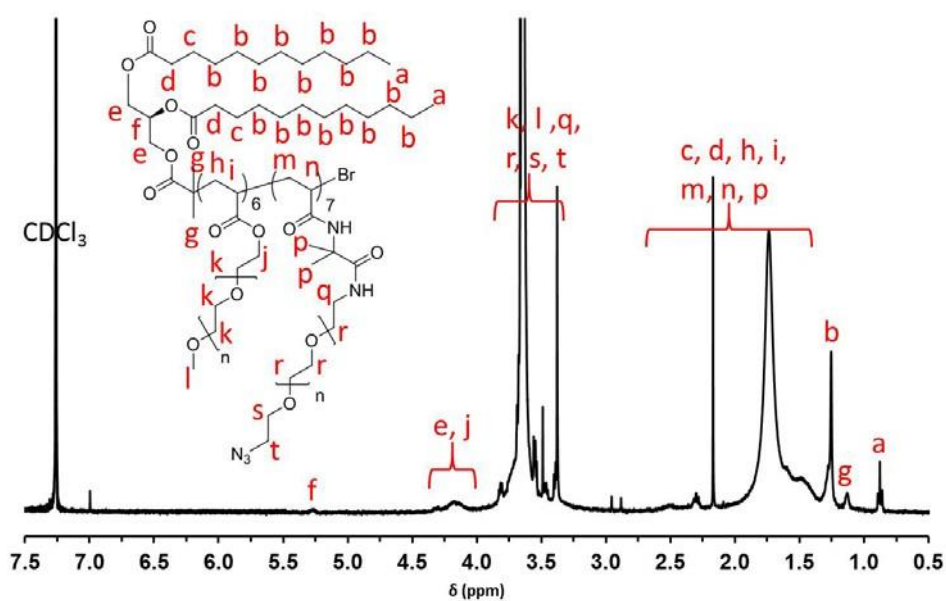
^{1}H NMR spectra of Polymer Long PEG
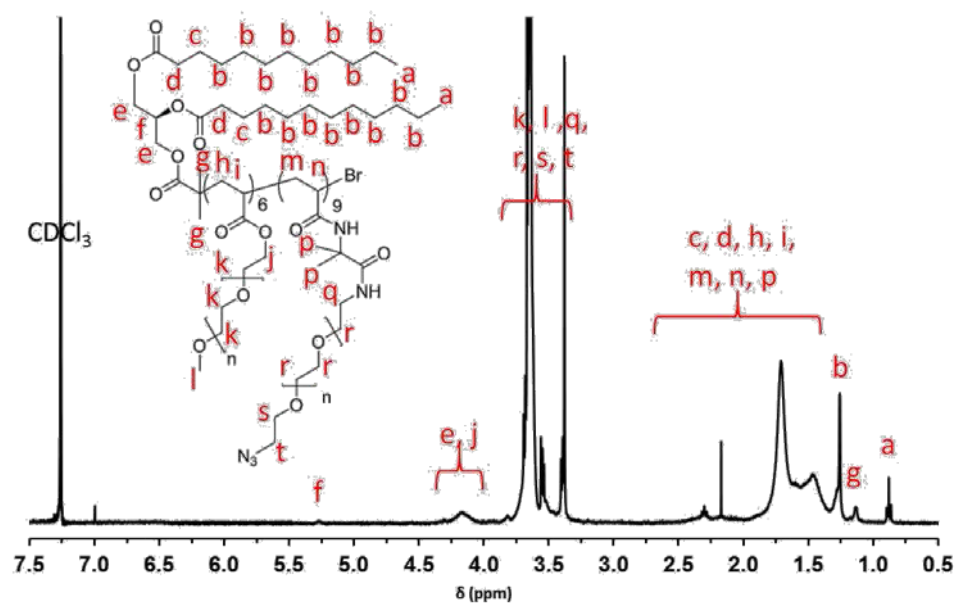
^{1}H NMR spectra of Polymer Short PEG

Stacked scattering profiles of SAXS temperature studies of phytantriol dispersions stabilised by lipidated polymers

Scattering profiles were acquired every 5ºC starting from 25ºC to 75ºC. The stacked plots generated have the lowest temperature (25ºC) at the bottom of the y-axis with the temperature increments above it respectively. For individual scattering profiles please contact the author.
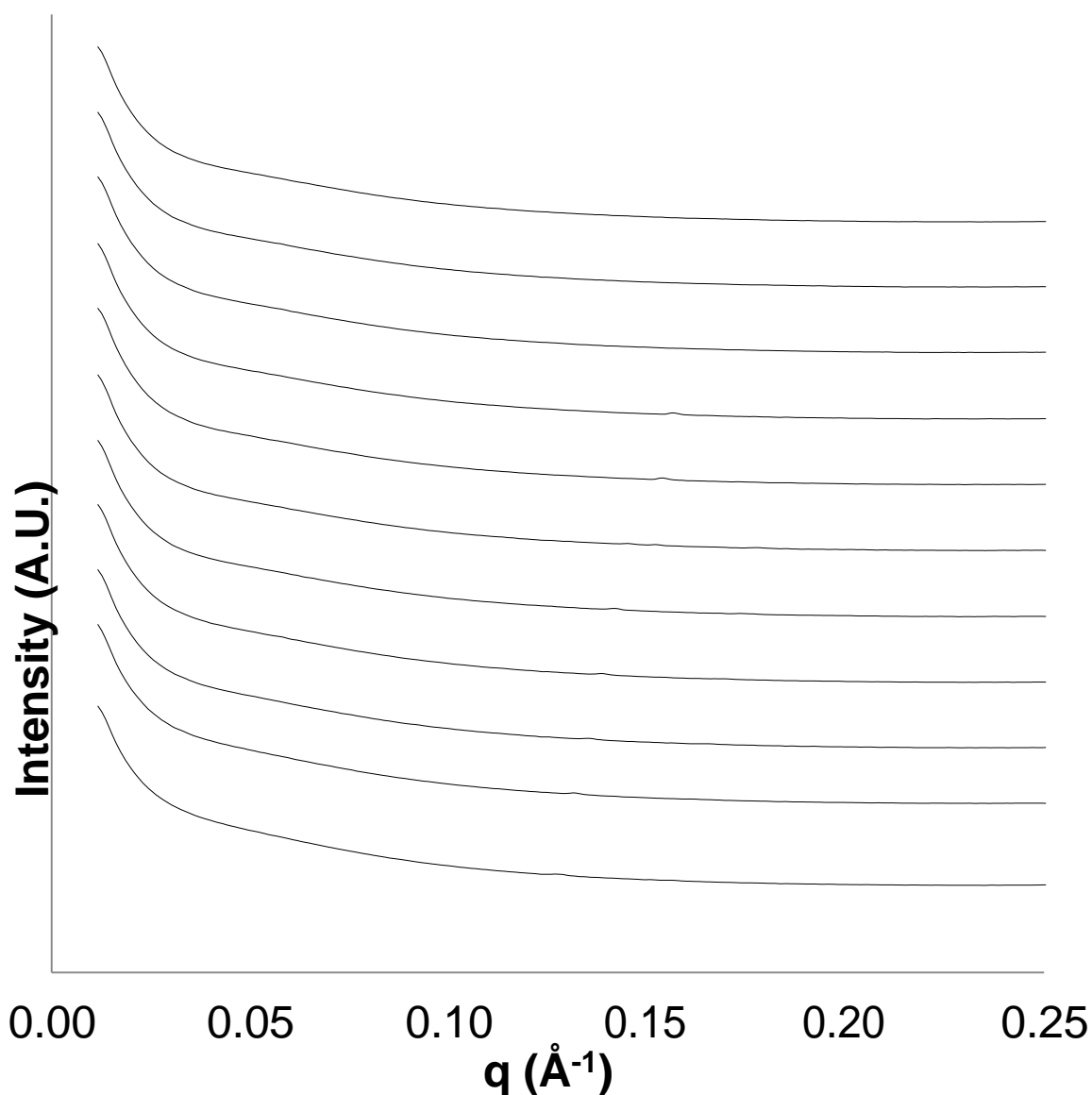
0.5% w/v C_{12}-PAEA stabilised phytantriol dispersions
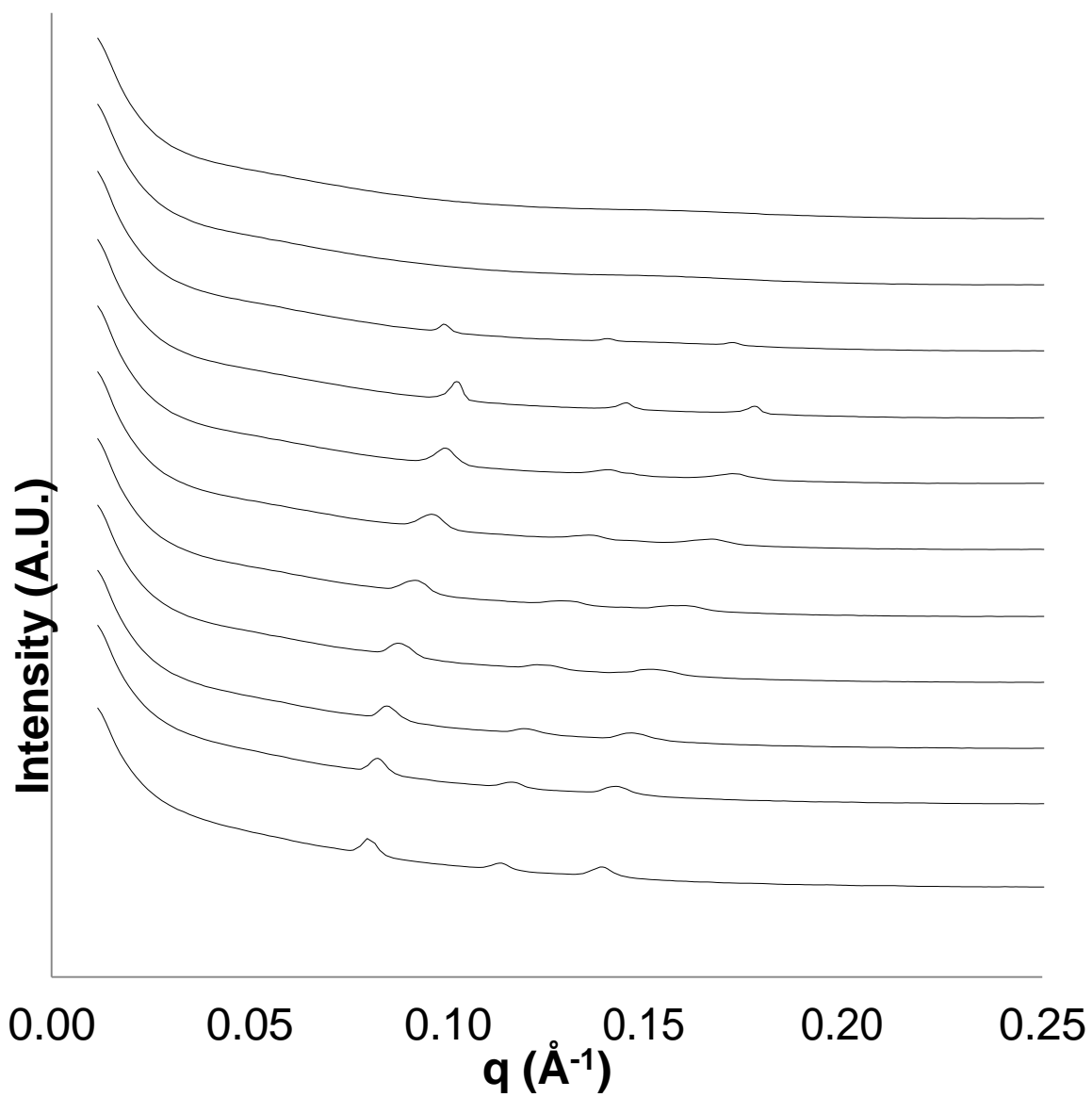
1% w/v C$_{12}$-PAEA stabilised phytantriol dispersions
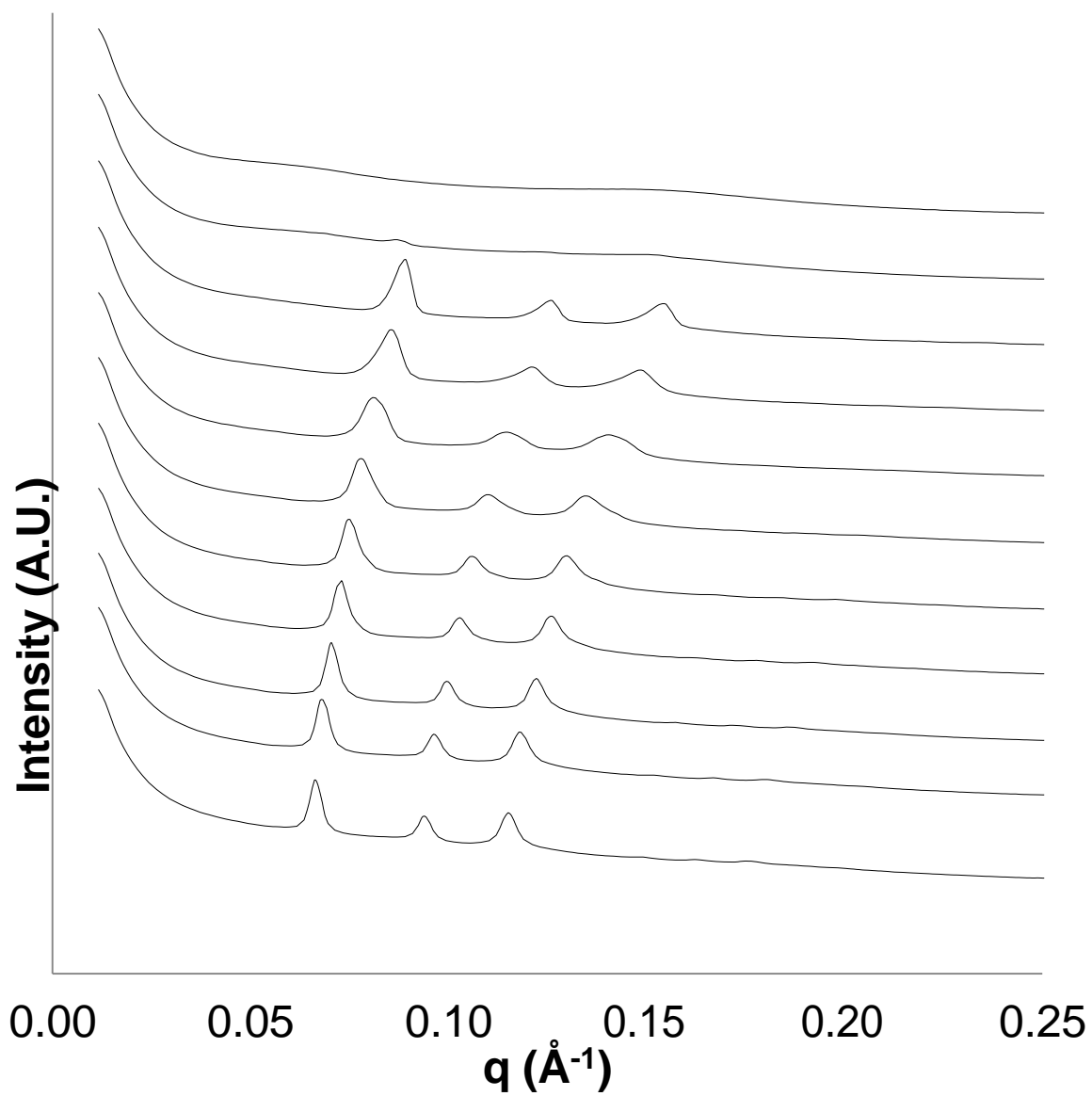
1.5% w/v C_{12}-PAEA stabilised phytantriol dispersions
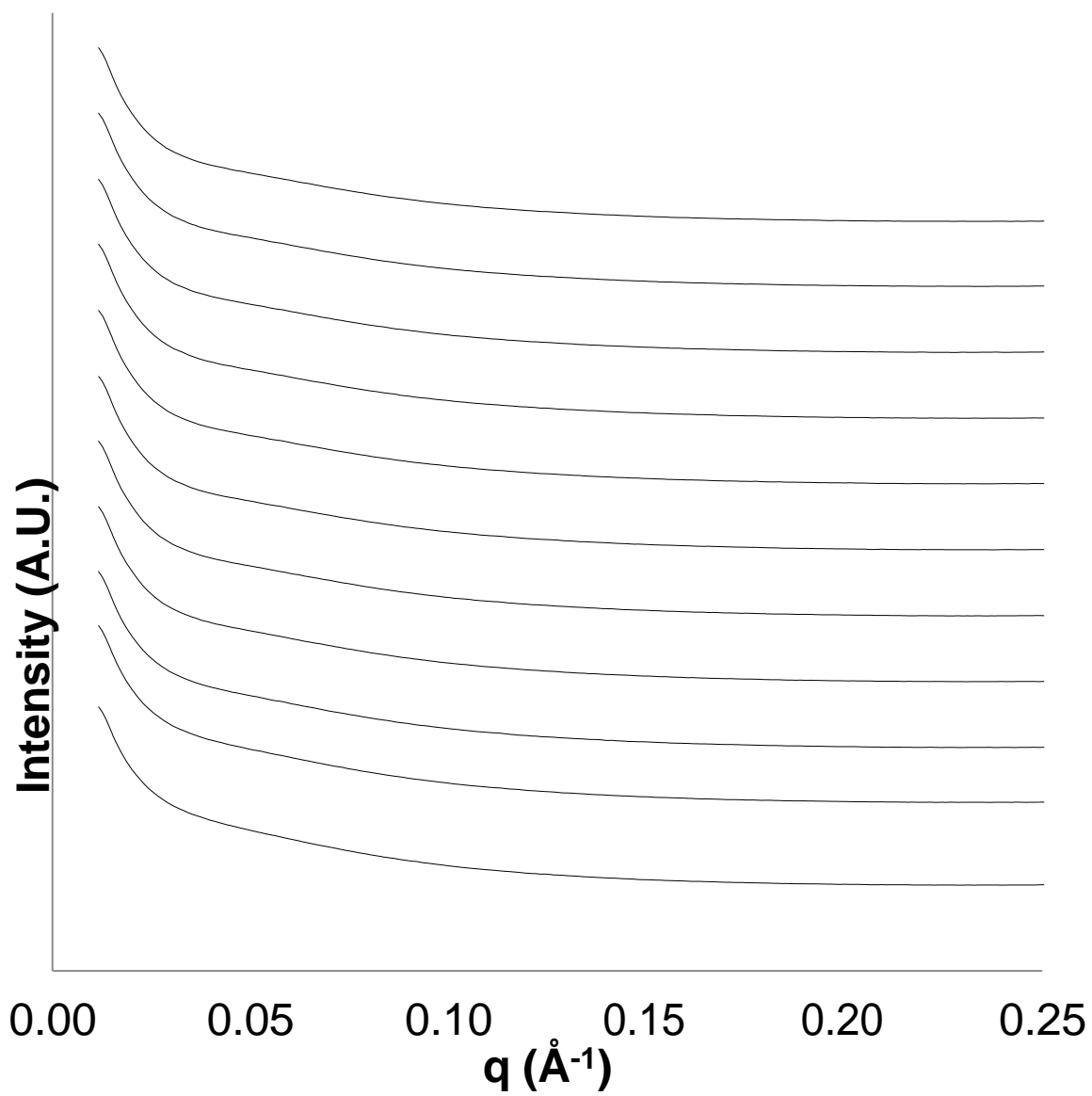
0.5% (w/v) di-C$_{12}$-PAEA stabilised phytantriol dispersions

1% (w/v) di-C$_{12}$-PAEA stabilised phytantriol dispersions

1.5% (w/v) di-C$_{12}$-PAEA stabilised phytantriol dispersions
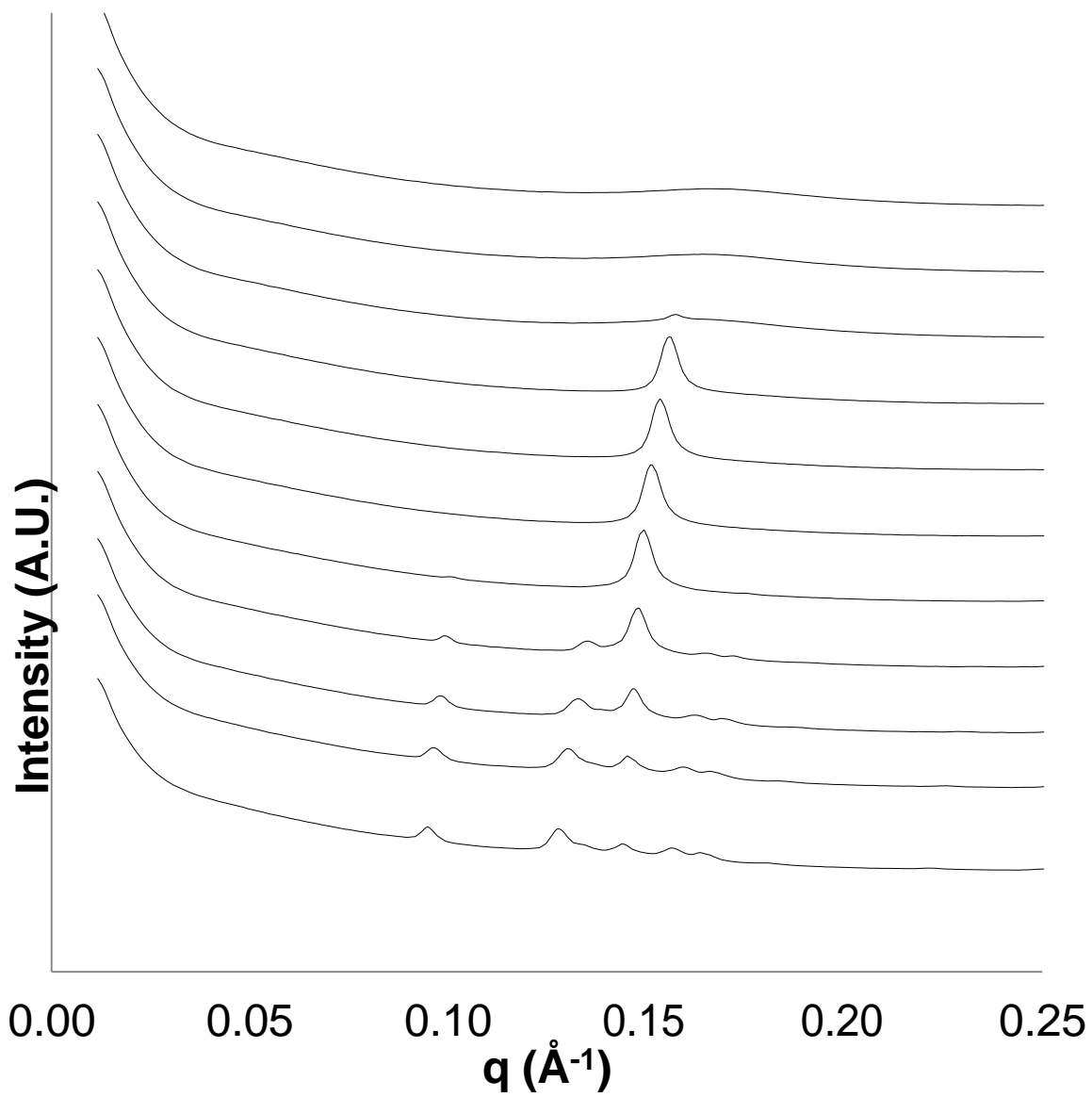
0.5% (w/v) C$_{12}$-PAA stabilised phytantriol dispersions

1% (w/v) C$_{12}$-PAA stabilised phytantriol dispersions

1.5% (w/v) C$_{12}$-PAA stabilised phytantriol dispersions

0.5% (w/v) di-C$_{12}$-PAA stabilised phytantriol dispersions
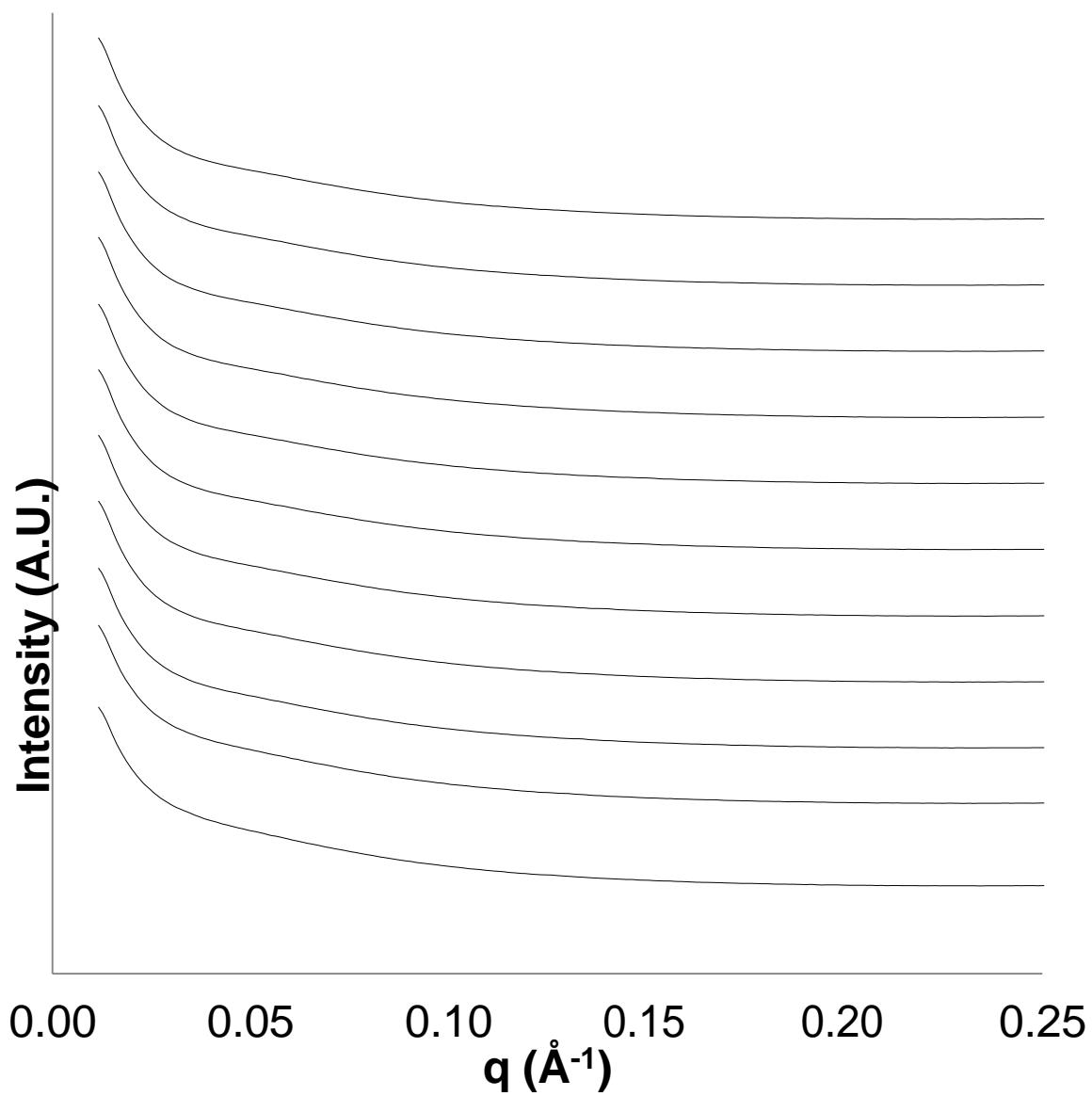
1% (w/v) di-C$_{12}$-PAA stabilised phytantriol dispersions
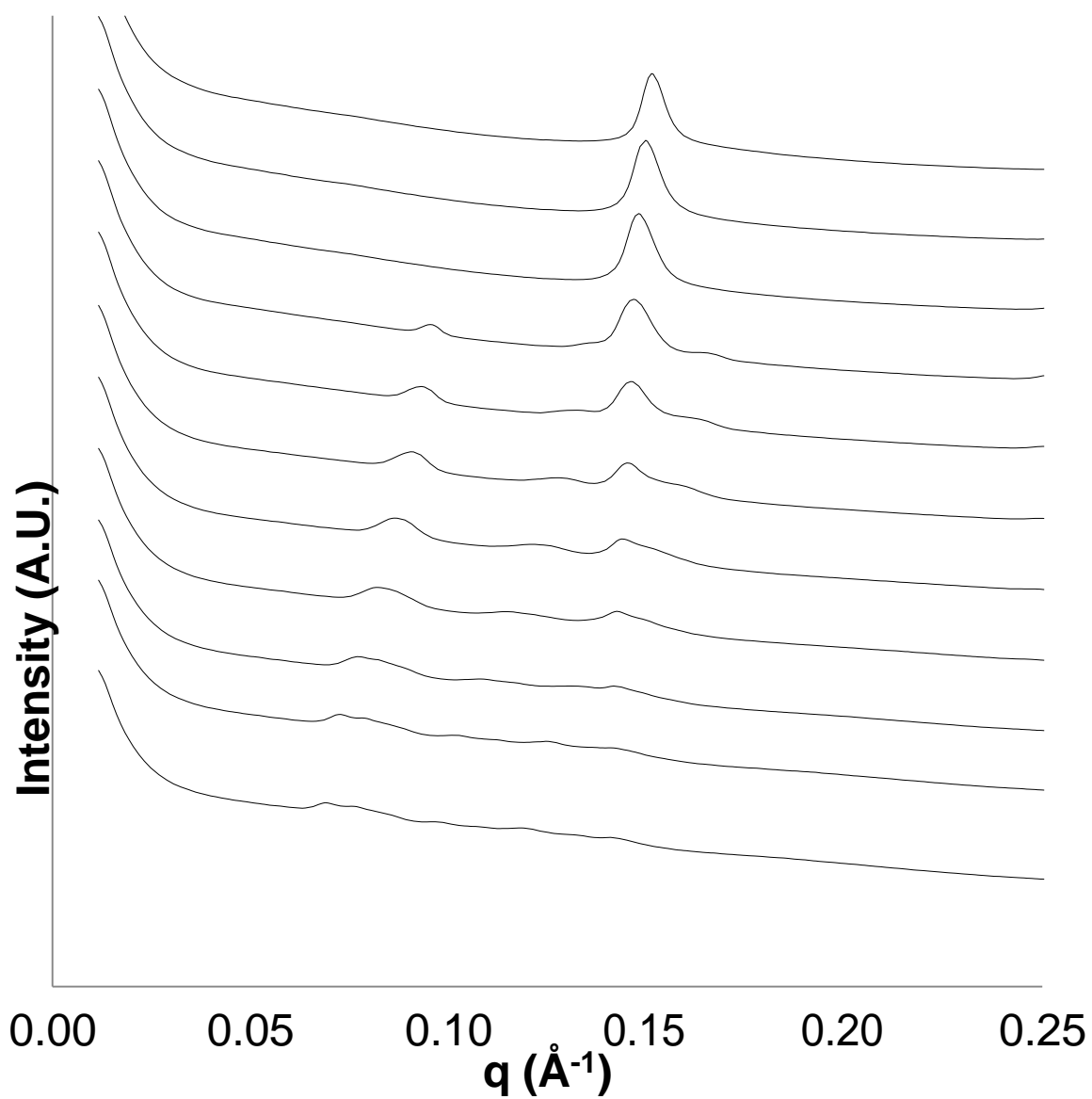
1% (w/v) di-C$_{12}$-PAA stabilised phytantriol dispersions
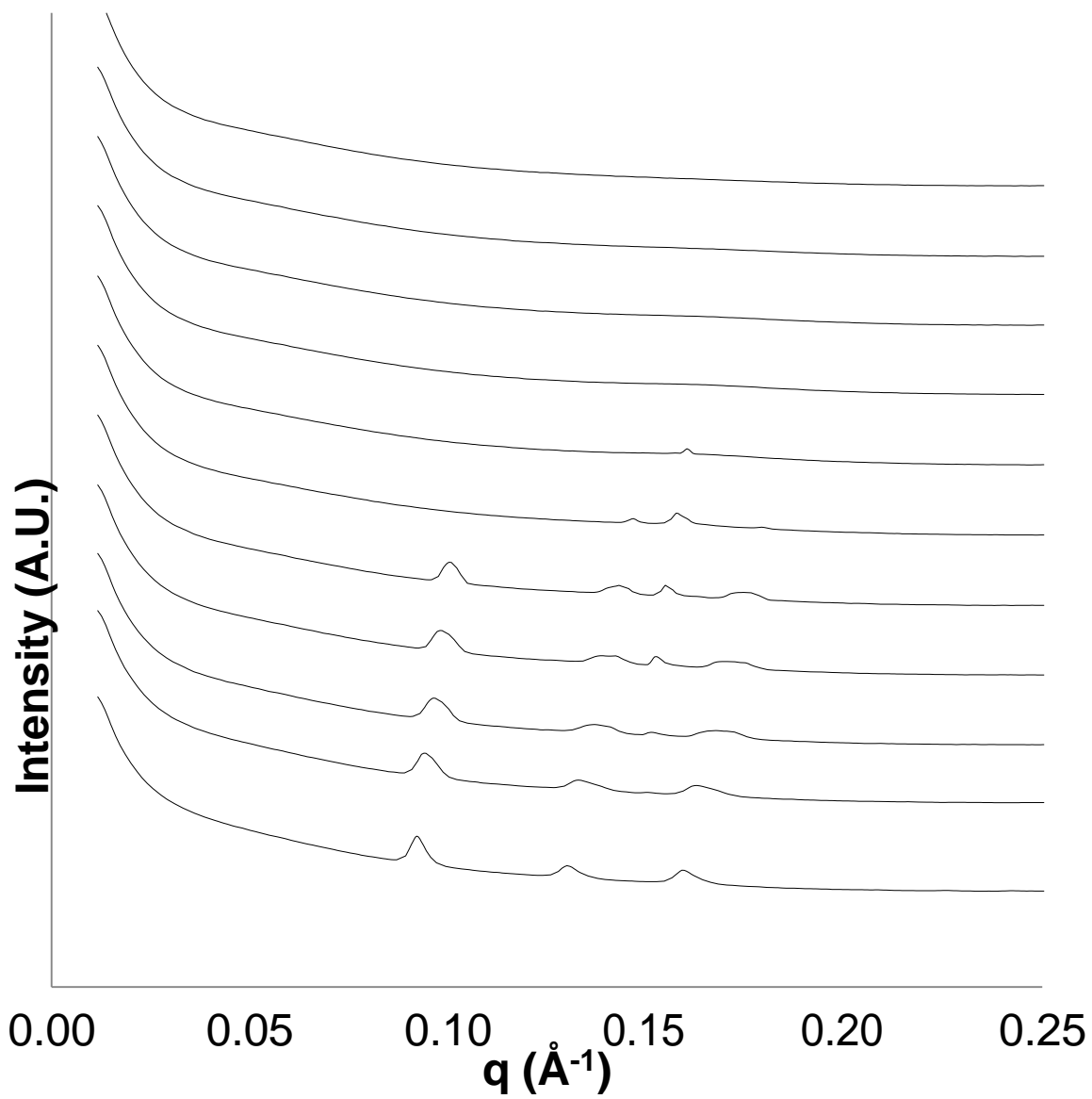
0.5% (w/v) C$_{12}$-PEGMEA stabilised phytantriol dispersions

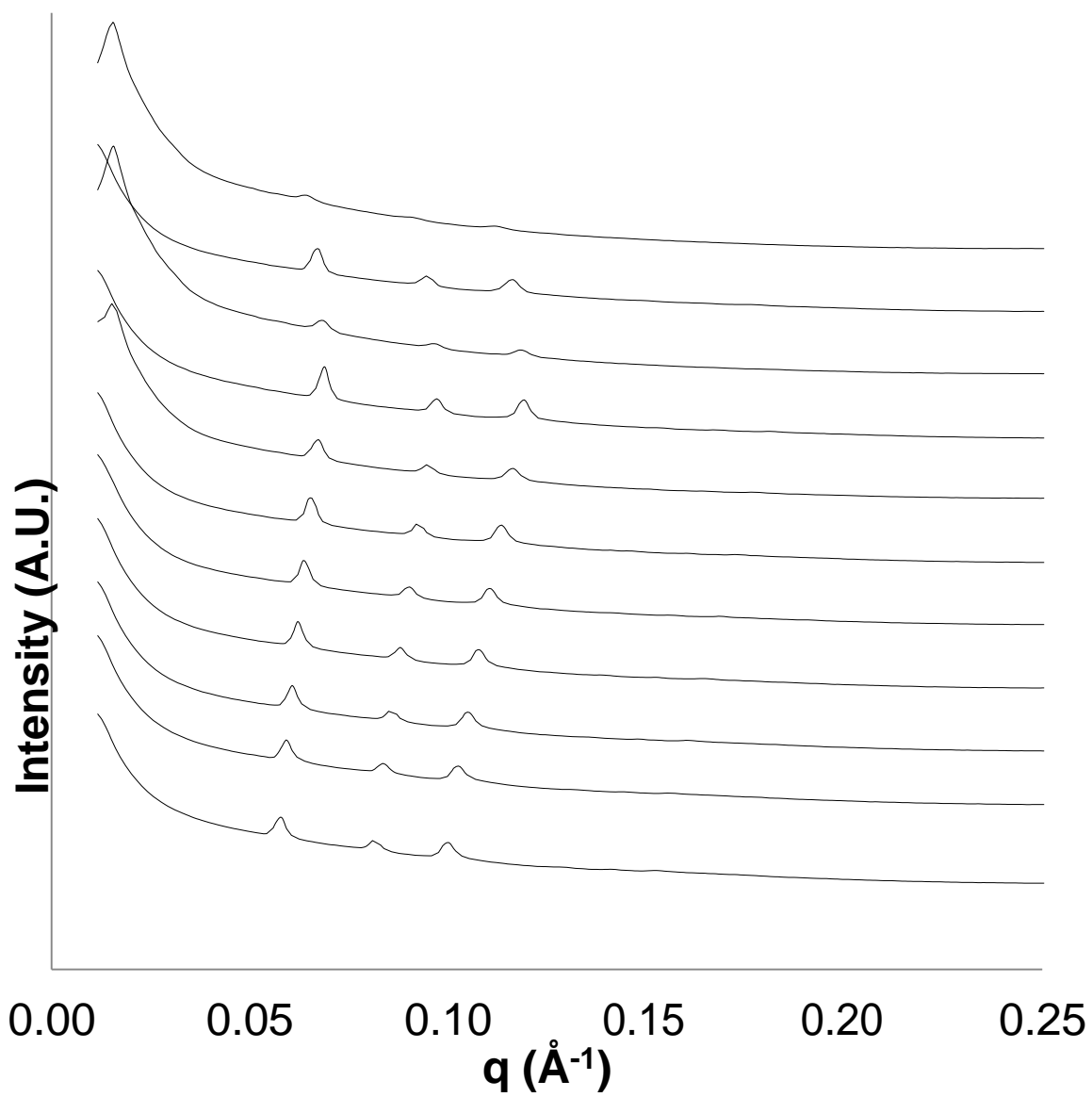1% (w/v) C$_{12}$-PEGMEA stabilised phytantriol dispersions

1.5% (w/v) C$_{12}$-PEGMEA stabilised phytantriol dispersions

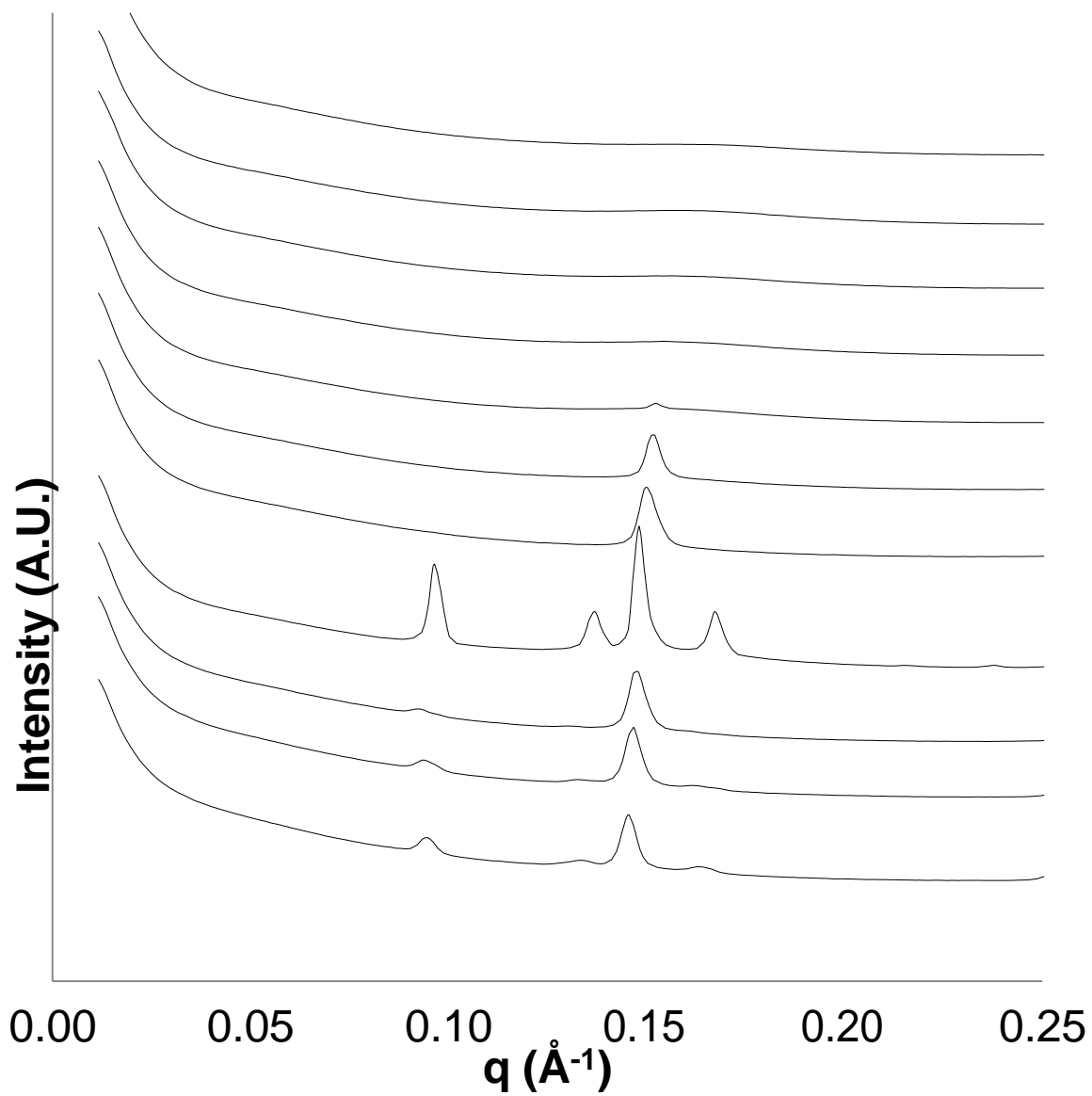0.5% (w/v) di-C$_{12}$-PEGMEA stabilised phytantriol dispersions

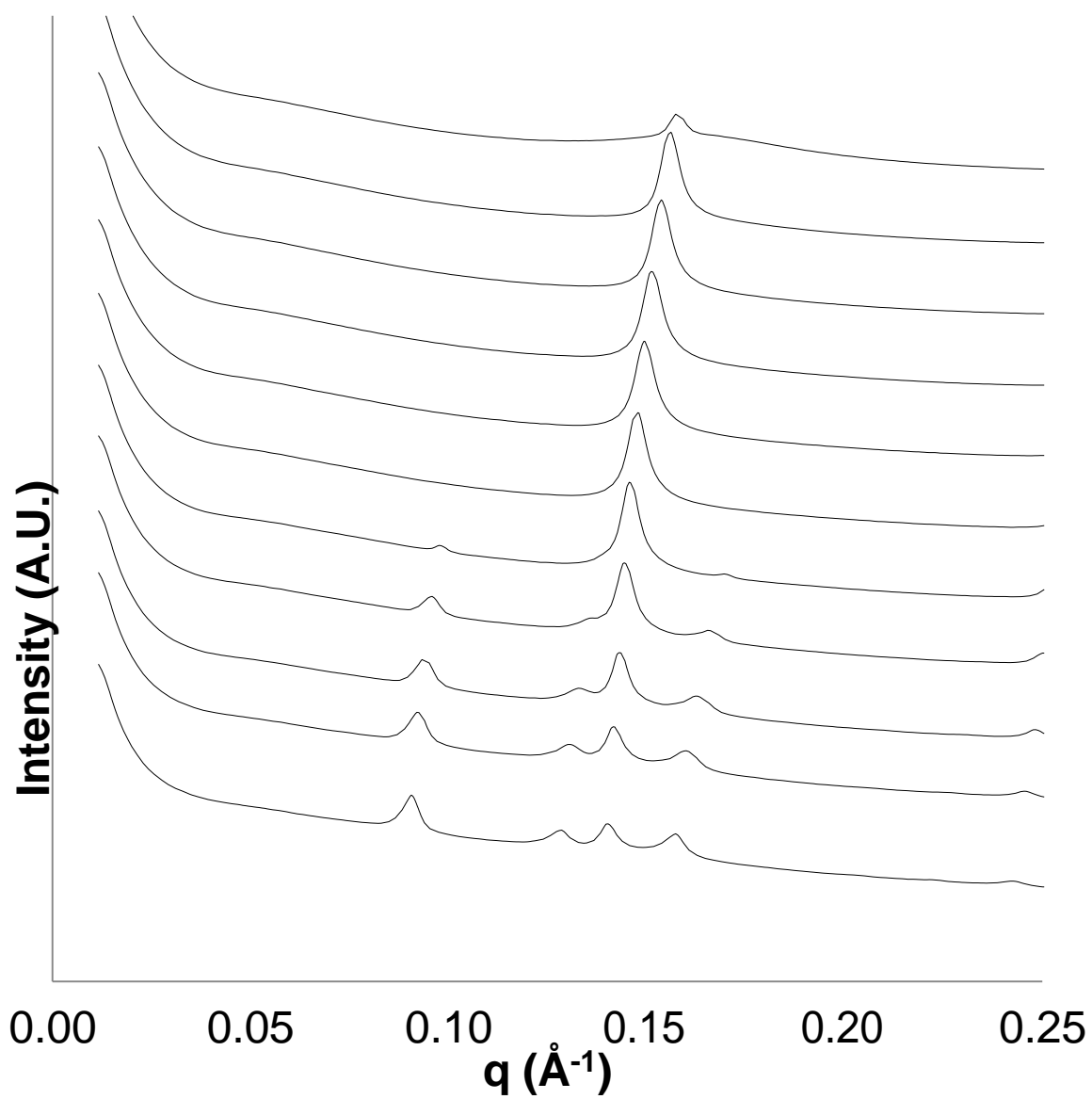1% (w/v) di-C$_{12}$-PEGMEA stabilised phytantriol dispersions

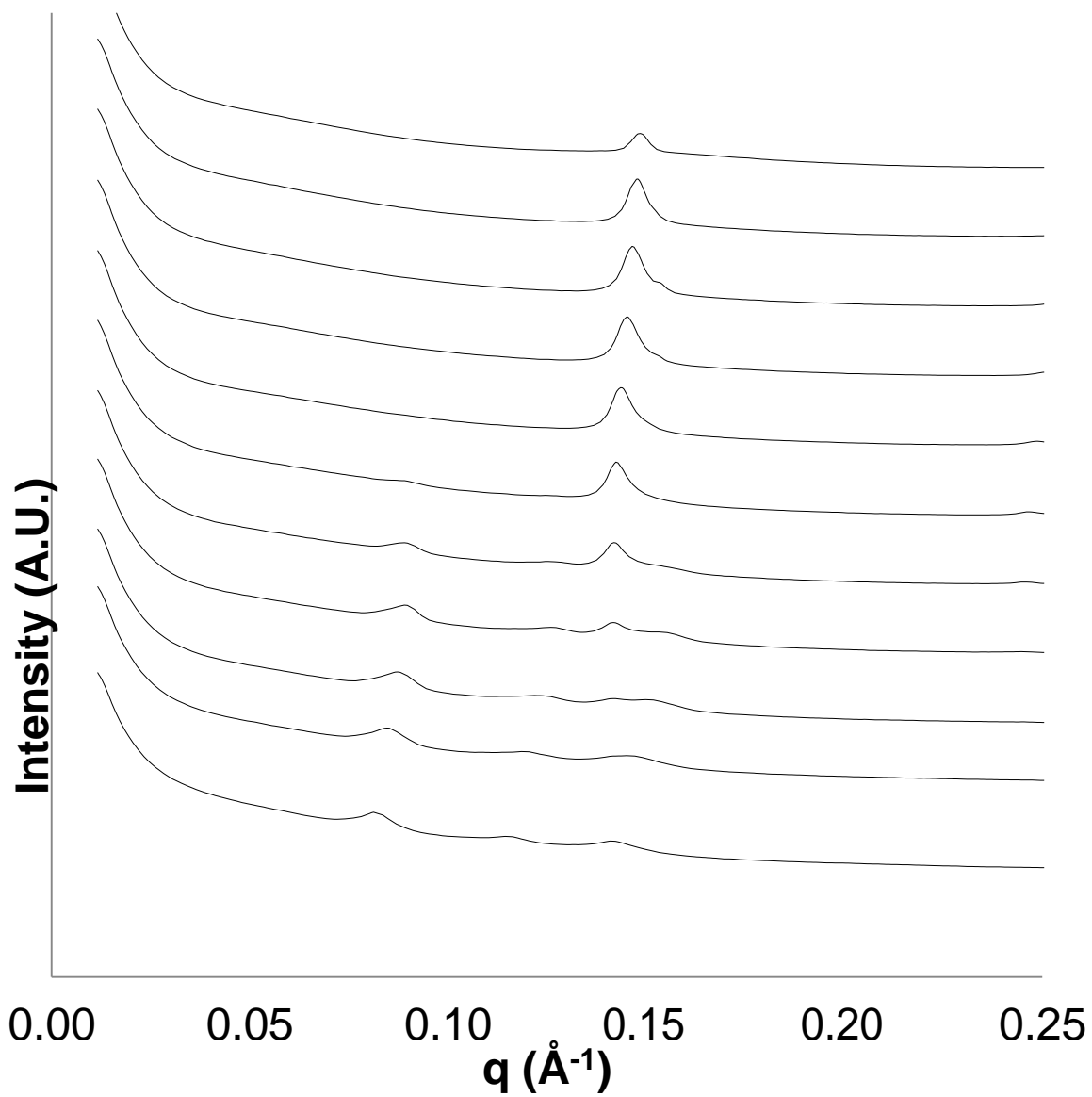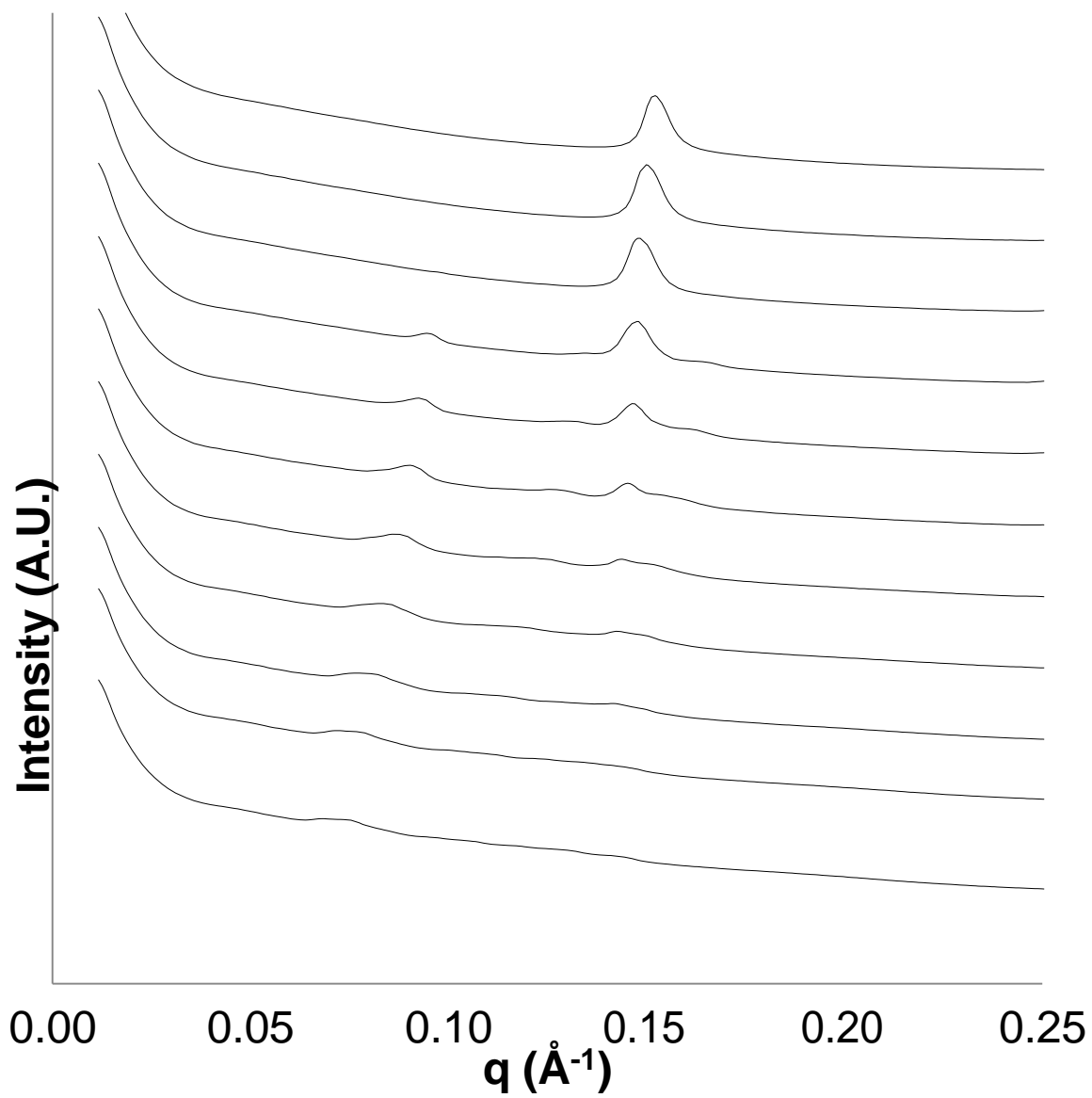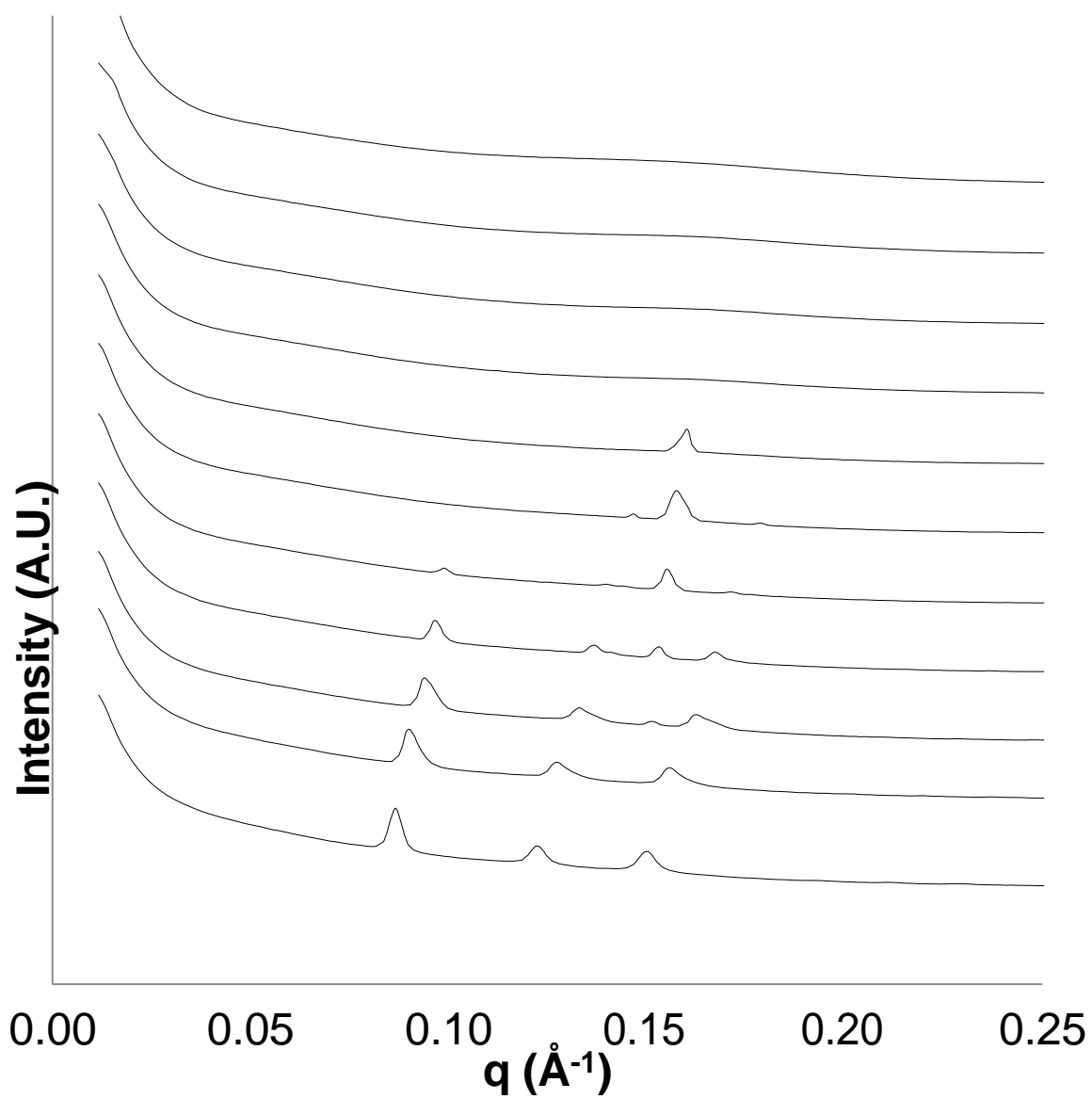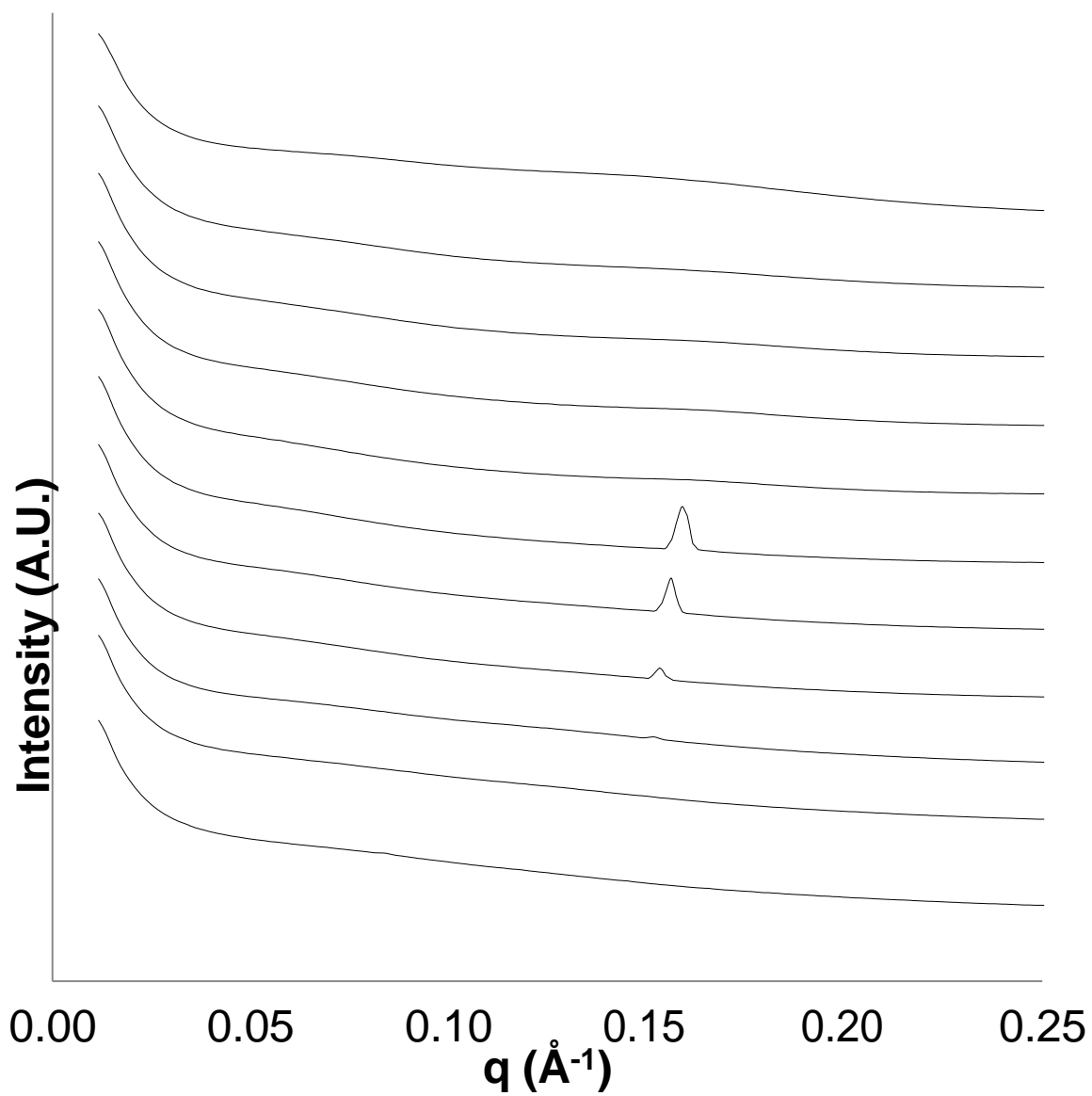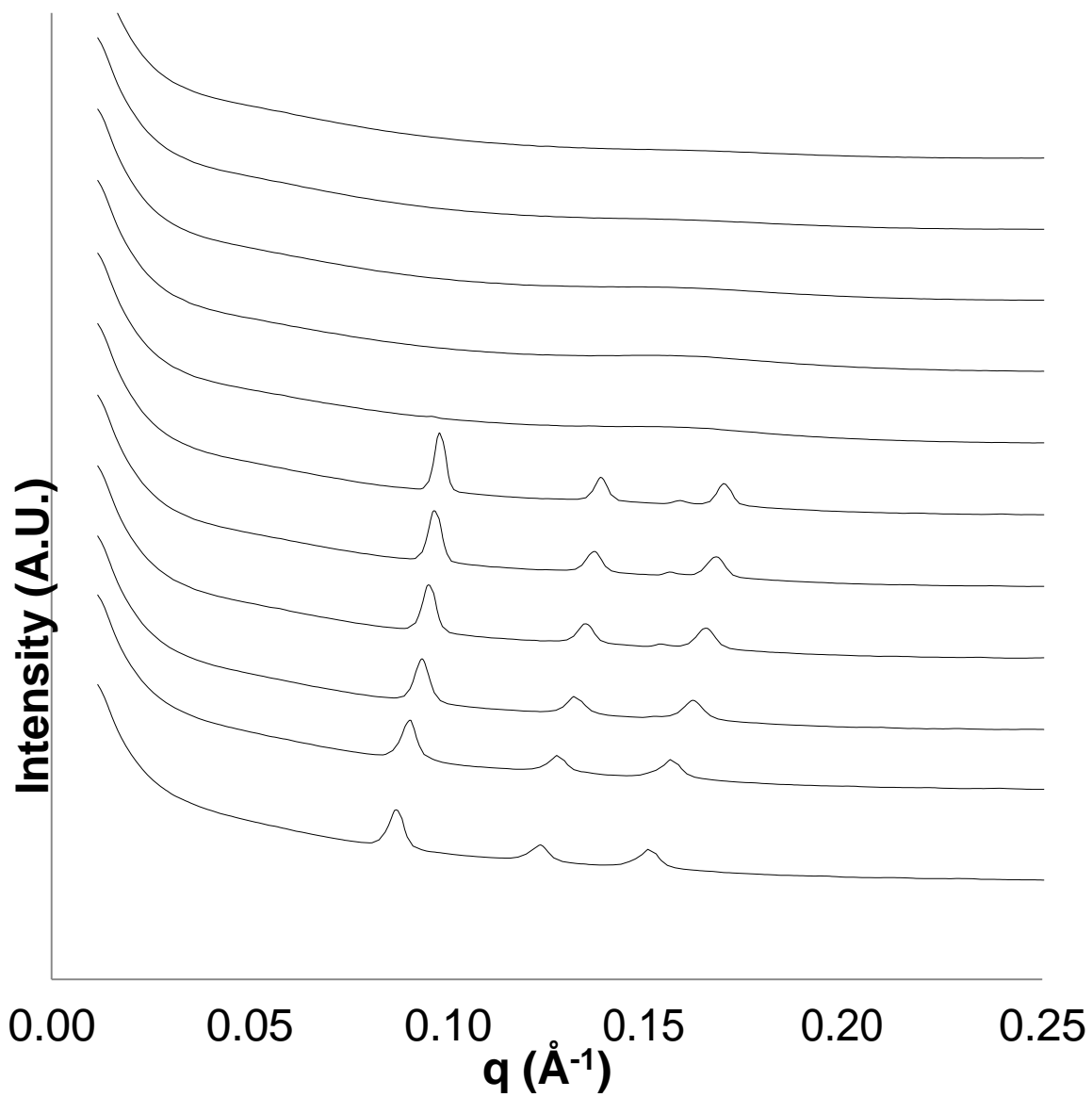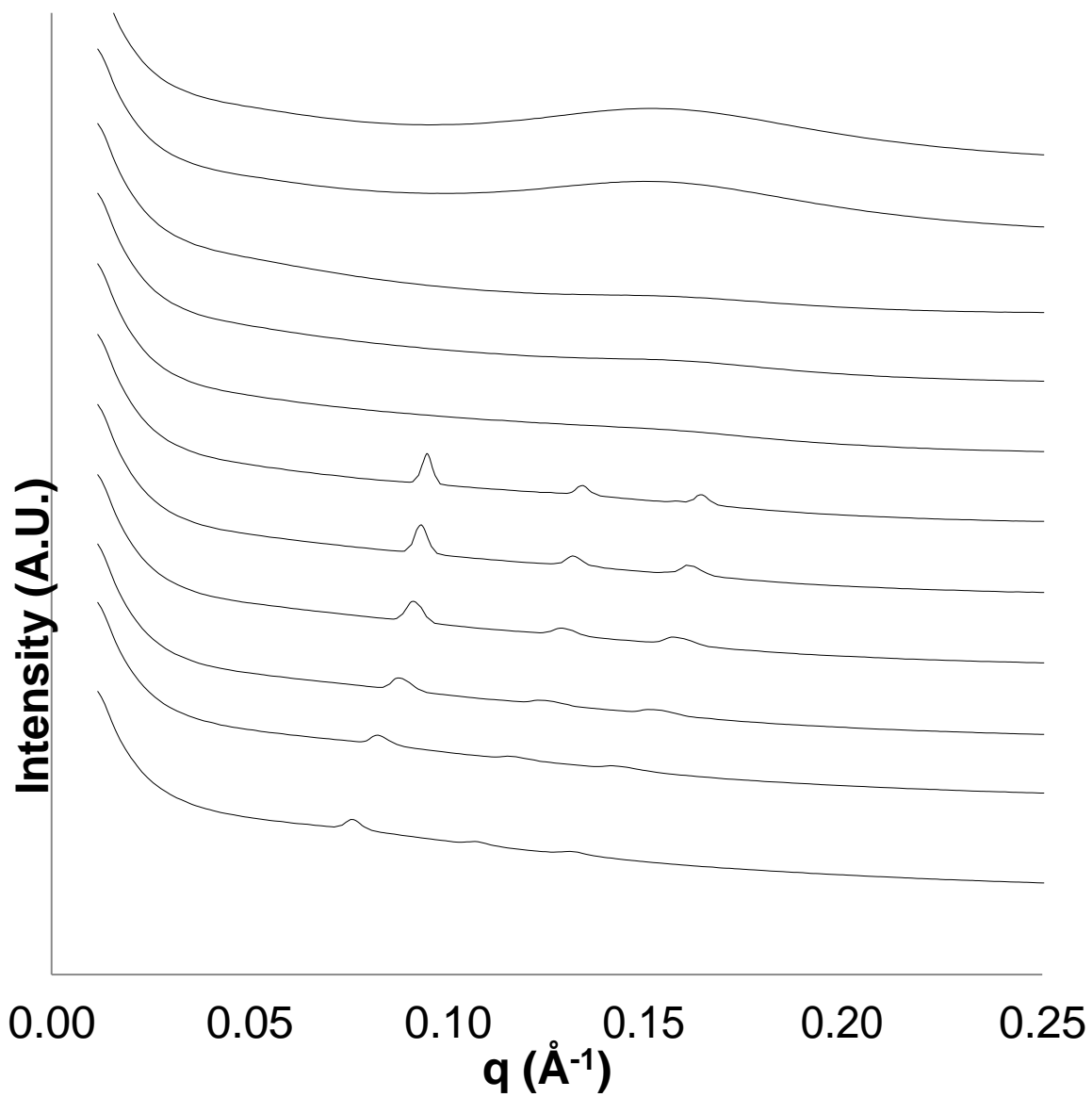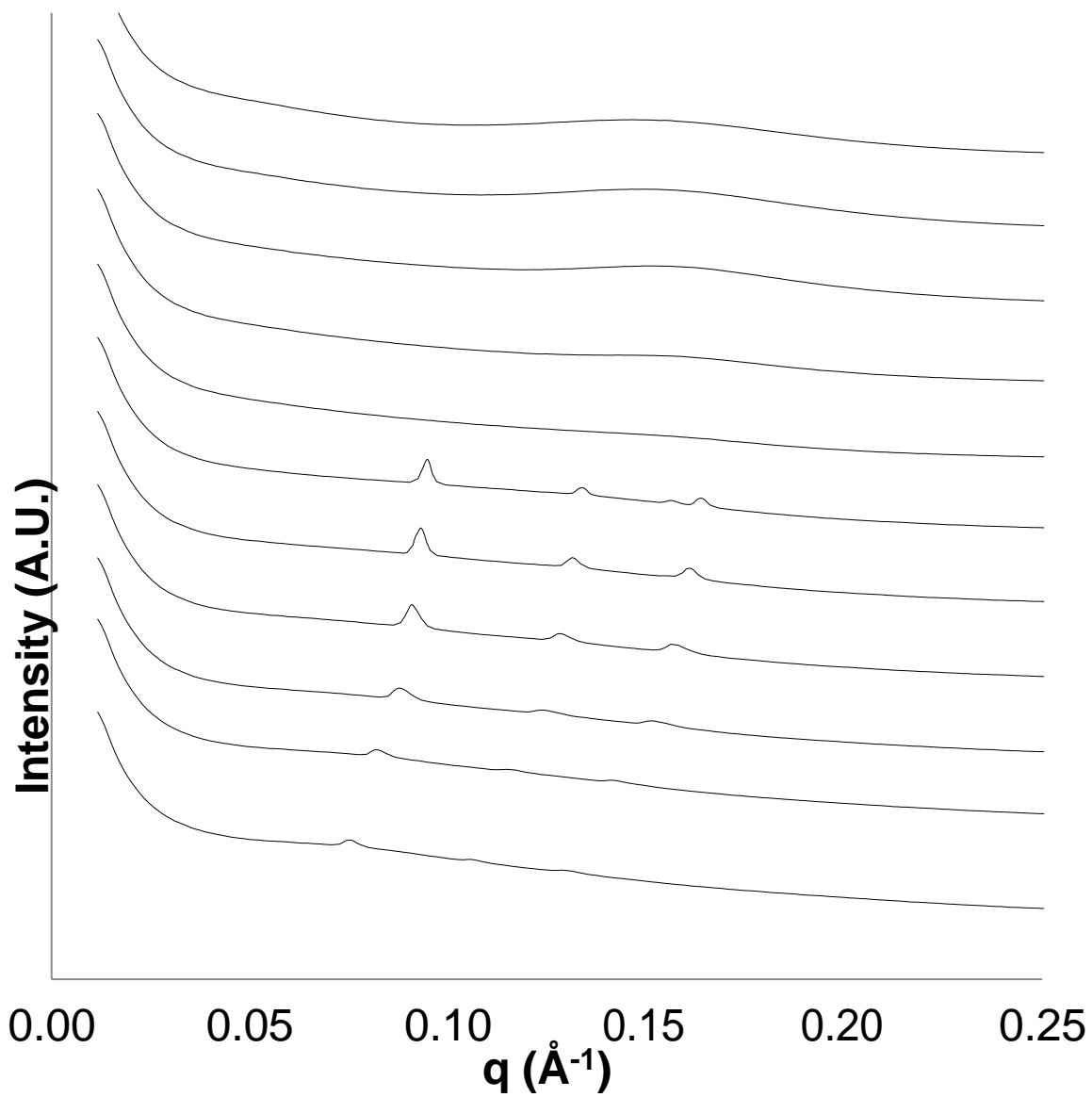1.5% (w/v) di-C$_{12}$-PEGMEA stabilised phytantriol dispersions

# Clickable Cubosomes for Antibody-Free Drug Targeting and Imaging Applications

Nicolas Alcaraz,[†,‡] Qingtao Liu,[†,‡] Eric Hanssen,[§] Angus Johnston,[†,‡] and Ben J. Boyd[*,†,‡]

[†]Drug Delivery, Disposition and Dynamics, Monash Institute of Pharmaceutical Science, Monash University, Parkville, VIC 3052, Australia

[‡]ARC Centre of Excellence in Convergent Bio-Nano Science and Technology, Monash Institute of Pharmaceutical Sciences, Parkville, VIC 3052, Australia

[§]Advanced Microscopy Unit, Bio21 Molecular Science and Biotechnology Institute, University of Melbourne, Parkville, VIC 3052, Australia

ABSTRACT: The combination of copper-free click chemistry with metabolic labeling offers new opportunities in drug delivery. The objective of this study was to determine whether cubosomes functionalized with azide or dibenzocyclooctyne (DBCO) groups are able to undergo copper-free click chemistry with a strained cyclooctyne or azide, respectively. Phytantriol-based cubosomes were functionalized using phospholipids bearing an azide or DBCO group. The modified cubosome dispersions were characterized using dynamic light scattering, cryo-TEM, and small-angle X-ray scattering. The efficiency of "clickability" was assessed by reacting the cubosomes with a complementary dye and determining bound and unbound dye via size exclusion chromatography. The clickable cubosomes reacted specifically and efficiently with a click-Cy5 dye with minor changes to the size, shape, and structure of the cubosomes. This indicates that cubosomes can retain their unique internal structure while participating in copper-free click chemistry. This proof of concept study paves the way for the use of copper-free click chemistry and metabolic labeling with cubosomes for targeted drug delivery and imaging.
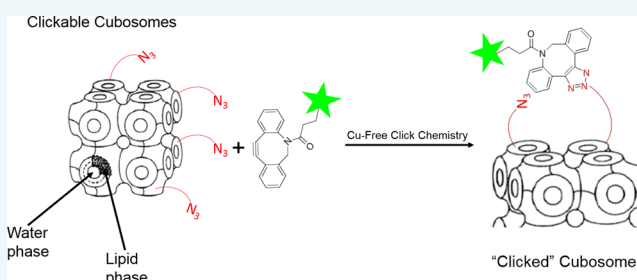
INTRODUCTION

A current trend in nanomedicine and drug delivery is to improve specificity of the treatment to in turn improve efficacy and avoid side effects. Nanoparticles have played a large role in this trend as they can accumulate in target tissues either passively (via the so-called Enhanced Permeation and Retention effect[1]) and actively using surface conjugated targeting ligands.[2]

Self-assembled lipid based liquid crystalline nanoparticles (LCNP) possessing an internal cubic phase structure, known as cubosomes, have been gathering attention as a drug delivery system as they can be loaded with both lipophilic and hydrophilic drugs and they have potential for on-demand reversible release which offers advantages over more commonly used liposomes.[3−6] Amphiphilic lipids such as phytantriol and glycerol monoleate (GMO) can self-assemble in excess water to form thermodynamically stable liquid crystalline phases such as the bicontinuous cubic phase.[7,8] Cubosomes can then be formed by the dispersion of the "bulk" cubic liquid crystalline phase, usually with the aid of a polymer stabilizer, such as Pluronic F127 or F108. The internal structure of the particles, and approaches to modification for drug delivery or imaging capabilities by incorporation of other agents such as lipids, phospholipids, or metallic nanoparticles have been well studied,[9−11] as has the influence of the stabilizer.[8] The cubosomes often have the same microstructure as the bulk

liquid crystalline phases but have a larger surface area and are much less viscous, enabling their potential deployment as injectable drug delivery or imaging systems.[12−14] The internal structure of the cubic phase particles makes them particularly interesting as MRI contrast agents, as the bound water behaves very differently to bulk water, providing a boost in relaxivity.[15,16] The use of cubosomes as contrast agent enhancers was recently reviewed.[17]

Active targeting of drug carriers is a challenge, with the most common approach involving the use of antibodies or ligands for a specific cell surface receptor. In cancer therapy an antibody or folic acid group targeting a receptor overexpressed by the diseased cells is often conjugated to the surface of the carrier particle. Potential drawbacks of these approaches include being expensive, having poor stability, lack of specificity if the target receptor is common or can mutate in the target cells, competition with other ligands, and poor pharmacokinetic consequences for the particle after injection.[18−20]

Metabolic labeling is gaining popularity as an approach to enable covalent attachment of "probes" to cell surfaces. A cellular substrate (commonly a monosaccharide) is modified to contain a target functional group such as an azide. The
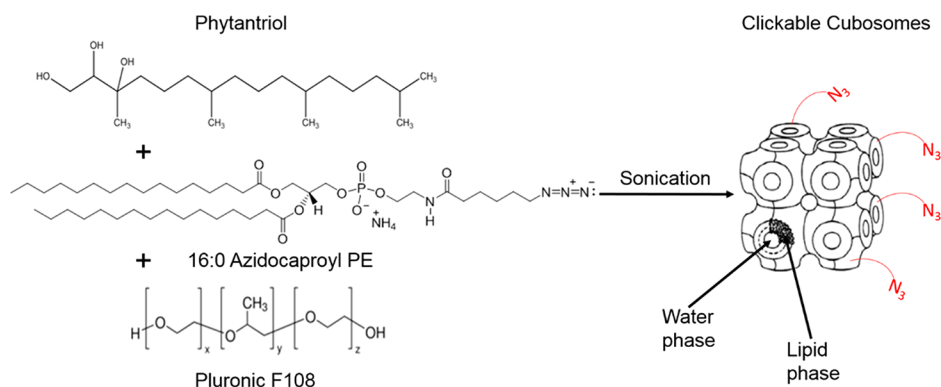
Figure 1. Schematic for the formation of copper-free "clickable" cubosomes. The lipid and phospholipid are mixed together and then hydrated with Pluronic F108 solution. The system is sonicated and the cubic phase disperses to form cubosomes. The click phospholipid is potentially both present in the interface within the internal aqueous channels, as well as at the external surface of the particles. Cubosome figure on right modified from ref 45 thanks to http://creativecommons.org/licenses/by/2.0.
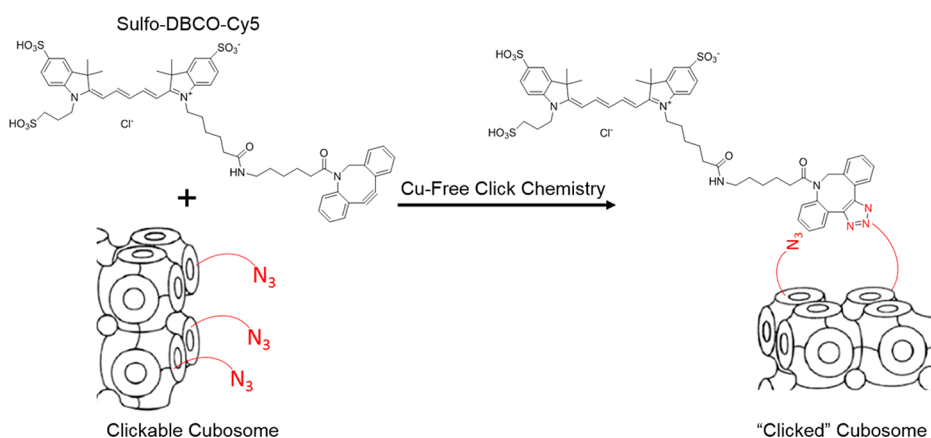

Figure 2. Simplified diagram of azide cubosome binding with dye through copper-free click chemistry. The azide and strained alkyne form a triazole and conjugate the dye to the nanoparticle. Cubosome figure modified from ref 45 thanks to http://creativecommons.org/licenses/by/2.0.

modification needs to be small and inert to not interfere with or be recognized by the cells' natural metabolic pathway. The functionalized sugar is then processed like a natural monosaccharide and is expressed in surface glycoproteins which results in the target functional group being present at the cell surface.

Following this surface expression, the functional group on the non-natural sugar can then be targeted by a probe molecule that contains the complementary functional group using biorthogonal chemical approaches. Bioorthogonal chemistry is defined as any chemical reaction that does not interfere with the native processes in a living system.[21−31] The benefits of bioorthogonal chemistry as an active targeting technique over other approaches are better stability, the materials are expectedly cheaper to synthesize than antibodies, and the process is not reliant on overexpression of natural receptors to target nonfunctionalized cell populations.[26,30,32]

Copper-free click chemistry is one class of reaction that is particularly useful in combination with metabolic labeling. The azide group expressed on the cell surface will react rapidly with strained cyclooctynes under physiological conditions, with one of the more commonly used strained cyclooctyne systems being dibenzocyclooctyne (DBCO). The target group and the probe react covalently to form a triazole, and the cell surface can thereby be imaged or targeted. Using this approach, imaging biological processes associated with sugars in cells and in live

animals, such as zebrafish, has been achieved.[33−38] Early studies focused on glycans such as sialic acid that can be incorporated into the natural metabolic machinery of cells; however, the field has expanded to DNA[39,40] and protein[41,42] labeling. Recently, nanoparticles have been used as probes in place of simple dyes and imaging agents. Chitosan nanoparticles and liposomes have been covalently reacted to tumors that had metabolized azide bearing sugars.[43,44] One approach to functionalizing lipid particles to click them to labeled cells is to add azide- or DBCO-functionalized phospholipids, as illustrated schematically for cubosomes in Figure 1.

There is no record of cubosomes designed to participate in copper-free click chemistry for use as cell-surface targeting systems through metabolic labeling. Given their aforementioned potential benefits in drug delivery and imaging, in this study we create copper-free click capable cubosomes, characterize them, and assess their ability to take part in copper-free click reactions using dye-conjugated to the DBCO click probe (Figure 2). The internal liquid crystalline nanostructure was confirmed before and after the reaction using synchrotron small-angle X-ray scattering (SAXS) while the morphology was assessed by cryogenic-transmission electron microscopy (cryo-TEM). Size measurements were carried out with dynamic light scattering (DLS). Binding efficiency of the cubosomes via copper-free click chemistry in solution was assessed through size exclusion chromatography and fluorescence measurements.

This paper establishes the "clickability" of these cubosomes with a view to future use as a drug delivery and imaging probe using metabolic labeling to couple these novel delivery systems to cells.

■ RESULTS AND DISCUSSION

Characterization of Copper Free Click-Capable Cubosomes. The volume-weighted size distributions of the cubosome dispersions are listed in Table 1. The size and

Table 1. Volume-Based Particle Size Distribution Measurements (Mean ± SD, n = 3) of the Different Cubosome Dispersions[a]

Additive into cubosome dispersion (2 mol %)	Size (nm) peak 1	Size (nm) peak 2	PDI
None	160 ± 10		0.15
PL-Azide	114 ± 1		0.11
PL-DBCO	102 ± 4	244 ± 56	0.19
PL-DSPC	151 ± 1		0.22
PL-PEG$_{2000}$-DBCO	32 ± 8	226 ± 67	0.27
PL-PEG$_{2000}$-Azide	91 ± 1	519 ± 19	0.52
PL-PEG$_{2000}$-DSPE	27 ± 3	129 ± 12	0.23

[a]PL denotes phospholipid.

polydispersity of the cubosomes doped with phospholipid differed from "traditional" cubosomes. The systems with PEG$_{2000}$ phospholipid displayed two populations indicating the formation of other lipid nanostructures, possibly some coexisting liposomal structures. This was also observed in the PL-DBCO doped system. It should be noted that the PL-PEG$_{2000}$-Azide modified cubosomes did exhibit considerably larger average size and higher polydispersity which is likely due to the presence of the charged polar headgroup which changes the dispersion behavior of the system. It has previously been shown that additives can alter the size and internal structure of cubosomes.[46]

Dynamic light scattering provides the size distribution assuming spherical particles but does not provide information about the shape or structure of the cubosomes. Therefore, further techniques were required to fully characterize these systems. CryoTEM was used to image and visualize the particle morphology in the different formulations (Figure 3). The cryo-TEM data supported the DLS measurements with the particle size populations apparent in the micrographs being in general agreement with the DLS data. The formulations containing phospholipids were mainly cubosomes but did show the presence of other structures such as some lipid vesicles, lamellar structures, and liposomal type structures. Again, this finding was reflected in the DLS data with more than one peak being detected. It is likely that the liposomes and other lipid structures in the samples containing PEG phospholipid led to the larger PDI values observed. This was more noticeable in the formulations containing a PEG phospholipid. This might be expected as the addition of phospholipid can alter the packing parameter of the system and this dictates the final structure.[47]

This can be understood through the critical packing parameter (CPP) concept where the double hydrophobic chain of the phospholipids induces formation of lamellar structures and phospholipids are a key component of liposomes. Additionally, phytantriol imparts a slightly negative curvature on the bilayer resulting in the formation of the cubic phase, but addition of a more polar phospholipid such as the PEG phospholipid would be expected to draw the mean curvature back toward a lamellar phase.

The internal structure of the cubosomes was determined using SAXS where the Bragg peaks were indexed and the internal structure thereby determined. The scattering profiles of the systems at 25 °C can be seen in Figure 4. The cubosomes containing the non-PEG$_{2000}$ additives retained the double diamond internal cubic phase structure of unmodified cubosomes. In contrast, the cubosomes with PEG$_{2000}$-based additives showed that the internal structure shifted to the more swollen primitive cubic phase. This behavior is consistent with the addition of hydrophilic additives to phytantriol-based cubic phases.[48] The scattering for the PEG$_{2000}$ phospholipid doped systems was also much weaker than the other systems potentially due to the presence of less geometrically ordered
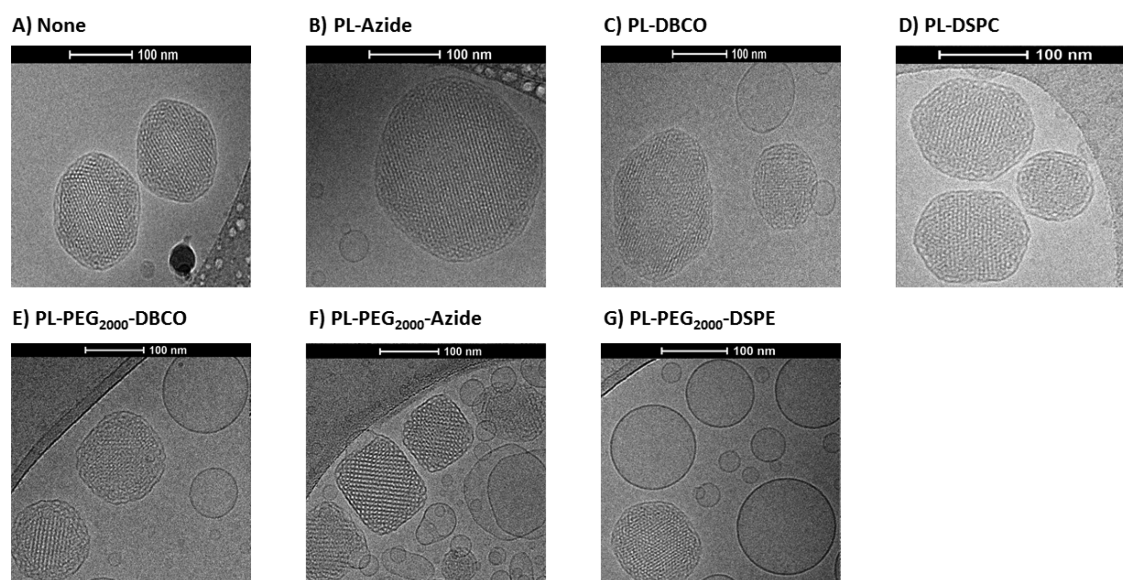

Figure 3. Cryo-TEM images of cubosome dispersions containing different additives as indicated on the respective panels. PL denotes phospholipid. Concentration of additive is 2 mol %.
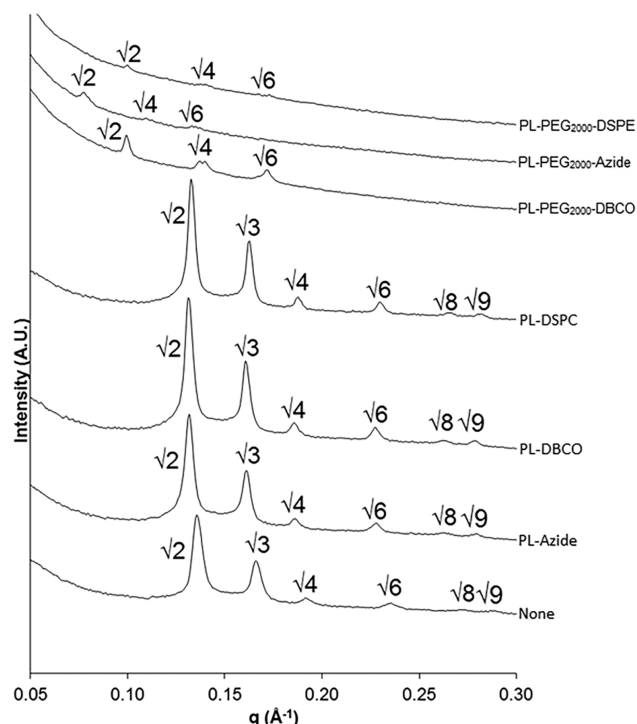
Figure 4. Dependence of internal structure on phospholipid-based additives in phytantriol-based cubosomes measured by small-angle X-ray scattering at 25 °C. The different cubosome dispersions contained different phospholipids loaded at 2 mol % relative to phytantriol. PL denotes phospholipid.

lipid structures that do not provide discrete diffraction peaks compared to the cubosomes.

The lattice parameters of the internal structures (Table 2) were determined from the SAXS data and showed similar

Table 2. Lattice Parameter of Cubosome Dispersions[a]

phospholipid added	cubic phase space group	lattice parameter (å)
None	double diamond	65.5 ± 0.2
PL-Azide	double diamond	67.7 ± 0.1
PL-DBCO	double diamond	66.9 ± 0.2
PL-DSPC	double diamond	67.5 ± 0.1
PL-PEG$_{2000}$-DBCO	primitive	89.7 ± 1.4
PL-PEG$_{2000}$-Azide	primitive	114.6 ± 0.7
PL-PEG$_{2000}$-DSPE	primitive	89.7 ± 0.2

[a]Lattice parameters were determined from the SAXS data presented in Figure 4. PL denotes phospholipid. All additives were at 2 mol %.

spacing to previously reported systems with double diamond and primitive cubic phase space groups, except for PL-PEG$_{2000}$-Azide containing cubosomes which had a considerably larger lattice parameter compared to typical phytantriol cubosomes (65−70 Å).[8,46,49,50] This is supported by the clearly larger lattice parameter seen in Figure 3 and as mentioned above is due to the increased hydrophilicity of the headgroup. This shift to primitive cubic phase space group has been reported previously upon addition of Tween 80 to phytantriol cubosomes as it favors a mean negative shift in spontaneous mean curvature at the lipid/water interface.[51]

A similar effect is likely to be occurring with the phospholipids containing PEG$_{2000}$ as they have both greater hydrophobic and greater hydrophilic regions compared to

Pluronic F108 or the non-PEGylated phospholipids. The cryo-TEM, DLS, and SAXS data indicate that the size, shape, and structure of the clickable cubosomes are relatively similar to those without click groups or additives when PEG$_{2000}$ was not conjugated to the phospholipid.

Binding Efficiency of Copper-Free Click-Capable Cubosomes. After confirmation that the dispersion contained cubosomes upon incorporation of copper-free click functional phospholipids and that they were similar to standard cubosomes, the ability of the cubosomes to covalently and specifically bind with a strained cyclooctyne or azide through copper-free click chemistry was assessed. A representative set of elution profiles showing the baseline separation between the cubosomes eluting at 2−5 mLs and the free dye eluting at 6−15 mLs are provided in Figure 5. The PL-Azide cubosomes sample was doped with Rhodamine B phospholipid to impart fluorescence to the cubosomes and this is why the total fluorescence observed is not in line with the other two elution profiles. Area under the curve for the distribution between the populations can be used to calculate a binding efficiency.

Each of the clickable cubosome systems showed over 85% binding with Sulfo-DBCO-Cy5 or Sulfo-Azide-Cy5 at 24 h after the complementary click-dye was added at a 1:1 mol ratio (Figure 6). The formulations with the greatest binding efficiency were the azide-containing cubosomes, specifically the PL-PEG$_{2000}$-Azide doped formulation binding to Sulfo-DBCO-Cy5 dye. This was over 8-times more efficient when compared to the three control samples that had under 5% binding. In the case of the controls, it is apparent that the dye is being partially nonspecifically bound to the particles, but one also needs to be mindful that a fraction of the PBS that contains dye is present within the internal water channels of the cubic phase.

The cubosomes containing bound dye were also studied using SAXS to determine whether there is an effect of the covalent attachment of dye on the structure of the cubosome system (Figure 7). The presence of dye bound to the cubosome had a generally minor impact on the structure, as all systems retained the phases they had displayed in previous SAXS experiments, but the scattering intensity was reduced and some peaks were less well-defined than before exposure to dye. This is likely due to the sample being diluted with the addition of dye solution. It should be noted that the PL-DSPC containing dispersion appeared to have a third peak emerging between the first two double diamond cubic phase peaks which often occurs when the hexagonal phase is also present as a liquid crystalline structure.

Additionally, lattice parameters were determined for the formulations after binding to the dye from the profiles in Figure 7 and there were no large changes aside from the PL-PEG$_{2000}$-Azide doped system that was similar to the other primitive cubic phase spacing found in this study and in the literature[52] (Table 3). It is likely that the formation of the triazole and attachment of dye to the PL-PEG$_{2000}$-Azide dispersion changed the hydrophilicity and therefore shifting the CPP, which lowered the lattice parameter to be similar to the other systems.

This confirms that the cubosomes can be functionalized using copper-free click reagents to enable covalent coupling to a complementary probe, and when used in a biorthogonal chemistry context they should retain their internal structure and consequently their drug delivery and imaging capabilities.

This finding is supported by other examples in the literature where cubosomes have been functionalized and used for
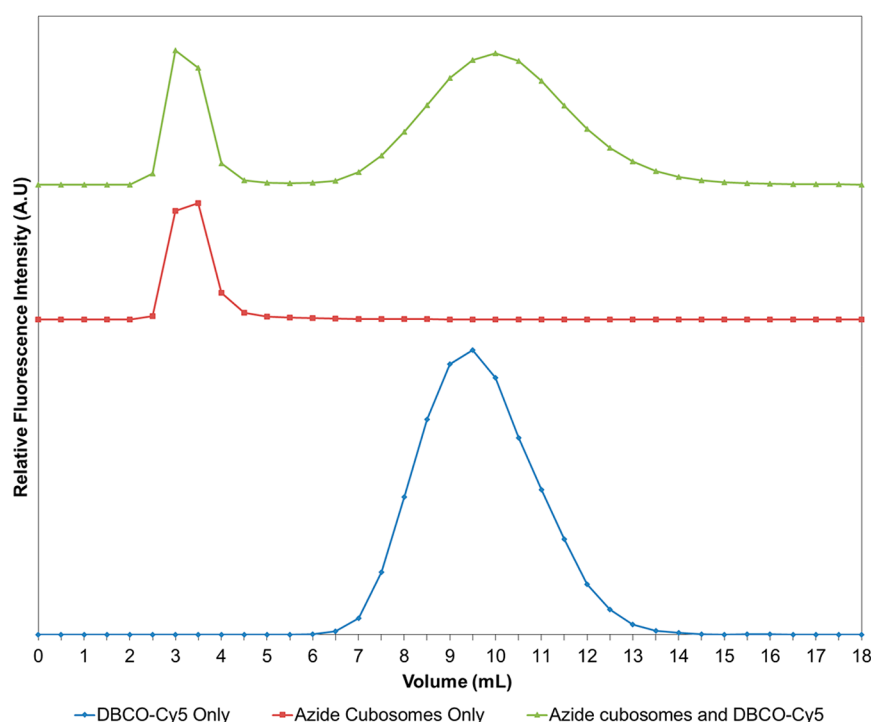
Figure 5. Representative elution profiles for Sulfo-DBCO-Cy5 dye only (blue/bottom), PL-Azide cubosomes only (red/middle), and Sulfo-DBCO-Cy5 dye mixed with PL-Azide cubosomes (green/top) from a Sephadex G50 column with PBS as the eluent.
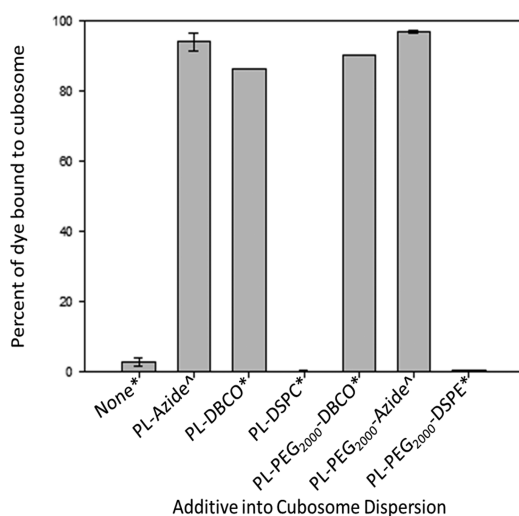
Figure 6. Percentage of dye bound to cubosomes (mean ± SD, $n = 3$) after size exclusion chromatography in a Sephadex G50 column with PBS as the eluent. Sulfo-Azide-Cy5 was used for all dispersions denoted with an asterisk (*) and sulfo-DBCO-Cy5 was used for those denoted with a carat (^). PL denotes phospholipid. All additives were at 2 mol %.

Figure 7. Effect of binding complementary dye probe on internal structures of clickable cubosomes. Scattering profiles were measured at 25 °C after mixing clickable cubosomes with the complementary Cy5 dye in PBS for 24 h. PL denotes phospholipid. All additives were at 2 mol %. The azide to DBCO ratio was 1:1 for all mixed samples.

immobilization or targeting. To the best of our knowledge there is one previous study using antibody functionalized cubosomes[53] and none using click functionalized cubosomes for targeting. Cubosomes have been doped with biotin-DSPE so that the cubosome can bind to avidin and be immobilized for biosensing.[54,55] Similarly, cubosomes have been functionalized with biotin through a biotin modified Pluronic F108 for active targeting of the receptors overexpressed by cancer cells.[56] Furthermore, two groups have used a folic acid modified Pluronic F108 to stabilize and functionalize cubosomes for

cancer cell targeted imaging and therapy.[57,58] All these examples showed only minor or no changes to the cubosomes upon binding, as was the case for the clickable cubosomes in this study.

Table 3. Lattice Parameters of Cubosome Dispersions after Being Mixed with Either Sulfo-N$_3$-Cy5 or Sulfo-DBCO-Cy5 for 24 h[a]

phospholipid added	dye added	cubic phase space group	lattice parameter (å)
None	Sulfo-Azide-Cy5	double diamond	66.76 ± 2.50
PL-Azide	Sulfo-DBCO-Cy5	double diamond	67.67 ± 1.20
PL-DBCO	Sulfo-Azide-Cy5	double diamond	66.47 ± 0.80
PL-DSPC	Sulfo-Azide-Cy5	double diamond	68.49 ± 0.27
PL−PEG$_{2000}$-DBCO	Sulfo-Azide-Cy5	primitive	90.24 ± 1.78
PL−PEG$_{2000}$-Azide	Sulfo-DBCO-Cy5	primitive	92.33 ± 0.13
PL−PEG$_{2000}$-DSPE	Sulfo-Azide-Cy5	primitive	91.96 ± 0.38

[a]Lattice parameters were determined from the SAXS data presented in Figure 4. PL denotes phospholipid. All additives were at 2 mol %.

The use of the long azide- or DBCO-PEG chain on the phospholipid additive is expected to increase the chance of the phospholipid being at the interface of the cubic phase due to its size and hydro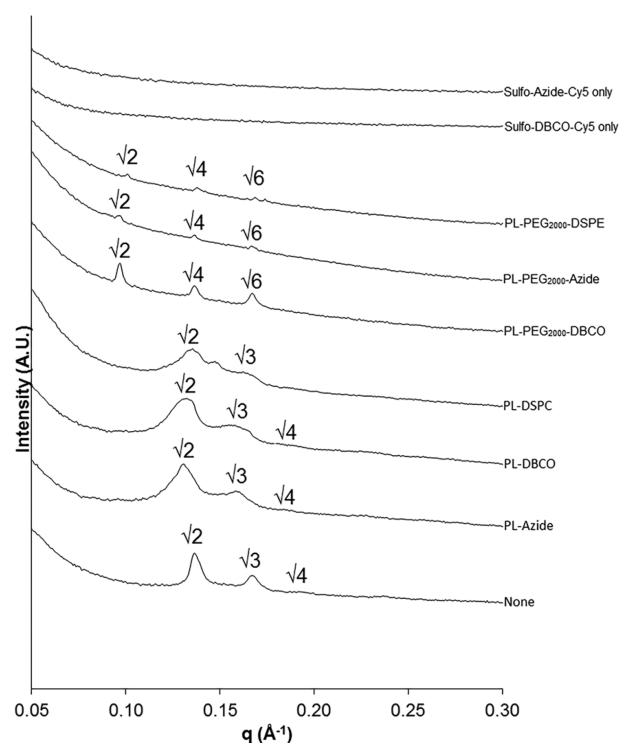philicity. This would benefit surface interactions as there would be a greater number of click groups extended from the surface. Additionally, the hydrophilic PEG chain might help reduce undesirable nonspecific hydrophobic interactions with a cell membrane or adsorption of opsonising proteins from the blood.

The findings presented in this manuscript pave the way for the use of these cubosomes with metabolic labeling to develop an improved delivery or imaging method. While the opportunities are significant for a new approach to delivery to come to the fore, it is very early days for cubosomes as delivery and imaging agents, for example understanding the in vitro cellular toxicity of cubosomes is still immature,[59,60] let alone understanding the pharmacokinetic aspects of these materials. Alternatively, these techniques and nanoparticles could have other uses such as biosensing and cell capture.

One limitation to functionalization through phospholipid doping is the lack of control over where the reactive groups present themselves. This does not appear to limit binding in solution but could present problems for future use paired with metabolic labeling. A potential solution is taking the approach mentioned above where the polymeric stabilizer is modified to contain the clickable functional group, as large stabilizer molecules tend to position at the external interface of the particles, presenting themselves to bulk aqueous phase rather than inside the aqueous cubic phase channels,[61,62] presenting the azides in a position where they are more readily available to react. Recently, lipid-like polymers were reported that can stabilize cubosomes[63] and an azide bearing version is currently being synthesized to assess the two different functionalization methods.

CONCLUSION

Novel functionalized cubosomes that can partake in copper-free click chemistry have been demonstrated. The incorporation of an azido or DBCO group to the cubosomes did not alter their phase and structure significantly. Additionally, the copper-free click reaction between the "clickable" cubosomes and DBCO or Azide-Cy5 was selective and very efficient while retaining the

structure of the unreacted cubosomes. This first study and proof of concept work is promising regarding the use of cubosomes combined with copper-free click chemistry and in the near future metabolic labeling to provide an antibody-free targeting option for these emerging drug delivery and imaging systems.

EXPERIMENTAL PROCEDURES

Materials. Phytantriol (3,7,11,15-tetramethylhexadecane-1,2,3-triol) was a gift from DSM Nutritional Products (Kaiseraugst, Switzerland). Pluronic F108 was purchased from Sigma-Aldrich (St. Louis, MO). 1,2-Distearoyl-sn-glycero-3-phosphocholine (DSPC), 1,2-dipalmitoyl-sn-glycero-3-phosphoethanolamine-N-(lissamine rhodamine B sulfonyl) (ammonium salt) (16:0 Liss RhoD PE), 1,2-distearoyl-sn-glycero-3-phosphoethanolamine-N-[dibenzocyclooctyl-(polyethylene glycol)-2000] (ammonium salt) (DSPE-PEG2000-DBCO), 1,2-distearoyl-sn-glycero-3-phosphoethanol-amine-N-[azido(polyethylene glycol)-2000] (ammonium salt) (DSPE-PEG2000-Azide), 1,2-distearoyl-sn-glycero-3-phosphoe-thanolamine-N-[methoxy(polyethylene glycol)-2000] (ammo-nium salt) (DSPE-PEG2000), 1,2-dipalmitoyl-sn-glycero-3-phosphoethanolamine-N-dibenzocyclooctyl (DPPE-DBCO), and 1,2-dipalmitoyl-sn-glycero-3-phosphoethanolamine-N-(6-azidohexanoyl)(ammonium salt) (DPPE-Azide) were pur-chased from Avanti Polar Lipids (Alabama, USA). Cy5-Dibenzocyclooctyne (DBCO) was purchased from Click Chemistry Tools (Scottsdale, USA). Water used in these studies was obtained from a Millipore Milli-Q purification system (Billerica, USA). Phosphate buffered saline (PBS) 1× pH 7.4 was prepared by dissolving 137 mM sodium chloride (≥99.7%), 2.7 mM potassium chloride (≥99%), 2 mM potassium dihydrogen phosphate (≥99%), and 8 mM disodium hydrogen phosphate (≥99%). The salts were purchased from Chemsupply (Port Adelaide, SA, Australia).

Methods. *Cubosome Preparation.* Cubosome dispersions were prepared by weighing 100 mg of phytantriol into a vial and adding 0.0025 molar ratio of 16:0 Liss Rhodamine B PE phospholipid. The two were dissolved and mixed in chloroform which was then removed. The mixture was then hydrated by addition of 900 mg of a 1.5% (w/v) Pluronic F108 solution in PBS for 12 h before ultrasonication via a Misonix S-4000 Tip sonicator (Farmingdale, NY) at 150 amplitude applied for 2 s on and 1 s off cycles for 2.5 min total sonication time. For the azide, DBCO and DSPC containing cubosomes the phospho-lipids were mixed in before hydration at a 0.02 molar ratio relative to phytantriol.

Dynamic Light Scattering (DLS). DLS was used to measure the size distribution of the cubosomes. DLS was conducted on a Malvern Zetasizer Nano ZS. Cubosome dispersions were diluted by a factor of 1000 into Milli-Q water before measurements were taken at 25 °C, assuming the viscosity of water. Volume PSD was used and each dispersion was measured three times.

Small Angle X-ray Scattering (SAXS). The internal structure of the clickable cubosomes was assessed using SAXS for comparison to nonclick traditional cubosomes. All SAXS measurements were performed at the SAXS/WAXS beamline at the Australian Synchrotron.[64] The synchrotron X-ray beam was tuned to a wavelength of 1.127 Å (11.0 keV) at a sample to detector distance of 1034.97 mm which gave the q-range of 0.0176 < q < 1.016 Å^{-1}, where q is the length of the scattering vector defined by $q = (4\pi/\lambda) \sin(\theta/2)$. The q range was

calibrated using a silver behenate standard. The 2D SAXS patterns were acquired over 1 s using a Pilatus 1 M detector with an active area of 169×179 mm^2 and with a pixel size of 172 μm. The cubosome dispersions were transferred to 1.5-mm-diameter glass capillaries and loaded into a custom 3D-printed capillary holder. The 2D scattering patterns were integrated into the 1D scattering function $I(q)$ using the in-house developed software package Scatterbrain. Scattering curves are plotted as a function of relative intensity and phase structures are identified by indexing the Bragg peaks to known relative spacing ratios.[65]

Cryogenic Transmission Electron Microscopy (cryo-TEM). Samples were frozen using a Vitrobot Mark III with ambient humidity of 80% for all experiments, and ambient temperature was 22 °C. Copper grids (200-mesh) coated with perforated carbon film (Lacey carbon film: ProSciTech, Qld, Australia) were glow discharged. Aliquots (3 μL) of the sample were pipetted onto each grid prior to plunging. After 15 s adsorption time the grid was blotted for 2 s. The grid was then plunged into liquid ethane cooled by liquid nitrogen. Frozen grids were stored in liquid nitrogen until required. The samples were examined using a Gatan 626 cryoholder (Gatan, Pleasanton, CA, USA) and Tecnai F30 Transmission Electron Microscope (FEI, Eindhoven, The Netherlands) at an operating voltage of 300 kV. At all times low dose procedures were followed, using an electron dose of $10-15$ electrons/Å^2 for all imaging. Images were recorded using a FEI CETA 4kx4k CMOS camera.

Binding Efficiency Studies. Size exclusion chromatography was used to separate bound and unbound dye from the cubosomes before measuring fluorescence of the fractions eluted from the column. A Sephadex G50 (GE Healthcare, Uppsala, Sweden) column was used with PBS as the eluent. Cubosome dispersions were mixed at a 1:1 ratio (of azide to DBCO) with Sulfo-DBCO-Cy5 or Sulfo-N$_3$-Cy5 in PBS for 24 h protected from light. Then 100 μL of sample was loaded and 18 mL was collected in 500 μL fractions. Aliquots (100 μL) of each fraction were loaded onto a black 96-well plate and diluted with 100 μL methanol and the fluorescence was measured by a PerkinElmer Enspire plate reader. Methanol was added to the elutions to break down the lipid structure and prevent quenching of the Cy5. The fluorescence from Rhodamine B was measured at 560/583 nm and from Cy5 at 649/662 nm. Standards were prepared through a series of serial volumetric dilutions of stock (1 mg/mL) dye solution and sample concentrations determined by comparison to this standard curve.

■ AUTHOR INFORMATION

Corresponding Author

*E-mail: Ben.Boyd@monash.edu.

ORCID ⓞ

Angus Johnston: 0000-0001-5611-4515

Ben J. Boyd: 0000-0001-5434-590X

Notes

The authors declare no competing financial interest.

■ REFERENCES

(1) Iyer, A. K., Khaled, G., Fang, J., and Maeda, H. (2006) Exploiting the enhanced permeability and retention effect for tumor targeting. *Drug Discovery Today 11*, 812−818.

(2) Torchilin, V. P. (2010) Passive and Active Drug Targeting: Drug Delivery to Tumors as an Example, in *Drug Delivery* (Schäfer-Korting, M., Ed.) pp 3−53, Springer, Berlin, Heidelberg.

(3) Garg, G., Saraf, S., and Saraf, S. (2007) Cubosomes: An Overview. *Biol. Pharm. Bull. 30*, 350−353.

(4) Karami, Z., and Hamidi, M. (2016) Cubosomes: remarkable drug delivery potential. *Drug Discovery Today 21*, 789−801.

(5) Spicer, P. T. (2005) Progress in liquid crystalline dispersions: Cubosomes. *Curr. Opin. Colloid Interface Sci. 10*, 274−279.

(6) Pan, X, Han, K., Peng, X., Yang, Z., Qin, L., Zhu, C., Huang, X., Shi, X., Dian, L., Lu, M., and Wu, C. (2013) Nanostructed Cubosomes as Advanced Drug Delivery System. *Curr. Pharm. Des. 19*, 6290−6297.

(7) Rizwan, S. B., Dong, Y. D., Boyd, B. J., Rades, T., and Hook, S. (2007) Characterisation of bicontinuous cubic liquid crystalline systems of phytantriol and water using cryo field emission scanning electron microscopy (cryo FESEM). *Micron 38*, 478−485.

(8) Zhai, J., Hinton, T. M., Waddington, L. J., Fong, C., Tran, N., Mulet, X., Drummond, C. J., and Muir, B. W. (2015) Lipid−PEG Conjugates Sterically Stabilize and Reduce the Toxicity of Phytantriol-Based Lyotropic Liquid Crystalline Nanoparticles. *Langmuir 31*, 10871−10880.

(9) Azmi, I. D. M., Moghimi, S. M., and Yaghmur, A. (2015) Cubosomes and hexosomes as versatile platforms for drug delivery. *Ther. Delivery 6*, 1347−1364.

(10) Chen, Y., Ma, P., and Gui, S. (2014) Cubic and Hexagonal Liquid Crystals as Drug Delivery Systems. *BioMed Res. Int. 2014*, 1.

(11) Boyd, B. J., and Fong, W.-K. (2012) Stimuli-Responsive Lipid-Based Self-Assembled Systems, in *Self-Assembled Supramolecular Architectures* (Garti, N., Somasundaran, P., and Mezzenga, R., Eds.) pp 257−288, John Wiley & Sons, Hoboken, NJ.

(12) Spicer, P. T. (2005) Progress in liquid crystalline dispersions: Cubosomes. *Curr. Opin. Colloid Interface Sci. 10*, 274−279.

(13) Naga, M. L., Prasanna, R. Y., Harini, C. V., Jyotsna, T., Gowri, Y., and Haritha, K. (2014) Cubosomes as Targeted Drug Delivery Systems - A Biopharmaceutical Approach. *Curr. Drug Discovery Technol. 11*, 181−188.

(14) Mulet, X., Boyd, B. J., and Drummond, C. J. (2013) Advances in drug delivery and medical imaging using colloidal lyotropic liquid crystalline dispersions. *J. Colloid Interface Sci. 393*, 1−20.

(15) Gupta, A., Stait-Gardner, T., de Campo, L., Waddington, L. J., Kirby, N., Price, W. S., and Moghaddam, M. J. (2014) Nanoassemblies of Gd-DTPA-monooleyl and glycerol monooleate amphiphiles as potential MRI contrast agents. *J. Mater. Chem. B 2*, 1225−1233.

(16) Muir, B. W., Acharya, D. P., Kennedy, D. F., Mulet, X., Evans, R. A., Pereira, S. M., Wark, K. L., Boyd, B. J., Nguyen, T.-H., Hinton, T. M., et al. (2012) Metal-free and MRI visible theranostic lyotropic liquid crystal nitroxide-based nanoparticles. *Biomaterials 33*, 2723−2733.

(17) Alcaraz, N., and Boyd, B. J. (2017) Cubosomes as Carriers for MRI Contrast Agents. *Curr. Med. Chem. 24*, 470−482.

(18) Chames, P., Van Regenmortel, M., Weiss, E., and Baty, D. (2009) Therapeutic antibodies: successes, limitations and hopes for the future. *Br. J. Pharmacol. 157*, 220−233.

(19) Zwicke, G. L., Ali Mansoori, G., and Jeffery, C. J. (2012) Utilizing the folate receptor for active targeting of cancer nano-therapeutics. *Nano Rev. 3*, 18496.

(20) Kularatne, S. A., and Low, P. S. (2010) Targeting of Nanoparticles: Folate Receptor, in *Cancer Nanotechnology: Methods and Protocols* (Grobmyer, S. R., and Moudgil, B. M., Eds.) pp 249−265, Humana Press, Totowa, NJ.

(21) Saxon, E., and Bertozzi, C. R. (2001) Chemical and Biological Strategies for Engineering Cell Surface Glycosylation. *Annu. Rev. Cell Dev. Biol. 17*, 1−23.

(22) Bertozzi, C. R., and Kiessling, L. L. (2001) Chemical Glycobiology. *Science 291*, 2357−2364.

(23) Vocadlo, D. J., Hang, H. C., Kim, E.-J., Hanover, J. A., and Bertozzi, C. R. (2003) A chemical approach for identifying O-GlcNAc-modified proteins in cells. *Proc. Natl. Acad. Sci. U. S. A. 100*, 9116–9121.

(24) Agard, N. J., Prescher, J. A., and Bertozzi, C. R. (2004) A Strain-Promoted [3 + 2] Azide–Alkyne Cycloaddition for Covalent Modification of Biomolecules in Living Systems. *J. Am. Chem. Soc. 126*, 15046–15047.

(25) Prescher, J. A., Dube, D. H., and Bertozzi, C. R. (2004) Chemical remodelling of cell surfaces in living animals. *Nature 430*, 873–877.

(26) Prescher, J. A., and Bertozzi, C. R. (2005) Chemistry in living systems. *Nat. Chem. Biol. 1*, 13–21.

(27) Agard, N. J., Baskin, J. M., Prescher, J. A., Lo, A., and Bertozzi, C. R. (2006) A Comparative Study of Bioorthogonal Reactions with Azides. *ACS Chem. Biol. 1*, 644–648.

(28) Laughlin, S. T., Agard, N. J., Baskin, J. M., Carrico, I. S., Chang, P. V., Ganguli, A. S., Hangauer, M. J., Lo, A., Prescher, J. A., and Bertozzi, C. R. (2006) Metabolic Labeling of Glycans with Azido Sugars for Visualization and Glycoproteomics, in *Methods in Enzymology* (Minoru, F., Ed.) pp 230–250, Academic Press, Cambridge, MA.

(29) Baskin, J. M., and Bertozzi, C. R. (2007) Bioorthogonal Click Chemistry: Covalent Labeling in Living Systems. *QSAR Comb. Sci. 26*, 1211–1219.

(30) Sletten, E. M., and Bertozzi, C. R. (2009) Bioorthogonal Chemistry: Fishing for Selectivity in a Sea of Functionality. *Angew. Chem., Int. Ed. 48*, 6974–6998.

(31) Bertozzi, C. R. (2011) A Decade of Bioorthogonal Chemistry. *Acc. Chem. Res. 44*, 651–653.

(32) McKay, C. S., and Finn, M. G. (2014) Click Chemistry in Complex Mixtures: Bioorthogonal Bioconjugation. *Chem. Biol. 21*, 1075–1101.

(33) Agarwal, P., Beahm, B. J., Shieh, P., and Bertozzi, C. R. (2015) Systemic Fluorescence Imaging of Zebrafish Glycans with Bioorthogonal Chemistry. *Angew. Chem., Int. Ed. 54*, 11504–11510.

(34) Baskin, J. M., Dehnert, K. W., Laughlin, S. T., Amacher, S. L., and Bertozzi, C. R. (2010) Visualizing enveloping layer glycans during zebrafish early embryogenesis. *Proc. Natl. Acad. Sci. U. S. A. 107*, 10360–10605.

(35) Dehnert, K. W., Baskin, J. M., Laughlin, S. T., Beahm, B. J., Naidu, N. N., Amacher, S. L., and Bertozzi, C. R. (2012) Imaging the sialome during zebrafish development with copper-free click chemistry. *ChemBioChem 13*, 353–357.

(36) Dehnert, K. W., Beahm, B. J., Huynh, T. T., Baskin, J. M., Laughlin, S. T., Wang, W., Wu, P., Amacher, S. L., and Bertozzi, C. R. (2011) Metabolic labeling of fucosylated glycans in developing zebrafish. *ACS Chem. Biol. 6*, 547–552.

(37) Jiang, H., Feng, L., Soriano del Amo, D., Seidel Iii, R. D., Marlow, F., and Wu, P. (2011) Imaging glycans in zebrafish embryos by metabolic labeling and bioorthogonal click chemistry. *J. Visualized Exp.*, 1 DOI: 10.3791/2686.

(38) Laughlin, S. T., Baskin, J. M., Amacher, S. L., and Bertozzi, C. R. (2008) In Vivo Imaging of Membrane-Associated Glycans in Developing Zebrafish. *Science 320*, 664–667.

(39) Neef, A. B., and Luedtke, N. W. (2014) An Azide-Modified Nucleoside for Metabolic Labeling of DNA. *ChemBioChem 15*, 789–793.

(40) Neef, A. B., and Luedtke, N. W. (2011) Dynamic metabolic labeling of DNA in vivo with arabinosyl nucleosides. *Proc. Natl. Acad. Sci. U. S. A. 108*, 20404–20409.

(41) Beynon, R. J., and Pratt, J. M. (2005) Metabolic Labeling of Proteins for Proteomics. *Mol. Cell. Proteomics 4*, 857–872.

(42) Krijgsveld, J., Ketting, R. F., Mahmoudi, T., Johansen, J., Artal-Sanz, M., Verrijzer, C. P., Plasterk, R. H. A., and Heck, A. J. R. (2003) Metabolic labeling of C. elegans and D. melanogaster for quantitative proteomics. *Nat. Biotechnol. 21*, 927–931.

(43) Koo, H., Huh, M. S., Sun, I.-C., Yuk, S. H., Choi, K., Kim, K., and Kwon, I. C. (2011) In Vivo Targeted Delivery of Nanoparticles for Theranosis. *Acc. Chem. Res. 44*, 1018–1028.

(44) Lee, S., Koo, H., Na, J. H., Han, S. J., Min, H. S., Lee, S. J., Kim, S. H., Yun, S. H., Jeong, S. Y., Kwon, I. C., et al. (2014) Chemical Tumor-Targeting of Nanoparticles Based on Metabolic Glycoengineering and Click Chemistry. *ACS Nano 8*, 2048–2063.

(45) Tresset, G. (2009) The multiple faces of self-assembled lipidic systems. *PMC Biophys. 2*, 3.

(46) Dong, Y.-D., Larson, I., Hanley, T., and Boyd, B. J. (2006) Bulk and Dispersed Aqueous Phase Behavior of Phytantriol: Effect of Vitamin E Acetate and F127 Polymer on Liquid Crystal Nanostructure. *Langmuir 22*, 9512–9518.

(47) Israelachvili, J. N., Mitchell, D. J., and Ninham, B. W. (1976) Theory of self-assembly of hydrocarbon amphiphiles into micelles and bilayers. *J. Chem. Soc., Faraday Trans. 2 72*, 1525–1568.

(48) Bisset, N. B., Boyd, B. J., and Dong, Y.-D. (2015) Tailoring liquid crystalline lipid nanomaterials for controlled release of macromolecules. *Int. J. Pharm. 495*, 241–248.

(49) Barauskas, J., and Landh, T. (2003) Phase Behavior of the Phytantriol/Water System. *Langmuir 19*, 9562–9565.

(50) Hartnett, T. E., Ladewig, K., O'Connor, A. J., Hartley, P. G., and McLean, K. M. (2014) Size and Phase Control of Cubic Lyotropic Liquid Crystal Nanoparticles. *J. Phys. Chem. B 118*, 7430–7439.

(51) Azhari, H., Strauss, M., Hook, S., Boyd, B. J., and Rizwan, S. B. (2016) Stabilising cubosomes with Tween 80 as a step towards targeting lipid nanocarriers to the blood–brain barrier. *Eur. J. Pharm. Biopharm. 104*, 148–155.

(52) Nilsson, C., Østergaard, J., Larsen, S. W., Larsen, C., Urtti, A., and Yaghmur, A. (2014) PEGylation of Phytantriol-Based Lyotropic Liquid Crystalline Particles—The Effect of Lipid Composition, PEG Chain Length, and Temperature on the Internal Nanostructure. *Langmuir 30*, 6398–6407.

(53) Zhai, J., Scoble, J. A., Li, N., Lovrecz, G., Waddington, L. J., Tran, N., Muir, B. W., Coia, G., Kirby, N., Drummond, C. J., et al. (2015) Epidermal growth factor receptor-targeted lipid nanoparticles retain self-assembled nanostructures and provide high specificity. *Nanoscale 7*, 2905–2913.

(54) Fraser, S. J., Dawson, R. M., Waddington, L. J., Muir, B. W., Mulet, X., Hartley, P. G., Separovic, F., and Polyzos, A. (2011) Development of Cubosomes as a Cell-Free Biosensing Platform. *Aust. J. Chem. 64*, 46–53.

(55) Tajik-Ahmadabad, B., Mechler, A., Muir, B. W., McLean, K., Hinton, T. M., Separovic, F., and Polyzos, A. (2017) A QCM-D and SAXS Study of the Interaction of Functionalised Lyotropic Liquid Crystalline Lipid Nanoparticles with siRNA. *ChemBioChem 18*, 921–930.

(56) Aleandri, S., Bandera, D., Mezzenga, R., and Landau, E. M. (2015) Biotinylated Cubosomes: A Versatile Tool for Active Targeting and Codelivery of Paclitaxel and a Fluorescein-Based Lipid Dye. *Langmuir 31*, 12770–12776.

(57) Caltagirone, C., Falchi, A. M., Lampis, S., Lippolis, V., Meli, V., Monduzzi, M., Prodi, L., Schmidt, J., Sgarzi, M., Talmon, Y., et al. (2014) Cancer-Cell-Targeted Theranostic Cubosomes. *Langmuir 30*, 6228–6236.

(58) Tian, Y., Li, J.-c., Zhu, J.-x., Zhu, N., Zhang, H.-m., Liang, L., and Sun, L. (2017) Folic Acid-Targeted Etoposide Cubosomes for Theranostic Application of Cancer Cell Imaging and Therapy. *Med. Sci. Monit. 23*, 2426–2435.

(59) Murgia, S., Falchi, A. M., Mano, M., Lampis, S., Angius, R., Carnerup, A. M., Schmidt, J., Diaz, G., Giacca, M., Talmon, Y., et al. (2010) Nanoparticles from Lipid-Based Liquid Crystals: Emulsifier Influence on Morphology and Cytotoxicity. *J. Phys. Chem. B 114*, 3518–3525.

(60) Zhai, J., Suryadinata, R., Luan, B., Tran, N., Hinton, T. M., Ratcliffe, J., Hao, X., and Drummond, C. J. (2016) Amphiphilic brush polymers produced using the RAFT polymerisation method stabilise and reduce the cell cytotoxicity of lipid lyotropic liquid crystalline nanoparticles. *Faraday Discuss. 191*, 545–563.

(61) La, Y., Park, C., Shin, T. J., Joo, S. H., Kang, S., and Kim, K. T. (2014) Colloidal inverse bicontinuous cubic membranes of block copolymers with tunable surface functional groups. *Nat. Chem. 6*, 534−541.

(62) Chong, J. Y. T., Mulet, X., Keddie, D. J., Waddington, L., Mudie, S. T., Boyd, B. J., and Drummond, C. J. (2015) Novel Steric Stabilizers for Lyotropic Liquid Crystalline Nanoparticles: PEGylated-Phytanyl Copolymers. *Langmuir 31*, 2615−2629.

(63) Grace, J. L., Alcaraz, N., Truong, N. P., Davis, T. P., Boyd, B. J., Quinn, J. F., and Whittaker, M. R. (2017) Lipidated polymers for the stabilization of cubosomes: nanostructured drug delivery vehicles. *Chem. Commun. 53*, 10552−10555.

(64) Kirby, N. M., Mudie, S. T., Hawley, A. M., Cookson, D. J., Mertens, H. D. T., Cowieson, N., and Samardzic-Boban, V. (2013) A low-background-intensity focusing small-angle X-ray scattering undulator beamline. *J. Appl. Crystallogr. 46*, 1670−1680.

(65) Hyde, S., Ninham, B. W., Andersson, S., Larsson, K., Landh, T., Blum, Z., and Lidin, S. (1997) The Language of Shape, in *The Language of Shape*, pp iii, Elsevier Science B.V., Amsterdam.

Lipidated polymers for the stabilization of cubosomes: nanostructured drug delivery vehicles†

James L. Grace, [ID] [ab] Nicolas Alcaraz, [ID] [ab] Nghia P. Truong, [ID] [ab]
Thomas P. Davis, [ID] [abc] Ben J. Boyd, [ID] *[ab] John F. Quinn [ID] *[ab] and
Michael R. Whittaker [ID] *[ab]

Lipidated polymers, like their protein counterparts, may be useful in fields as diverse as biochemistry and drug delivery. As such, strategies for preparing lipidated polymers with defined molecular architecture are clearly warranted. Herein, we describe a broadly-applicable methodology for synthesizing such lipidated materials, and demonstrate how they can be applied to the preparation of nanostructured drug delivery vehicles.

Diglycerides, fatty acid esters of glycerol in which two of the hydroxyls are esterified, are both industrially and biochemically significant molecules. For example, diglycerides have been employed as solubilizing agents for oral and injectable pharmaceutical formulations,[1] and are commonly applied as emulsifiers in the food industry.[2] Moreover, diglycerides with the *sn*-1,2 isoform have been shown to be critically important to a range of cell signalling processes.[3] As such, the development of polymeric materials which incorporate diglyceride moieties is potentially of interest to a broad section of the chemical community. For example, such "lipidated" materials would be useful to researchers at the interface of biochemistry and polymer chemistry interested in how materials can be engineered to manipulate cell signalling processes, or to pharmaceutical scientists seeking next-generation, nanostructured materials for drug delivery.

Nanostructured drug delivery vehicles, for example cubosomes, can be prepared by using lipid-based liquid crystalline mesophases, such as the reversed bicontinuous cubic (V_2) (see Fig. 1), inverse hexagonal (H_2), and lamellar phase. Cubosome formation,

geometry and potential uses, including as nanostructured drug delivery vehicles, has been reviewed recently by Spicer *et al.*,[4] Garg *et al.*,[5] and in the Language of Shape by Hyde.[6] By exploiting the fact that cubic phases exhibit a faster release rate of encapsulated material compared to the hexagonal phase,[7] these systems can be engineered to provide highly controlled drug release profiles. Specifically, the release rate of an encapsulated molecule can be increased by triggering changes in phase from inverse hexagonal to cubic with either environmental cues (such as pH) or by application of an external trigger (such as light).[8] As such, the development of novel surface-active agents capable of stabilizing particulate forms of these interesting materials is highly desirable.

The development of novel surface-active polymers frequently employs one of the so-called reversible-deactivation radical polymerization techniques (RAFT, ATRP, NMP, *etc.*). Of these, Cu(0)-mediated polymerization is particularly powerful in that it enables the preparation of polymers with narrow molecular weight distributions from acrylates,[9] methacrylates,[10] acrylamides,[11] methacrylamides,[11a,12] styrene,[13] acrylonitrile,[14] and vinyl chloride.[15] For a more detailed overview of Cu(0)-mediated polymerization refer to the reviews by the groups of Percec[16] and Haddleton.[17] Moreover, the well-documented high end-group fidelity associated with the technique has enabled the preparation of a variety of interesting multiblock[18] and di-end group

[a] *ARC Centre of Excellence in Convergent Bio-Nano Science and Technology, Monash Institute of Pharmaceutical Sciences, Monash University, Parkville, VIC 3052, Australia. E-mail: ben.boyd@monash.edu, john.f.quinn@monash.edu, michael.whittaker@monash.edu*

[b] *Drug Delivery, Disposition and Dynamics Theme, Monash Institute of Pharmaceutical Sciences, Monash University, Parkville, VIC 3052, Australia*

[c] *Department of Chemistry, University of Warwick, Coventry, ULCV4 7AL, UK*

† Electronic supplementary information (ESI) available: Materials, initiator synthesis, polymer synthesis, NMR, kinetic study conversion plot and GPC, ATR-FTIR, size measurements, cryo-TEM, SAXS measurements, phase summaries, lattice parameters. See DOI: 10.1039/c7cc05842j

Fig. 1 Structure of an *Im3m* cubosome. Cubosome structure was created by 3D printing.

functionalised materials.[19] As such, Cu(0)-mediated polymerization is ideally suited to the preparation of novel lipidated materials with precisely defined molecular architecture.

Herein, we describe the preparation of lipidated polymers with terminal diglyceride functionality by employing a new initiator based on 1,2-dilauroyl-*sn*-glycerol, (*i.e.*, (*R*)-3-((2-bromo-2-methylpropanoyl)oxy)propane-1,2-diyl didodecanoate (BMPD)). Specifically, we have synthesized both poly(methyl acrylate) (PMA) and poly(poly(ethylene glycol) methyl ether acrylate) (PPEGMEA) using Cu(0)-mediated polymerization initiated with BMPD. We also demonstrate the effectiveness of this new material for stabilization of cubosomes, in contrast to polymers having the same degree of polymerization and chemistry but having a monoalkyl endgroup. To our knowledge there are no other reports where a diglyceride has been exploited to incorporate two alkyl chains into the chain terminus of narrow molecular weight distribution polymers prepared *via* reversible-deactivation radical polymerization. Perhaps the closest example is that of Lowe and co-workers, who have employed RAFT polymerization with difunctional benzodithioates to prepare interesting materials with difunctionalised endgroups.[20] Recently, Matyjaszewski and co-workers have synthesized a tetherable initiator based on the structure of fatty acids for surface-initiated atom transfer radical polymerization from metal oxide surfaces.[21] However, these materials only employ a single aliphatic chain fatty acid at the chain terminus.

BMPD was synthesized as a dual aliphatic tail Cu(0)-mediated polymerization initiator using 1,2-dilauroyl-*sn*-glycerol as the starting material. Specifically, the reaction of 1,2-dilauroyl-*sn*-glycerol and α-bromoisobutyryl bromide in the presence of triethylamine afforded the product as shown in Scheme 1.

Synthesis of BMPD was confirmed by both ^{1}H and ^{13}C NMR spectroscopy, infrared (IR) spectroscopy, and high resolution mass spectrometry (HRMS). As shown in Fig. SI1 (ESI†), ^{1}H NMR spectroscopy indicated the transformation of 1,2-DLG to BMPD by the disappearance of peak 'g' at 3.73 ppm, and the appearance of a new peak 'g' at 1.91 ppm (Fig. SI1A and SI1B, ESI†). Further, the emergence of a new carbonyl signal at 171.31

consistent with the formation of a new ester linkage (Fig. SI2, ESI†) also indicates successful synthesis of the initiator. As shown in Fig. SI3 (ESI†), conversion of 1,2-DLG to BMPD was also evident from the corresponding IR spectra. Specifically, loss of the peaks associated with the hydroxyl group (3450 cm^{-1}, O–H stretch) and (1040 cm^{-1}, C–O stretch) confirmed successful esterification of the 1,2-DLG. In the HRMS analysis, the sodium adduct was observed.

BMPD was then employed as the initiator for polymerization of both methyl acrylate (MA) and poly(ethylene glycol) methyl ether acrylate (PEGMEA). The kinetics of the polymerization reaction were monitored by ^{1}H NMR (shown in Fig. SI4, ESI†), and GPC was employed to follow the evolution of the molecular weight distribution. In both cases the polymerization proceeded to above 80% conversion within three hours (Fig. SI5, ESI†), with a slight induction time observed for the polymerization of PEGMEA. Moreover, as shown in Fig. 2A and Fig. SI6A (ESI†), there was good agreement between the experimental molecular weights and the theoretical values, confirming that the polymerization was well-controlled. The dispersity values remained low throughout the polymerization (<1.10 for PMA, and <1.18 for PPEGMEA), indicating good control over the polymerization and the absence of major side reactions that might be visible in the molecular weight distribution.

To investigate the utility of BMPD for preparing more sophisticated molecular architectures, we investigated the chain end fidelity of the diglyceride-terminated polymer by chain extending with a further segment of MA. These results, shown in Fig. SI7 (ESI†), demonstrated that there was minimal dead polymer formed after the first block, and indicate a high level of "livingness" after polymerization of the first segment.

Given the propensity of diglycerides to form ordered structures and to insert into hydrophobic environments, we hypothesized that one application for these new materials might be in the stabilization of liquid crystalline nanoparticles such as cubosomes. Traditionally, block copolymer surfactants such as Pluronic F108® or F127® are employed to aid the dispersion of bulk mesophases. The polymer typically sits at the interface of the hydrophobic lipid phase and the hydrophilic water phase and thus reduces interfacial tension.[22] Previous work has shown that the type of stabiliser used has an effect on the ease of dispersal, phase formation and stability.[23] As such, we predicted that the novel diglyceride-terminated material prepared herein will impart a high level of stability, as it would be expected to exhibit a strong affinity for the lipid phase given that the structure of the endgroup mimics that of a phospholipid.

To investigate this possibility, potential stabilisers were synthesized by polymerizing PEGMEA using either BMPD or a single C_{12} aliphatic chain initiator (dodecyl 2-bromoisobutyrate, DBiB) (Table SI1 and Fig. SI8, ESI†). The ability of the synthesized polymers to act as stabilisers and aid the formation of cubosomes was assessed by dispersing phytantriol in the presence of 1.5 wt% of the polymers synthesized. The resulting particles were then interrogated using dynamic light scattering (DLS) and small angle X-ray scattering (SAXS). Initial size estimations using DLS for the phytantriol particles stabilised by C_{12}-terminated and di-C_{12}-terminated PPEGMEA were 632.2 nm (PDI = 0.434) and
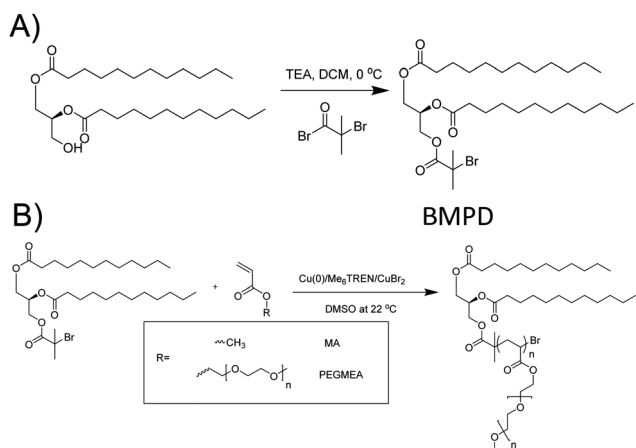
Scheme 1 (A) Synthesis of the diglyceride derived initiator BMPD. (B) Cu(0)-Mediated polymerization using BMPD as the initiator.
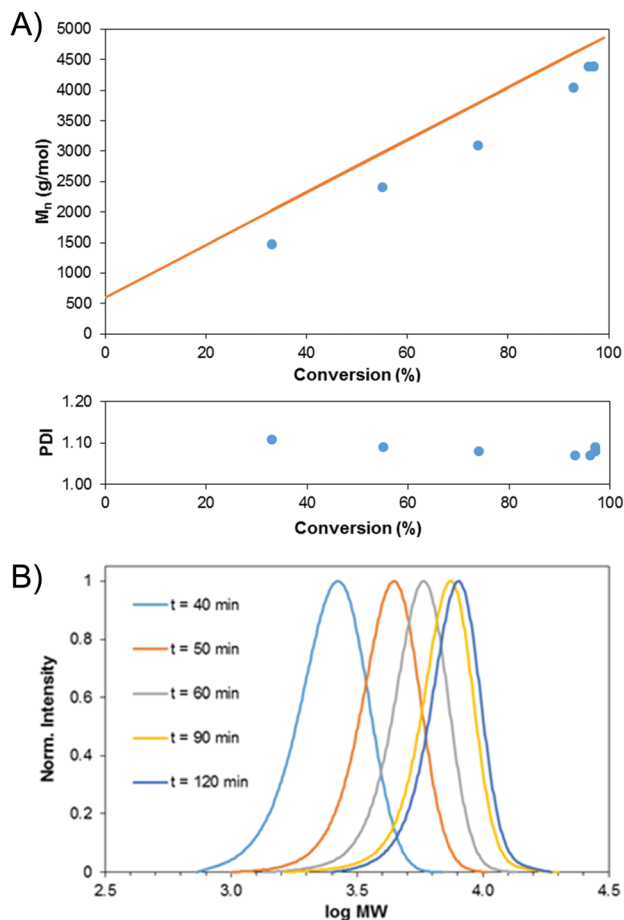
Fig. 2 Evolution of molecular weight with conversion for polymerization of MA ([M] = 3.68 M, [I] = 0.0736 M, [Me_6TREN] = 0.0118 M, [$CuBr_2$] = 0.00368 M) in DMSO at 22 °C. (A) M_n and PDI vs. conversion plot. The full line represents the theoretically expected molar mass. M_n values were derived from ^{1}H NMR DP calculations by the integration of peak 'a' against peak 'j' from Fig. SI4A (ESI†). (B) GPC spectra of molecular weight distribution over the time of the kinetic study. MWD at time points t = 180, 240 and 300 min were removed due to overlapping distributions.

Fig. 3 (A) SAXS profile of 1.5% w/v di-C_{12}-PPEGMEA stabilised phytantriol cubosomes at 25 °C indicating the presence of Im3m cubic spacing. (B) Cryo-TEM image of 1.5% w/v di-C_{12}-terminated PPEGMEA stabilised phytantriol cubosomes (indicated with a black circle). (C) Fourier transform of B. (D) Temperature phase study of 1.5% di-C_{12}-PPEGMEA and 1.5% C_{12}-PPEGMEA stabilised phytantriol cubosomes.

632 nm (PDI = 0.454), respectively. The presence of the large polymeric stabilisers are likely to have increased the size and polydispersity of the cubosomes when compared to Pluronic stabilized systems.[24] The internal structure of the resulting particles was subsequently investigated using SAXS. At ambient temperature the di-C_{12}-terminated PPEGMEA was shown to effectively stabilise cubosomes with Im3m phase (Fig. 3A), while particles stabilised with the monofunctional C_{12}-terminated PPEGMEA did not exhibit any internal structure under the same conditions possibly due to its more surfactant like structure. The cubosomes stabilised with the di-C_{12}-terminated PPEGMEA were then imaged via cryo-TEM, with cubic structure clearly evident (Fig. 3B and Fig. SI9, ESI†). The corresponding Fourier transform of the cryo-TEM (Fig. 3C) shows the internal structure of the cubosomes by focussing on the reciprocal spacing and supports the appearance of cubic structure, with the Im3m spacing observed consistent with the SAXS measurements.[25] The internal structure of both C_{12}-terminated PPEGMEA- and di-C_{12}-terminated PPEGMEA-stabilised phytantriol particles was
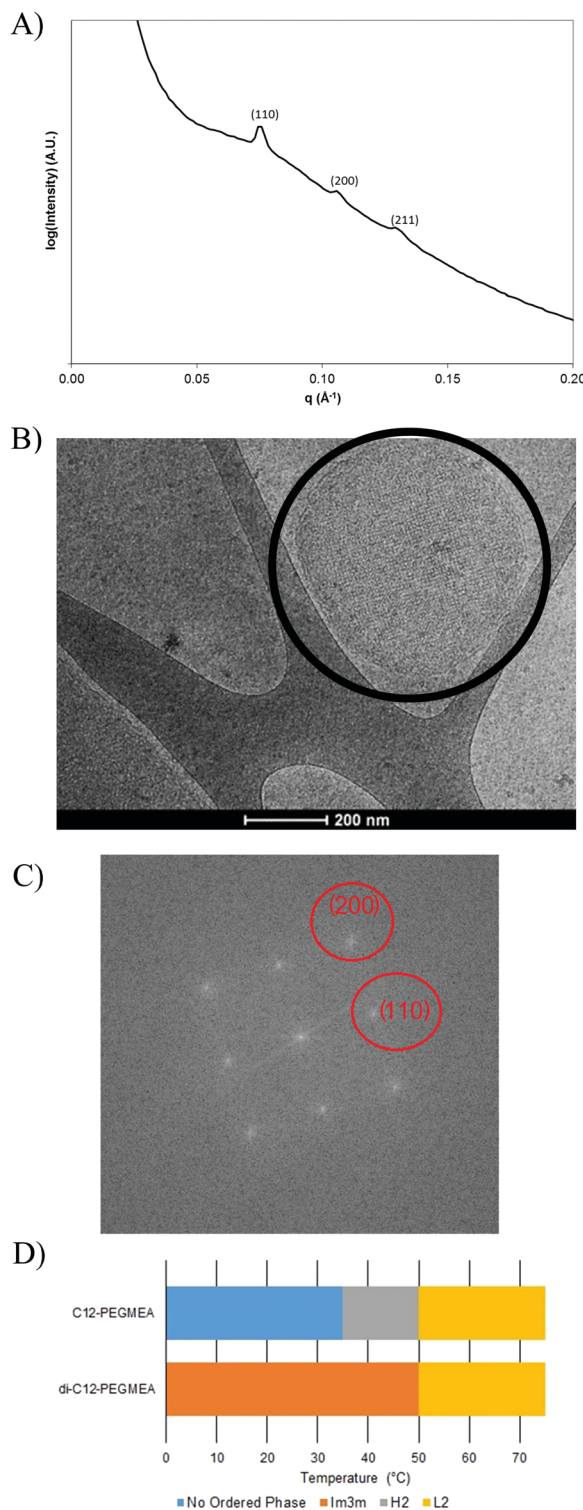
determined as a function of temperature using SAXS (see Fig. SI10 to SI15, ESI†). Fig. 3D summarises the phase transitions observed

over the temperature range studied (25–75 °C) for 1.5% w/v (see Fig. SI16 and SI17 (ESI†) for other concentrations). As noted above, particles stabilised with a monofunctional stabiliser (*i.e.*, C_{12}-terminated PPEGMEA) exhibited no distinguishable phase up until 35 °C, at which point hexagonal phase became observable. Further heating led to a phase change to lamellar at 50 °C. Stabilization *via* di-C_{12}-terminated PPEGMEA provided phase behaviour consistent with reports on Pluronic stabilized phytantriol, with *Im3m* cubic phase observed up to 50 °C after which the phase changed to lamellar. The lattice parameters were calculated (see Fig. SI18 and SI19, ESI†) using the SAXS data obtained and this showed similar spacing to Pluronic F127 stabilised cubosomes in the 1 and 1.5% di-C_{12}-terminated PPEG-MEA stabilised systems with the spacing around 120 Å at 25 °C. The spacing of the C_{12}-terminated PPEGMEA was around 100 Å which is commonly seen in the *Pn3m* cubic phase. A decrease in lattice parameter with an increase in temperature was observed as was an increase in lattice parameter with an increase in stabiliser concentration which is in line with previous works.[24–26] These results indicate that di-C_{12}-terminated PPEGMEA more effectively stabilised cubic LC structures across a broad range of temperatures compared to a monofunctional analogue (C_{12}-terminated PPEGMEA). Clearly, incorporating a phospholipid-mimicking end-group into a polymeric stabiliser is a convenient method for stabilising cubosomes, presumably by reducing the interfacial tension of the cubic LC structures.

In conclusion, lipidated polymers have been prepared by employing Cu(0)-mediated polymerization of MA and PEGMEA with a new initiator based on 1,2-dilauroyl-*sn*-glycerol. The resulting materials were shown to be applicable as novel stabilizers for liquid crystalline nanoparticles, enabling preservation of the internal LC structure. These interesting lipidated materials are likely to find application in various aspects of drug delivery, where diglycerides are of considerable importance.

Conflicts of interest

There are no conflicts to declare.

Notes and references

1 R. G. Strickley, *Pharm. Res.*, 2004, **21**, 201.
2 C. Maier, B. Zeeb and J. Weiss, *Colloids Surf., B*, 2014, **117**, 368.
3 T. O. Eichmann and A. Lass, *Cell. Mol. Life Sci.*, 2015, **72**, 3931.
4 P. T. Spicer, K. L. Hayden, M. L. Lynch, A. Ofori-Boateng and J. L. Burns, *Langmuir*, 2001, **17**, 5748.
5 G. Garg, S. Saraf and S. Saraf, *Biol. Pharm. Bull.*, 2007, **30**, 350.
6 S. Hyde, Z. Blum, T. Landh, S. Lidin, B. Ninham, S. Andersson and K. Larsson, in *The Language of Shape*, Elsevier Science B.V., Amsterdam, 1997, p. iii.
7 S. Phan, W. K. Fong, N. Kirby, T. Hanley and B. J. Boyd, *Int. J. Pharm.*, 2011, **421**, 176.
8 W. K. Fong, R. Negrini, J. J. Vallooran, R. Mezzenga and B. J. Boyd, *J. Colloid Interface Sci.*, 2016, **484**, 320.
9 (*a*) S. R. Samanta, V. Nikolaou, S. Keller, M. J. Monteiro, D. A. Wilson, D. M. Haddleton and V. Percec, *Polym. Chem.*, 2015, **6**, 2084; (*b*) N. H. Nguyen, J. Kulis, H. J. Sun, Z. F. Jia, B. Van Beusekom, M. E. Levere, D. A. Wilson, M. J. Monteiro and V. Percec, *Polym. Chem.*, 2013, **4**, 144; (*c*) Q. Zhang, P. Wilson, Z. D. Li, R. McHale, J. Godfrey, A. Anastasaki, C. Waldron and D. M. Haddleton, *J. Am. Chem. Soc.*, 2013, **135**, 7355; (*d*) Q. Zhang, J. Collins, A. Anastasaki, R. Wallis, D. A. Mitchell, C. R. Becer and D. M. Haddleton, *Angew. Chem., Int. Ed.*, 2013, **52**, 4435; (*e*) M. R. Whittaker, C. N. Urbani and M. J. Monteiro, *J. Polym. Sci., Part A: Polym. Chem.*, 2008, **46**, 6346; (*f*) G. Lligadas, J. S. Ladislaw, T. Guliashvili and V. Percec, *J. Polym. Sci., Part A: Polym. Chem.*, 2008, **46**, 278; (*g*) N. H. Nguyen and V. Percec, *J. Polym. Sci., Part A: Polym. Chem.*, 2011, **49**, 4756; (*h*) J. L. Grace, J. X. Huang, S. Cheah, N. P. Truong, M. C. Cooper, J. Li, T. P. Davis, J. F. Quinn, T. Velkov and M. R. Whittaker, *RSC Adv.*, 2016, **6**, 15469.
10 (*a*) B. D. Hornby, A. G. West, J. C. Tom, C. Waterson, S. Harrisson and S. Perrier, *Macromol. Rapid Commun.*, 2010, **31**, 1276; (*b*) M. Khan, Y. K. Feng, D. Z. Yang, W. Zhou, H. Tian, Y. Han, L. Zhang, W. J. Yuan, J. Zhang, J. T. Guo and W. C. Zhang, *J. Polym. Sci., Part A: Polym. Chem.*, 2013, **51**, 3166; (*c*) N. H. Nguyen, X. F. Leng, H. J. Sun and V. Percec, *J. Polym. Sci., Part A: Polym. Chem.*, 2013, **51**, 3110.
11 (*a*) U. Edlund, C. Rodriguez-Emmenegger, E. Brynda and A. C. Albersson, *Polym. Chem.*, 2012, **3**, 2920; (*b*) F. Alsubaie, A. Anastasaki, P. Wilson and D. M. Haddleton, *Polym. Chem.*, 2015, **6**, 406; (*c*) T. Tischer, C. Rodriguez-Emmenegger, V. Trouillet, A. Welle, V. Schueler, J. O. Mueller, A. S. Goldmann, E. Brynda and C. Barner-Kowollik, *Adv. Mater.*, 2014, **26**, 4087.
12 N. H. Nguyen, C. Rodriguez-Emmenegger, E. Brynda, Z. Sedlakova and V. Percec, *Polym. Chem.*, 2013, **4**, 2424.
13 J. Tom, B. Hornby, A. West, S. Harrisson and S. Perrier, *Polym. Chem.*, 2010, **1**, 420.
14 X. H. Liu, G. B. Zhang, B. X. Li, Y. G. Bai and Y. S. Li, *J. Polym. Sci., Part A: Polym. Chem.*, 2010, **48**, 5439.
15 T. Hatano, B. M. Rosen and V. Percec, *J. Polym. Sci., Part A: Polym. Chem.*, 2010, **48**, 164.
16 (*a*) B. M. Rosen and V. Percec, *Chem. Rev.*, 2009, **109**, 5069; (*b*) G. Lligadas, S. Grama and V. Percec, *Biomacromolecules*, 2017, **18**, 1039.
17 A. Anastasaki, V. Nikolaou, G. Nurumbetov, P. Wilson, K. Kempe, J. F. Quinn, T. P. Davis, M. R. Whittaker and D. M. Haddleton, *Chem. Rev.*, 2016, **116**, 835.
18 A. H. Soeriyadi, C. Boyer, F. Nyström, P. B. Zetterlund and M. R. Whittaker, *J. Am. Chem. Soc.*, 2011, **133**, 11128.
19 (*a*) A. Simula, V. Nikolaou, A. Anastasaki, F. Alsubaie, G. Nurumbetov, P. Wilson, K. Kempe and D. M. Haddleton, *Polym. Chem.*, 2015, **6**, 2226; (*b*) A. Simula, G. Nurumbetov, A. Anastasaki, P. Wilson and D. M. Haddleton, *Eur. Polym. J.*, 2015, **62**, 294.
20 J. Y. Quek, X. C. Liu, T. P. Davis, P. J. Roth and A. B. Lowe, *Polym. Chem.*, 2015, **6**, 118.
21 J. J. Yan, X. C. Pan, Z. Y. Wang, Z. Lu, Y. Wang, L. Liu, J. N. Zhang, C. E. Ho, M. R. Bockstaller and K. Matyjaszewski, *Chem. Mater.*, 2017, **29**, 4963.
22 J. Y. T. Chong, X. Mulet, L. J. Waddington, B. J. Boyd and C. J. Drummond, *Langmuir*, 2012, **28**, 9223.
23 (*a*) J. Y. T. Chong, X. Mulet, L. J. Waddington, B. J. Boyd and C. J. Drummond, *Soft Matter*, 2011, **7**, 4768; (*b*) J. Y. T. Chong, X. Mulet, D. J. Keddie, L. Waddington, S. T. Mudie, B. J. Boyd and C. J. Drummond, *Langmuir*, 2015, **31**, 2615.
24 Y. D. Dong, I. Larson, T. Hanley and B. J. Boyd, *Langmuir*, 2006, **22**, 9512.
25 (*a*) J. Barauskas, M. Johnsson, F. Johnson and F. Tiberg, *Langmuir*, 2005, **21**, 2569; (*b*) P. Spicer, in *Encyclopedia of Nanoscience and Nanotechnology*, ed. J. Schwarz, C. Contescu and K. Putyera, Marcel Dekker, New York, 2004, pp. 881–892.
26 (*a*) G. Popescu, J. Barauskas, T. Nylander and F. Tiberg, *Langmuir*, 2007, **23**, 496; (*b*) M. Nakano, A. Sugita, H. Matsuoka and T. Handa, *Langmuir*, 2001, **17**, 3917; (*c*) T. E. Hartnett, K. Ladewig, A. J. O'Connor, P. G. Hartley and K. M. McLean, *J. Phys. Chem. B*, 2014, **118**, 7430; (*d*) J. L. Zhai, T. M. Hinton, L. J. Waddington, C. Fong, N. Tran, X. Mulet, C. J. Drummond and B. W. Muir, *Langmuir*, 2015, **31**, 10871.
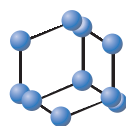
REVIEW ARTICLE

Cubosomes as Carriers for MRI Contrast Agents

Nicolas Alcaraz and Ben J. Boyd[*]

Drug Delivery, Disposition and Dynamics, Monash Institute of Pharmaceutical Sciences and ARC Centre of Excellence in Convergent Bio-Nano Science and Technology, Monash University (Parkville Campus), 381 Royal Pde, Parkville VIC 3052, Australia

Abstract: Cubosomes are self-assembled nanostructures that often form on dispersion of polar lipids in aqueous environments. The nanoparticles are analogous to liposomes but contain a complex internal self-assembled structure providing a point of difference to relatively simple liposomes. They exhibit a range of attractive properties such as having a high surface area, being able to incorporate both hydrophobic and hydrophilic molecules and controlled release. Consequently cubosomes are of increasing interest in fields such as drug delivery, and diagnostic imaging, in particular as a carrier for magnetic resonance imaging contrast agents. Over the last decade the incorporation of various contrast agents into the cubic mesophases has demonstrated improved relaxivity and resolution, as well as addressing other limitations of commercially available agents by increasing circulation time, stability and targeting. This minireview provides a brief overview of what cubosomes are, how they can be made, how they are characterised and also summarise the findings from the studies that have used cubosomes to develop better contrast agents for MRI, as well as highlight some potential for future developments.

WHAT ARE CUBOSOMES?

Lipids, surfactants and polymers can all possess amphiphilic structures such that in polar solvents the hydrophobic effect largely drives association of the hydrophobic parts of the molecules, presenting the hydrophilic parts to the (usually) aqueous environment [1]. One familiar example of this type of self-assembly is the formation of bilayers by many phospholipids, the bilayer structures being termed a 'lamellar phase', which forms the basis of cellular membranes. However, amphiphilic molecules may self-assemble into a wide range of other geometries illustrated in Fig. (**1**). The type of structure formed on self-assembly is dictated by the packing of molecules, which in turn is determined by molecular geometry, temperature, pressure

and solution conditions [2]. It is possible to switch between such structures by dynamically changing these conditions 'on demand'.

Some modes of self-assembly of lipids are liquid crystalline structures. These structures are a matter of state that exhibit properties between a traditional liquid and a solid, such as the long range order of crystalline materials and the local disorder of liquid systems. With reference to Fig. (**1**), in the bicontinuous cubic phase, the lipids are locally in a liquid state but the material contains crystallographic order and has an overall three dimensional geometry compared to lamellar phase which has repeated units only in one dimension. This also imparts a very high viscosity on the bulk cubic phase such that it resembles a self-supporting solid gel-like material despite comprising approximately equal parts lipid and water.

Cubosomes are formed on dispersion of cubic phase-forming lipids in excess water, this alleviates the handling issues associated with the highly viscous bulk

*Address correspondence to this author at the Drug Delivery, Disposition and Dynamics, Monash Institute of Pharmaceutical Sciences and ARC Centre of Excellence in Convergent Bio-Nano Science and Technology, Monash University (Parkville Campus), 381 Royal Pde, Parkville VIC 3052, Australia;
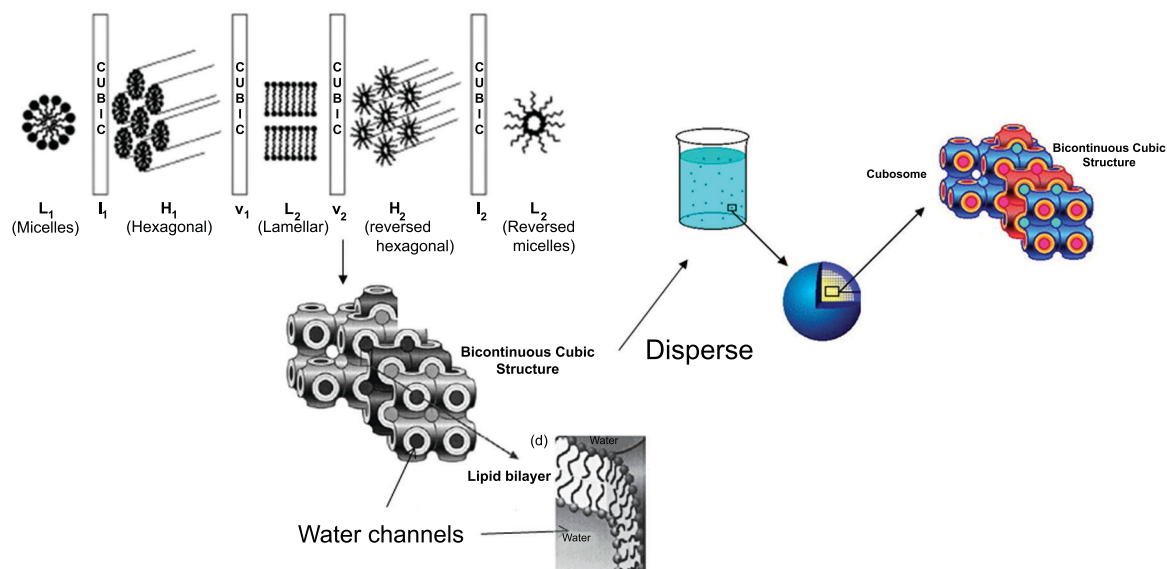E-mail: Ben.Boyd@monash.edu

Fig. (1). Schematic of self-assembly structures formed in increasing water content/hydrophobicity/packing order. The structures often formed by lipids in excess water are the lamellar, inverse cubic, inverse hexagonal and inverse micellar phases. Cubosomes are obtained upon dispersion of the bicontinuous cubic phase (V_2), analogous to formation of liposomes on dispersion of lamellar phase. (Modified with permission from Kaasgaard and Drummond [2]).

cubic phase material [3]. While there are reports of forming dispersed cubic phase particles using polymers [4], the vast majority of literature on cubosomes has described their formation using lipid systems. Cubosomes have been described as having unique internal structures that consist of a single lipid bilayer twisted and warped around two separate water domains, hence the terminology 'bicontinuous'. There have been three subtly different internal structures observed for these materials as represented in Fig. (**2**), which fit discrete mathematical solutions for the geometry of such structures [5].

Cubosomes are relatively novel having been discovered in the 1980s by Kare Larsson, coining the term

due to their similarities to liposomes and the molecular crystallography of cubic phase [1]. Cubosomes typically range in size from as small as 100 nm to as large as 500 nm in diameter [3] as seen in Fig. (**3**). However, there is no physical limitation to growing macrosized particles. Most research is focussed on making small dispersed cubic phase particles, in order to use them as injectable drug delivery systems, hence the focus on preparation and understanding of dispersions with submicron dimensions. In order to prepare them in a stable form, a small amount of a stabilizing surfactant or polymer is necessary to prevent particle aggregation.

Some benefits of cubosomes over other nano-delivery systems include that, unlike liposomes, they
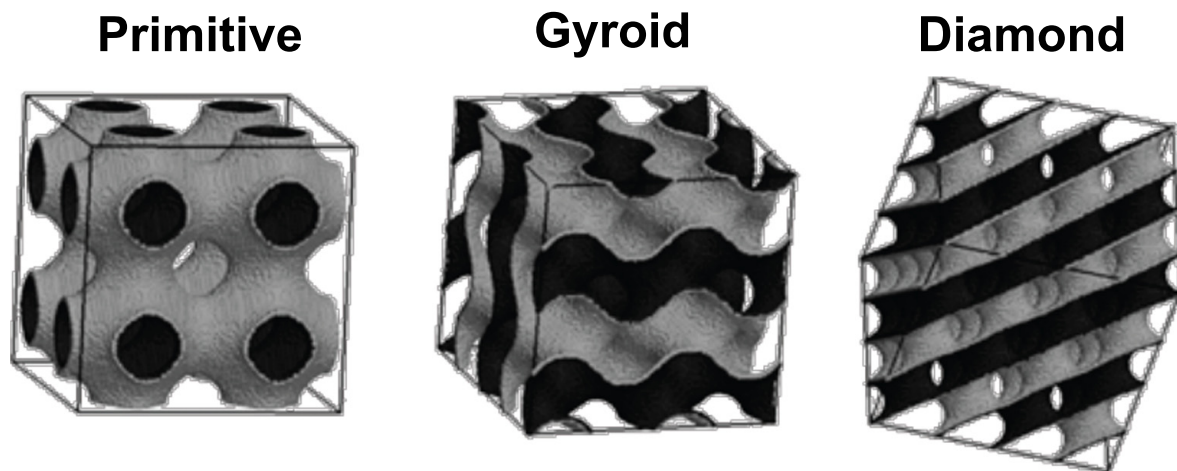

Fig. (2). Surface representation of the three main cubic phase structures. These internal structures are also commonly known as Im3m (Q229), Ia3d (Q229) and Pn3m (Q224) respectively. (Reused with permission from Marrink *et al.* [6]).

are not spherical, presenting interesting opportunities in surface specific delivery. Additionally, due to their intricate internal channels cubosomes provide a much higher surface area for binding delivery agents to the bilayer rather than passive solubilization. The internal lipid content also means that they can incorporate much larger amounts of hydrophobic and amphiphilic payloads [7-9]. Finally, the phase change of cubosomes between other structures is reversible, allowing for switchable on-demand release as opposed to a burst on-demand release of other nanoparticle systems. Consequently, cubosomes are under investigation for a number of different uses with the most prominent being drug delivery and pharmaceutics. This is primarily due to their diffusion controlled release that is phase dependent but also their ability to uptake both hydrophilic and hydrophobic payloads [7, 8]. Within this scope there are applications of cancer therapy, oral drug delivery, intravenous systems, and topical systems [7, 10, 11]. Outside of this area there are potential applications in agrochemical delivery [12, 13], cosmetics [14-17] and food products [18-21]. While drug delivery is receiving most of the current literature focus for cubosomes [22] there is an opportunity to also use these particles as carriers of hydrophobic, hydrophilic and amphiphilic imaging agents. Hence, for this mini-review the focus will be on lipid-based materials as they are most commonly used to formulate cubosomes and have only been applied relatively recently to develop new MRI agents.

METHODS OF PREPARATION OF CUBOSOMES

There are a number of ways to create cubosomes with the most common being known as the top-down approach [24-27] which involves dispersion of the am-phiphile or preformed bulk cubic phase in excess aqueous solution (generally with an added colloidal stabiliser) using high amounts of mechanical energy such as with an ultrasonicator probe or other high energy process. The dispersing droplets of lipid amphiphile will self-assemble into the cubosome dispersion. This is not an energy efficient method and requires a lot of energy per unit volume which can result in degradation of components. Another drawback of the sonication method is the potential for vesicles and liposomes to form as opposed to cubosomes. An alternative method, that is potentially more suitable for larger scale production, is known as the bottom-up approach [3], involving dilution of a hydrotope-containing mixture into excess water, which induces precipitation of cubosomes from an unstructured solution or emulsion.

In the absence of steric stabilising surfactants such as Pluronic polymers, upon dispersion the cubosomes will aggregate due to the hydrophobic surface. Pluronic F127 (also known as Poloxamer 407 and Lutrol F127), a non-ionic block copolymer surfactant, is the most common stabiliser and has shown to provide the best stability for cubosomes and similar dispersions [26]. It acts by incorporating itself into the nanostructure and is a physical barrier that repels the nanoparticles and prevents them from colliding and aggregating [23, 28]. It also ensures hydrophilic groups are present on the surface of the cubosome and in contact with the bulk water reducing unfavourable interfacial tension [28].

CHARACTERIZATION OF CUBOSOMES

To confirm the formation of cubosomes and characterise their shape, size, stability and structure there are a number of techniques that can be combined to get a complete picture.
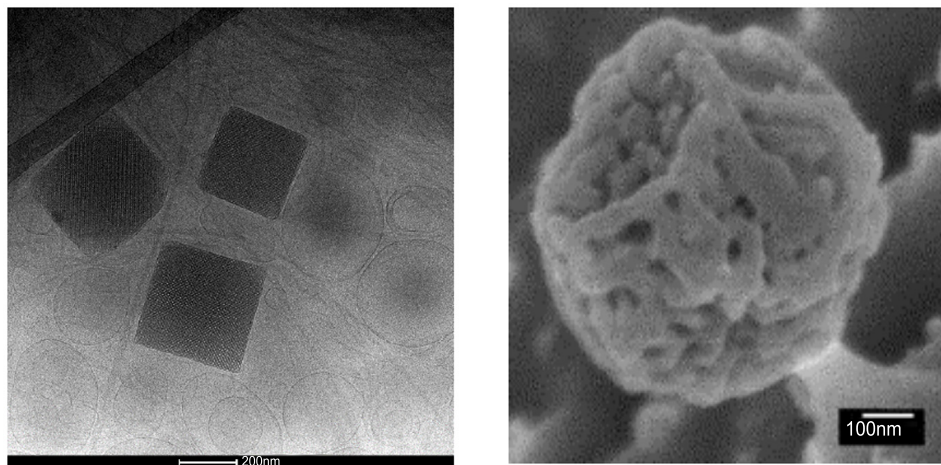

Fig. (3). Cryo-TEM and cryoFESEM images of cubosomes. (CryoFESEM image adapted with permission from Rizwan *et al.* [23]).

The external properties of the particles such as size, shape and morphology are important in dictating their interactions in biological systems. Dynamic light scattering (DLS) is commonly used for measurements of particle size distribution of cubosomes [29-32]. The technique tracks the scattering intensity of the nanoparticles as they diffuse through the medium [33]. By measuring the size distribution of cubosomes over a period of time the stability can be deduced as an increase in size will indicate aggregation. Imaging allows the visualization of the nanoparticles to determine their size, structure and shape [9, 23, 27, 34]. As cuboso-mes must be hydrated to retain their structure, cryo-TEM, rather than regular TEM, is the main mode of imaging used to characterise them. Additionally, cryo-FESEM has also been applied to obtain 3-dimensional information on particle shape and surface features, with examples of both shown in Fig. (**3**).

By far, the most important and widely used approach to determine the internal structure of cubosomes is small angle X-ray scattering. Because cubosomes generally retain the internal cubic phase order of the parent cubic phase (schematically shown in Fig. **1**), the crystallographic order gives rise to periodicity that interacts with X-rays. This results in scattering of incident X-rays at angles defined by the geometric ordering in the sample (Fig. **2**). The two-dimensional scattering profile is converted to a one-dimensional intensity vs q profile, where q is the scattering vector related to the angle. The 'Bragg peaks' occur at specific angles depending on both the structure present and the dimensions of that structure. These are used as both a fingerprint for the type of phase present but also the absolute positions provide information on water channel swelling [24, 25, 35-37].

MAGNETIC RESONANCE IMAGING

MRI is a diagnostic tool used heavily in the medical world as it allows physicians to create 3D images of soft tissue regions and helps diagnosis of illnesses and track the progression of treatment.

The images are created by a computer analysing the detected variations of the spin in hydrogen protons in water within the body [38]. First, a strong magnetic field is applied to align the protons and then a secondary variable field is introduced to flip the protons. A scanner monitors the recovery of the alignment after the removal of the variable field (analogous to NMR for molecular identification) and an image is created with this information. A typical scanner is pictured be-low in Fig. (**4**), and scanners come in a range of magnetic power and sizes, suitable for small rodents up to humans and larger animals. For *in vitro* work up, samples can be mounted in disk-like holders to enable comparison of the intrinsic contrast between different contrast agents prior to progressing to *in vivo* evaluations.

The benefits of MRI over other imaging modalities is that it is non-invasive, does not use ionising radiation and gives a very high amount of spatial resolution and soft-tissue contrast. This makes it practical in finding irregularities and damage to muscular groups and other soft tissue abnormalities, such as tumors. However, the main limitation of the technique is its low sensitivity which is overcome in clinical settings by commonly using contrast agents.

There are three main parameters which affect image contrast, namely the spin density, longitudinal relaxation time (T1) and transverse relaxation time (T2) [40]. Therefore, contrast agents work by either by changing T1, T2 or both as they alter the relaxation times of the water protons within and around the tissue.

There are a number of commercially available contrast agents that are placed into two main groups depending on their mechanism of action. As mentioned, all contrast agents reduce the relaxation time of the water protons within the tissue but some will effect either the longitudinal or transverse relaxation times. Generally, paramagnetic metal ions such as Gd [41] and Mn (II) are known as positive, T1 or R1 contrast agents as they effect the longitudinal relaxation times [42, 43]. Alternatively, superparamagnetic iron oxide (SPION) based nanomaterials are known as negative, T2 or R2 contrast agents as they affect the transverse relaxation times [44]. It should be noted that the superparamagnetic iron oxide materials also act as T1 contrast agents however they provide a greater T2 effect [45, 46]. Although, commonly used and successful in clinical settings, contrast agents do have some drawbacks. The contrast agents have a lack of targeting or specificity which limits their sensitivity, they generally have short half-lives in the body meaning that the dosing and imaging events need to occur at close timeframes and the contrast agents, particularly gadolinium, can be toxic [47-51].

Therefore, there is a growing body of research related to improving contrast agents for MRI to extend their half-lives, increasing their specificity by giving them passive or active targeting capabilities and reducing their toxicity.
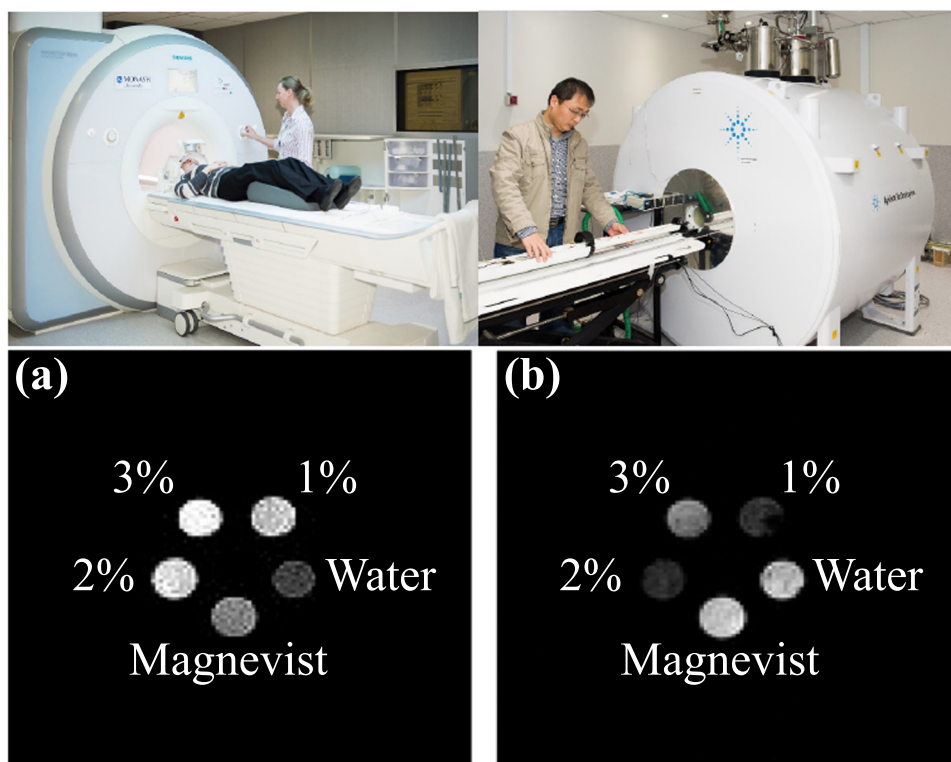
Fig. (4). A Siemens Skyra 3T MRI for human use on the top left and an Agilent 9.4T MRI Small Animal Scanner on the top right. Bottom: Image of *in vitro* contrasting of various Gd-DTPA-MP/PT dispersions and Magnevist at the same Gd concentration. T1 **(a)** and T2 **(b)** weighted MRI show improved brightness in T1 and improved darkness in T2 resulting in greater contrasting. (Reused with permission from Gupta *et al.* [39]).

The effectiveness of contrast agents is usually compared by assessing the degree to which they can enhance the longitudinal or transverse water relaxation rate constant ($R_1 = 1/T_1$ or $R_2 = 1/T_2$, respectively) normalized to concentration of the contrast agent and this is termed relaxivity [52]. The relaxation rate constant is impacted by the properties of water in the local vicinity of the contrast agent, hence different tissues, with different water availability will provide different relaxivities leading to contrast. Thus the nature of the aqueous environment in which the contrast agent resides is important for understanding where contrast may be limited by concentration or by relaxivity. This becomes important shortly in highlighting a key feature of cubosomes when used as carriers for MRI contrast agents.

An approach that is increasing in popularity particularly for cancer diagnosis involves making high molecular weight contrast agents that will have a longer circulation time and will be influenced by the enhanced permeation and retention effect [53, 54] leading to accumulation in tumors. The main benefit of these higher molecular weight contrast agents is that they provide superior contrast due to greater accumulated concentrations in the local tissue when compared to their lower molecular weight counterparts [55, 56].

CUBOSOMES AND MRI

While cubosomes may present certain benefits over liposomes in application to imaging, there have been some reports of the use of liposomes for this purpose. To be used as contrast agents the liposomes are loaded with either a heavy metal ion such as Gd [41] or SPION into their internal aqueous phase or the lipid bilayer itself [57]. In general, they have demonstrated improved relaxivity and in turn contrasting enhancement over commercially available agents and the contrast agents loaded on their own. This is likely due to similar properties that would make cubosomes desirable as a carrier for contrast agents. These properties include a high loading capacity, the ability to incorporate both hydrophilic and hydrophobic entities, being biologically safe, securing the toxic heavy metal ions and increasing circulation time and accumulation in tissues.

It has been shown that placing the contrast agent in the rigid lipid bilayer over the aqueous phase is favourable due to reducing how much the contrast agents rotate or tumble.

Over the last 8 years there has been increasing interest using liquid crystalline colloidal dispersions such as cubosomes and hexosomes as a basis for improved MRI contrast agents. The interest in using cubosomes has arisen from the theory that the 3-D framework of the bicontinuous cubic phase may facilitate coordination of the water around the metal ion (typically gadolinium) and that the ease of water transfer between the cubic phase and the bulk water would lower the lifetime of the water in the inner sphere, increasing the relaxation rate. Additionally, the structure may impede some rotational movement of Gd [41], further improving the relaxation of water. The reported studies into the use of liquid crystalline materials and dispersions as carriers for MRI agents are summarised in Table **1**. The general strategy for developing such systems is to create an amphiphilic chelating molecule or amphiphilic MRI sensitive molecule that is incorporated into the self-assembled structure, exposing the contrast agent to modified water conditions compared to in bulk water.

To this end the strategy of using Gd-chelated amphiphiles incorporated into cubosomes was pioneered by the Drummond group in 2009 reporting the synthesis of gadolinium-oleate and incorporating it into bulk cubic phase and dispersing as cubosomes [58]. Concentrations of Gd-oleate greater than 1% lead to partial phase separation in the bulk systems. It was also discovered that upon dispersing the bulk phase, the presence of the gadolinium oleate disrupted the cubic phase. Nevertheless, these bulk systems showed 3-4 fold greater relaxivity over free Gd-Oleate and the commercially available contrast agent Magnevist indicating that there is potential for liquid crystalline based contrast agents. Interestingly, increasing the Gd-oleate concentration in Myverol, the commercial name of a distilled monoglyceride consisting of saturated fatty acids with similar properties to glycerol mono-oleate (GMO), led to a decrease in relaxivity, indicating that the environment is more important than the Gd content in providing greater relaxivity. This is consistent with the hypothesis presented above for the benefit of using cubosomes as hosts for MRI contrast agents.

As a result of the promising findings in the work, phytanyl–tailed chelated amphiphiles (phytantyl-ethylenediaminetetraacetic acid (EDTA) derivatives) were developed with an anticipation that the amphiphiles themselves may form liquid crystalline structures on dispersion [59]. Depending on the number of conjugations a lamellar phase or inverse hexagonal and micellar cubic mixed phase was promoted. However, due to a propensity not to form bicontinuous cubic phase on dispersion and the formation of non-swelling materials, chelation with the metal ion after dispersion was studied with the intention of less disruption to preformed particles. This method allows the potential for addition of the metal immediately before use – an advantage for short lived isotopes. This new strategy resulted in small unilamellar liposomal particles that had much greater contrasting abilities, with the single-tailed derivatives showing enhanced relaxitivity compared to EDTA-Gd or EDTA-Mn in aqueous solution, however the dispersions were not cubosomes.

In order to address some of the issues regarding creating cubosomes EDTA was replaced by another chelator, diethylenetriaminepentaacetic acid (DTPA), due to the headgroup having an extra carboxylate and amine group which provides more stable chelates of trivalent ions [60]. Additionally, the different structure and intermolecular interactions could lead to more favourable packing conditions resulting in cubosomes. In this work they developed Gd-DTPA- mono or bis oleyl (MO and BO) and phytanyl (MP and BP) molecules, the structures of which can be seen in Fig. (**5**). The studies showed that creating dispersions from the four amphiphiles resulted in a range of different liquid crystalline structures. No relaxivity tests were conducted but the four amphiphiles neat and bulk properties were characterised. Generally, the DTPA amphiphiles exhibited mesophases with slightly lower interfacial curvature when compared to EDTA amphiphiles previously studied.

Drummond's group [61] continued their work by mixing the new DTPA-amphiphiles with stabiliser and dispersing them. The structure formed was dependent on the amphiphile used. However, regardless of the structure formed all the Gd-DTPA-lipid systems had higher relaxivities than that of commercially available low molecular weight Magnevist at all magnetic field strengths tested. It was noted that there were different relaxivities between the different structures alluding to the importance of structure and the system's ability to enhance the contrast agent. They also attempted to improve the targeting of the contrast agent by bioconjugation of an antibody to the surfaces of the nanosystems and were able to show that antigen binding could occur, implying targeted delivery was possible. Finally, they conducted *in vivo* cytotoxicity studies showing these systems were not cytotoxic within the relevant toxicological range.

In a similar study by Gupta *et al.* [62] the Gd-DTPA-monooleyl amphiphile was assessed as an MRI contrast agent. By incorporating different concentra-

Table 1.   Summary of studies into the use of lipid liquid crystalline materials as carriers for MRI contrast agents.

| Contrast agent	Host lipid system	Impact on self-assembly	Impact on relaxivity	Contrast agent type	Ref.
Gd-Oleate	Myverol - As bulk and dispersions	Disrupts cubic phase with phase separation over 1% w/w	Enhanced relaxivity *vs.* Magnevist	R1	[58]
Gd-EDTA- phytanyl (Mono and Bis)	Itself – As bulk and dispersions	Mono – Unilamellar liposomal nanoparticles Bis – Hexosomes and unilamellar liposomal nanoparticles	Enhanced relaxivity *vs.* Magnevist and Gd-EDTA	R1	[59]
Mn-EDTA- phytanyl (Mono and Bis)	Itself – As bulk and dispersions	Mono – Unilamellar liposomal nanoparticles Bis – Hexosomes and unilamellar liposomal nanoparticles	Enhanced relaxivity *vs.* Magnevist and Mn-EDTA	R1	[59]
Gd-DTPA-Oleyl (Mono and Bis)	Itself – As bulk and dispersions	Mono – Rod shaped micelles Bis – Uni and multilamellar liposomes As Gd mol ratio increases the formation of multilayered nanospheres is promoted	Mono – Best of the Gd-DTPA-Amphiphiles and ~8 times greater relaxitivty over Magnevist Bis – ~3 times greater relaxitivty over Magnevist	R1	[60, 61]
Gd-DTPA-Phytanyl (Mono and Bis)	Itself – As bulk and dispersions	Mono – Unilamellar liposomes Bis – Hexosomes and cubosomes As Gd mol ratio increases a phase shift occurs from hexosomes or liposomes to cubosomes and then to multilayered nanospheres	Mono – ~4 times greater relaxtivity over Magnevist Bis – ~3 times greater relaxtivity over Magnevist	R1	[60, 61]
Gd-DTPA-Monooleyl	GMO– As bulk and dispersions	Cubic phase present until 5 mol % loading At 10 mol % loading myelins form Increased loading shifts the system from Pn3m cubic phase to Im3m cubic phase	All dispersions created had a ~2 fold greater relaxtivity when compared to Magnevist at all field strengths	R1	[62]
Gd-DTPA-Monophytanyl	Phytantriol – As dispersions	Cubosomes retained until 2 mol % loading Above 2 mol % loading leads to flattened planar bilayers of liposomal nanoassemblies	Enhanced relaxivity *vs.* Magnevist	R1	[39]
SPION	Phytantriol – As dispersions	Easily incorporated into the structure and cubosomes were formed	Enhanced relaxivity *vs.* unbound SPION	R2	[63]
Nitroxide-lipid	Phytantriol – As dispersions GMO – As dispersions	Easily dispersed into cubosomes and hexosomes using Pluronic F127 stabiliser up to the studied 14% w/w loading Cubic phase promoted at 2% w/w loading or lower. As loading increases hexagonal phase beings forming	Enhanced relaxivity *vs.* free nitroxides Phytantriol provided better relaxivity enhancement *vs.* GMO Cubic phase (lower loading) had enhanced relaxivity *vs.* hexagonal phase (higher loading)	R1	[68]
O/L/Do/C Nox ("Kinked" tail nitroxide lipid)	GMO – As dispersions	Hexosomes were intentionally formed due to a more desirable toxicity profile at up to 10% w/w loading	Enhanced relaxivity (~x2) *vs.* previously reported nitroxide lipids	R1	[69]
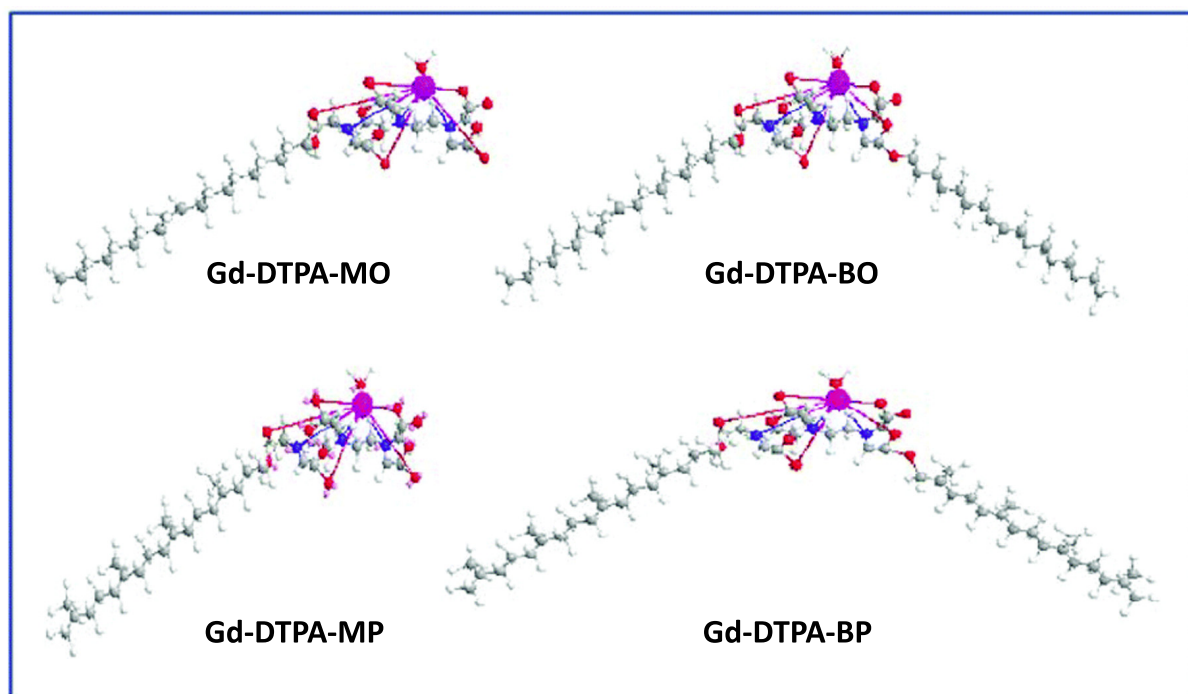
Fig. (5). Molecular structure of Gd-DTPA amphiphiles based off oleyl and phytantyl in both a mono or bis conjugation. (Reused with permission from Moghaddam *et al.* [60]).

tions of the amphiphile into glycerol monooleate and dispersing them, liquid crystalline dispersions were formed. If the loading was above 1 mol % then the system would form liposomes instead of cubosomes. Much like before, these systems proved to have greater relaxivities at four different magnetic field strengths per Gd ion when compared to Magnevist. The cubosomes were particularly better at high magnetic field strengths showing potential as a high strength MRI contrast agent as can be seen in Fig. (**6**).

The same group continued their work and created phytantriol based systems to assess any differences with GMO based systems [39]. Phytantriol is often seen as more desirable due to the lack of an ester bond that can undergo hydrolysis leading to instability. These different systems could tolerate an increased loading at twice that of the original systems tested. The systems were able to remain in the Pn3m cubic mesophase up until 10 mol % of Gd-DTPA-MP in the bulk systems in excess water and 2 mol % in dispersions. As before, these systems showed much greater relaxivities and image contrast when compared to Magnevist at both high and low strengths. These improvements are attributed to the larger sizes which results in longer reorientational correlation times and the unique continuous water channels of the cubosomes which may allow more efficient water exchange which also results from high magnetic field.
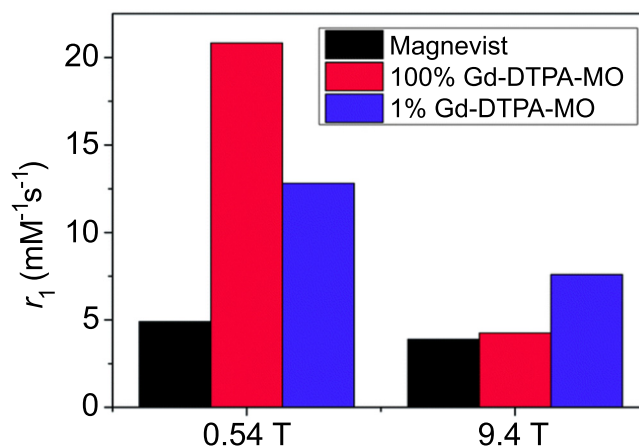
Fig. (6). Longitudinal relaxivity measurements at low and high field strengths of Magnevist and dispersions made from Gd-DTPA-MO. (Reused with permission from Gupta *et al.* [62].

Acharya *et al.* [63] took a different approach which involved doping cubic mesophases with superparamagnetic iron oxide nanoparticles. The unique structure of the cubosomes was not altered with the introduction of the metallic nanoparticles which can be visualised in Fig. (**7**). They also found that as the concentration of iron oxide nanoparticles increased so did the T2 relaxivity. This indicates that if there is a secondary desired use of the cubosome structure such as drug delivery, it is still possible but also that by doping the cubosomes with a contrast agent the potential of the contrast agent is improved. This is likely due to the

Fig. (7). Cryo-TEM images of cubosomes loaded with 8 nm spherical SPIONs at a concentration of 0.3 wt% Fe in phytantriol. These images s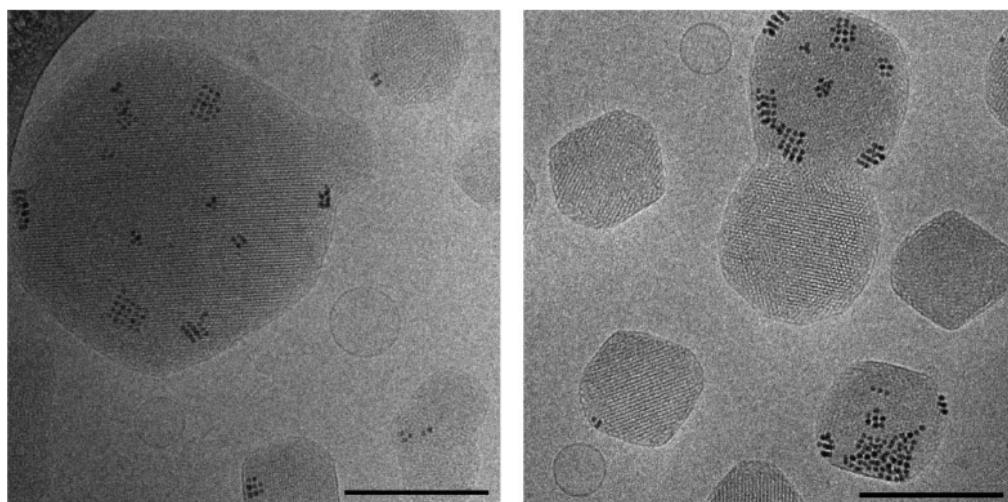how a lack of uniformity of SPION loading into the lipid nanosystem. (Adapted with permission from Acharya *et al.* [63]).

SPIONs interacting with the water inside the bi-continuous water channels and also the surrounding bulk water of the dispersion. Additionally, these improvements in the efficacy of the contrast agent can be attributed to a couple of physical phenomena. Finally, they were able to show that the contrast agent had effect one hour post injection in rats which is a significant improvement over the commercially available Resovist®. These results are promising for the future application of cubosomes in conjunction with contrast agents to improve MRI imaging.

One of the less conventional classes of contrast agents are nitroxides. Nixtroxides are stable, organic free radicals with an unpaired electron which is paramagnetic making it a possible contrast agent due to its ability to shorten relaxation times [64]. Imaging agents based from nitroxides exhibit certain benefits as the metal based contrast agents are toxic if not chelated or bound [42, 52, 65]. Other drawbacks of more traditional contrast agents are that a possible adverse effect in some patients can be renal failure resulting in a disease called nephrogenic systemic fibrosis [66]. Aside from overcoming said drawbacks, other benefits of nitroxides include that they have been shown to help control hypertension and weight, prevent damage from reperfusion injury and some abilities to treat neurodegenerative diseases and ocular damage [67].

In order to capitalise on these sought after properties Muir *et al.* [68] created metal-free nitroxide-based lyotropic liquid crystalline nanoparticles for MRI imaging enhancement. Their work involved synthesising a nitroxide group containing lipid which were then formulated into cubosomes and hexosomes. They quickly noticed through cryo-TEM imaging that loading a higher percentage of their lipid resulted in structure changes to the nanosystems. Relaxivity studies indicated that the contrast enhancement was more greatly affected by the structure of the mesophase as opposed to the content of nitroxide present. The cubic structure performed better than the hexagonal structure that was brought on by a higher nitroxide lipid loading.

One possible explanation is that the cubic phase nanoparticles have a much greater internal surface area when compared to hexagonal phase as there are bicontinuous water and oil channels. Another explanation touched upon previously is that the cubic phase has a faster exchange of water molecules from the confined water and the bulk water. Muir *et al.* were able to show that nitroxide-loaded lyotropic liquid crystalline nanosystems were more effective than previously attempted nixotride-loaded liposomes *in vivo* and those made from Myverol were shown to be non-toxic as opposed to heavy metals such as gadolinium.

They followed up this work by synthesising four novel nitroxide lipids with a "kinked" tail (Fig. **8**) which would allow a higher loading but not alter the packing parameter in a way that leads to a phase shift away from the more effective cubic structure [69]. They discovered a direct link with the lattice parameter of the system to the longitudinal relaxation rate (T1). Their results further support the importance of the role of the structure in the agents ability to act as a contrast enhancer. Similarly, they again showed that including the nitroxide into the nanostructure improved relaxivity

when compared to a free nitroxyl group which is also more likely to undergo degradation. Using hexosomes as opposed to cubosomes due to previously found toxicity issues, Bye *et al.* [69] were able to formulate metal-free MRI contrast agents with limited targeting capabilities and long circulating half-lives demonstrating a possible alternative in contrast agent development. It should be mentioned that toxicity studies regarding cubosomes are limited and require further investigation as there is evidence to suggest it can also be cell line specific [70-73].
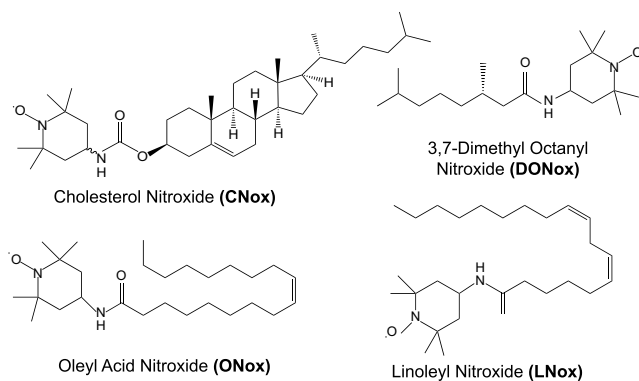

Fig. (8). Molecular structure of nitroxide lipids synthesised for use as MRI contrast agents (Reused with permission from Bye *et al.* [69]).

LOOKING FORWARD

As shown there is still a lot to explore with cubosomes but especially in regards to MRI imaging contrast agents. Due to their special properties such as having both polar and non-polar domains, internal and external water channels and being biocompatible there is a lot of untapped potential with these systems as theranostic agents.

An area that still must be explored is the role of the mesophase in controlling the efficacy as a MRI contrast agent. Some of the mentioned studies noted that relaxivity was more dependent on the phase of the system as opposed to the amount of contrast agent loaded. It is still unclear whether the size of the water channels or their shape have greater effect on relaxivity and the ability of these systems to perform as a contrast agent.

Further developments in targeting cubosomes to specific tissue type could further improve the potential of these systems as MRI contrast agents. Current approaches involve creating more sophisticated nanoparticles with the use of novel stabilisers and phospholipids that can introduce functional groups onto the surface. These functional groups can be utilised in active targeting of tumours using antibodies or other ligands

to receptors on the cells of interest. One avenue our research group is taking involves using cubosomes with the fairly new technique of metabolic labelling. This approach uses a cells natural metabolic pathway by generating chemical reporters that can then be targeted for covalent attachment. These experiments are ongoing but preliminary results are promising which reveal another approach for targeted and improved MRI contrast agents.

CONCLUSION

To summarise, MRI is an important tool in clinical settings to help health professionals come to a diagnosis and create treatment plans for patients without requiring invasive or radiating measures. However, to be more effective and clear the modality requires contrast agents to help improve resolution. Current contrast agents have limited specificity and circulation times putting certain restraints on their efficacy. For this reason there is a need to develop longer circulating and more tissue specific contrast agents and one potential avenue is using lyotropic liquid crystalline nanoparticles as a carrier. These nanosystems have already been researched for their potential uses as drug delivery agents and as mentioned in this minireview there are a few groups of researchers that have combined current contrast agents with cubosomes with different degrees of early success. Overall, they have shown that regardless of which type of contrast agent is used that loading them into the nanoparticles has improved their imaging performance when compared to commercially available alternatives. The unique mesophase structure plays a large role in these systems capabilities as a contrast agent due to how it changes the interactions of the water protons which in turn effects the technique. More work is needed to continue to assess and determine the full potential of cubosomes as contrast agents but the current body of work indicates early success in proving the concept.

LIST OF ABBREVIATIONS

Cryo-FESEM	=	Cryo-Field Emission Scanning Electron Microscopy
Cryo-TEM	=	Cryo-Transmission Electron Microscopy
DLS	=	Dynamic Light Scattering
DTPA	=	Diethylenetriaminepentaacetic acid
EDTA	=	Ethylenediaminetetraacetic acid
GMO	=	Glycerol Mono-Oleate

MRI = Magnetic Resonance Imaging

SAXS = Small Angle X-ray Scattering

SPION = Super Paramagnetic Iron Oxide Nanoparticle

CONFLICT OF INTEREST

The authors confirm that this article content has no conflict of interest.

ACKNOWLEDGEMENTS

REFERENCES

[1] Larsson, K. Cubic lipid-water phases: structures and biomembrane aspects. *J. Phys. Chem.,* **1989**, *93*(21), 7304-7314.

[2] Kaasgaard, T.; Drummond, C.J. Ordered 2-D and 3-D nanostructured amphiphile self-assembly materials stable in excess solvent. *Phys. Chem. Chem. Phys.,* **2006**, *8*(43), 4957-4975.

[3] Spicer, P.T.; Hayden, K.L.; Lynch, M.L.; Ofori-Boateng, A.; Burns, J.L. Novel process for producing cubic liquid crystalline nanoparticles (Cubosomes). *Langmuir,* **2001**, *17*(19), 5748-5756.

[4] La, Y.; Park, C.; Shin, T.J.; Joo, S.H.; Kang, S.; Kim, K.T. Colloidal inverse bicontinuous cubic membranes of block copolymers with tunable surface functional groups. *Nat. Chem.,* **2014**, *6*(6), 534-541.

[5] Hyde, S.; Ninham, B.W.; Andersson, S.; Larsson, K.; Landh, T.; Blum, Z.; Lidin, S., Chapter 1 - The Mathematics of Curvature. In: *The Language of Shape;* Elsevier Science B.V.: Amsterdam, **1997**; pp. 1-42.

[6] Marrink, S.-J.; Tieleman, D.P. Molecular dynamics simulation of a lipid diamond cubic phase. *J. Am. Chem. Soc.,* **2001**, *123*(49), 12383-12391.

[7] Garg, G.; Saraf, S.; Saraf, S. Cubosomes: an overview. *Biol. Pharm. Bull.,* **2007**, *30*(2), 350-353.

[8] Karami, Z.; Hamidi, M. Cubosomes: remarkable drug delivery potential. *Drug Discov. Today,* **2016**, *21*(5), 789-801.

[9] Spicer, P.T. Progress in liquid crystalline dispersions: Cubosomes. *Curr. Opin. Colloid Interface Sci.,* **2005**, *10*(5–6), 274-279.

[10] Han, S.; Shen, J.Q.; Gan, Y.; Geng, H.M.; Zhang, X.X.; Zhu, C.L.; Gan, L. Novel vehicle based on cubosomes for ophthalmic delivery of flurbiprofen with low irritancy and high bioavailability. *Acta Pharmacol. Sin.,* **2010**, *31*(8), 990-998.

[11] Pan, X.; Han, K.; Peng, X.; Yang, Z.; Qin, L.; Zhu, C.; Huang, X.; Shi, X.; Dian, L.; Lu, M.; Wu, C. Nanostructured cubosomes as advanced drug delivery system. *Curr. Pharm. Des.,* **2013**, *19*(35), 6290-6297.

[12] Nadiminti, P.P.; Rookes, J.E.; Dong, Y.D.; Sayer, C.; Boyd, B.J.; Cahill, D.M. Nanostructured liquid crystalline particle assisted delivery of 2,4-dichlorophenoxyacetic acid to weeds, crops and model plants. *Crop .Prot.,* **2016**, *82*, 17-29.

[13] Nadiminti, P.P.; Dong, Y.D.; Sayer, C.; Hay, P.; Rookes, J.E.; Boyd, B.J.; Cahill, D.M. Nanostructured liquid crystalline particles as an alternative delivery vehicle for plant agrochemicals. *ACS Appl. Mater. Interfaces,* **2013**, *5*(5), 1818-1826.

[14] Afriat, I.; Biatry, B. Use of cubic gel particles as an anti-pollution agent, in particular in a cosmetic composition. U.S. Patent 20,020,071,820, June 13, 2002.

[15] Ribier, A.; Simonnet, J.T.; Michelet, J. Cosmetic or dermatological composition comprising an oil-in-water emulsion comprising oily globules with a lamellar liquid crystal coating. U.S Patent 5,925,364, July 20, 1999.

[16] Albrecht, H.; Schreiber, J. Hair care products with disperse liquid crystals exhibiting the cubic phases. W.O Patent 2,002,041,850, May 30, 2002.

[17] Leng, F.J.; Parrott, D.T. Antiperspirant materials and compositions. U.S Patent 5,593,663, January 14, 1997.

[18] Barauskas, J.; Nylander, T. 4 - *Lyotropic Liquid Crystals as Delivery Vehicles for Food Ingredients A2 - Garti, Nissim. Delivery and Controlled Release of Bioactives in Foods and Nutraceuticals.* Woodhead Publishing, U.K., **2008**, pp. 107-131.

[19] Hernandez, E.M. 5 - *Structured Lipids as Delivery Systems A2 - Garti, Nissim. Delivery and Controlled Release of Bioactives in Foods and Nutraceuticals.* Woodhead Publishing, U.K., **2008**, pp. 135-148.

[20] Garti, N.; Yuli-Amar, I. 6 - *Micro- and Nano-Emulsions for Delivery of Functional Food Ingredients. Delivery and Controlled Release of Bioactives in Foods and Nutraceuticals.* Woodhead Publishing, U.K., **2008**, pp. 149-183.

[21] Ramon, O.; Danino, D. *8 - Lipid Self-Assembled Particles for the Delivery of Nutraceuticals A2 - Garti, Nissim. Delivery and Controlled Release of Bioactives in Foods and Nutraceuticals.* Woodhead Publishing, U.K., **2008**, pp. 207-233.

[22] Mulet, X.; Boyd, B.J.; Drummond, C.J. Advances in drug delivery and medical imaging using colloidal lyotropic liquid crystalline dispersions. *J. Colloid Interface Sci.,* **2013**, *393*, 1-20.

[23] Rizwan, S.B.; Dong, Y.D.; Boyd, B.J.; Rades, T.; Hook, S. Characterisation of bicontinuous cubic liquid crystalline systems of phytantriol and water using cryo field emission scanning electron microscopy (cryo FESEM). *Micron,* **2007**, *38*(5), 478-485.

[24] Barauskas, J.; Johnsson, M.; Joabsson, F.; Tiberg, F. Cubic phase nanoparticles (Cubosome): principles for controlling size, structure, and stability. *Langmuir,* **2005**, *21*(6), 2569-2577.

[25] Gustafsson, J.; Ljusberg-Wahren, H.; Almgren, M.; Larsson, K. Cubic lipid−water phase dispersed into submicron particles. *Langmuir,* **1996**, *12*(20), 4611-4613.

[26] Gustafsson, J.; Ljusberg-Wahren, H.; Almgren, M.; Larsson, K. Submicron particles of reversed lipid phases in water stabilized by a nonionic amphiphilic polymer. *Langmuir,* **1997**, *13*(26), 6964-6971.

[27] Yaghmur, A.; de Campo, L.; Sagalowicz, L.; Leser, M.E.; Glatter, O. Emulsified microemulsions and oil-containing liquid crystalline phases. *Langmuir,* **2005**, *21*(2), 569-577.

[28] Nakano, M.; Sugita, A.; Matsuoka, H.; Handa, T. Small-angle x-ray scattering and ^{13}C NMR investigation on the internal structure of "cubosomes". *Langmuir,* **2001**, *17*(13), 3917-3922.

[29] Salentinig, S.; Yaghmur, A.; Guillot, S.; Glatter, O. Preparation of highly concentrated nanostructured dispersions of controlled size. *J. Colloid Interface Sci.,* **2008**, *326*(1), 211-220.

[30] Fraser, S.J.; Mulet, X.; Hawley, A.; Separovic, F.; Polyzos, A. Controlling nanostructure and lattice parameter of the inverse bicontinuous cubic phases in functionalised phytantriol dispersions. *J. Colloid Interface Sci.,* **2013**, *408*, 117-124.

[31] Driever, C.D.; Mulet, X.; Waddington, L.J.; Postma, A.; Thissen, H.; Caruso, F.; Drummond, C.J. Layer-by-layer

polymer coating on discrete particles of cubic lyotropic liquid crystalline dispersions (cubosomes). *Langmuir,* **2013**, *29*(42), 12891-12900.

[32] Hartnett, T.E.; Ladewig, K.; O'Connor, A.J.; Hartley, P.G.; McLean, K.M. Size and phase control of cubic lyotropic liquid crystal nanoparticles. *J. Phys. Chem. B,* **2014**, *118*(26), 7430-7439.

[33] Goldburg, W.I. Dynamic light scattering. *Am. J. Phys.,* **1999**, *67*(12), 1152-1160.

[34] Borné, J.; Nylander, T.; Khan, A. Effect of lipase on monoolein-based cubic phase dispersion (cubosomes) and vesicles. *J. Phys. Chem. B,* **2002**, *106*(40), 10492-10500.

[35] Barauskas, J.; Johnsson, M.; Tiberg, F. Self-assembled lipid superstructures: beyond vesicles and liposomes. *Nano Lett.,* **2005**, *5*(8), 1615-1619.

[36] Boyd, B.J.; Dong, Y.-D.; Rades, T. Nonlamellar liquid crystalline nanostructured particles: advances in materials and structure determination. *J. Liposome Res.,* **2009**, *19*(1), 12-28.

[37] Johnsson, M.; Barauskas, J.; Tiberg, F. Cubic phases and cubic phase dispersions in a phospholipid-based system. *J. Am. Chem. Soc.,* **2005**, *127*(4), 1076-1077.

[38] Doan, B.-T.; Meme, S.; Beloeil, J.-C. *General Principles of MRI. The Chemistry of Contrast Agents in Medical Magnetic Resonance Imaging.* John Wiley & Sons, Ltd; **2013**, pp. 1-23.

[39] Gupta, A.; de Campo, L.; Rehmanjan, B.; Willis, S.A.; Waddington, L.J.; Stait-Gardner, T.; Kirby, N.; Price, W.S.; Moghaddam, M.J. Evaluation of Gd-DTPA-monophytanyl and phytantriol nanoassemblies as potential MRI contrast agents. *Langmuir,* **2015**, *31*(4), 1556-1563.

[40] Brown, R. W.; Cheng, Y.-C. N.; Haacke, E. M.; Thompson, M. R; Venkatesan, R. Magnetic Resonance Imaging. In: *Magnetic Resonance Imaging*, John Wiley & Sons Ltd: **2014**, pp. 1-17.

[41] Jiang, H.; Feng, L.; Soriano del Amo, D.; Seidel Iii, R.D.; Marlow, F.; Wu, P. Imaging glycans in zebrafish embryos by metabolic labeling and bioorthogonal click chemistry. *J. Vis. Exp.,* **2011**, *52*, 2686.

[42] Caravan, P.; Ellison, J.J.; McMurry, T.J.; Lauffer, R.B. Gadolinium(III) chelates as MRI contrast agents: structure, dynamics, and applications. *Chem. Rev.,* **1999**, *99*(9), 2293-2352.

[43] Aime, S.; Crich, S.G.; Gianolio, E.; Giovenzana, G.B.; Tei, L.; Terreno, E. High sensitivity lanthanide(III) based probes for MR-medical imaging. *Coord. Chem. Rev.,* **2006**, *250*(11–12), 1562-1579.

[44] Qin, J.; Laurent, S.; Jo, Y.S.; Roch, A.; Mikhaylova, M.; Bhujwalla, Z.M. A high-performance magnetic resonance imaging T2 contrast agent. *Adv. Mater.,* **2007**, *19*(14), 1874-1878.

[45] Borges, M.; Yu, S.; Laromaine, A.; Roig, A.; Suarez-Garcia, S.; Lorenzo, J. Dual T1/T2 MRI contrast agent based on hybrid SPION@coordination polymer nanoparticles. *RSC Adv.,* **2015**, *5*(105), 86779-86783.

[46] Ma, X.; Gong, A.; Chen, B.; Zheng, J.; Chen, T.; Shen, Z.; Wu, A. Exploring a new SPION-based MRI contrast agent with excellent water-dispersibility, high specificity to cancer cells and strong MR imaging efficacy. *Colloids Surf. B Biointerfaces,* **2015**, *126*, 44-49.

[47] Biagi, B.A.; Enyeart, J.J. Gadolinium blocks low- and high-threshold calcium currents in pituitary cells. *Am. J. Physiol.,* **1990**, *259*(3 Pt. 1), C515-C520.

[48] Molgó, J.; del Pozo, E.; Baños, J.E.; Angaut-Petit, D. Changes of quantal transmitter release caused by gadolinium ions at the frog neuromuscular junction. *Br. J. Pharmacol.,* **1991**, *104*(1), 133-138.

[49] Hingorani, D.V.; Bernstein, A.S.; Pagel, M.D. A review of responsive MRI contrast agents: 2005-2014. *Contrast Media Mol. Imaging,* **2015**, *10*(4), 245-265.

[50] Strijkers, G.J.; Mulder, W.J.; van Tilborg, G.A.; Nicolay, K. MRI contrast agents: current status and future perspectives. *Anticancer. Agents Med. Chem.,* **2007**, *7*(3), 291-305.

[51] Natalin, R.A.; Prince, M.R.; Grossman, M.E.; Silvers, D.; Landman, J. Contemporary applications and limitations of magnetic resonance imaging contrast materials. *J. Urol.,* **2010**, *183*(1), 27-33.

[52] Caravan, P. Strategies for increasing the sensitivity of gadolinium based MRI contrast agents. *Chem. Soc. Rev.,* **2006**, *35*(6), 512-523.

[53] Mulder, W.J.; Strijkers, G.J.; van Tilborg, G.A.; Griffioen, A.W.; Nicolay, K. Lipid-based nanoparticles for contrast-enhanced MRI and molecular imaging. *NMR Biomed.,* **2006**, *19*(1), 142-164.

[54] Strijkers, G.J.; Mulder, W.J.; van Heeswijk, R.B.; Frederik, P.M.; Bomans, P.; Magusin, P.C. Relaxivity of liposomal paramagnetic MRI contrast agents. Magnetic Resonance Materials in Physics. *Biol. Med.,* **2005**, *18*(4), 186-192.

[55] Gløgård, C.; Stensrud, G.; Klaveness, J. Novel high relaxivity colloidal particles based on the specific phase organisation of amphiphilic gadolinium chelates with cholesterol. *Int. J. Pharm.,* **2003**, *253*(1-2), 39-48.

[56] Nicolle, G.M.; Tóth, E.; Schmitt-Willich, H.; Radüchel, B.; Merbach, A.E. The impact of rigidity and water exchange on the relaxivity of a dendritic MRI contrast agent. *Chemistry,* **2002**, *8*(5), 1040-1048.

[57] Estelrich, J.; Sánchez-Martín, M.J.; Busquets, M.A. Nanoparticles in magnetic resonance imaging: from simple to dual contrast agents. *Int. J. Nanomedicine,* **2015**, *10*, 1727-1741.

[58] Liu, G.; Conn, C.E.; Waddington, L.J.; Mudie, S.T.; Drummond, C.J. Colloidal amphiphile self-assembly particles composed of gadolinium oleate and myverol: evaluation as contrast agents for magnetic resonance imaging. *Langmuir,* **2010**, *26*(4), 2383-2391.

[59] Moghaddam, M.J.; de Campo, L.; Waddington, L.J.; Drummond, C.J. Chelating phytanyl-EDTA amphiphiles: self-assembly and promise as contrast agents for medical imaging. *Soft Matter,* **2010**, *6*(23), 5915-5929.

[60] Moghaddam, M.J.; de Campo, L.; Kirby, N.; Drummond, C.J. Chelating DTPA amphiphiles: ion-tunable self-assembly structures and gadolinium complexes. *Phys. Chem. Chem. Phys.,* **2012**, *14*(37), 12854-12862.

[61] Moghaddam, M.J.; de Campo, L.; Hirabayashi, M.; Bean, P.A.; Waddington, L.J.; Scoble, J.A. Gadolinium-DTPA amphiphile nanoassemblies: agents for magnetic resonance imaging and neutron capture therapy. *Biomater. Sci.,* **2014**, *2*(6), 924-935.

[62] Gupta, A.; Stait-Gardner, T.; de Campo, L.; Waddington, L.J.; Kirby, N.; Price, W.S. Nanoassemblies of Gd-DTPA-monooleyl and glycerol monooleate amphiphiles as potential MRI contrast agents. *J. Mater. Chem. B Mater. Biol. Med.,* **2014**, *2*(9), 1225-1233.

[63] Acharya, D.P.; Moffat, B.A.; Polyzos, A.; Waddington, L.; Coia, G.; Wright, D.K. Cubic mesophase nanoparticles doped with superparamagnetic iron oxide nanoparticles: a new class of MRI contrast agent. *RSC Adv.,* **2012**, *2*(16), 6655-6662.

[64] Hyodo, F.; Chuang, K-H.; Goloshevsky, A.G.; Sulima, A.; Griffiths, G.L.; Mitchell, J.B.; Koretsky, A.P.; Krishna, M.C. Brain redox imaging using blood-brain barrier-permeable nitroxide MRI contrast agent. *J. Cereb. Blood Flow Metab.,* **2008**, *28*(6), 1165-1174.

[65] Laurent, S.; Elst, L.V.; Muller, R.N. Comparative study of the physicochemical properties of six clinical low molecular

weight gadolinium contrast agents. *Contrast Media Mol. Imaging,* **2006**, *1*(3), 128-137.

[66]   Sadowski, E.A.; Bennett, L.K.; Chan, M.R.; Wentland, A.L.; Garrett, A.L.; Garrett, R.W.; Djamali, A. Nephrogenic systemic fibrosis: risk factors and incidence estimation. *Radiology,* **2007**, *243*(1), 148-157.

[67]   Soule, B.P.; Hyodo, F.; Matsumoto, K.; Simone, N.L.; Cook, J.A.; Krishna, M.C.; Mitchell, J.B. Therapeutic and clinical applications of nitroxide compounds. *Antioxid. Redox Signal.,* **2007**, *9*(10), 1731-1743.

[68]   Muir, B.W.; Acharya, D.P.; Kennedy, D.F.; Mulet, X.; Evans, R.A.; Pereira, S.M.; Wark, K.L.; Boyd, B.J.; Nguyen, T.H.; Hinton, T.M.; Waddington, L.J.; Kirby, N.; Wright, D.K.; Wang, H.X.; Egan, G.F.; Moffat, B.A. Metal-free and MRI visible theranostic lyotropic liquid crystal nitroxide-based nanoparticles. *Biomaterials,* **2012**, *33*(9), 2723-2733.

[69]   Bye, N.; Hutt, O.E.; Hinton, T.M.; Acharya, D.P.; Waddington, L.J.; Moffat, B.A.; Wright, D.K.; Wang, H.X.; Mulet, X.; Muir, B.W. Nitroxide-loaded hexosomes provide MRI contrast *in vivo. Langmuir,* **2014**, *30*(29), 8898-8906.

[70]   Barauskas, J.; Cervin, C.; Jankunec, M.; Špandyreva, M.; Ribokaitė, K.; Tiberg, F.; Johnsson, M. Interactions of lipid-based liquid crystalline nanoparticles with model and cell membranes. *Int. J. Pharm.,* **2010**, *391*(1-2), 284-291.

[71]   Murgia, S.; Falchi, A.M.; Mano, M.; Lampis, S.; Angius, R.; Carnerup, A.M.; Schmidt, J.; Diaz, G.; Giacca, M.; Talmon, Y.; Monduzzi, M. Nanoparticles from lipid-based liquid crystals: emulsifier influence on morphology and cytotoxicity. *J. Phys. Chem. B,* **2010**, *114*(10), 3518-3525.

[72]   Shen, H-H.; Crowston, J.G.; Huber, F.; Saubern, S.; McLean, K.M.; Hartley, P.G. The influence of dipalmitoyl phosphatidylserine on phase behaviour of and cellular response to lyotropic liquid crystalline dispersions. *Biomaterials,* **2010**, *31*(36), 9473-9481.

[73]   Zhai, J.; Hinton, T.M.; Waddington, L.J.; Fong, C.; Tran, N.; Mulet, X.; Drummond, C.J.; Muir, B.W. Lipid-PEG conjugates sterically stabilize and reduce the toxicity of phytantriol-based lyotropic liquid crystalline nanoparticles. *Langmuir,* **2015**, *31*(39), 10871-10880.